Title

Amidinates and Guanidinates as Supporting Ligands for Expanding the Reactivity of Thorium and Uranium Complexes

Author

Settineri, Nicholas Salvatore

Publication Date

2018

Peer reviewed|Thesis/dissertation

Amidinates and Guanidinates as Supporting Ligands for Expanding the Reactivity of Thorium and Uranium Complexes

By

Nicholas Salvatore Settineri

A dissertation submitted in partial satisfaction of the
requirements for the degree of
Doctor of Philosophy
in
Chemistry
in the
Graduate Division
of the
University of California, Berkeley

Committee in charge:

Professor John Arnold, Chair
Professor Matthew Francis
Professor Alexander Katz

Summer 2018

Amidinates and Guanidinates as Supporting Ligands for Expanding the Reactivity of Thorium and Uranium Complexes

By

Nicholas Salvatore Settineri

Abstract

Amidinates and Guanidinates as Supporting Ligands for Expanding the Reactivity of Thorium and Uranium Complexes

By

Nicholas Salvatore Settineri

Doctor of Philosophy in Chemistry
University of California, Berkeley
Professor John Arnold, Chair

Chapter 1:

A series of thorium and uranium tris-amidinate complexes featuring a rare O-bound terminal phosphaethynolate (OCP^{1-}) ligand were synthesized and fully characterized. These are the first actinide complexes featuring the OCP^{1-} moiety, and the coordination through the O-atom donor is unique compared to all previously reported metal complexes, which feature P-bound OCP^{1-} ligands. The cyanate (OCN^{1-}) and thiocyanate (SCN^{1-}) analogs were prepared for structural comparison and feature preferential N-coordination to the metal center. Calculations suggest the binding in all these complexes is charge-driven. The thorium OCP complex reacts with $Ni(COD)_2$ to yield a heterobimetallic adduct as addition across the C≡P triple bond is observed; this new species features an unprecedented reduced OCP^{1-} bent fragment which bridges the two metal centers.

Chapter 2:

A new thorium monoalkyl complex, $Th(CH_2SiMe_3)(BIMA)_3$ (**2.2**; BIMA = $MeC(N^iPr)_2$), undergoes insertion of chalcogen atoms resulting in a series of thorium chalcogenolate complexes, $Th(ECH_2SiMe_3)(BIMA)_3$ (where E = S, SS, Se, Te; **2.5-2.8**). Complex **2.6** represents the first alkyl disulfide thorium species and illustrates the ability of **2.2** to undergo controllable, stoichiometric atom insertion. All complexes have been characterized by ^1H and $^{13}C\{^1H\}$ NMR spectroscopy, FTIR, EA, and melting point, and in the case of **2.1**, **2.2**, and **2.4-2.8**, X-ray crystallography. X-ray diffraction studies reveal the η^2-coordination mode of the sulfur atoms in **2.6**, the acute nature of the Th-Se-C bond in **2.7**, and the first molecular Th-Te single bond in **2.8**. Insertion was achieved by balancing the thermodynamic driving force of chalcogenolate formation versus the BDE of the pnictogen-chalcogen bond in the transfer reagent. Utilizing Me_3NO as an oxygen atom

transfer reagent led to C-H activation and $SiMe_4$ elimination rather than oxygen atom insertion, resulting in the alkoxide complex $Th(OCH_2NMe_2)(BIMA)_3$ (**2.4**).

Chapter 3:

The reactivity of the thorium monoalkyl complex $Th(CH_2SiMe_3)(BIMA)_3$ (**2.2**; BIMA = $MeC(N^iPr)_2$) with various small molecules is presented. While steric congestion prohibits the insertion of *N*,*N'*-diisopropylcarbodiimide into the Th-C bond in **2.2**, the first thorium tetrakis(amidinate) complex, $Th(BIMA)_4$ (**3.1**), is synthesized *via* an alternative salt metathesis route. Insertion of *p*-tolyl azide leads to the triazenido complex Th[(*p*-tolyl)NNN(CH_2SiMe_3)-$\kappa^2N^{1,2}$](BIMA)$_3$ (**3.2**), which undergoes thermal decomposition to the amido species Th[(*p*-tolyl)N($SiMe_3$)](BIMA)$_3$ (**3.3**). The reaction of **2.2** with 2,6-dimethylphenylisocyanide results in the thorium iminoacyl complex Th[η^2-(C=N)-2,6-Me_2-$C_6H_3(CH_2SiMe_3)$](BIMA)$_3$ (**3.4**), while the reaction with isoelectronic CO leads to the products Th[OC(=CH_2)$SiMe_3$](BIMA)$_3$ (**3.5**) and Th[OC(N^iPr)C(CH_2SiMe_3)(C(Me)N(^{i}Pr))O-κ^2O,O′](BIMA)$_2$ (**3.6**), the latter being the result of CO coupling and insertion into an amidinate ligand. Protonolysis is achieved with several substrates, producing amido (**3.8**), aryloxide (**3.9**), phosphide (**3.10**, **3.11**), acetylide (**3.12**), and cationic (**3.13**) complexes. Ligand exchange with 9-borabicyclo[3.3.1]nonane (9-BBN) results in the formation of the thorium borohydride complex $(BIMA)_3Th(\mu\text{-}H)_2[B(C_8H_{14})]$ (**3.14**). Complex **2.2** also reacts under photolytic conditions to eliminate $SiMe_4$ and produce $Th(BIMA)_2$(BIMA*) [**3.15**, BIMA* = (^{i}Pr)NC(CH_2)N(^{i}Pr)], featuring a rare example of a dianionic amidinate ligand. Complexes **3.1**, **3.2**, **3.4**, **3.5**, and **3.11-3.15** were characterized by ^{1}H and $^{13}C\{^1H\}$ NMR spectroscopy, FTIR, EA, melting point and X-ray crystallography. All other complexes were identified by one or more of these spectroscopic techniques.

Chapter 4:

A series of uranium tris-guanidinate complexes is presented, including the first homoleptic U(III) guanidinate species (**4.2**). Reaction of **4.2** with diphenyldiazomethane results in the two-electron oxidation of U(III) to U(V), producing the first isolable U(V) diphenyldiazomethane complex (**4.3**), featuring a short U-N_{imido} bond. Corresponding U(V) imido (**4.4**), U(V) oxo (**4.5**), and U(IV) azido (**4.6**) complexes were also synthesized for spectroscopic comparison. All complexes were characterized by ^{1}H NMR spectroscopy, FTIR, EA, melting point, and X-ray crystallography.

Chapter 5:

Thorium dialkyl complexes featuring bis-amidinate and bis-guanidinate frameworks are reported, and their ability to insert molecular oxygen is evaluated. The bis-amidinate system $Th(BTBA)_2(CH_2SiMe_3)_2$ (**5.2**; BTBA = $PhC(NSiMe_3)_2$) is able to undergo instantaneous oxygen insertion to form the corresponding dialkoxide complex (**5.3**), as well as selenium atom insertion to form the diselenolate (**5.4**). The bis-guanidinate system $Th(TIG)_2(CH_2SiMe_3)_2$ (**5.6**; TIG = $^iPr_2NC(N^iPr)_2$) undergoes oxygen insertion at a significantly slower rate, and preliminary mechanistic studies suggest a radical-type mechanism is at play. All complexes were characterized by ^{1}H and $^{13}C\{^1H\}$ NMR spectroscopy, FTIR, EA, melting point, and X-ray crystallography.

Table of Contents

Acknowledgements……...iii

Chapter 1

Uranium and Thorium Complexes of the Phosphaethynolate Ion…….1

Overview……..2
Introduction……..2
Results and Discussion…….3
Synthesis of Actinide OCP Complexes……3
Synthesis of Actinide NCO and NCS Complexes……5
DFT Calculations……7
Reactivity of OCP Moiety……..13
Conclusions……18
Experimental Details……..19
References……..23

Chapter 2

A Thorium Chalcogenolate Series Generated by Atom Insertion into Thorium-Carbon Bonds…….27

Overview……28
Introduction……28
Results and Discussion……...29
Synthesis of $Th(CH_2SiMe_3)(BIMA)_3$…….29
C-H Activation of OAT Reagents……...31
Synthesis of Heavier Thorium Chalcogenolates……34
Conclusions……44
Experimental Details……..45
References……..50

Chapter 3

Insertion, Protonolysis and Photolysis Reactivity of a Thorium Monoalkyl Amidinate Complex……54

Overview……55
Introduction……55

Table of Contents

Results and Discussion……...56
Insertion Reactivity of $Th(CH_2SiMe_3)(BIMA)_3$……56
Protonolysis Reactivity of $Th(CH_2SiMe_3)(BIMA)_3$……...65
Photolysis Reactivity of $Th(CH_2SiMe_3)(BIMA)_3$……..71
Conclusions……76
Experimental Details…….....77
References……..84

Chapter 4

Two-Electron Oxidation of a Homoleptic U(III) Guanidinate Complex by Diphenyldiazomethane……88

Overview……89
Introduction……89
Results and Discussion……...90
Synthesis of Uranium Guanidinate Systems……..90
Two-Electron Oxidation of $U(TIG)_3$……..92
Conclusions……..102
Experimental Details……103
References……107

Chapter 5

Dioxygen Reactivity with Thorium Dialkyls Supported by Amidinate and Guanidinate Frameworks……109

Overview……..110
Introduction……..110
Results and Discussion……112
Synthesis of Amidinate-Supported Thorium Dialkyls……..112
Synthesis of Guanidinate-Supported Thorium Dialkyls……...119
Conclusions……..127
Experimental Details……128
References……132

Acknowledgements

How can I adequately thank everyone who has helped me reach this point in my life? I don't think I can; I suppose this small section of my thesis will have to suffice. Let it be known to everyone mentioned in this section – your importance to me and impact on my life is far greater than I can put into words. And to those are aren't mentioned but think they deserve it: better luck next time, suckers.

It seems only appropriate to first express my unending gratitude and love for my family, for they have helped me along this journey every step of the way. To my brothers Tony and Gaetano, and my sister Anna, there exists no people on Earth I would've rather grown up with and called my siblings. Having good brothers and sisters doesn't necessitate that you always get along; what it does necessitate is that you know, without a doubt, that they love you unconditionally and will always be there for you. Luckily for me, this has always been the case. I would like to personally thank Tony and Gaetano for actively being a part of my upbringing, despite the sizable age difference, and Anna for being my friend and partner in crime, as well as always knowing what I'm thinking (twin powers). I can't imagine a childhood filled with as much joy, laughter and tears (of joy, due to laughter) if not for the three of you, and for that I am eternally thankful. If you're wondering how much longer it'll take you to read the rest of these acknowledgments, it'll be about a half hour.

To my mother, who clearly wanted me to get a PhD only so she could refer to me as "Dr." to all her friends and family, you have been a symbol of resilience, determination, and patience my whole life. I could not have made it this far without learning these qualities from you. Our mutual competitive nature, manifested mostly in our arduous and hard-fought games of cribbage, has helped propel me to be better every day. I'd be remiss not to mention that those very same games of cribbage taught me a lot about humility and how to suffer defeat with grace and humor. To my father – you have been the single greatest influence in my life, with that influence growing more and more with each passing day. All my best qualities come from you, and I am forever thankful that I am your son, and you are my father. You've taught me, among countless other things, how to be a good person and friend not only to people I know, but to people I don't. You've taught me the power of a friendly conversation with a complete stranger, and how life is so much more than money, possessions and status; it's about the people in it and how you treat them, and the joy they can bring to your life and you to theirs. You are my role model and hero. To Mom and Dad – I love you both, and thank you for always loving me, even when I acted like a little shit. It means more than you know. I would also like to thank all of my extended family, as they have always supported and been proud of my endeavors.

Next in line, naturally, come my friends Matt, Colin, Max and Brandon (the boys). It's difficult to imagine what kind of life I would've lived these past 18 years if I hadn't met the four of you. Your friendship means everything to me, and I can only hope I've been as good a friend to you four as you've been to me these many years. Much of the person I am today is thanks to your influence, and your collective support and intellectual stimulation has pushed me to be the best version of myself. Whether it was playing video games, making zombie movies, star-gazing at meteor showers, or road tripping across half the United States, every minute spent with you guys has been a privilege and a blessing. I frankly cannot wait for the many adventures that still lie ahead of us.

Acknowledgements

Christine, I owe you so much. Graduate school is a difficult road, and I would've succumbed to its challenges and stresses without you by my side. Your sustained friendship and involvement in my life is one I am continuously thankful for, and I am grateful for the years of love and wonderful memories we shared together.

To my Berkeley chums – Parker, Rodi, Tyler, Matt Smith, Matt Kap, Phil, Mercedes, and Cindy – I wouldn't have wanted to go through this journey with anyone else. People ask me all the time if I would've been happier at any other institution and I always, bluntly, tell them "no." It's the people here that make Berkeley great, and the friendships I've formed here are frankly more valuable to me than my own PhD. You guys are what made this place special.

Building off that, I can't fail to mention the wonderful friends and colleagues I had in the Arnold group. To my mentors, Ashleigh and Clement, I owe you a great deal of gratitude for training me and guiding me through the world of actinide chemistry. Getting started with research in grad school can be rough, but thanks to your help I was able get started on the right foot. To the previous members of the lab, especially Thomas, Bernie, Ben, and Dan, who helped create a lab environment that I always wanted to be a part of, thank you for being fun, unique, and accepting. To my current lab members of Mary, Trevor, Michael and Jade, I've learned far more from you all than you've learned from me I'm sure, and I couldn't have asked for better lab mates and friends these past few years. I think it's clear that our lab dynamic and camaraderie is the envy of many of the groups here at Berkeley, and it's because of you wonderful individuals. I am eternally thankful that several visiting students, specifically my boi Jimmy Dank, as well as Marketa and Anki, made their way through our lab and have become part of my life.

In particular, a certain Jessica Ziegler deserves a great deal of praise. As my fellow 5th year and dear friend, we both felt a little overwhelmed when we first arrived in the Arnold group. With little air-sensitive chemistry between the two of us, joining a heavily synthetic, inorganic lab was daunting, and we faced many struggles and hurdles together. But there is no person I would've rather faced these challenges with; somehow, despite all the setbacks, uncertainty and doubt, we made it to the finish line. We helped turn the group dynamic around and brought back the fun and collectiveness that was missing during our first few years here. And while I like to think of myself as a good leader, it was clear that you became the true leader of the lab in our finals years, and I know you'll continue to lead everywhere you go, whether at Intel or places beyond. The laughs, stories, and experiences we've shared together are irreplaceable, and I thank you for every single one. You should also consider a career in stand-up since your GRS introduction for me brought the house down.

Luckily, I had the great opportunity and pleasure of mentoring a brilliant undergrad by the name of Angela Shiau, who now resides as a graduate student at Caltech. Angela did an excellent job working on analogous guanidinate systems, and much of chapters 4 and 5 are the results of her labors. Angela's quirky sense of humor, cheerful nature and friendly personality are only a few of her many amazing qualities, and I know she'll do nothing but great things with the rest of her life. The numerous Post-it note doodles I have thanks to her will forever be a staple of my office.

I would like to thank a variety of members of the Long, Raymond, and Tilley groups for helpful advice, instrumentation assistance and supplies. I also owe an exorbitant amount of gratitude to Hasan, for not only keeping the NMR facility afloat (a truly daunting task) but also keeping me afloat as I simultaneously ran CheXray and tried to finish the work in this thesis.

Acknowledgements

Hasan, your selfless nature and willingness to help anyone in any situation is nothing short of inspiring. Speaking of selfless individuals always willing to help, every graduate student would be completely lost without the aid of Lynn Keithlin, so I would like to personally thank her for always being patient and treating all of my silly requests with the utmost dedication.

Finally, there is no one left to thank but the boss man himself. John, being in your lab these past five years has truly been a wonderful experience. At times it's been exhausting, frustrating, and challenging, but the payoff has been worth it. You gave me the space to develop my own project and supported my directions, even if at first, they didn't seem all that fruitful. I always greatly appreciated your presence; it can't often be said that PIs are consistently around and available (or even willing) to chat with their graduate students, but you made that a priority and it certainly benefited my development as a researcher and chemist. It was always clear that you cared about us as people and not just as employees, and it meant a lot to me to have a boss that cared not only about my research but my life outside of lab. Thank you for believing in me and guiding me on this ill-advised path we take as graduate students. It has been the most rewarding experience of my life.

Chapter 1

Uranium and Thorium Complexes of the Phosphaethynolate Ion

Chapter 1

Overview

Efficient syntheses of the phosphaethynolate anion (OCP^{1-}) have only appeared within the last decade, and the chemistry involving this moiety is continuing to expand at a rapid rate. As the phosphorus analog of the cyanate anion, there is an interest in exploring the analogous reactivity of the OCP^{-1} anion, and reports have shown that this ligand shows the potential to act as a phosphorus-transfer reagent, as well as generate metal phosphides through loss of carbon monoxide from M-PCO starting materials. The following chapter describes the synthesis and characterization of the first actinide complexes incorporating the phosphaethynolate anion, in which the complexes exhibit rare O-bound coordination to the metal center. Both thorium and uranium amidinate complexes containing the OCP ligand were synthesized, as well as cyanate and thiocyanate analogs for structural comparison. Portions of this chapter have previously been published in: Camp, C., Settineri, N., Lefèvre, J., Jupp, A. R., Goicoechea, J. M., Maron, L. and Arnold, J. "Uranium and thorium complexes of the phosphaethynolate ion." *Chem. Sci.*, **2015**, *6*, 6379-6384.

Introduction

Synthetically accessible salts of the phosphaethynolate ion (OCP^{1-}) – the phosphorus analog of cyanate – have only appeared recently,[1,2] and since then the chemistry of this anion has begun to burgeon. The Grützmacher and Goicoechea groups have done extensive work in this area, having shown that the OCP^{1-} moiety exhibits rich cycloaddition and redox chemistry, resulting in the synthesis of various phosphorus-containing organic derivatives.[1,3-8] Two recent studies which showed the OCP^{1-} could act as a P-transfer reagent when treated with imidazolium salts[9] or cyclotrisilene[10] are of particular interest, as they suggest that the phosphaethynolate ion could be used as a readily accessible phosphide source. Recent computational studies also predicated the possibility to generate transition-metal phosphides from M-PCO precursors through carbonyl loss.[11] The Cummins group was able to confirm this idea experimentally, through the synthesis of a terminal tungsten phosphide via loss of carbonyl from a transient W-OCP complex, although the parent W-OCP species was never isolated.[12] The first transition-metal complex featuring the phosphaethynolate ion was $Re(P{=}C{=}O)(CO)_2(triphos)$ (triphos = $MeC(CH_3PPh_2)_3$),[13] which featured a terminal OCP^{1-} ligand P-bound to Re(I) and strongly bent around the pnictogen center. Since then, transition-metal complexes of copper, cobalt, iridium, and gold have been synthesized, all featuring P-bound phosphaethynolate moieties (Figure 1.1).[14] While recent work by Grützmacher and co-workers has shown that OCP^{1-} possesses an ambident nucleophilicity,[15] several questions remain to be answered concerning its interaction with metal centers throughout the periodic table and how this compares with its cyanate and thiocyanate counterparts, as well as determining the reactivity profile of the metal-bound phosphaethynolate species.

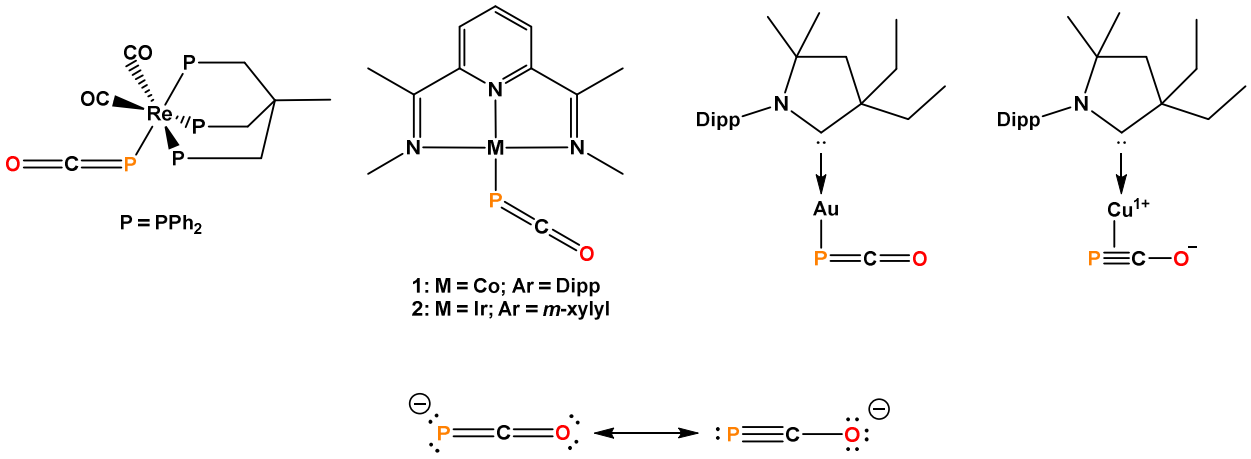

Figure 1.1. Top: transition-metal complexes incorporating the OCP^{1-} moiety. Bottom: resonance structures for the OCP^{1-} anion.

We thus targeted the use of $Na(OCP)(dioxane)_n$[2] as a source of the OCP^{1-} ligand in order to explore its coordination chemistry with actinides. We reasoned that these oxophilic metals were suitable candidates to polarize the OCP^{1-} moiety, with O-bound coordination preferential over the softer binding of the phosphorus atom. Interaction of heteroallenes with actinide species has attracted substantial interest over the past few years notably due to the propensity of low-valent actinides to activate small molecules (CO_2,[16-23] CS_2,[21,24-27], azides[28-34]). Additionally, uranium-mediated formations of cyanate have also been described, involving reductive co-coupling of CO and NO[35,36] and carbonylation of terminal nitrido[37] or silylimido[38] uranium derivatives. Here we report a series of uranium and thorium tris-amidinate complexes featuring linear OCP^{1-}, OCN^{1-} and SCN^{1-} ligands as well as preliminary reactivity studies involving the actinide-bound phosphaethynolate moiety with Ni(0). These studies have also inspired additional actinide work with the phosphaethynolate moiety, as Meyer and co-workers recently investigated the reactivity of OCP^{1-} with both trivalent and tetravalent uranium complexes supported by their bulky, tris-aryloxide ligand framework.[39]

Results and Discussion

Synthesis of Actinide OCP Complexes. Previous work by Edelmann and co-workers established $UCl(BTBA)_3$ (BTBA = *N*,*N'*-bis(trimethylsilyl)benzamidinate) as an accessible actinide tris-amidinate platform,[40] and we envisioned this molecule, as well as the thorium analog, would prove suitable as starting materials for installation of the OCP^{1-} ligand. Carrying out salt-metathesis reactions between $MCl(BTBA)_3$ (**1.1**: M = U; **1.2**: M = Th) and $Na(OCP)(dioxane)_{2.9}$ afforded the targeted phosphaethynolate complexes $M(OCP)(BTBA)_3$ (**1.3**: M = U; **1.4**: M = Th) as block shaped crystals in 76% and 63% isolated yields, respectively (Scheme 1.1). Averaged C_3-symmetry is observed for both complexes in their respective ^1H NMR spectra, and this symmetry

is maintained in their X-ray crystal structures (*vide infra*). The ^{31}P NMR resonance of the OCP^{1-} moiety in **1.4** in C_6D_6 is shifted noticeably downfield (δ -334 ppm) compared to that reported for the rhenium complex $Re(PCO)(CO)_2$(triphos) (δ -398 ppm)[13] and group I and II phosphaethynolate

Scheme 1.1. Synthesis of Uranium and Thorium Complexes **1.3-1.8**

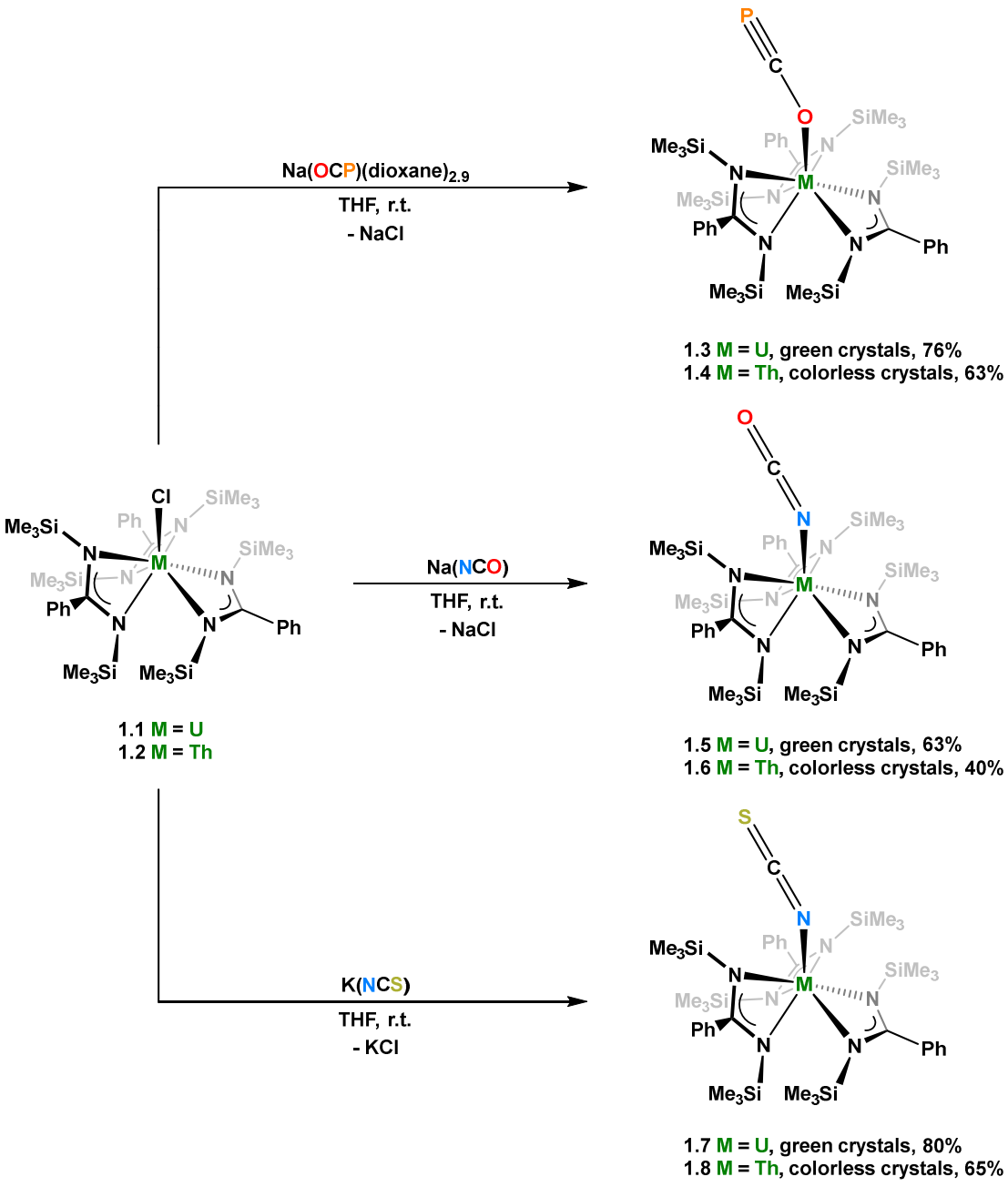

salts (δ range: -362 to -397 ppm).[1,2,41] The ^{31}P signal of **1.3** (δ -285 ppm) is shifted even more downfield than that seen in **1.4** due to the paramagnetism of the U(IV) metal center. The strong C-O stretching frequency of the OCP^{1-} ligand was observable in the IR spectra for compounds **1.3** and **1.4** at nearly identical wavenumbers (1685 cm^{-1} vs. 1683 cm^{-1} for **1.3** and **1.4**, respectively); this stretch appeared at lower wavenumbers than that seen in $Re(PCO)(CO)_2$(triphos) (1860 cm^{-1}) and the alkali OCP^{1-} salts (1730 to 1780 cm^{-1}), indicative of a lower C-O bond order. These metrics (IR and ^{31}P NMR) taken together provide insight into the bonding motif of the OCP^{1-} moiety, with it best described as a phosphaalkyne-type ligand (see Figure 1.1). This is in noticeable contrast to that observed with the transition-metal complexes, which exhibit P-bound phosphaketene-type binding of the OCP^{1-} moiety.[13,14]

While the IR and ^{31}P NMR spectroscopy data were telling of O-bound coordination of the OCP^{1-} ligand in **1.3** and **1.4**, this suspicion was confirmed by X-ray diffraction studies (Figure 1.2). Complex **1.4** crystallized as two independent molecules in the asymmetric unit, one of which featured an OCP^{1-} moiety disordered over two positions with the C≡P fragment pointing in two different directions in a 45:55 ratio. Therefore, the metrical parameters of the non-disordered molecule will be solely discussed. As observed by ^{1}H NMR spectroscopy, C_3-symmetry is maintained in the crystal structures of both **1.3** and **1.4**, with the amidinate ligands positioned around the metal center in a propeller-like motif, with the OCP^{1-} ligand in the axial position, pointing out of the steric pocket created by the tris-amidinate framework. Near-linearity is observed for the O-C-P (179.1(4)° and 179.7(4)° for **1.3** and **1.4**, respectively) and An-O-C (170.9(3)° and 176.4(3)° for **1.3** and **1.4**, respectively) angles. The C≡P (1.576(5) and 1.561(4) Å for **1.3** and **1.4**, respectively) and C-O (1.219(6) and 1.246(4) Å for **1.3** and **1.4**, respectively) are consistent with that seen in [K(18-crown-6)][PCO] (1.579(3) and 1.212(4) Å for C≡P and C-O bonds, respectively).[1] These metrics also indicate a strengthening of the C≡P triple bond and weakening of the C-O bond when compared to the theoretical values computed for the OCP^{1-} anion (C≡P = 1.625 Å; C-O = 1.203 Å).[13] The An-O bond distances (U-O = 2.297(3) Å; Th-O = 2.318(2) Å) are consistent with the larger ionic radius of Th(IV) vs U(IV).[42] These distances are unremarkable and fall in the range between actinide complexes with strongly donating aryloxide or siloxide ligands and dative oxygen donors.[43-48] The U-N_{amid} and Th-N_{amid} bond distances average 2.44(3) and 2.49(3) Å, respectively, and are consistent with that observed in comparable complexes.[40,49-51]

Synthesis of Actinide NCO and NCS Complexes. In order to directly compare structural analogs of **1.3** and **1.4**, the cyanate and thiocyanate complexes were targeted for synthesis. Complexes **1.5-1.8** were prepared in a similar fashion to **1.3** and **1.4**, either by reaction of **1.1** or **1.2** with sodium cyanate or potassium thiocyanate (Scheme 1.1). ^{1}H NMR spectroscopy of complexes **1.5-1.8** exhibited averaged C_3-symmetry in solution, consistent with that seen previously for **1.1-1.4**. IR spectroscopy of **1.5-1.8** displayed strong C-N stretches (2199 cm^{-1} in **1.5**, 2200 cm^{-1} in **1.6**, 2021 cm^{-1} in **1.7** and 2018 cm^{-1} in **1.8**) that fall in the range of previously reported N-bound cyanate[37,38,52] and thiocyanate[53,54] actinide complexes. The molecule structures of **1.5-1.8** were determined by X-ray diffraction studies; these complexes feature cyanate and

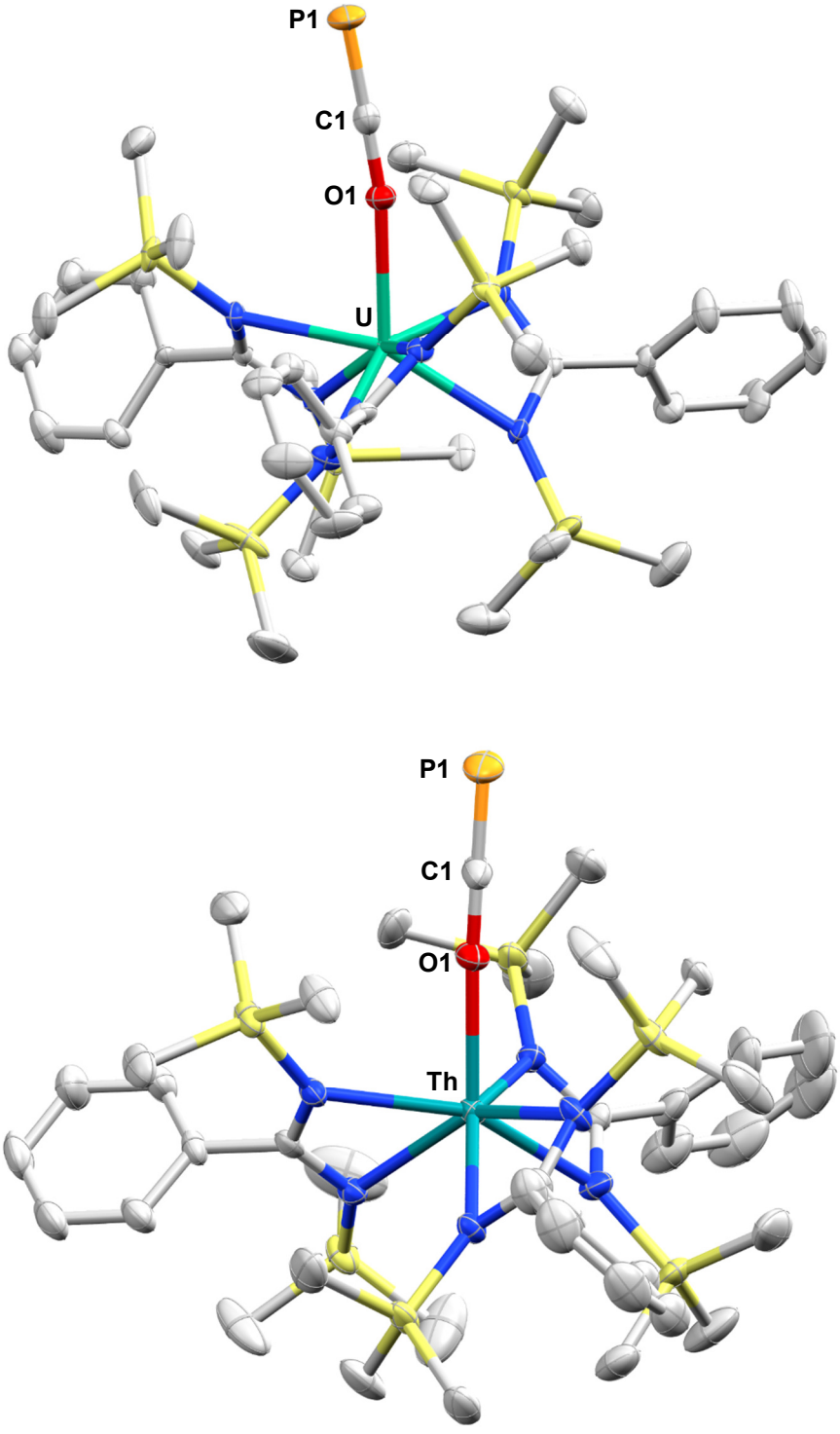

Figure 1.2. Molecule structures of **1.3** (top) and **1.4** (bottom). Thermal ellipsoids drawn at the 50% probability level. Hydrogen atoms omitted for clarity.

thiocyanate ligands bound to the actinide metal center through the N-donor in a linear fashion (Figures 1.3, 1.4). The An-N_{OCN} (2.340(3) Å in **1.5**, 2.410(2) Å in **1.6**) and An-N_{SCN} (2.385(4) Å in **1.7**, 2.428(4) Å in **1.8**) bond lengths are consistent with those previously reported An(IV) cyanate and thiocyanate complexes.[37,38-52-55] Within each heteroallene system, the binding is similar for U(IV) and Th(IV). However, the notable difference between these systems is the preferential O-coordination mode for OCP^{1-} compared to the N-coordination for OCN^{1-} and SCN^{1-}. Selected bond lengths and angles observed for complexes **1.3-1.8** are listed in Table 1.1.

Initially, it may seem counterintuitive for these binding motifs to occur. As the actinides are extremely oxophilic, the N-coordination mode of the OCN^{1-} ligand is particularly surprising, especially given the O-coordination of OCP^{1-}. Or, had the molecular structures of **1.5** and **1.6** been determined first, perhaps one would have expected OCP^{1-} to behave similarly and bind through the pnictogen donor, consistent with that seen with the structurally characterized transition-metal species.[13,14] As pointed out in Figure 1.1, two major resonance structures must be considered when describing the possible binding modes of these ambiphilic heteroallene anions. What is observed experimentally, however, is consistent with the computed partial charges found for the two anions, as the OCP^{1-} anion (q(O) = -0.65; q(P) = -0.44) and OCN^{1-} anion (q(O) = -0.75; q(N) = -0.81)[13] have the majority of their negative charge on the atoms bound to the actinide metal center. Thus, the preference is largely charge-driven.

DFT Calculations. This result is also supported by DFT calculations, which show that the N-bonding motif is preferred with cyanate and thiocyanate anions, while O-binding is favored for the phosphaethynolate anion. While there are only a few studies which address this issue,[11,13,15] this observation contrasts with those prior results, as these previous studies reported that the P-bound products are thermodynamically favored. However, it was found that the O-bound complex **1.4** is 7.7 kcal mol^{-1} lower in energy than the hypothetical P-bound analog (Table 1.3). IR calculations also agree with the experimental results, as the C-O stretching frequency is 235 cm^{-1} lower for the O-bound complex **1.4** (1666 cm^{-1}) than for the theoretical P-bound complex (1901 cm^{-1}). Regarding the OCN^{1-} ligand, the computed CO stretching frequency for N-bound complex **1.6** is 15 cm^{-1} lower than that for the theoretical Th-OCN complex (2230 vs. 2245 cm^{-1}, respectively), while the C=N stretch for the SCN^{1-} moiety is 132 cm^{-1} lower in complex **1.8** than its theoretical counterpart Th-SCN (2016 vs. 2148 cm^{-1}, respectively). This is in line with the stretches observed experimentally (Table 1.4).

NBO analysis of **1.4** indicates that the O-bound complex is preferred over the P-bound analog due to the donation from the oxygen lone pairs to the empty hybrid d/f orbital of the metal (Wiberg index of 0.42). Interestingly, there is no interaction between the C≡P and C-O bonds, as their molecular orbitals are localized entirely onto either one or the other within the OCP^{1-} unit.

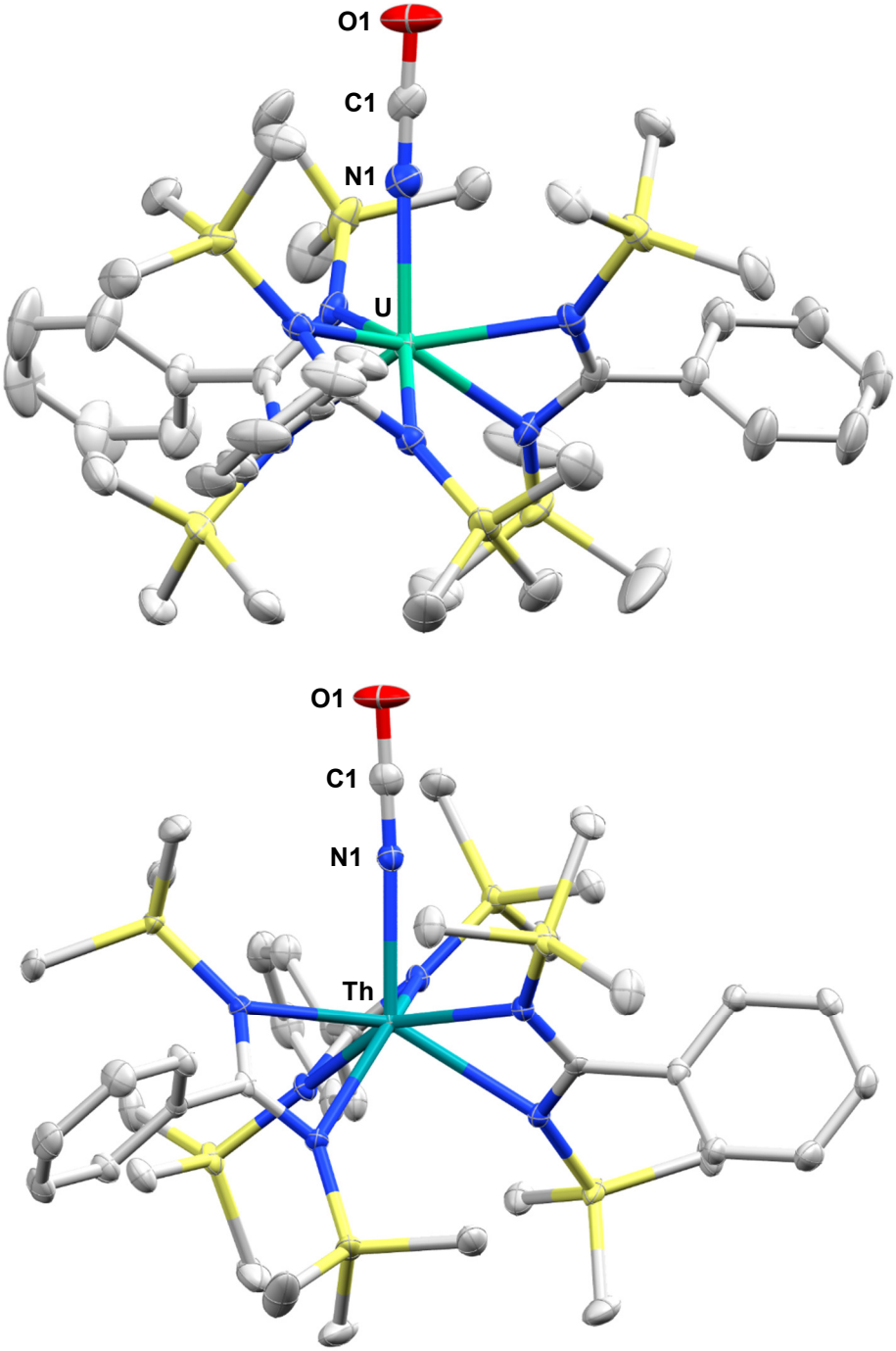

Figure 1.3. Molecule structures of **1.5** (top) and **1.6** (bottom). Thermal ellipsoids drawn at the 50% probability level. Hydrogen atoms omitted for clarity.

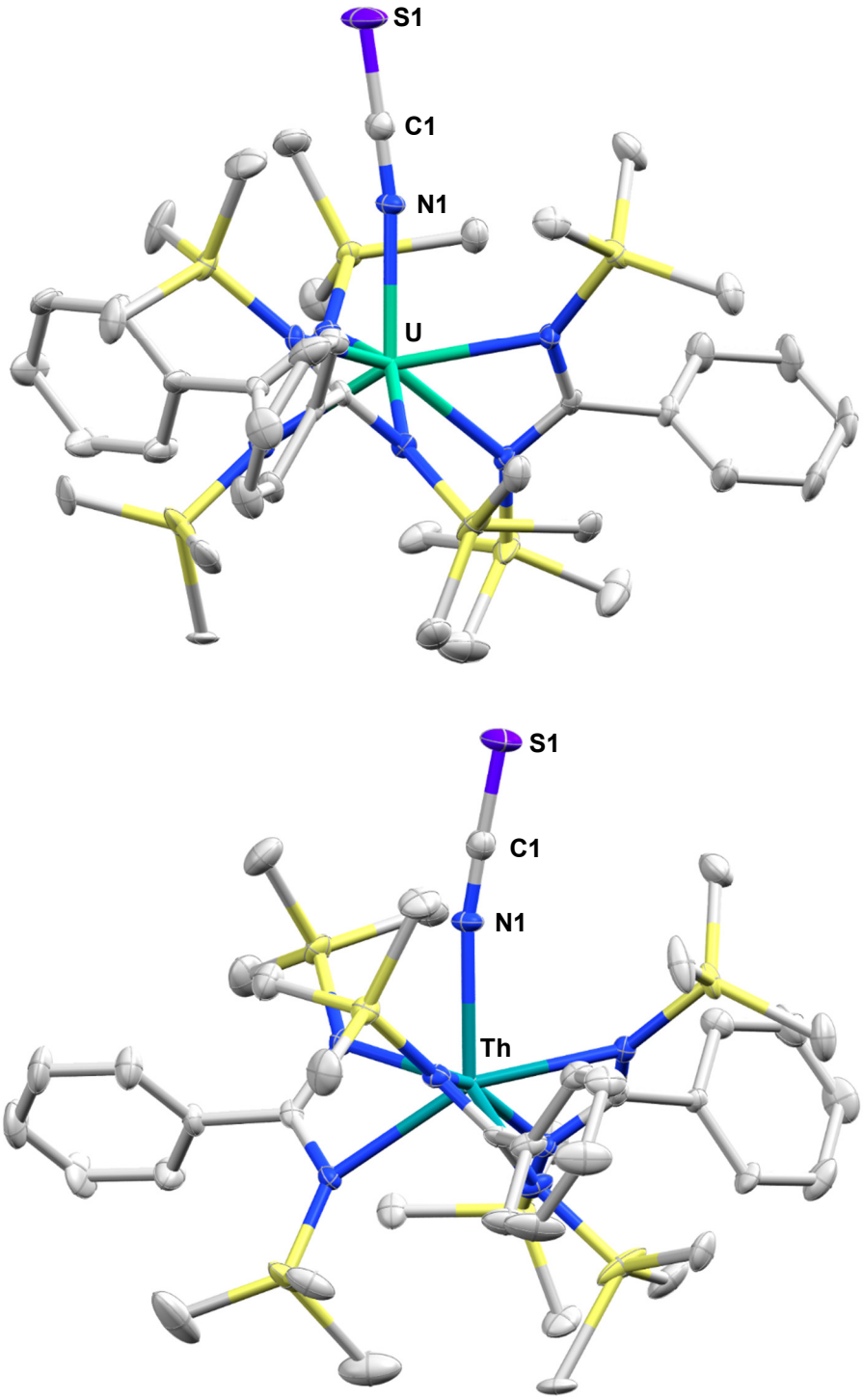

Figure 1.4. Molecule structures of **1.7** (top) and **1.8** (bottom). Thermal ellipsoids drawn at the 50% probability level. Hydrogen atoms omitted for clarity.

Table 1.1. Selected Bond Lengths (Å) and Angles (°) for Complexes **1.3**-**1.8**

Complex	**1.3**	**1.4**[a]	**1.5**	**1.6**[b]	**1.7**	**1.8**
Bond Lengths (Å)						
M-O1	2.296(4)	2.318(2)	-	-	-	-
M-N1	-	-	2.340(3)	2.408(3)	2.385(5)	2.427(4)
O1-C1	1.219(7)	1.246(4)	1.212(5)	1.208(5)	-	-
N1-C1	-	-	1.128(5)	1.135(5)	1.166(8)	1.170(7)
C1-P1	1.576(6)	1.561(4)	-	-	-	-
C1-S1	-	-	-	-	1.609(7)	1.607(6)
Bond Angles (°)						
M-O1-C1	170.9(3)	176.4(2)	-	-	-	-
M-N1-C1	-	-	171.6(3)	174.3(2)	171.3(4)	169.7(4)
O1-C1-P1	179.1(4)	179.7(3)	-	-	-	-
N1-C1-O1	-	-	179.2(4)	179.4(4)	-	-
N1-C1-S1	-	-	-	-	179.3(5)	178.7(5)

[a]Complex **1.4** contains two molecules in the asymmetric unit, with the OCP^{1-} moiety of one molecule disordered over two sites. The metrics presented are thus only for the non-disordered molecule.

[b]Complex **1.6** contains two molecules in the asymmetric unit and as a result all bond lengths and angles are presented as an average.

Table 1.2. Crystal and Refinement Data for Complexes **1.3-1.8**

Complex	**1.3**	**1.4**	**1.5**	**1.6**	**1.7**	**1.8**
Chemical formula	$C_{40}H_{69}N_6OPSi_6U\cdot0.5(C_7H_8)$	$C_{40}H_{69}N_6OPSi_6Th$	$C_{40}H_{69}N_7OSi_6U$	$C_{40}H_{69}N_7OSi_6Th\cdot0.5(C_7H_8)$	$C_{40}H_{69}N_7SSi_6U\cdot0.5(C_7H_8)$	$C_{40}H_{69}N_7SSi_6Th\cdot0.5(C_7H_8)$
Formula weight	1133.61	1081.56	1070.59	1110.66	1132.71	1126.72
Temperature (K)	100(2)	100(2)	100(2)	100(2)	100(2)	100(2)
Crystal system	Triclinic	Triclinic	Monoclinic	Triclinic	Triclinic	Triclinic
Space group	P-1	P-1	C 2/c	P-1	P-1	P-1
a (Å)	11.5703(12)	11.4301(9)	15.5201(7)	11.2966(19)	11.5810(7)	11.6047(6)
b (Å)	11.7055(13)	21.3302(16)	17.9868(8)	23.057(4)	11.6278(7)	11.6602(6)
c (Å)	21.152(2)	24.614(2)	37.3806(17)	23.270(4)	21.1150(13)	21.2040(11)
α (°)	86.747(5)	99.881(4)	90	66.405(6)	86.775(2)	86.479(2)
β (°)	83.810(5)	90.073(4)	97.783(2)	87.390(6)	83.982(2)	83.836(2)
γ (°)	75.030(5)	95.606(4)	90	77.614(6)	75.259(3)	75.464(2)
V ($Å^3$)	2750.1(5)	5882.7(8)	10388.9(8)	5419.7(16)	2733.3(3)	2759.5(2)
Z	2	4	8	4	2	2
Densitiy (Mg m^{-3})	1.369	1.221	1.376	1.361	1.376	1.356
F(000)	1150	2192	4336	2260	1150	1146
Radiation Type	MoK_α	MoK_α	MoK_α	MoK_α	MoK_α	MoK_α
μ (mm^{-1})	3.146	2.715	3.314	2.921	3.174	2.905
Meas. Refl.	67609	89182	90811	86355	45826	50449
Indep. Refl.	10048	21550	9521	19891	9978	10054
R(int)	0.033	0.036	0.034	0.033	0.024	0.028
Final R indices [$I > 2\sigma(I)$]	R = 0.0279 R_w = 0.0702	R = 0.0282 R_w = 0.0683	R = 0.0285 R_w = 0.0545	R = 0.0195 R_w = 0.0482	R = 0.0294 R_w = 0.0796	R = 0.0278 R_w = 0.0781
GOF	1.371	0.975	1.319	1.019	1.383	1.417
$\Delta\rho_{max}$, $\Delta\rho_{min}$ (e $Å^{-3}$)	0.865, -2.201	3.278, -0.874	1.204, -1.664	2.311, -0.454	1.005, -2.243	1.059, -2.196

Table 1.3. DFT Computed Energy Difference Between the Different Coordination Isomers in kcal mol^{-1}

		ΔE/kcal mol^{-1}
Th	Th-OCP/Th-PCO	-7.7
	Th-NCO/Th-OCN	-13.4
	Th-NCS/Th-SCN	-17.5
U	U-OCP/U-PCO	-6.2
	U-NCO/U-OCN	-15.4
	U-NCS/U-SCN	-19.4

Table 1.4. Infrared Stretches for the Anisotropic Vibration of the Heteroallene Ligand in Complexes **1.3-1.8**

Complex	ν (cm^{-1})
1.3	**1685**
1.4	**1683**
1.5	**2199**
1.6	**2200**
1.7	**2021**
1.8	**2018**

However, this localization is flipped when the OCP^{1-} ligand is coordinated through the lone pair of the phosphorus. A more covalent interaction is observed (Wiberg index of 0.90), and there is a strong interaction between the oxygen lone pairs and the Th-P bond, resulting in an interaction between the three centers (P, C and O) best described as allylic in nature. Due to the hard Lewis acidity of thorium and its tendency to prefer ionic interactions, the O-bound isomer is the most energetically prominent.

For the cyanate and thiocyanate anions, the N-bound isomers are 13.4 and 17.5 kcal mol^{-1} lower in energy, respectively, than their O- and S-bound counterparts for thorium, and 15.4 and 19.4 kcal mol^{-1} lower in energy for uranium. This large ΔE for OCN^{1-} and SCN^{1-} is somewhat surprising, considering the calculated charge density difference is more significant in OCP^{1-}

compared to OCN^{1-}. Additionally, there is a greater hard/soft mismatch for An-P than for An-N, all of which would suggest that the ΔE for OCP^{1-} should be larger than that seen for OCN^{1-} or SCN^{1-}. This indicates that subtle differences in the nature of the metal can have significant effects on the binding motif of the phosphaethynolate ligand.

Reactivity of OCP Moiety. Looking to capitalize on the phosphaalkyne nature of the OCP^{1-} ligand in **1.4** (as well as the diamagnetic nature of thorium vs. uranium), preliminary reactivity studies were carried out on this complex. Formation of SCP^{1-} has been seen upon reaction of alkali salts of the OCP^{1-} anion with CS_2;[56] however, complex **1.4** is stable with respect to [2 + 2] cycloaddition with CS_2. With the P-atom in **1.4** protruding above the steric pocket created by the trimethylsilyl groups, it was thought that this soft-donor atom could be accessible and bind to late transition-metals. Treatment of **1.4** with one equivalent of $Ni(COD)_2$ resulted in a darkening of the solution and led to the formation of the heterobimetallic complex $(BTBA)_3Th(\mu\text{-}\eta^1(O):\eta^2(C,P)\text{-}OCP)Ni(COD)$ (**1.9**) (Scheme 1.2). Although complex **1.9** is the only product resulting from the reaction of **1.4** with $Ni(COD)_2$, NMR spectroscopy studies performed in C_6D_6 show that the two species are in equilibrium. Due to their similar solubilities in common organic solvents, the two complexes could not be separated, and thus **1.9** could not be isolated in pure form. The ^{31}P NMR resonance of **1.9** is observed at δ -7.7 ppm, significantly downfield from that of **1.4** (δ -334 ppm), indicative of significant rearrangement of the phosphaethynolate moiety. Strong deshielding of the phosphorus atom is often observed in similar η^2-phosphaalkene derivatives.[57-62] An asymmetric environment for the COD ligand in **1.9** is confirmed by ^1H NMR spectroscopy, as two vinylic resonances are observed at δ 6.1 and 5.5 ppm.

The activation of the phosphaethynolate moiety was confirmed by X-ray diffraction studies

Scheme 1.2. Synthesis of Complex **1.9**. COD = 1,5-cyclooctadiene

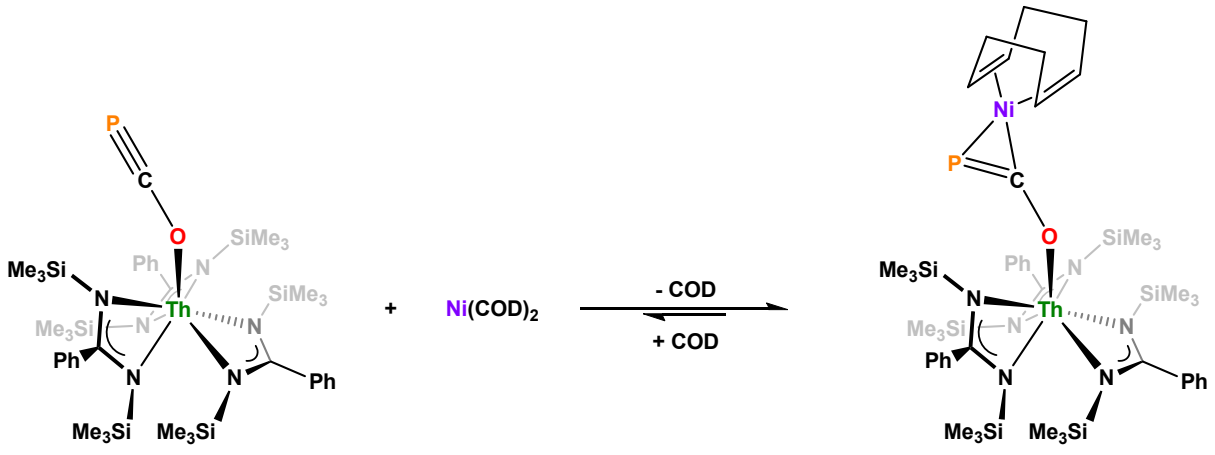

1.4 **1.9**

of **1.9**, which unequivocally confirmed the formation of a three-membered nickel phosphametallacycle, resulting from the addition of the Ni(0) center across the C≡P bond (Figure 1.5). The crystal structure contains two molecules in the asymmetric unit, thus the metrics described will be an average of these two molecules. The nickel phosphametallacycle features an acute C-P-Ni bond angle of 57.3(2)°, as well as P-Ni and C-Ni bond lengths of 2.168(2) and 1.893(5) Å, respectively. These values are in the expected range and compare well with the related phosphaalkyne complex [Ni(trop$_2$NMe)(η^2-(Ph$_3$C)C≡P)], which features Ni-C and Ni-P bond distances of 1.887(4) and 2.2188(13) Å, respectively.[62] The bending of the OCP^{1-} and its use as a bridging ligand between the two metal centers is a particularly prominent feature, with the near linearity of the O-C-P ligand lowered to 147.0(4)°, and the Th-O-C angle also reduced from 176.4(2)° in **1.4** to 159.2(3)° in **1.9**. An elongation of the C≡P bond length is observed from 1.561(4) Å in **1.4** to 1.677(5) Å in **1.9**, resulting from electron-donation from the nickel center to the antibonding π* orbital of the C-P fragment. This bond length falls in the range observed for

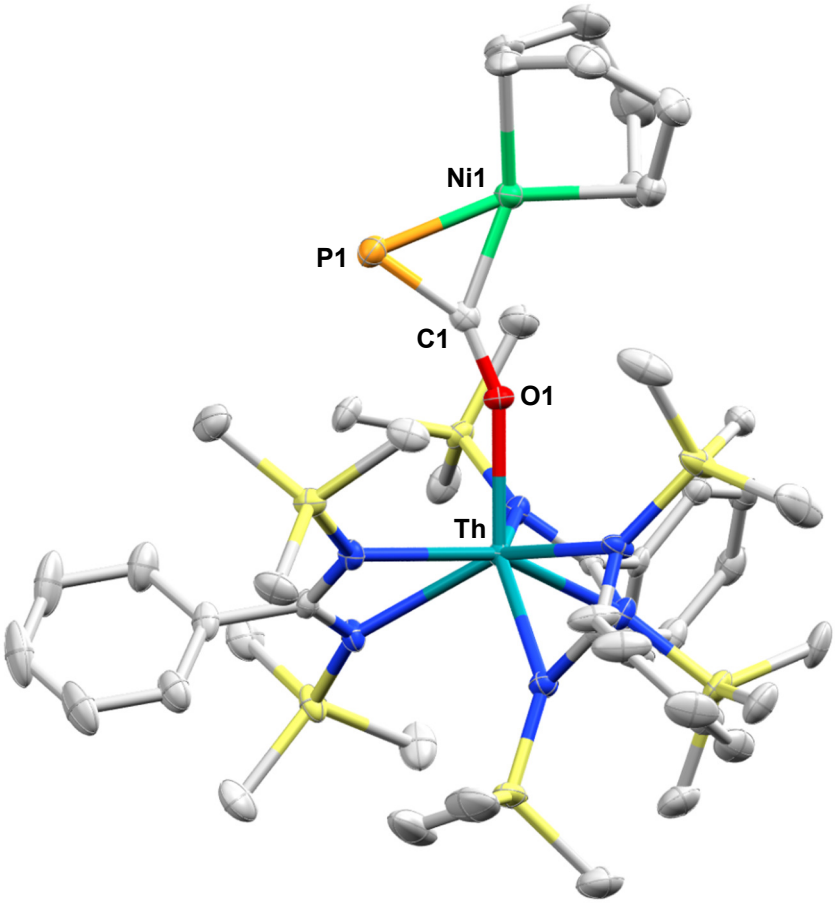

Figure 1.5. Molecule structure of **1.9**. Thermal ellipsoids drawn at the 50% probability level. Hydrogen atoms omitted for clarity.

side-on coordinated phosphaalkynes to nickel[57,62] and other d-block metals.[58-61] The slightly elongated C-O bond distance of 1.275(6) Å (compared to 1.246(4) Å in **1.4**) and the shortened Th-O distance of 2.283(3) Å (compared to 2.318(2) Å in **1.4**) are both indicative of increased electron density on the OCP^{1-} moiety. These structural characteristics are similar to that observed with Ni(0) activation of phosphaalkynes[57,62] and heteroallenes,[63-66] but the bonding situation of the Ni(COD) moiety to the OCP^{1-} ligand in **1.9** is decidedly unique. Analyzing the structure of **1.9** by DFT calculations provided an optimized structure which was able to reliably reproduce the main structural features. NBO analysis showed that the oxygen atom is bonding with the thorium metal center via an ionic bond involving donation from an oxygen lone pair to an unoccupied hybrid d/f orbital of thorium. The π orbital of C≡P fragment of the OCP^{1-} ligand overlaps with a nickel d-orbital to give the HOMO (Figure 1.6).

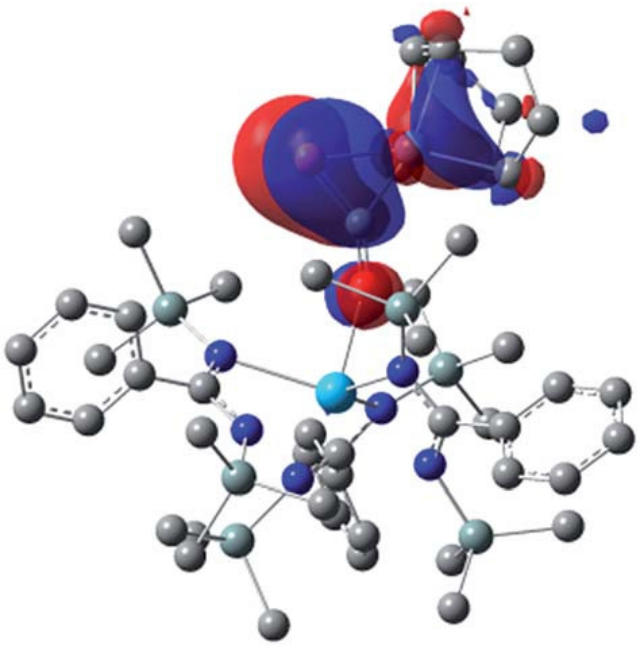

Figure 1.6. Computed HOMO orbital for **1.9**

Table 1.5. Selected Bond Lengths (Å) and Angles (°) for Complex **1.9**

Complex	**1.9**[a]
Bond Lengths (Å)	
M-O1	2.283(3)
O1-C1	1.275(6)
C1-P1	1.677(5)
P1-Ni1	2.168(2)
C1-Ni1	1.893(5)
Bond Angles (°)	
M-O1-C1	159.2(3)
O1-C1-P1	147.0(4)
C1-P1-Ni1	57.3(2)

[a]Complex **1.9** contains two molecules in the asymmetric unit, and as a result all bond lengths and angles are presented as an average.

Table 1.6. Crystal and Refinement Data for Complexes **1.9**

Complex	**1.9**
Chemical formula	$C_{48}H_{81}N_6NiOPSi_6Th \cdot 0.75(C_6H_{14})$
Formula weight	1313.07
Temperature (K)	100(2)
Crystal system	Triclinic
Space group	P-1
a (Å)	14.8598(10)
b (Å)	19.6824(13)
c (Å)	24.2681(17)
α (°)	105.8698(27)
β (°)	101.3208(26)
γ (°)	95.5472(27)
V (Å^3)	6587.8(8)
Z	4
Densitiy (Mg m^{-3})	1.324
F(000)	2694
Radiation Type	MoK_α
μ (mm^{-1})	2.711
Meas. Refl.	171492
Indep. Refl.	23909
R(int)	0.031
Final R indices [I > 2σ(I)]	R = 0.0333 R_w = 0.0857
GOF	1.034
$\Delta\rho_{max}$, $\Delta\rho_{min}$ (e Å^{-3})	3.024, -3.064

Conclusions

Our studies have proven that the tris-amidinate framework can be a useful platform for stabilizing actinide complexes of the phosphaethynolate moiety, and that Na(OCP)(dioxane)$_n$ is a useful reagent for generating these species. Unlike that observed with previous transition-metal OCP complexes, which favor a P-bound coordination mode, the thorium and uranium complexes prefer O-coordination, whereas the analogous cyanate and thiocyanate complexes adopt N-bound ligands. Calculations suggest that this is differing interaction is based on negative charge distribution along the heteroallene, as well as the interactions being principally ionic in nature. As an O-bound ligand, the OCP^{1-} is best described as phosphaalkyne-like, and this character was demonstrated by the addition of Ni(0) across the C≡P bond of the thorium phosphaethynolate species, resulting in formation of an unprecedented reduced OCP^{1-} moiety bridging two metal centers. These results provide a basis for developing metal phosphaethynolate complexes for the purpose of studying reactivity as well as generating unique heterometallic structures.

Experimental Details

General procedures. Unless otherwise noted, all reactions were performed either using standard Schlenk line techniques or in an MBraun inert atmosphere glovebox under an atmosphere of purified nitrogen (<1 ppm O_2/H_2O). Glassware and cannulae were stored in an oven at ~160 °C for at least 12 h prior to use. Hexanes, THF and toluene were dried and degassed using a commercially available Phoenix SDS from JC Meyer Solvent Systems. C_6D_6 was dried over sodium/benzophenone and then vacuum-transferred to a storage flask and freeze-pump-thaw degassed before being stored over activated molecular sieves in the glovebox. UCl_4,[67] $ThCl_4(DME)_2$,[68] Li(BTBA)(TMEDA),[69] and $Na(OCP)(dioxane)_{2.9}$[2] were prepared using literature procedures. All other reagents were acquired from commercial sources and used as received. NMR spectra were recorded on Bruker AVQ-400, AVB-400, DRX-500, AV-500 and AV-600 spectrometers. Chemical shifts were measured relative to residual solvent peaks, which were assigned relative to an external TMS standard set at 0.00 ppm. ^{31}P chemical shifts were referenced to an external standard (Ph_3PO for ^{31}P set at 23 ppm). ^{1}H and ^{13}C NMR assignments were routinely confirmed by ^{1}H-^{1}H COSY and ^{1}H-^{13}C HSQC experiments. Infrared (IR) spectra were recorded with a Thermo Scientific Nicolet iS10 series FTIR spectrophotometer as a Nujol mull between KBr plates. The uncorrected melting points were determined using sealed capillaries prepared under nitrogen on an Optimelt SRS. Elemental analyses were performed at the School of Human Sciences, Science Center, London Metropolitan University. The X-ray structural determinations were performed at CHEXRAY, University of California, Berkeley on a Bruker APEX II Quazar diffractometer. Solution magnetic moments were obtained by Evans Method.

$UCl(PhC(NSiMe_3)_2)_3$ (1.1). This compound was prepared according to a modified published procedure.[40] A 50 mL THF solution of Li(BTBA)(TMEDA) (3.15 g, 8.13 mmol) was added to UCl_4 (1.03 g, 2.71 mmol) and the reaction mixture was vigorously stirred at ambient temperature for 15 h, affording a green suspension. The volatiles were removed under reduced pressure, and the resulting residue was triturated with toluene (2 x 10 mL) and dried under vacuum. The green solid was then extracted with toluene (3 x 30 mL) and the solution filtered through Celite. The resulting green filtrate was concentrated to 30 mL and placed in a -40 °C freezer for 24 h, resulting in large, bright green crystals of **1.1** (2.55 g, 88%). ^{1}H NMR (400 MHz, C_6D_6, 293 K): δ 15.3 (br s, 3H, C*H*$_{Ar}$), 10.9 (br s, 3H, C*H*$_{Ar}$), 9.3 (br s, 6H, C*H*$_{Ar}$), 8.8 (t, 3H, C*H*$_{Ar}$), 1.3 (s, 27H, $SiMe_3$), -3.1 (s, 27H, $SiMe_3$). FTIR (cm^{-1}): 1245 (s), 1157 (w), 1075 (w), 1000 (w), 973 (s), 920 (w), 841 (s), 784 (s), 759 (s), 704 (s), 477 (s). Mp: 317(2) °C (decomp.). Anal. Calcd for $C_{39}H_{69}N_6Si_6ClU$ (1064.0): C, 44.02; H, 6.54; N, 7.90. Found: C, 43.98; H, 6.47; N, 7.93.

$ThCl(PhC(NSiMe_3)_2)_3$ (1.2). A 50 mL THF solution of Li(BTBA)(TMEDA) (5.01 g, 12.9 mmol) was added to a stirred THF solution (75 mL) of $ThCl_4(DME)_2$ (2.39 g, 4.31 mmol), and the resulting solution was allowed to stir at ambient temperature for 16 h. The volatiles were then removed under reduced pressure, and the resulting residue was triturated with hexane (2 x 10 mL) and dried under vacuum. The colorless solid was then extracted with toluene (3 x 30 mL)

and the solution filtered through Celite. The resulting colorless filtrate was concentrated to 30 mL and placed in a -40 °C freezer for 24 h, resulting in large, colorless crystals of **1.2** (2.71 g, 59%). X-ray quality crystals were grown from a concentrated toluene solution stored at -35 °C for 16 h. ^{1}H NMR (500 MHz, C_6D_6, 293 K): δ 7.5 (br s, 6H, C*H*$_{Ar}$), 7.0 (m, 9H, C*H*$_{Ar}$), 0.4 (s, 27H, SiMe$_3$), 0.2 (s, 27H, SiMe$_3$). ^{13}C NMR (125.8 MHz, C_6D_6, 293 K): δ 181.7 (N*C*N), 143.0 (*C*$_{Ar}$), 128.8 (*C*$_{Ar}$), 126.8 (*C*$_{Ar}$), 3.4 (Si*Me*$_3$), 2.7 (Si*Me*$_3$). FTIR (cm^{-1}): 1246 (s), 1160 (w), 1025 (w), 1000 (2), 978 (s), 920 (w), 842 (s), 785 (m), 761 (s), 717 (s), 479 (s). Mp: 317(2) °C (decomp.). Anal. Calcd $C_{39}H_{69}N_6Si_6ClTh$ (1058.0): C, 44.15; H, 6.84; N, 7.92. Found: C, 44.16; H, 6.71; N, 7.85.

U(OCP)(PhC(NSiMe$_3$)$_2$)$_3$ (1.3). A 10 mL THF solution of **1.1** (0.300 g, 0.282 mmol) and NaOCP(dioxane)$_{2.9}$ (0.100 g, 0.296 mmol) was stirred at ambient temperature for 24 h. Volatiles were then removed under reduced pressure and the resulting residue was extracted with toluene (2 mL) and filtered through Celite. The green filtrate was then placed in a -35 °C freezer for 48 h, resulting in green, block-shaped crystals of **1.3** (0.234 g, 76%). X-ray quality crystals were grown from a concentrated toluene solution stored at -35 °C for 48 h. ^{1}H NMR (400 MHz, C_6D_6, 293 K): δ 13.7 (br s, 3H, C*H*$_{Ar}$), 10.3 (br s, 3H, C*H*$_{Ar}$), 8.9 (t, 6H, C*H*$_{Ar}$), 8.4 (t, 3H, C*H*$_{Ar}$), 0.5 (s, 27H, SiMe$_3$), -2.6 (s, 27H, SiMe$_3$). ^{13}C NMR (125.8 MHz, C_6D_6, 293 K): δ 142.7 (*C*$_{Ar}$), 132.9 (*C*$_{Ar}$), 4.6 (Si*Me*$_3$), 1.8 (Si*Me*$_3$). ^{31}P NMR (243 MHz, C_6D_6, 293 K): δ -285.2. FTIR (cm^{-1}): 1685 (s, PCO), 1247 (s), 1179 (w), 1157 (w), 1000 (w), 974 (s), 931 (w), 920 (w), 838 (s), 783 (s), 761 (s), 704 (s). Mp: 233(2) °C (decomp.). μ_{eff} = 3.23 μ_B. Anal. Calcd for $C_{40}H_{69}N_6OPSi_6U$ (1087.6): C, 44.18; H, 6.40; N, 7.73. Found: C, 43.83; H, 6.31; N, 7.62.

Th(OCP)(PhC(NSiMe$_3$)$_2$)$_3$ (1.4). A 10 mL THF solution of **1.2** (0.298 g, 0.282 mmol) and NaOCP(dioxane)$_{2.9}$ (0.100 g, 0.296 mmol) was stirred at ambient temperature for 24 h. Volatiles were then removed under reduced pressure and the resulting residue was extracted with toluene (2 mL) and filtered through Celite. The colorless filtrate concentrated to 1 mL and was then placed in a -35 °C freezer for 48 h, resulting in colorless, block-shaped crystals of **1.4** (0.191 g, 63%). X-ray quality crystals were grown from a concentrated toluene solution stored at -35 °C for 16 h. ^{1}H NMR (400 MHz, C_6D_6, 293 K): δ 7.3 (br s, 6H, C*H*$_{Ar}$), 7.0 (m, 9H, C*H*$_{Ar}$), 0.3 (s, 27H, SiMe$_3$), 0.1 (s, 27H, SiMe$_3$). ^{13}C NMR (125.8 MHz, C_6D_6, 293 K): δ 182.2 (N*C*N), 142.5 (*C*$_{Ar}$), 129.0 (*C*$_{Ar}$), 126.6 (*C*$_{Ar}$), 3.2 (Si*Me*$_3$), 2.3 (Si*Me*$_3$). ^{31}P NMR (243 MHz, C_6D_6, 293 K): δ -334.4. FTIR (cm^{-1}): 1683 (s, PCO), 1248 (s), 978 (s), 839 (s), 785 (s), 761 (s), 703 (s). Mp: 277(2) °C. Anal. Calcd for $C_{40}H_{69}N_6OPSi_6Th$ (1081.6): C, 44.42; H, 6.43; N, 7.77. Found: C, 44.35; H, 6.35; N, 7.69.

U(NCO)(PhC(NSiMe$_3$)$_2$)$_3$ (1.5). A 5 mL THF suspension of **1.1** (0.195 g, 0.183 mmol) and sodium cyanate (0.014 g, 0.211 mmol) was stirred at ambient temperature for 24 h. The volatiles were removed under reduced pressure and the resulting residue was extracted with toluene (1.5 mL) and filtered through Celite. The green filtrate was then placed in a -35 °C freezer for 48 h, resulting in green, block-shaped crystals of **1.5** (0.123 g, 63%). X-ray quality crystals were grown from a concentrated toluene solution stored at -35 °C for 48 h. ^{1}H NMR (400 MHz, C_6D_6, 293 K): δ 13.2 (br s, 3H, C*H*$_{Ar}$), 10.1 (br s, 3H, C*H*$_{Ar}$), 8.8 (t, 6H, C*H*$_{Ar}$), 8.4 (t,

3H, CH_{Ar}), 0.5 (s, 27H, SiMe$_3$), -2.5 (s, 27H, SiMe$_3$). ^{13}C NMR (125.8 MHz, C_6D_6, 293 K): δ 144.0 (C_{Ar}), 132.7 (C_{Ar}), 3.4 (SiMe_3), 1.9 (SiMe_3). FTIR (cm^{-1}): 3063 (w), 2199 (s, OCN), 1246 (s), 1157 (w), 1074 (w), 1000 (w), 973 (s), 920 (w), 847 (s), 784 (s), 758 (s), 706 (s). Mp: 288(2) °C (decomp.). Anal. Calcd for $C_{40}H_{69}N_7OSi_6U$ (1070.6): C, 44.88; H, 6.50; N, 9.16. Found: C, 44.72; H, 6.61; N, 9.06.

Th(NCO)(PhC(NSiMe$_3$)$_2$)$_3$ (1.6). A 10 mL THF suspension of **1.2** (0.297 g, 0.281 mmol) and sodium cyanate (0.040 g, 0.615 mmol) was stirred at ambient temperature for 96 h. The volatiles were removed under reduced pressure and the resulting residue was extracted with toluene (4 mL) and filtered through Celite. The colorless filtrate was then concentrated to 1 mL and placed in a -35 °C freezer for 24 h, resulting in colorless, block-shaped crystals of **1.6** (0.120 g, 40%). X-ray quality crystals were grown from a concentrated toluene solution stored at -35 °C for 16 h. ^{1}H NMR (400 MHz, C_6D_6, 293 K): δ 7.4 (br s, 6H, CH_{Ar}), 7.0 (m, 9H, CH_{Ar}), 0.3 (s, 27H, SiMe$_3$), 0.2 (s, 27H, SiMe$_3$). ^{13}C NMR (125.8 MHz, C_6D_6, 293 K): δ 181.7 (N*C*N), 143.0 (C_{Ar}), 128.8 (C_{Ar}), 126.6 (C_{Ar}), 3.2 (SiMe_3), 2.3 (SiMe_3). FTIR (cm^{-1}): 2200 (s, OCN), 1663 (w), 1246 (s), 1157 (w), 1074 (w), 1000 (w), 978 (s), 842 (s), 785 (w), 758 (m), 716 (m), 703 (m), 630 (w), 479 (s). Mp: 205(2) °C (decomp.) Anal. Calcd for $C_{40}H_{69}N_7OSi_6Th$ (1064.6): C, 45.15; H, 6.53; N, 9.21. Found: C, 44.93; H, 6.72; N, 9.15.

U(NCS)(PhC(NSiMe$_3$)$_2$)$_3$ (1.7). A 5 mL THF suspension of **1.1** (0.163 g, 0.153 mmol) and potassium thiocyanate (0.017 g, 0.176 mmol) was stirred at ambient temperature for 24 h. The volatiles were removed under reduced pressure and the resulting residue was extracted with toluene (1.5 mL) and filtered through Celite. The green filtrate was then placed in a -35 °C freezer for 48 h, resulting in green, block-shaped crystals of **1.7** (0.133 g, 80%). X-ray quality crystals were grown from a concentrated toluene solution stored at -35 °C for 48 h. ^{1}H NMR (500 MHz, C_6D_6, 293 K): δ 15.6 (br s, 3H, CH_{Ar}), 11.1 (br s, 3H, CH_{Ar}), 9.5 (br s, 6H, CH_{Ar}), 8.9 (t, 3H, CH_{Ar}), 0.9 (s, 27H, SiMe$_3$), -3.4 (s, 27H, SiMe$_3$). ^{13}C NMR (125.8 MHz, C_6D_6, 293 K): δ 151.1 (C_{Ar}), 133.7 (C_{Ar}), 4.6 (SiMe_3), 0.8 (SiMe_3). FTIR (cm^{-1}): 3062 (w), 3024 (w), 2021 (s, SCN), 1247 (s), 1179 (w), 1158 (w), 1000 (w), 973 (s), 922 (w)834 (s), 783 (s), 761 (s), 704 (s). Mp: 288(2) °C (decomp.). Anal. Calcd for $C_{40}H_{69}N_7SSi_6U$ (1086.6): C, 44.21; H, 6.40; N, 9.02. Found: C, 44.19; H, 6.50; N, 8.98.

Th(NCS)(PhC(NSiMe$_3$)$_2$)$_3$ (1.8). A 10 mL THF suspension of **1.2** (0.303 g, 0.286 mmol) and potassium thiocyanate (0.034 g, 0.350 mmol) was stirred at ambient temperature for 24 h. The volatiles were removed under reduced pressure and the resulting residue was extracted with toluene (4 mL) and filtered through Celite. The colorless filtrate was then concentrated to 1 mL and placed in a -35 °C freezer for 48 h, resulting in colorless, block-shaped crystals of **1.8** (0.201 g, 65%). X-ray quality crystals were grown from a concentrated toluene solution stored at -35 °C for 16 h. ^{1}H NMR (400 MHz, C_6D_6, 293 K): δ 7.4 (br s, 6H, CH_{Ar}), 7.0 (m, 9H, CH_{Ar}), 0.3 (s, 27H, SiMe$_3$), 0.1 (s, 27H, SiMe$_3$). ^{13}C NMR (125.8 MHz, C_6D_6, 293 K): δ 182.1 (N*C*N), 142.7 (C_{Ar}), 129.0 (C_{Ar}), 126.6 (C_{Ar}), 3.1 (SiMe_3), 2.3 (SiMe_3). FTIR (cm^{-1}): 2018 (s, SCN), 1246 (s), 1179 (w), 1158 (w), 1001 (w), 978 (s), 921 (w), 846 (s), 784 (w), 760 (m), 702 (s), 604 (w), 479

(s). Mp: 308(2) °C (decomp.). Anal. Calcd for $C_{40}H_{69}N_7SSi_6Th$ (1080.7): C, 44.46; H, 6.44; N, 9.07. Found: C, 44.51; H, 6.51; N, 8.89.

(PhC(NSiMe$_3$)$_2$)$_3$Th(μ-η^1(O):η^2(C,P)-OCP)Ni(COD) (1.9). A 2 mL toluene solution of **1.4** (0.255 g, 0.236 mmol) and *bis*(1,5-cyclooctadiene)nickel(0) (0.065 g, 0.236 mmol) was stirred at ambient temperature for 12 h during which time the solution turned from pale yellow to dark brown within a few hours. Monitoring the reaction by ^{1}H and ^{31}P NMR spectroscopy showed that the reaction reached equilibrium after approximately 12 h at ambient temperature. The volatiles were then removed under reduced pressure and the resulting residue extracted with hexanes (0.5 mL) and filtered through Celite. The dark brown filtrate was then placed in a -35 °C freezer for 72 h, resulting in a dark brown crystalline material (0.122 g) containing **1.9** as well as **1.4** and Ni(COD)$_2$. Full purification of **1.9** proved too difficult to achieve, although a few crystals of **1.9** (1% yield) were obtained upon four successive recrystallizations from hexanes at -35 °C. This was sufficient to get X-ray diffraction and NMR spectroscopy data. The latter revealed that **1.9** exhibits limited stability in C_6D_6 solution and is converted back to **1.4** through the loss of free COD, Ni(COD)$_2$ and other non-identified Ni species. ^{1}H NMR (600 MHz, C_6D_6, 293 K): δ 7.5 (m, 6H, C*H*$_{Ar}$), 7.0 (m, 9H, C*H*$_{Ar}$), 6.1 (m, 2H, C*H*=CH$_{COD}$), 5.5 (m, 2H, CH=C*H*$_{COD}$), 2.4 (m, 2H, C*H*$_{2,COD}$), 2.2 (m, 2H, C*H*$_{2,COD}$), 2.0 (m, 2H, C*H*$_{2,COD}$), 1.9 (m, 2H, C*H*$_{2,COD}$), 0.3 (s, 54H, SiMe$_3$). ^{31}P NMR (243 MHz, C_6D_6, 293 K): δ -7.7.

Crystallographic Procedures. Single-crystal X-ray diffraction experiments were performed at the UC Berkeley CHEXRAY crystallographic facility. Measurements of all complexes were performed on either a Bruker APEX-I or APEX-II CCD area detector using Mo Kα radiation (λ = 0.71073 Å). Crystals were kept at 100(2) K throughout collection. Data collection was performed with Bruker APEX2 software (v. 2014.11). Data refinement and reduction were performed with Bruker SAINT (V8.34A). All structures were solved with SHELXT.53.[70] Structures were refined with SHELXL-2014.[71] Molecular graphics were computed with Mercury 3.10. All non-hydrogen atoms were refined anisotropically, and hydrogen atoms were included at the geometrically calculated positions and refined using a riding model.

Computational Details. Calculations were carried out at the DFT level using the hybrid functional B3PW91[72,73] with the Gaussian 03[74] suite of programs. Polarized all-electron triple-ζ 6-31G(d,p)[75] basis sets were used for C, H and N. Thorium, uranium, phosphorus and silicon atoms were treated with an effective core potential from the Stuttgart-Dresden-Köln group in association with its adapted basis set.[76] Geometry optimizations were carried out without any symmetry restriction. The nature of the extrema (minimum) was verified with analytical frequency calculations. NBO analysis[77] was also carried out in order to analyze the bonding.

References

(1) Jupp, A. R.; Goicoechea, J. M. *Angew. Chem., Int. Ed.* **2013**, *52*, 10064-10067.
(2) Puschamnn, F. F.; Stein, D.; Heift, D.; Hendriksen, C.; Gal, Z. A.; Grützmacher, H.-F.; Grützmacher, H. *Angew. Chem., Int. Ed.* **2011**, *50*, 8420-8423.
(3) Heift, D.; Benkő, Z.; Grützmacher, H. *Angew. Chem., Int. Ed.* **2014**, *53*, 6757-6761.
(4) Heift, D.; Benkő, Z.; Grützmacher, H. *Dalton Trans.* **2014**, *43*, 831-840.
(5) Heift, D.; Benkő, Z.; Grützmacher, H. *Chem. – Eur. J.* **2014**, *20*, 11326-11330.
(6) Chen, X.; Alidori, S.; Puschmann, F. F.; Santiso-Quinones, G.; Benkő, Z.; Li, Z.; Becker, G.; Grützmacher, H.-F.; Grützmacher, H. *Angew. Chem., Int. Ed.* **2014**, *53*, 1641-1645.
(7) Jupp, A. R.; Goicoechea, J. M. *J. Am. Chem. Soc.* **2013**, *135*, 19131-19134.
(8) Heift, D.; Benkő, Z.; Grützmacher, H.; Jupp, A. R.; Goicoechea, J. M. *Chem. Sci.* **2015**, *6*, 4017-4024.
(9) Tondreau, A. M.; Benkő, Z.; Harmer, J. R.; Grützmacher, H. *Chem. Sci.* **2014**, *5*, 1545-1554.
(10) Robinson, T. P.; Cowley, M. J.; Scheschkewitz, D.; Goicoechea, J. M. *Angew. Chem., Int. Ed.* **2015**, *54*, 683-686.
(11) Lü, W.; Wang, C.; Luo, Q.; Li, Q.; Xie, Y.; King, R. B.; Schaefer III, H. F. *New J. Chem.* **2015**, *39*, 1390-1403.
(12) Joost, M.; Transue, W. J.; Cummins, C. C. *Chem. Commun.* **2017**, *53*, 10731-10733.
(13) Alidori, S.; Heift, D.; Santiso-Quinones, G.; Benkő, Z.; Grützmacher, H.; Caporali, M.; Gonsalvi, L.; Rossin, A.; Peruzzini, M. *Chem. – Eur. J.* **2012**, *18*, 14805-14811.
(14) Liu, L.; Ruiz, D. A.; Dahcheh, F.; Bertrand, G.; Suter, R.; Tondreau, A. M.; Grützmacher, H. *Chem. Sci.* **2016**, *7*, 2335-2341.
(15) Heift, D.; Benkő, Z.; Grützmacher, H. *Dalton Trans.* **2014**, *43*, 5920-5928.
(16) Castro-Rodriquez, I.; Nakai, H.; Zakharov, L. N.; Rheingold, A. L.; Meyer, K. *Science* **2004**, *305*, 1757-1759.
(17) Summerscales, O. T.; Frey, A. S. P.; Cloke, F. G. N.; Hitchcock, P. B. *Chem. Commun.* **2009**, 198-200.
(18) Castro-Rodriguez, I.; Meyer, K. *J. Am. Chem. Soc.* **2005**, *127*, 11242-11243.
(19) Bart, S. C.; Anthon, C.; Heinemann, F. W.; Bill, E.; Edelstein, N. M.; Meyer, K. *J. Am. Chem. Soc.* **2008**, *130*, 12536-12546.
(20) Tsoureas, N.; Castro, L.; Kilpatrick, A. F. R.; Cloke, F. G. N.; Maron, L. *Chem. Sci.* **2015**, *5*, 3777-3788.
(21) Mougel, V.; Camp. C.; Pécaut, J.; Copéret, C.; Maron, L.; Kefalidis, C. E.; Mazzanti, M. *Angew. Chem., Int. Ed.* **2012**, *51*, 12280-12284.
(22) Cooper, O.; Camp, C.; Pécaut, J.; Kefalidis, C. E.; Maron, L.; Gambarelli, S.; Mazzanti, M. *J. Am. Chem. Soc.* **2014**, *136*, 6716-6723.
(23) Mansell, S. M.; Kaltsoyannis, N.; Arnold, P. L. *J. Am. Chem. Soc.* **2011**, *133*, 9036-9051.
(24) Brennan, J. G.; Andersen, R. A.; Zalkin, A. *Inorg. Chem.* **1986**, *25*, 1756-1760.

(25) Camp, C.; Cooper, O.; Andrez, J.; Pécaut, J.; Mazzanti, M. *Dalton Trans*. **2015**, *44*, 2650-2656.
(26) Lam, O. P.; Heinemann, F. W.; Meyer, K. *Angew. Chem., Int. Ed.* **2011**, *50*, 5965-5968.
(27) Lam, O. P.; Castro, L.; Kosog, B.; Heinemann, F. W.; Maron, L.; Meyer, K. *Inorg. Chem.* **2012**, *51*, 781-783.
(28) Nocton, G.; Pécaut, J.; Mazzanti, M. *Angew. Chem., Int. Ed.* **2008**, *47*, 3040-3042.
(29) King, D. M.; Tuna, F.; McInnes, E. J. L.; McMaster, J.; Lewis, W.; Blake, A. J.; Liddle, S. T. *Science* **2012**, *337*, 717-720.
(30) Camp, C.; Pécaut, J.; Mazzanti, M. *J. Am. Chem. Soc.* **2013**, *135*, 12101-12111.
(31) Thomson, R. K.; Cantat, T.; Scott, B. L.; Morris, D. E.; Batista, E. R.; Kiplinger, J. L. *Nat. Chem.* **2010**, *2*, 723-729.
(32) Evans, W. J.; Kozimor, S. A.; Ziller, J. W. *Science* **2005**, *309*, 1835-1838.
(33) Fox, A. R.; Arnold, P. L.; Cummins, C. C. *J. Am. Chem. Soc.* **2010**, *132*, 3250-3251.
(34) Fortier, S.; Wu, G.; Hayton, T. W. *J. Am. Chem. Soc.* **2010**, *132*, 6888-6889.
(35) Frey, A. S. P.; Cloke, F. G. N.; Coles, M. P.; Hitchcock, P. B. *Chem. – Eur. J.* **2010**, *16*, 9446-9448.
(36) Kefalidis, C. E.; Frey, A. S. P.; Roe, S. M.; Cloke, F. G. N.; Maron, L. *Dalton Trans.* **2014**, *43*, 11202-11208.
(37) Cleaves, P. A.; King, D. M.; Kefalidis, C. E.; Maron, L.; Tuna, F.; McInnes, E. J. L.; McMaster, J.; Lewis, W.; Blake, A. J.; Liddle, S. T. *Angew. Chem., Int. Ed.* **2014**, *53*, 10412-10415.
(38) Castro-Rodriguez, I.; Nakai, H.; Meyer, K. *Angew. Chem., Int. Ed.* **2006**, *45*, 2389-2392.
(39) Hoerger, C. J.; Heinemann, F. W.; Louyriac, E.; Maron, L.; Grützmacher, H.; Meyer, K. *Organometallics* **2017**, *36*, 4351-4354.
(40) Wedler, M.; Knosel, F.; Noltemeyer, M.; Edelmann, F. T.; Behrens, U. *J. Organomet. Chem.* **1990**, *388*, 21-45.
(41) Westerhausen, M. *J. Organomet. Chem.* **2002**, *644*, 189-193.
(42) Shannon, R. D. *Acta Crystallogr., Sect. A: Cryst. Phys., Diffr., Theor. Gen. Crystallogr.* **1976**, *32*, 751-767.
(43) Clark, D. L.; Grumbine, S. K.; Scott, B. L.; Watkin, J. G. *Organometallics* **1996**, *15*, 949-957.
(44) Lu, E.; Lewis, W.; Blake, A. J.; Liddle, S. T. *Angew. Chem., Int. Ed.* **2014**, *53*, 9356-9359.
(45) Camp, C.; Andrez, J.; Pécaut, J.; Mazzanti, M. *Inorg. Chem.* **2013**, *52*, 7078-7086.
(46) Camp, C.; Kefalidis, C. E.; Pécaut, J.; Maron, L.; Mazzanti, M. *Angew. Chem., Int. Ed.* **2013**, *52*, 12646-12650.
(47) Pool, J. A.; Scott, B. L.; Kiplinger, J. L. *J. Am. Chem. Soc.* **2005**, *127*, 1338-1339.
(48) Camp, C.; Mougel, V.; Pécaut, J.; Maron, L.; Mazzanti, M. *Chem. – Eur. J.* **2013**, *19*, 17528-17540.
(49) Karmel, I. S. R.; Elkin, T.; Fridman, N.; Eisen, M. S. *Dalton Trans.* **2014**, *43*, 11376-11387.

(50) Villiers, C.; Thuéry, P.; Ephritikhine, M. *Eur. J. Inorg. Chem.* **2004**, *2004*, 4624-4632.
(51) Camp, C.; Antunes, M. A.; Garcia, G.; Ciofini, I.; Santos, I. C.; Pécaut, J.; Almeida, M.; Marcalo, J.; Mazzanti, M. *Chem. Sci.* **2014**, *5*, 841-846.
(52) Thomson, R. K.; Scott, B. L.; Morris, D. E.; Kiplinger, J. L. *C. R. Chim.* **2010**, *13*, 790-802.
(53) Al-Daher, A. G. M.; Bagnall, K. W.; Castellani, C. B.; Benetollo, F.; Bombieri, G. *Inorg. Chim. Acta.* **1984**, *95*, 269-277.
(54) Fischer, R. D.; Klähne, E.; Kopf, J. *Z. Naturforsch., B: Anorg. Chem., Org. Chem.* **1978**, *33*, 1393-1397.
(55) Bagnall, K. W.; Benetollo, F.; Forsellini, E.; Bombieri, G. *Polyhedron* **1992**, *11*, 1765-1770.
(56) Becker, G.; Hübler, K. *Z. Anorg. Allg. Chem.* **1994**, *620*, 405-417.
(57) Schaub, T.; Radius, U. *Z. Anorg. Allg. Chem.* **2006**, *632*, 981-984.
(58) Burkett-St. Laurent, J. C. T. R.; Hitchcock, P. B.; Kroto, H. W.; Nixon, J. F. *J. Chem. Soc., Chem. Commun.* **1981**, 1141-1143.
(59) Binger, P.; Biedenbach, B.; Herrmann, A. T.; Langhauser, F.; Betz, P.; Goddard, R.; Krüger, C. *Chem. Ber.* **1990**, *123*, 1617-1623.
(60) Mansell, S. M.; Green, M.; Russell, C. A. *Dalton Trans.* **2012**, *41*, 14360-14368.
(61) Burrows, A. D.; Dransfeld, A.; Green, M.; Jeffery, J. C.; Jones, C.; Lynam, J. M.; Nguyen, M. T. *Angew. Chem., Int. Ed.* **2001**, *40*, 3221-3224.
(62) Trincado, M.; Rosenthal, A. J.; Vogt, M.; Grützmacher, H. *Eur. J. Inorg. Chem.* **2014**, *2014*, 1599-1604.
(63) Aresta, M.; Nobile, C. F.; Albano, V. G.; Forni, E.; Manassero, M. *J. Chem. Soc., Chem. Commun.* **1975**, 636-637.
(64) Anderson, J. S.; Iluc, V. M.; Hillhouse, G. L. *Inorg. Chem.* **2010**, *49*, 10203-10207.
(65) Mindiola, D. J.; Hillhouse, G. L. *Chem. Commun.* **2002**, 1840-1841.
(66) Iluc, V. M.; Hillhouse, G. L. *J. Am. Chem. Soc.* **2014**, *136*, 6479-6488.
(67) Kiplinger, J. L.; Morris, D. E.; Scott, B. L.; Burns, C. J. *Organometallics* **2002**, *21*, 5978-5982.
(68) Cantat, T.; Scott, B. L.; Kiplinger, J. L. *Chem. Commun.* **2010**, *46*, 919-921.
(69) Volkis, V.; Nelkenbaum, E.; Lisovskii, A.; Hasson, G.; Semiat, R.; Kapon, M.; Botoshansky, M.; Eishen, Y.; Eisen, M. S. *J. Am. Chem. Soc.* **2003**, *125*, 2179-2194.
(70) Sheldrick, G. M. *Acta. Crystallogr. Sect. A* **2015**, *71*, 3-8.
(71) Sheldrick, G. M. *Acta. Crystallogr. Sect. A* **2008**, *64*, 112-122.
(72) Becke, A. D. *J. Chem. Phys.* **1993**, *98*, 5648-5652.
(73) Perdew, J. P.; Wang, Y. [*Phys. Rev. B* **1992**, *46*, 12947-12954]. *Phys. Rev. B* **1997**, *56*, 7018-7018.
(74) Gaussian 03 (Pittsburgh PA **2006**).
(75) Hehre, W. J.; Ditchfield, R.; Pople, J. A. *J. Chem. Phys.* **1972**, *56*, 2257-2261.
(76) Kuechle, W.; Dolg, M.; Stoll, H.; Preuss, H. *J. Chem. Phys.* **1994**, *100*, 7535-7542. (b) Cao, X.; Dolg, M.; Stoll, H. *J. Chem. Phys.* **2003**, *118*, 487-496. (c) Cao, X.; Dolg, M. *J.*

Molec. Struct. (Theochem) **2004**, *673*, 203-209. (d) Bergner, A.; Dolg, M.; Kuechle, W.; Stoll, H.; Preuss, H. *Mol. Phys.* **1993**, *80*, 1431-1441.
(77) Reed, A. E.; Curtiss, L. A.; Weinhold, F. *Chem. Rev.* **1988**, *88*, 899-926.

Chapter 2

A Thorium Chalcogenolate Series Generated by Atom Insertion into Thorium-Carbon Bonds

Chapter 2

Overview

The successful separation and recycling of spent nuclear fuel is critical for making nuclear power a viable alternative energy source. Currently, there is great interest in utilizing chalcogen-based ligands as selective extraction agents for the separation of trivalent actinides and lanthanides, the latter of which are neutron poisons and diminish the efficiency of nuclear fuel. It is believed that the stronger covalent interactions between the soft-donor ligands and the actinides is what facilitates the selective binding of these metals to these chalcogen chelators. Most of this research has focused on uranium binding, but as the possibility of thorium-based reactors is becoming more prominent, investigations into the interactions between thorium and chalcogen-donors is necessary. The following chapter describes the synthesis and characterization of a thorium monoalkyl complex supported by a tris-amidinate framework, which is able to support the formation of a series of chalcogenolate species, which are generated by atom insertion into thorium-carbon bonds. Portions of this chapter have previously been published in: Settineri, N. S., Garner, M. E. and Arnold, J. "A Thorium Chalcogenolate Series Generated by Atom Insertion into Thorium-Carbon Bonds." *J. Am. Chem. Soc.*, **2017**, *139*, 6261-6269.

Introduction

The chemistry of early actinide elements continues to be a flourishing field of active research.[1-5] While a major focus has been nuclear fuel applications,[6,7] the large size, oxidation state accessibility, and 5*f*-orbital availability in the actinides have distinguished their coordination chemistry from that of other metals in the periodic table.[8] In particular, actinide-chalcogen chemistry has undergone a resurgence in recent years due to the success of chalcogenide soft-donor ligands in actinide-lanthanide separation, a necessary step in spent nuclear fuel recycling.[9-11] The nature of the bonds in these actinide chalcogenides has been of particular interest, with the focus predominantly on uranium-chalcogen species and the participation of the 5*f*-orbitals in covalent bonding.[12-14] Thorium chalcogen (Th-E; E = O, S, Se, Te) species have received far less attention, and only a few molecular thorium species containing Th-E bonds of the heavier chalcogen elements have been reported (Figure 2.1).[15-20]

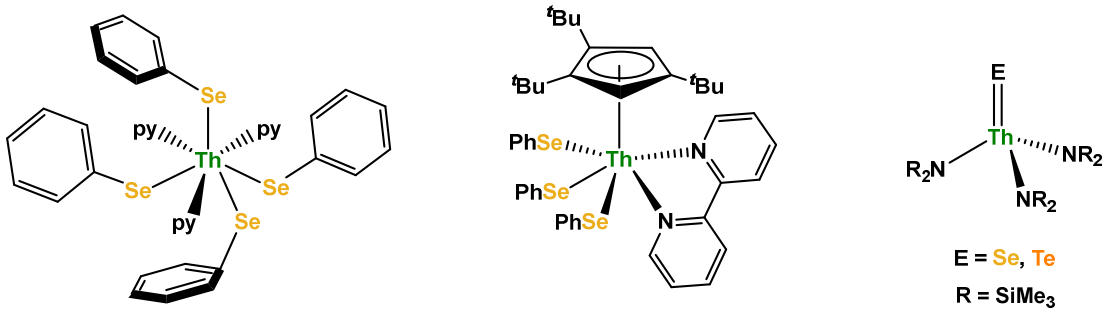

Figure 2.1. Examples of thorium complexes of the heavier chalcogens.

To address the dearth of thorium chalcogenides, we sought to develop a new strategy for the generation of these complexes. Salt metathesis,[18,19] reductive cleavage,[16,17,20] and addition across unsaturated moieties[15] have been employed in synthesizing complexes bearing Th-E bonds of the heavier chalcogens. Thorium-alkyl bonds are prone to insertion reactivity, and we postulated that these Th-C bonds could be utilized for chalcogen atom insertion chemistry by exploiting appropriate transfer reagents.[12] This would provide a convenient route to thorium chalcogenolate (ER; R = organic) complexes, which may serve as potential precursors for nanoscale material synthesis.[21-23] The reactivity of actinide alkyl complexes with a variety of small molecules and organic substrates has been extensively explored, predominantly with Cp-based ancillary ligands[24-33] and to a lesser extent with other supporting frameworks.[34-37] Having previously established the utility of amidinates as ancillary ligands in both transition metal[38-42] and actinide[43] chemistry, we sought the use of a tris-amidinate framework to stabilize a thorium monoalkyl complex (**2.2**), and examine its ability to incorporate chalcogen atoms *via* insertion. The resulting Th-SR, Th-SSR, Th-SeR and Th-TeR complexes represent rare examples of such linkages, and to the best of our knowledge are the first such bonds formed *via* insertion of a chalcogen atom into a thorium-carbon bond.

Results and Discussion

Synthesis of Th(CH$_2$SiMe$_3$)(BIMA)$_3$. The bis(isopropyl)methylamidinate (BIMA) ligand was chosen for its ease of synthesis and diagnostic ^{1}H NMR spectrum. We envisioned the isopropyl moieties would provide sufficient steric protection to the metal center, while still allowing space for coordination of incoming substrates. Treatment of $ThCl_4(DME)_2$[44] with 3.05 equiv. of Li(BIMA)(THF)[45] afforded Th(Cl)(BIMA)$_3$ (**2.1**) in 82% yield. Salt metathesis with $LiCH_2SiMe_3$ provided the alkyl species, Th(CH_2SiMe_3)(BIMA)$_3$ (**2.2**), as large, colorless blocks in 89% yield (Scheme 2.1). The ^{1}H NMR spectrum of **2.2** confirmed the incorporation of the alkyl fragment. Two new singlets appeared in the spectrum at δ 0.48 and -0.08 ppm for the $SiMe_3$-methyls and thorium-bound methylene groups, respectively, alongside resonances attributable to the equivalent

Scheme 2.1. Synthesis of Complexes **2.1** and **2.2**

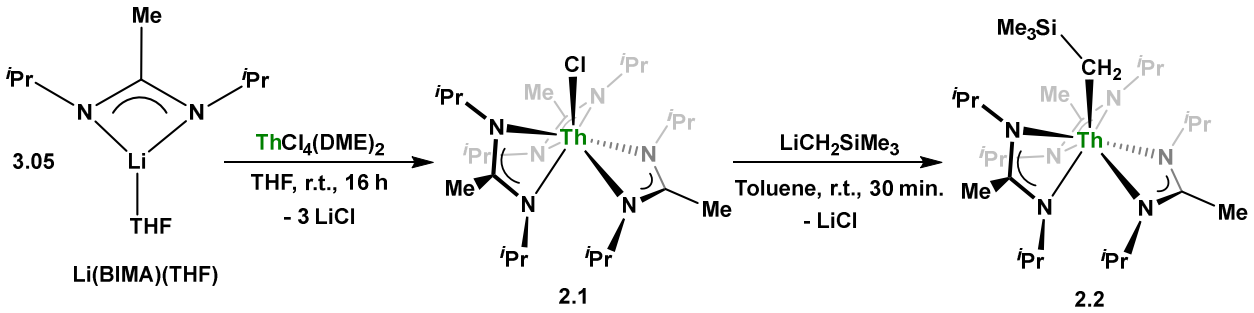

amidinate ligands, consistent with averaged C_3-symmetry in solution. The upfield resonance corresponding to the methylene protons, common in other thorium complexes bearing the same alkyl fragment,[46-48] serves as a useful diagnostic tool for quickly determining the success of a variety of reactions. This is also observable in the ^{13}C NMR spectrum, with the methylene carbon resonance (δ 83.3 ppm) most sensitive to change upon reacting with a substrate. The $^{1}J_{C,H}$ coupling constant of 99 Hz for the -CH_2SiMe$_3$ group (as measured from the ^{13}C satellites observed in the ^{1}H NMR spectrum) is lower than typically observed for an sp^3-hybridized carbon atom; this has been previously proposed as evidence for C-H-Th α-agostic interactions and is consistent with coupling constants observed in analogous actinide alkyl systems.[46-51] Analysis of **2.2** by variable-temperature ^{1}H NMR spectroscopy provided no further evidence for α-agostic interactions. While significant broadening of the -CH_2- signal did occur, no change to the $^{1}J_{C,H}$ coupling constant was observed upon cooling from 300 K to 210 K in toluene-d_8.

The molecular structure of **2.2** was determined by single-crystal X-ray diffraction studies (Figure 2.2). The Th-C25 bond length of 2.557(3) Å was found to be slightly longer than most thorium (IV) complexes bearing the -CH$_2$SiMe$_3$ ligand.[46-50,52] The Th-C25-Si1 bond angle of 135.98(16)° falls in the range reported for other thorium-CH$_2$SiMe$_3$ species. The amidinate ligands

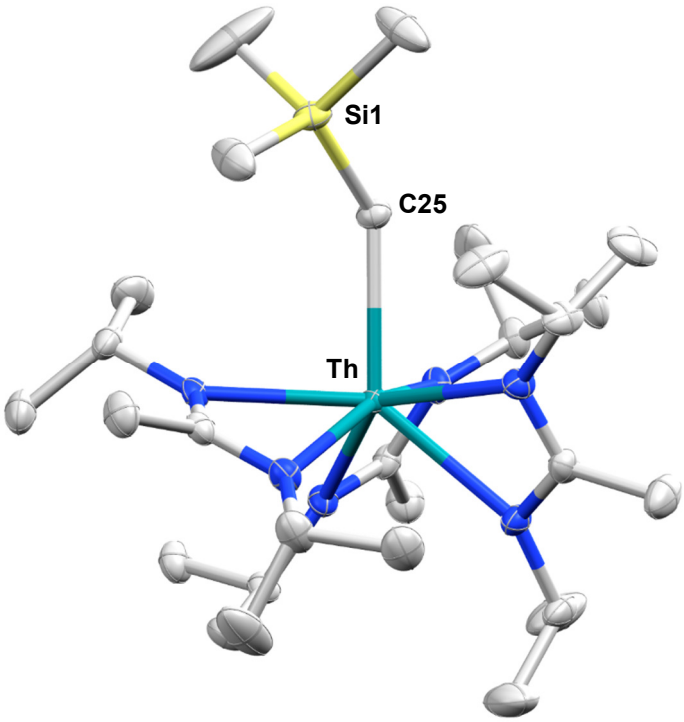

Figure 2.2. Molecular structure of **2.2**. Thermal ellipsoids drawn at the 50% probability level. Hydrogen atoms omitted for clarity.

all show C-N bond lengths between 1.33 and 1.34 Å, indicating delocalization of electron density within the NCN fragment, while the Th-N_{amid} bond lengths vary between 2.49 and 2.54 Å, which is in the range of previously reported thorium amidinate complexes.[31,53-55] With **2.2** in-hand, we began to explore the insertion reactivity of the alkyl fragment with various chalcogen atom transfer reagents.

C-H Activation of OAT Reagents. Actinides are known to be highly oxophilic,[56] and thus the corresponding thorium alkoxide from **2.2** was sought as an initial synthetic target. Pyridine *N*-oxide is a convenient choice for oxygen atom transfer (OAT),[57] as the pyridine formed upon atom transfer can either bind as a Lewis base or be removed under vacuum. However, instead of the intended OAT reactivity, treatment of **2.2** with one equivalent of pyridine *N*-oxide caused a gradual color change from colorless to red to yellow. Upon workup, the cyclometalated complex Th[η^2-(O,C)-ONC_5H_4]$(BIMA)_3$ (**2.3**) was isolated as a yellow solid in 68% yield (Scheme 2.2). Monitoring the reaction by ^{1}H NMR spectroscopy showed nearly complete (>95%) conversion to **3** within 10 minutes at room temperature, along with the generation of one equivalent of free $SiMe_4$. No resonances attributable to an OAT alkoxide product were observed. Consistent with the assignment of a cyclometalated product, the ^{1}H NMR spectrum of **3** in C_6D_6 displayed the absence

Scheme 2.2 C-H Activation of OAT Reagents by **2.2**

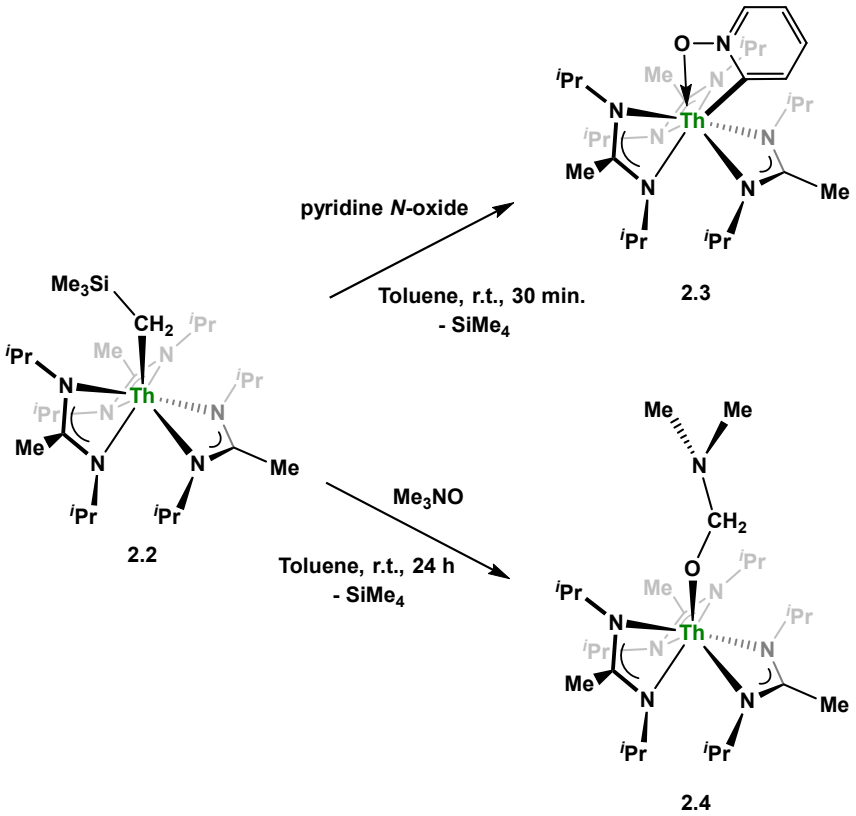

of -CH_2SiMe_3 alkyl resonances, small shifts in the BIMA ligand resonances compared to those in **2.2**, and the presence of four resonances in the aromatic region integrating to 1H each. We note that a related C-H activation of pyridine *N*-oxide has been reported by Kiplinger. Comparison of this Cp*-supported thorium dialkyl system helps support our assignment of **2.3** as a cyclometalated product.[58] Mechanistic studies performed by Kiplinger and co-workers revealed that pyridine *N*-oxide coordination followed by C-H activation was operative, and we expect a similar scenario is at play in the formation of **2.3**. Since the activation of pyridine N-oxide appeared to be favored over oxygen atom transfer, we turned our attention to trimethylamine N-oxide as an alternative OAT reagent. Monitoring the reaction of **2.2** with one equivalent of trimethylamine N-oxide by ^{1}H NMR spectroscopy showed the formation of a new Th-BIMA containing product (**2.4**) with no detectable amount of trimethylamine. Instead, one equivalent of free $SiMe_4$ was produced and two new singlets at δ 4.78 and 2.42 ppm were observed, integrating to 2H and 6H, respectively. The generation of $SiMe_4$ indicated C-H activation had again occurred preferably over OAT: the downfield resonance at δ 4.78 ppm integrating to 2H implied that the Th-CH_2 bond formed after C-H activation then underwent oxygen atom insertion (the Th-CH_2 resonance observed in **2.2** is noticeably upfield at δ -0.08 ppm). The identity of **2.4** was confirmed by X-ray diffraction (Figure 2.3). This revealed the thorium center was bound to a (dimethylamino)methanolate (-OCH_2NMe_2)

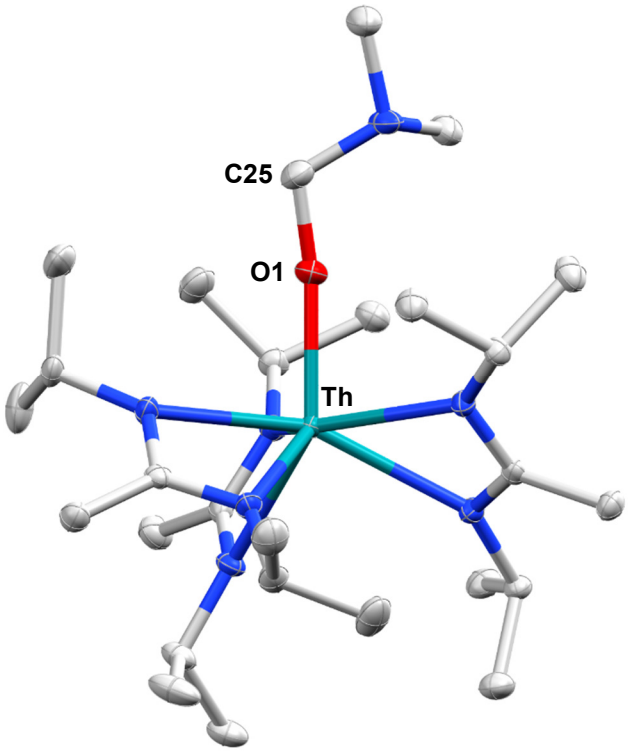

Figure 2.3. Molecular structure of **2.4**. Thermal ellipsoids drawn at the 50% probability level. Hydrogen atoms omitted for clarity.

moiety. The Th-O1 bond length of 2.1663(15) and near linear Th-O1-C25 bond angle of 166.14(15)° are within the range observed for known thorium alkoxide and aryloxide species.[59-62] Rather than succumbing to oxygen atom transfer, the basic $–CH_2SiMe_3$ ligand of **2.2** preferentially deprotonated a methyl group of the trimethylamine N-oxide followed by oxygen atom insertion to form **2.4** (Scheme 2.3). We propose the 4-membered metallocycle shown in Scheme 2.3 as a likely intermediate, although this was not detected by ^{1}H NMR spectroscopy. This mode of reactivity for trimethylamine N-oxide is uncommon, and to the best of our knowledge has only been observed once before involving a bis(amino)germylene species.[63] The thermodynamics of this transformation were investigated computationally at the DFT level. The calculated Gibbs free energy (ΔG) of the conversion of **2.2** to **2.4** was found to be -97.81 kcal mol^{-1}. Additionally, the intended OAT reaction leading to the targeted insertion product, $Th(OCH_2SiMe_3)(BIMA)_3$, was also examined computationally, and was found to have a $\Delta G°_{rxn}$ of -87.04 kcal mol^{-1}, indicating both reaction pathways are thermodynamically very favorable. Efforts to locate a transition state for the activation of trimethylamine N-oxide by computational methods were not successful. Use of alternative OAT reagents (N_2O, Ph_2S=O, TEMPO, O_2, Ph_3P=O) did not result in the desired $Th(OCH_2SiMe_3)(BIMA)_3$ complex; these reactions displayed either no reactivity or produced a mixture of products. Based on these results, it appears that the $Th(BIMA)_3$ framework supports an unusually basic $–CH_2SiMe_3$ alkyl moiety, which renders OAT difficult with reagents bearing accessible C-H protons. The oxophilic nature of thorium likely assists initial coordination of the OAT reagent and favors the deprotonation pathway. With this in mind, we hypothesized that moving down the chalcogen series would promote the desired atom transfer reactivity, as coordination of the larger and less electronegative atom becomes increasingly less favored.

Scheme 2.3. Proposed Activation Pathway of Me_3NO by **2.2**

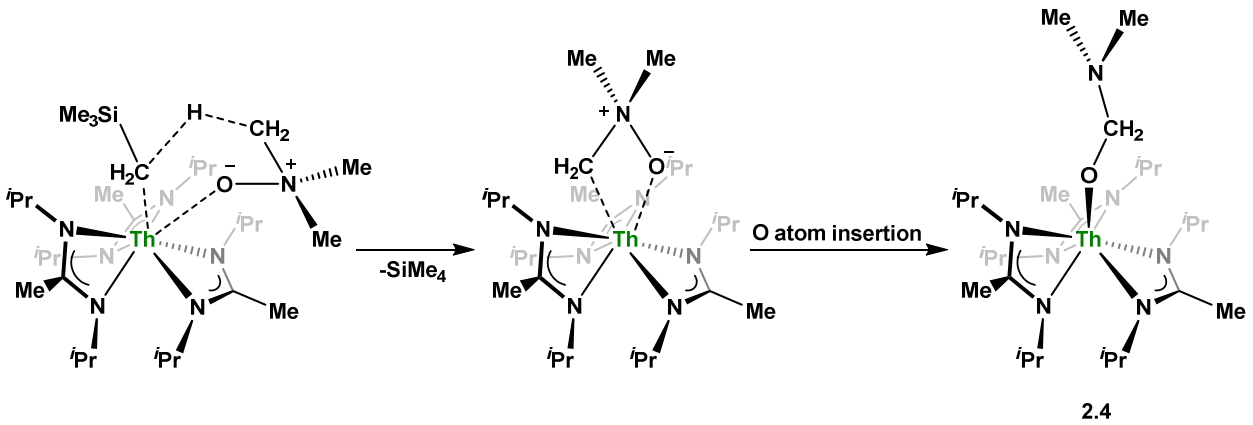

Synthesis of Heavier Thorium Chalcogenolates. The oxophilicity of the thorium atom combined with the strong basicity of the $-CH_2SiMe_3$ ligand in **2.2** led to unavoidable C-H activation products with the OAT reagents employed. To circumvent this and instead elicit atom transfer reactivity with **2.2**, we began exploring softer chalcogen atom transfer reagents. The reaction of elemental sulfur (S_8, 0.125 eq.) with **2.2** led to an intractable mixture of several products. The interaction of trimethylphosphine sulfide ($Me_3P{=}S$) with **2.2** did not lead to any observable reaction, despite elevated temperatures and extended reaction times. Looking to exploit a weaker P=S bond,[64] the reaction of $Ph_3P{=}S$ with **2.2** unfortunately proved equally ineffective. This stark contrast between immediate versus non-existent reactivity of **2.2** with oxygen and sulfur atom transfer reagents, respectively, further supports the notion that adduct formation precedes chalcogen atom transfer with the OAT reagents. Presumably, C-H activation was successfully avoided because thorium does not possess the same strong affinity for sulfur that it does for oxygen. To achieve the desired atom transfer, and thermodynamically drive the formation of the Th-S bond, we turned our attention to reagents bearing weaker X=S (X = pnictogen atom) bonds. Hoff and co-workers reported that triphenylantimony sulfide ($Ph_3Sb{=}S$) has a Sb=S BDE roughly 20 kcal mol^{-1} lower than the P=S BDE in $Ph_3P{=}S$.[64] Monitoring the reaction between **2.2** and one equivalent of $Ph_3Sb{=}S$ at 100 °C by ^1H NMR spectroscopy over a period of ten days showed clean conversion of **2.2** to a new product and no formation of free $SiMe_4$. The methylene resonance of **2.2** observed at δ -0.08 ppm disappeared as a new singlet integrating to 2H appeared further downfield at δ 2.42 ppm. This diagnostic downfield shift of the methylene resonance is an indicator of successful chalcogen atom insertion. Isolation from Et_2O furnished the product, $Th(SCH_2SiMe_3)(BIMA)_3$ (**2.5**), in 80% yield (Scheme 2.4). The identity of **2.5** as the single insertion product was confirmed by X-ray diffraction (Figure 2.4). The Th-S1 bond length of

Scheme 2.4. General Synthesis of Heavier Thorium Chalcogenolate Species

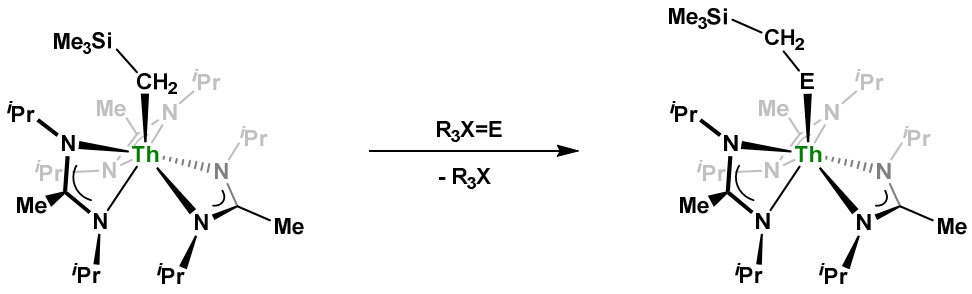

2.5: E = S; $R_3X = Ph_3Sb$
2.6: E = SS; $R_3X = Ph_3Sb$ (2 eq.)
2.7: E = Se; $R_3X = Ph_3P$, Me_3P
2.8: E = Te; $R_3X = Cy_3P$

2.8235(6) Å is ~0.1 Å longer than that observed in comparable Th-SR systems: 2.7488(11) and 2.7451(10) Å in $Cp^*_2Th(SPh)_2$,[65] 2.704(1) in $[Th(SCPh_3)(NR_2)_3]$ (R = $SiMe_3$),[66] and 2.718(3) in $Cp^*_2Th(SCH_2CH_2CH_3)_2$.[67] The Th-S1-C25 bond angle of 107.27(8)° is in the range observed with previously reported complexes. The Th-C25 distance of 3.801(2) Å and the $-CH_2SiMe_3$ $^1J_{C,H}$ coupling constant of 130 Hz indicate no appreciable C-H-Th α-agostic interactions.

Upon addition of $Ph_3Sb{=}S$ to **2.2** at room temperature, ^{1}H NMR spectroscopy revealed formation of another product alongside **2.5**, unreacted **2.2**, and Ph_3Sb (Figure 2.5). This product had a singlet downfield at δ 2.26 ppm, as well as shifted resonances corresponding to the BIMA and alkyl ligands. Under the reaction conditions necessary to generate **2.5**, this product and **2.2** slowly disappeared, leaving **2.5** as the sole thorium-containing species in solution. The downfield shift of the methylene protons in this unknown species seemed to indicate successful sulfur insertion. We hypothesized that the most likely explanation involved the formation of an alkyl disulfide complex, $Th(SSCH_2SiMe_3)(BIMA)_3$ (**2.6**), as a result of two successive sulfur atom insertions. This would explain the formation of both products initially, along with unreacted **2.2**. This disulfide complex then acted as a sulfur atom transfer reagent at high temperatures, yielding only **2.5** upon reaction completion. The reaction of **2.2** with 2 equivalents of $Ph_3Sb{=}S$ lead to

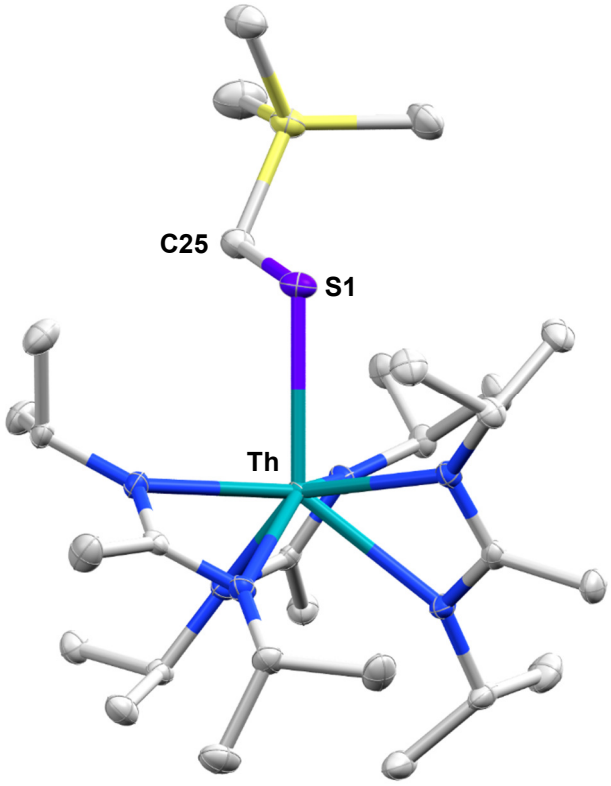

Figure 2.4. Molecular structure of **2.5**. Thermal ellipsoids drawn at the 50% probability level. Hydrogen atoms omitted for clarity.

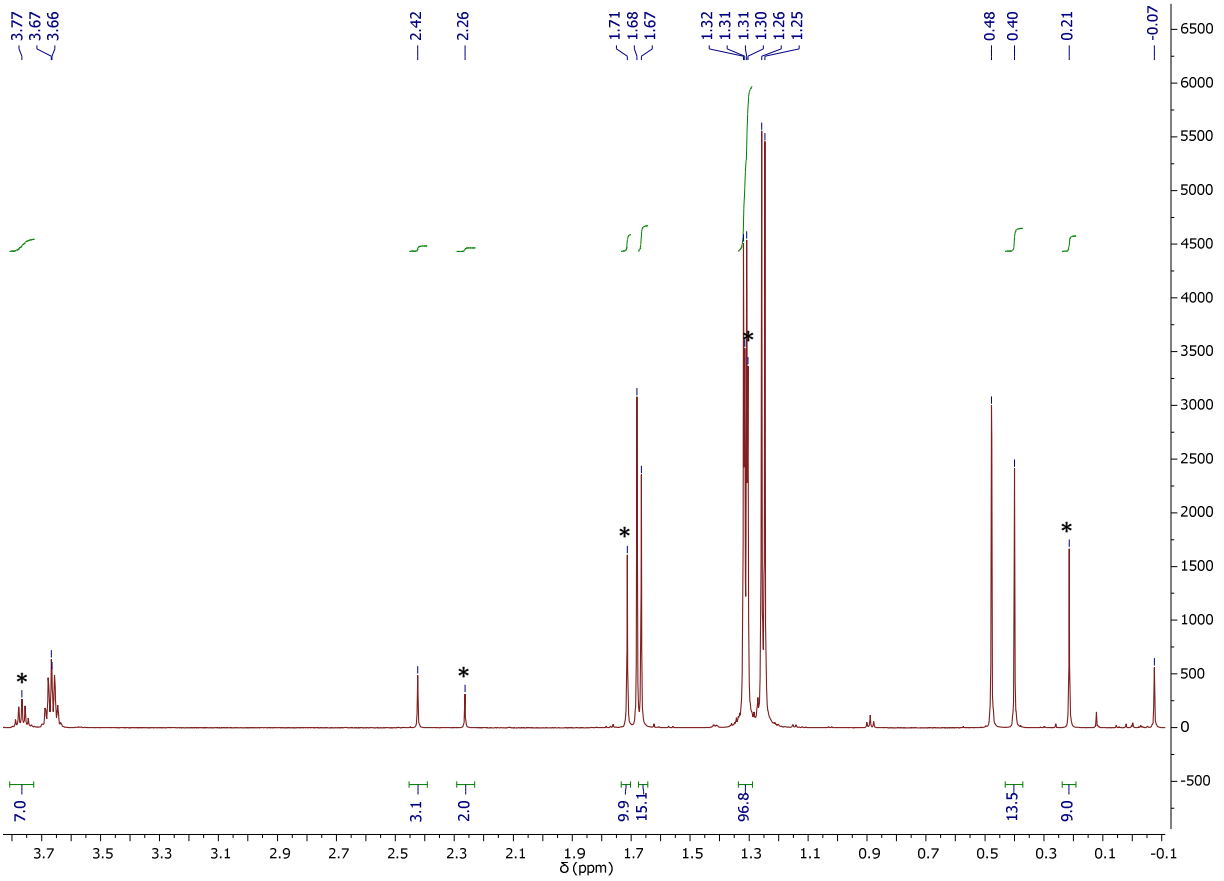

Figure 2.5. ^{1}H NMR spectrum of both products initially seen in the reaction of **2.2** with $Ph_3Sb{=}S$ at 298 K in C_6D_6. Starting material **2.2** and any product resonances overlapping with resonances of **2.2** are not integrated. The C_6D_6 resonance (δ 7.16) and Ph_3Sb resonances (δ 7.07 and 7.44, multiplets) are not shown. *Resonances corresponding to **2.6**.

formation of **2.6** as the major species at room temperature, and isolation from HMDSO (necessary due to the high solubility of this complex) afforded **2.6** in 52% yield. X-ray diffraction studies confirmed the identity of **2.6** and revealed an η^2-S_2 moiety inserted into the Th-C bond (Figure 2.6). Coordination of an alkyl disulfide to a metal center is well precedented in transition metal chemistry,[68-72] but only one example has been observed with uranium[73] and none to our knowledge with thorium. Related η^2-S_2 structural motifs have been observed in other thorium complexes, specifically $[\{\eta^5\text{-}1,2,4\text{-}(^t\text{Bu})_3C_5H_2\}_2\text{Th}\{\text{N}(p\text{-tolyl})\text{S-S}\}]$[74] and $Cp^*_2ThS_5$.[75] The Th-S1 and Th-S2 bond lengths of 2.8203(7) and 3.0439(7) Å, respectively, are in the range of Th-S bonds previously observed in the other thorium η^2-S_2 complexes. The difference of 0.2236 Å between the Th-S bond lengths promotes the notion that the Th-S1 bond is best described as ionic and the Th-S2 bond as dative, which is consistent with the description of the bonding in $Cp^*_2ThS_5$.[75] The Th-C25 bond distance of 4.174(2) Å and the $-CH_2SiMe_3$ $^{1}J_{C,H}$ coupling constant of 131 Hz indicate a lack of α-agostic interactions. With the identity of **2.6** established, we wished to test the capability of **2.6** to transfer a sulfur atom to **2.2**. A C_6D_6 solution containing both **2.2** and **2.6** was heated at 100 °C

over a period of 7 days, resulting in the generation of **2.5**, confirming the ability of **2.6** to act as a sulfur atom transfer reagent. Finally, a solution of **2.6** in C_6D_6 was heated to 100 °C for 48 h to gauge whether **2.5** could be generated by thermal decomposition of **2.6**. The formation of a small amount of **2.5** and an even smaller amount of an unidentified product was observed; we postulated that **2.6** was acting as a sulfur atom transfer reagent to itself, generating **2.5** and a triple-insertion product. The reaction of **2.2** with 3 eq. of $Ph_3Sb{=}S$ resulted in a mixture of **2.6** and the same presumed triple-insertion product seen in the thermal decomposition of **2.6** (Figure 2.7). Further identification has proven difficult as complete conversion and isolation of this product in pure form has not yet been achieved. The ^{1}H NMR shifts of **2.5**, **2.6**, and the presumed triple insertion product (**TIP**) are summarized in Table 2.1.

Despite the forcing conditions needed for sulfur insertion, we predicted that the weak X=Se BDE observed in common selenium transfer reagents would facilitate insertion into the Th-C bond of **2.2** under relatively mild conditions.[64] Monitoring the reaction of **2.2** with one equivalent of either $Ph_3P{=}Se$ or $Me_3P{=}Se$ at 50 °C by ^{1}H NMR confirmed the formation of a new product along with free of PR_3 (verified by ^{31}P NMR). As observed with successful sulfur transfer to **2.2**, a diagnostic downfield singlet integrating to 2H emerged at δ 2.25 ppm, concomitant with the disappearance of all resonances attributable to **2.2**. We assigned this new product as $Th(SeCH_2SiMe_3)(BIMA)_3$ (**2.7**). Purification of **2.7** was simplified by utilizing $Me_3P{=}Se$ as the

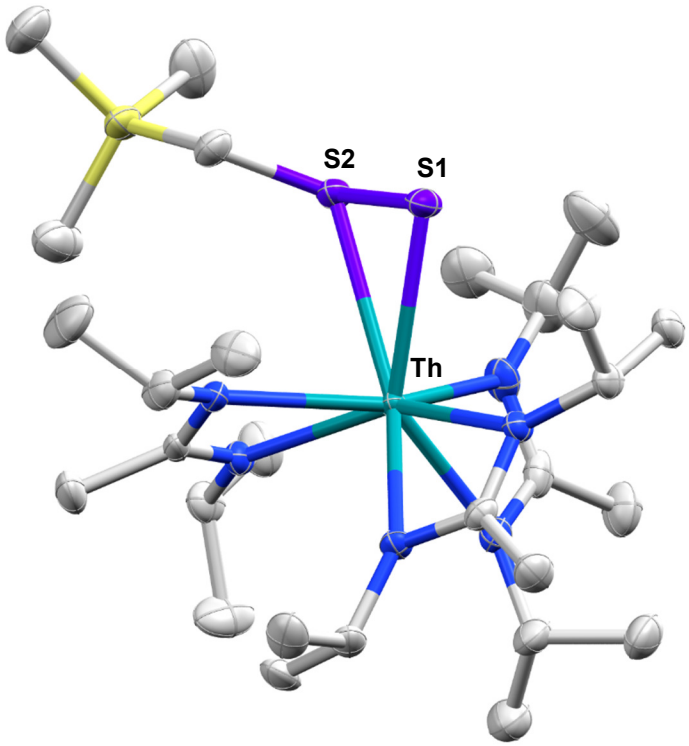

Figure 2.6. Molecular structure of **2.6**. Thermal ellipsoids drawn at the 50% probability level. Hydrogen atoms omitted for clarity.

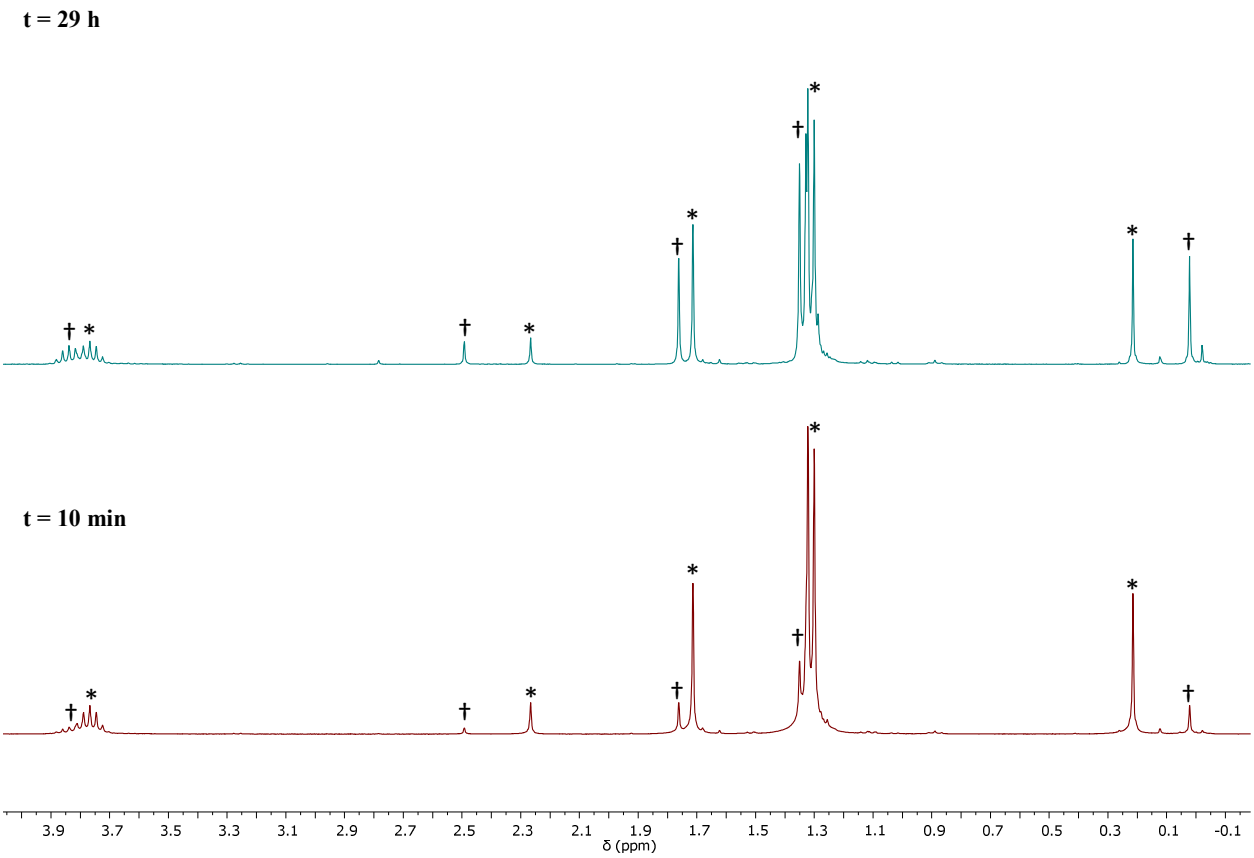

Figure 2.7. Stacked ^{1}H NMR spectrum of **2.2** with 3 eq. $Ph_3Sb{=}S$ in C_6D_6 (300 MHz). The C_6D_6 resonance (δ 7.16 ppm) and Ph_3Sb resonances (δ 7.07 and 7.44 ppm, multiplets) are not shown. *Resonances attributable to **2.6**. †Resonances attributed to triple-insertion product. After 24 h at room temperature the reaction was heated at 60 °C for 5 h. Further conversion to the triple-insertion product was not achieved with additional heating, as several unidentified products began to appear.

Table 2.1. ^{1}H NMR Resonances (ppm) for Complexes **2.5**, **2.6**, and **TIP**

Resonance	2.5	2.6	TIP
6H septet	3.67	3.77	3.84
2H singlet	2.42	2.27	2.49
9H singlet	1.67	1.71	1.76
36H doublet	1.31	1.32	1.34
9H singlet	0.40	0.21	0.02

selenium transfer reagent, as the volatile Me_3P by-product could be removed under reduced pressure. Crystallization from pentane afforded colorless crystals of **2.7** in 74% yield (Scheme 2.4). The identity of **2.7** as the selenolate complex was confirmed by X-ray diffraction. The Th-Se1 bond length of 2.9317(5) Å in **2.7** falls in the range observed for previously reported Th-Se complexes.[15-20] This is the first example of a Th-Se complex formed via chalcogen insertion into a Th-C bond, as those previously characterized have been formed through salt metathesis,[18,19] reductive cleavage of a diselenide,[16,17,20] or [2 + 2] cycloaddition across a terminal thorium-imido moiety.[15] In the solid state, **2.7** was found to exhibit an unusually acute Th-Se1-C25 bond angle of 80.98(13)° and a Th-C25 distance of 3.281(5) Å, a difference of ~26° and ~0.5 Å, respectively, compared to that observed in **2.5** (Figure 2.8). Of the molecular complexes containing Th-Se bonds that have been structurally characterized, none have a bond angle close to that observed in **2.7**. For comparison, the groups of Walter and Brennan have reported Th-Se-C_{aryl} bond angles ranging from 105-115°, more than 20° larger than that seen in **2.7**.[16,17,20] These large bond angles (>100°) are prevalent in group 4 selenolates.[76,77] We believe this notable difference is caused by a combination of crystal packing effects and steric congestion imposed by the more rigid phenyl substituents on selenium. C-H-Th α-agostic interactions were ruled out as the cause of the unusually acute Th-Se-C bond angle in **2.7** through variable temperature ^{1}H NMR experiments. Specifically, the $^1J_{C,H}$

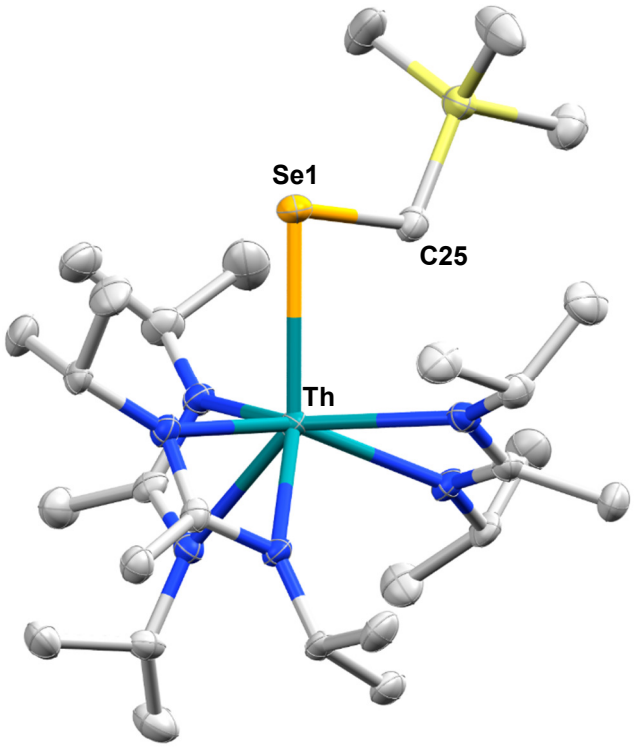

Figure 2.8. Molecular structure of **2.7**. Thermal ellipsoids drawn at the 50% probability level. Hydrogen atoms omitted for clarity.

coupling constant of the $-CH_2SiMe_3$ group in **2.7** was measured over a range of temperatures to probe the likelihood of a temperature-dependent equilibrium between a product that favors α-agostic interactions and one that does not. Cooling a solution of **2.7** in toluene-d_8 from 300 K to 210 K caused a gradual broadening of the methylene resonance but no significant change in the $^1J_{C,H}$ coupling constant of 128 Hz. The unusual bond angle of **2.7** was also investigated computationally at the DFT level. The lowest energy structure resulting from a geometry optimization calculation revealed an even more acute Th-Se-C bond angle of 73.65° (Figure 2.9). Vibrational analyses were performed on this optimized structure as well as an independently optimized structure of **2.7** wherein the Th-Se-C bond angle was constrained to the experimentally obtained value of 80.98°. The calculated Gibbs free energies (ΔG) of these two structures were found to be essentially thermoneutral, with an energy difference of less than 1.4 kcal mol^{-1}. Furthermore, a gas phase potential energy scan was performed on the Th-Se-C angle which revealed that the optimized structure calculated for **2.7** sits at the minimum of a very shallow potential energy well. Therefore, as seen previously with other metal complexes,[78,79] the effects of crystal packing likely play a key role in the unique solid-state structure of **2.7**.

While only a handful of molecular complexes contain Th-Se bonds, to date only two bearing Th-Te bonds have been crystallographically characterized, one featuring a Th(η^2-Te_2) interaction and the other a Th=Te double bond.[19] To this end, no discrete Th-Te single bond featuring a Te^{2-} moiety has been crystallographically characterized, and no thorium tellurolates have been synthesized despite the availability of reagents such as diphenyl ditelluride, which is

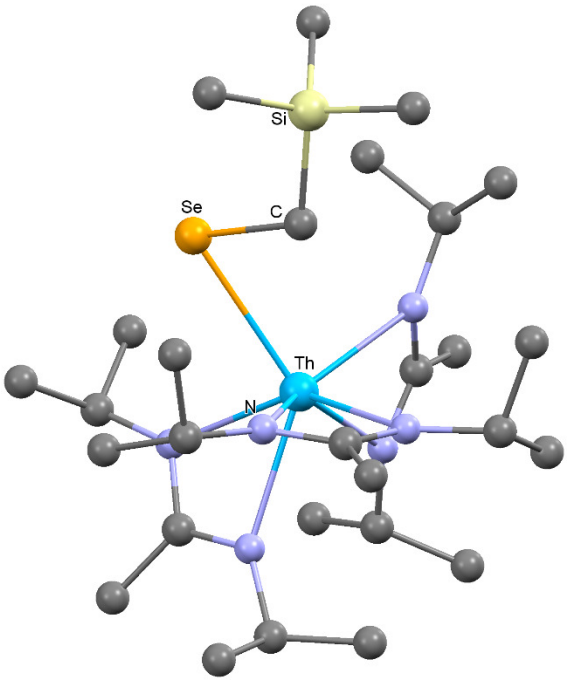

Figure 2.9. Geometry optimized structure for complex **2.7**

known to undergo reductive cleavage to generate anionic PhTe units. The reaction of **2.2** with one equivalent of $Cy_3P{=}Te$[80] (Scheme 2.4) resulted in the disappearance of **2.2** and the diagnostic downfield shift of the methylene resonance from δ -0.08 to δ 2.20 ppm in the ^{1}H NMR spectrum, along with free PCy_3 (confirmed by ^{31}P NMR). Crystallization from hexane afforded $Th(TeCH_2SiMe_3)(BIMA)_3$ (**2.8**) in 67% isolated yield. Single crystals suitable for X-ray diffraction were grown from a concentrated Et_2O solution. Complex **2.8** crystallized with two independent molecules in the asymmetric unit. However, one molecule contained a disordered $-CH_2SiMe_3$ alkyl fragment; thus, only the non-disordered molecule will be discussed (Figure 2.10). The Th-Te1 bond length of 3.2275(3) Å is longer than the average Th-Te bond length of 3.173 Å seen in [K(18-crown-6)][$Th(Te_2)(NR_2)_3$] (R = $SiMe_3$), and substantially longer than that of the double bonded species [K(18-crown-6)][$Th(Te)(NR_2)_3$] (avg. 2.933 Å).[19] Complex **2.8** is the first example of a molecular thorium tellurolate; as such, **2.8** has no structural analog to which the Th-Te1-C25 bond angle of 110.82(12)° could be compared. However, this angle is ~30° larger than the analogous angle seen in **2.7**, but only ~3° larger than in **2.5**. The Th-C25 distance is 4.498(5) Å, and the $^1J_{C,H}$ coupling constant for the $-CH_2SiMe_3$ group in **2.8** was found to be 128 Hz. Taken together, these metrics indicate no appreciable C-H-Th α-agostic interactions, and the similar coupling constants observed in complexes **2.5**-**2.7** support the notion that the acute angle observed in **2.7** is the result of factors not influenced by C-H-Th α-agostic interactions.

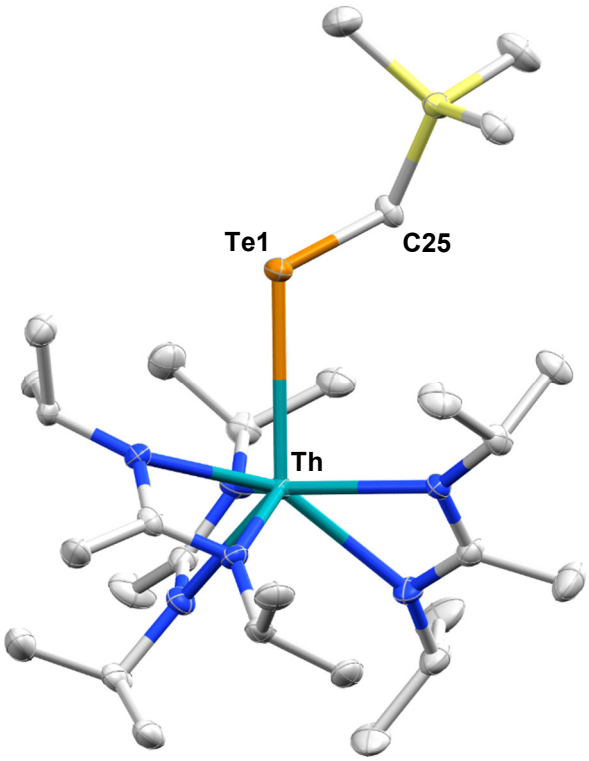

Figure 2.10. Molecular structure of **2.8**. Thermal ellipsoids drawn at the 50% probability level. Hydrogen atoms omitted for clarity.

Table 2.2. Selected Bond Lengths (Å) and Angles (°) for Complexes **2.2, 2.4**-**2.8**

Complex	**2.2**	**2.4**	**2.5**	**2.6**	**2.7**	**2.8**
Bond Lengths (Å)						
Th-X	2.557(3)	2.1663(15)	2.8235(6)	2.8203(7), 3.0439(7)	2.9317(5)	3.2275(3)
X-C25	-	1.386(3)	1.841(2)	1.809(2)	2.002(5)	2.188(5)
Th-C25[a]	2.557(3)	3.527(2)	3.801(2)	4.174(2)	3.281(5)	4.498(5)
Bond Angles (°)						
Th-X-C25	-	166.14(15)	107.27(8)	116.29(8)	80.98(13)	110.82(12)
X-C25-Y	135.98(16)	113.30(19)	112.15(12)	112.5(1)	112.2(2)	113.0(2)

*X is the atom bound directly to Th not coming from the amidinate ligands. Y is the atom bound directly to C25 in the structures (mostly Si, for **2.4** is N). For complex **2.2**, X = Th for X-C25-Y. For **2.6**, the Th-X bond distances correspond to Th-S1 and Th-S2, respectively, and X = S2 for Th-X-C25 and X-C25-Y. Complex **2.8** crystallized with two independent molecules in the asymmetric unit, with the second molecule containing a disordered Te1-C25-Si1 fragment. Therefore, the discussion of metrical parameters for these complexes is relevant to the Th1 molecule only.*

[a]No structure contains thorium bound directly to C25 (except **2.2**); this is a measurement of the distance between the two atoms.

Table 2.3. Crystal and Refinement Data for Complexes **2.2, 2.4-2.8**

Complex	**2.2**	**2.4**	**2.5**	**2.6**	**2.7**	**2.8**
Chemical formula	$C_{28}H_{62}N_6SiTh$	$C_{27}H_{59}N_7OTh$	$C_{28}H_{62}N_6SiSTh$	$C_{28}H_{62}N_6SiS_2Th$	$C_{28}H_{62}N_6SiSeTh$	$C_{28}H_{62}N_6SiTeTh$
Formula weight	742.96	729.85	775.02	807.08	821.92	870.56
Temperature (K)	100(2)	100(2)	100(2)	100(2)	100(2)	100(2)
Crystal system	Monoclinic	Triclinic	Monoclinic	Monoclinic	Monoclinic	Triclinic
Space group	P 21/n	P-1	P 21/c	P 21/n	P 21/n	P-1
a (Å)	11.8539(5)	9.4910(3)	10.8680(8)	11.3345(10)	11.1273(4)	13.6129(5)
b (Å)	16.0933(7)	10.5346(4)	16.4185(13)	18.1535(17)	16.9733(6)	16.3848(6)
c (Å)	18.5690(9)	17.7484(6)	20.9253(17)	18.6885(17)	19.4029(7)	17.5895(7)
α (°)	90	84.9754(16)	90	90	90	105.0224(18)
β (°)	99.3271(11)	75.7195(14)	103.045(3)	101.817(4)	99.500(2)	90.6966(18)
γ (°)	90	70.3210(14)	90	90	90	104.7327(17)
V (Å^3)	3495.5(3)	1619.26(10)	3637.5(5)	3763.9(6)	3614.3(2)	3651.8(2)
Z	4	2	4	4	4	4
Densitiy (Mg m^{-3})	1.412	1.497	1.415	1.424	1.510	1.583
F(000)	1504	736	1568	1632	1640	1712
Radiation Type	MoK_α	MoK_α	MoK_α	MoK_α	MoK_α	MoK_α
μ (mm^{-1})	4.324	4.634	4.214	4.129	5.190	4.923
Meas. Refl.	138464	89862	184008	169148	48829	177437
Indep. Refl.	6415	5953	6689	6911	6648	13420
R(int)	0.0385	0.0279	0.0345	0.0299	0.0558	0.0435
Final R indices [I > 2σ(I)]	R = 0.0235 R_w = 0.0528	R = 0.0150 R_w = 0.0321	R = 0.0164 R_w = 0.0330	R = 0.0157 R_w = 0.0351	R = 0.0306 R_w = 0.0652	R = 0.0293 R_w = 0.0669
GOF	1.161	1.109	1.173	1.077	1.095	1.109
$\Delta\rho_{max}$, $\Delta\rho_{min}$ (e Å^{-3})	3.044, -1.019	2.104, -0.752	1.893, -0.700	1.238, -0.505	2.701, -1.144	2.536, -1.047

Conclusions

The amidinate-supported thorium monoalkyl complex **2.2** inserts chalcogen atoms to form thorium chalcogenolate complexes, including species containing rare Th-S, Th-η^2-S_2, Th-Se and Th-Te bonds. The oxophilicity of thorium coupled with the ease of intramolecular deprotonation favors C-H activation with oxygen atom transfer reagents. Rapid C-H activation is avoided by utilizing softer chalcogen donors for atom transfer, with successful insertion readily observable in the diagnostic downfield shift of the methylene resonance. Chalcogen atom insertion is realized for S, Se, and Te by balancing the thermodynamics of thorium chalcogenolate formation with the X=E bond strength of the transfer reagent. Complexes **2.5** and **2.6** demonstrate the ability of **2.2** to stoichiometrically insert sulfur atoms and generate unique thiolate and disulfide species, with preliminary studies indicating additional sulfur atom insertions occur. The Th-Se complex **2.7** contains an unusually acute Th-Se-C bond angle of 81°, which is more than 20° lower than comparable angles observed in other Th-Se complexes. Spectroscopic and computational evidence implies that C-H-Th α-agostic interactions do not play a role in producing this acute angle.

Experimental Details

General procedures. Unless otherwise stated, all reactions were performed under an atmosphere of dry N_2 using standard Schlenk line techniques or in an MBraun N_2 atmosphere glovebox (<1.0 ppm of O_2/H_2O). All solvents were dried and degassed using a commercially available Phoenix SDS from JC Meyer Solvent Systems. All glassware, syringes, and cannulas were stored in a 140 °C oven for a minimum of 16 h prior to use. Prior to use, deuterated solvents (C_6D_6, tol-d_8) were dried over sodium/benzophenone, followed by three freeze−pump−thaw cycles and vacuum transfer. Li(BIMA)(THF),[45] $ThCl_4(DME)_2$,[44] $Me_3P{=}Se$,[81] and $Cy_3P{=}Te$[80] were prepared according to previously reported literature procedures. Pyridine-N-oxide was sublimed prior to use. Trimethylamine N-oxide was obtained by dissolving trimethylamine N-oxide dihydrate in dry dimethylformamide (DMF) and removing the volatiles by distillation, resulting in an oil that then solidified. (Trimethylsilyl)methyllithium was purchased from SigmaAldrich as a 1.0 M solution in pentane; solid $LiCH_2SiMe_3$ was obtained by crystallization from this pentane solution at -40 °C. All other reagents were purchased from commercial sources and used as received. Unless otherwise stated, NMR spectra were collected at ambient temperature on a Bruker AV-300, AVB-400, AV-500, DRX-500 or AV-600 spectrometer. ^1H and $^{13}C\{^1H\}$ NMR chemical shifts (δ) are reported in ppm and were calibrated to residual solvent peaks. $^{77}Se\{^1H\}$ spectra were recorded at an operating frequency of 76.3 MHz and referenced to PhSeSePh in C_6D_6 (δ = 460 ppm).[82] $^{125}Te\{^1H\}$ spectra were recorded at an operating frequency of 189 MHz and referenced to $Te(OH)_6$ in H_2O (δ = 707 ppm).[83] Melting points were determined on an Optimelt SRS instrument using capillary tubes sealed under dry N_2. Elemental analysis samples were either sealed under vacuum or inert gas (N_2) and analyzed at either the London Metropolitan University or the University of California, Berkeley Microanalytical Facility. Infrared spectra were collected on a Thermo Scientific Nicolet iS10 FTIR spectrophotometer using Nujol mulls pressed between KBr plates.

$ThCl(MeC(N^iPr)_2)_3$ (2.1): $ThCl_4(DME)_2$ (4.00 g, 7.22 mmol) was added to a 250 mL Schlenk flask containing a magnetic stir bar and dissolved in 75 mL THF. To this stirred solution was added a solution of Li(BIMA)(THF) (4.85 g, 22.0 mmol) in THF (50 mL) slowly *via* cannula. The resulting colorless solution was allowed to stir at ambient temperature for 16 h. The volatiles were removed under reduced pressure, and the resulting sticky solid was triturated with hexanes (2 x 30 mL). The colorless solid was extracted into toluene (2 x 50 mL), filtered through Celite and concentrated to 20 mL. The solution was stored at -40 °C overnight, yielding **2.1** as analytically pure, colorless crystals (4.09 g, 82.0%). ^1H NMR (300 MHz, C_6D_6, 293 K): δ 3.63 (sept, C*H*Me$_2$, 6H), 1.62 (s, NC(C*H*$_3$)N, 9H,), 1.33 (d, CH*Me*$_2$, 36H). $^{13}C\{^1H\}$ NMR (151 MHz, C_6D_6, 293 K): δ 173.7 (N*C*N), 48.7 (Me$_2$*C*H), 24.7 (*Me*$_2$CH), 12.3 (NC(*C*H$_3$)N). Anal. Calcd for $C_{24}H_{51}N_6ClTh$ (691.2): C, 41.70; H, 7.44; N, 12.16. Found: C, 41.57; H, 7.57; N, 12.08. Mp: 133-135 °C (dec.). FTIR (Nujol): 2602 (w), 1360 (s), 1336 (s), 1313 (s), 1200 (s), 1175 (s), 1138 (s), 1125 (s), 1050 (m), 1013 (s), 940 (w), 805 (s), 727 (w), 618 (s), 572 (m), 545 (s). Crystals suitable for single-crystal X-ray diffraction studies were grown from a concentrated toluene solution stored at -35 °C for 16 h.

$Th(CH_2SiMe_3)(MeC(N^iPr)_2)_3$ (2.2): Solid **2.1** (1.49 g, 2.16 mmol) was added to a 20 mL scintillation vial containing a magnetic stir bar and was dissolved in 10 mL toluene. To this stirred

solution was added a solution of $LiCH_2SiMe_3$ (0.212 g, 2.25 mmol) in toluene (2 mL) dropwise, resulting in immediate precipitation of a colorless solid. The resulting suspension was allowed to stir at ambient temperature for 30 min. The volatiles were removed under reduced pressure, and the resulting solid was extracted into HMDSO (10 mL), filtered through Celite and concentrated to 6 mL. The solution was stored at -35 °C overnight, yielding **2.2** as analytically pure, colorless crystals (1.42 g, 88.8%). ^{1}H NMR (600 MHz, C_6D_6, 293 K): δ 3.66 (sept, C*H*Me$_2$, 6H), 1.68 (s, NC(C*H*$_3$)N, 9H,), 1.26 (d, CH*Me*$_2$, 36H), 0.48 (s, CH_2Si*Me*$_3$, 9H), -0.08 (s, C*H*$_2$SiMe$_3$, 2H) . ^{13}C{^{1}H} NMR (151 MHz, C_6D_6, 293 K): δ 173.4 (N*C*N), 83.3 (*C*H$_2$SiMe$_3$), 48.6 (Me$_2$*C*H), 25.1 (*Me*$_2$CH), 13.4 (NC(*C*H$_3$)N), 5.8 (CH_2Si*Me*$_3$). Anal. Calcd for $C_{28}H_{62}N_6SiTh$ (743.0): C, 45.27; H, 8.41; N, 11.31. Found: C, 45.13; H, 8.53; N, 11.15. Mp: 190 °C (dec.) FTIR (Nujol): 1486 (s), 1359 (s), 1335 (s), 1314 (s), 1247 (w), 1236 (m), 1197 (s), 1173 (s), 1120 (m), 1050 (w), 1013 (m), 854 (s), 805 (s), 747 (m), 720 (m), 671 (w), 620 (w), 573 (w), 542 (w). Crystals suitable for single-crystal X-ray diffraction studies were grown from a concentrated HMDSO solution stored at -35 °C for 16 h.

Th[η^2-(O,C)-ONC$_5$H$_4$](MeC(N^{i}Pr)$_2$)$_3$ (2.3): Solid **2.2** (0.401 g, 0.540 mmol) was added to a 20 mL scintillation vial containing a magnetic stir bar and was dissolved in 5 mL toluene. To this stirred solution was added a solution of pyridine *N*-oxide (0.0520 g, 0.547 mmol) in toluene (4 mL) dropwise over 5 minutes, resulting in a gradual solution color change from colorless to light red. The solution was allowed to stir at ambient temperature for 1 h, at which point the solution had become yellow in color. The volatiles were removed under reduced pressure, and the resulting solid was triturated with hexane (2 x 4 mL) and extracted into HMDSO (6 mL). The solution was concentrated to 2 mL, filtered through Celite, and placed in the freezer at -35 °C for 16 h, resulting in **2.3** as a yellow solid (0.273 g, 67.5%). ^{1}H NMR (300 MHz, C_6D_6, 293 K): δ 7.65 (d, pyrNO, 1H), 7.49 (d, pyrNO, 1H), 6.76 (t, pyrNO, 1H), 6.35 (t, pyrNO, 1H), 3.74 (sept, C*H*Me$_2$, 6H), 1.72 (s, NC(C*H*$_3$)N, 9H), 1.27 (d, CH*Me*$_2$, 36H). ^{13}C{^{1}H} NMR (151 MHz, C_6D_6, 293 K): δ 210.0 (C_{pyrNO}), 172.3 (N*C*N), 134.7 (C_{pyrNO}), 134.3 (C_{pyrNO}), 120.2 (C_{pyrNO}), 48.7 (Me$_2$*C*H), 25.2 (*Me*$_2$CH), 12.7 (NC(*C*H$_3$)N). Anal. Calcd for $C_{29}H_{55}N_7OTh$ (749.9): C, 46.45; H, 7.39; N, 13.08. Found: C, 46.21; H, 7.63; N, 13.30. Mp: 165-174 °C (dec.) FTIR (Nujol): 1493 (s), 1358 (s), 1335 (s), 1313 (s), 1248 (w), 1197 (s), 1173 (s), 1123 (m), 1088 (w), 1050 (w), 1013 (m), 816 (m), 803 (m), 765 (m), 722 (w), 691 (w), 654 (w), 619 (w), 572 (w), 559 (w), 537 (m), 421 (w).

Th(OCH$_2$NMe$_2$)(MeC(N^{i}Pr)$_2$)$_3$ (2.4): Solid **2.2** (0.300 g, 0.404 mmol) was added to a 20 mL scintillation vial containing a magnetic stir bar and was dissolved in 2 mL toluene. In a separate vial, trimethylamine *N*-oxide (0.0318 g, 0.423 mmol) was suspended in 4 mL toluene, and to this suspension was added the solution of **2**. The suspension was allowed to stir at ambient temperature for 24 h, at which point the volatiles were removed under reduced pressure, and the resulting solid was triturated with pentane (2 x 2 mL) and extracted into pentane (8 mL). The solution was concentrated to 2 mL, filtered through Celite, and placed in the freezer at -35 °C for 16 h, resulting in colorless crystals of **2.4** (0.194 g, 65.8 %). ^{1}H NMR (600 MHz, C_6D_6, 293 K): δ 4.78 (s, OC*H*$_2$NMe$_2$, 2H), 3.68 (sept, C*H*Me$_2$, 6H), 2.42 (s, OCH$_2$N*Me*$_2$, 6H), 1.72 (s, NC(C*H*$_3$)N, 9H), 1.29 (d, CH*Me*$_2$, 36H). ^{13}C{^{1}H} NMR (151 MHz, C_6D_6, 293 K): δ 172.6 (N*C*N), 93.5 (O*C*H$_2$NMe$_2$), 48.4 (Me$_2$*C*H), 42.5 (OCH$_2$N*Me*$_2$), 25.1 (*Me*$_2$CH), 12.5 (NC(*C*H$_3$)N). Anal. Calcd for $C_{27}H_{59}N_7OTh$ (729.9): C, 44.43; H, 8.15; N, 13.43. Found: C, 44.31; H, 8.40; N, 13.27. Mp: 270-280 °C (dec.) FTIR (Nujol): 2805 (m), 2760 (m), 2700 (m), 2600 (w), 1488 (s), 1359 (s), 1335

(s), 1314 (s), 1262 (w), 1199 (s), 1174 (s), 1162 (s), 1123 (s), 1094 (s), 1050 (m), 1012 (m), 853 (m), 804 (s), 722 (w), 619 (s), 573 (w), 544 (w), 435 (w). Crystals suitable for single-crystal X-ray diffraction studies were grown from a concentrated HMDSO solution stored at -35 °C for 16 h.

Th(SCH$_2$SiMe$_3$)(MeC(N^{i}Pr)$_2$)$_3$ (2.5): Solid **2.2** (0.150 g, 0.202 mmol) was added to a 4 mL dram vial and dissolved in 1 mL C_6D_6. To a separate dram vial was added Ph_3Sb=S (0.0790 g, 0.205 mmol), which was dissolved in 0.5 mL C_6D_6. The Ph_3Sb=S solution was then added to the solution of **2.2**, resulting in a change from colorless to light yellow/green and the solution became cloudy. The solution was then filtered directly into a *J*-Young NMR tube and was sealed with a Teflon screw cap. The NMR tube was then placed in an aluminum heating block at 100 °C for 10 days and was monitored by ^{1}H NMR spectroscopy. Upon completion, the contents of the NMR tube were emptied into a 20 mL scintillation vial and the volatiles were removed under reduced pressure. The residue was then triturated with pentane (2 x 2 mL) and extracted into pentane (4 mL). The solution was concentrated to 1.5 mL, filtered through Celite, and placed in the freezer at -35 °C for 16 h, resulting in the precipitation of Ph_3Sb as determined by ^{1}H NMR spectroscopy. The mother liquor was isolated and volatiles were then removed under reduced pressure. The resulting residue was extracted into Et_2O (2 mL), and concentrated to an oil. This oil was then placed in the freezer at -35 °C for 16 h, resulting in solid **2.5** (0.136 g). By ^{1}H NMR, 0.20 eq. of Ph_3Sb remained in the solid isolated, which could not be purified further. The yield of **2.5** was thus reduced to 0.125 g (79.9%). ^{1}H NMR (600 MHz, C_6D_6, 293 K): δ 3.67 (sept, C*H*Me$_2$, 6H), 2.42 (s, C*H*$_2$SiMe$_3$, 2H), 1.67 (s, NC(C*H*$_3$)N, 9H), 1.31 (d, CH*Me*$_2$, 36H), 0.40 (s, CH$_2$Si*Me*$_3$, 9H). ^{13}C{^{1}H} NMR (151 MHz, C_6D_6, 293 K): δ = 173.6 (N*C*N), 48.8 (Me$_2$*C*H), 25.0 (*Me*$_2$CH), 14.6 (*C*H$_2$SiMe$_3$), 13.2 (NC(*C*H$_3$)N), -0.9 (CH$_2$Si*Me*$_3$). Anal. Calcd for $C_{28}H_{62}N_6SiSTh$ (775.0): C, 43.39; H, 8.06; N, 10.84. Found: C, 44.58; H, 7.80; N, 10.02. Anal. Calcd for $C_{28}H_{62}N_6SiSTh$ w/0.20 eq. $C_{18}H_{15}Sb$: C, 44.91; H, 7.75; N, 9.94. Mp: 51-54 °C. FTIR (Nujol): 1487 (s), 1361 (s), 1335 (s), 1314 (s), 1253 (m), 1242 (s), 1198 (s), 1174 (s), 1124 (s), 1051 (m), 1014 (s), 859 (s), 840 (s), 805 (s), 776 (w), 752 (w), 729 (s), 696 (s), 646 (w), 619 (m), 574 (w), 543 (w), 461 (w). Crystals suitable for single-crystal X-Ray diffraction studies were grown from a concentrated Et_2O solution stored at -35 °C for 16 h.

Th(SSCH$_2$SiMe$_3$)(MeC(N^{i}Pr)$_2$)$_3$ (2.6): Solid **2.2** (0.0745 g, 0.100 mmol) was added to a 20 mL scintillation vial containing a magnetic stir bar and was dissolved in 2 mL toluene. To this stirred solution was added a toluene solution (4 mL) of Ph_3Sb=S (0.0770 g, 0.200 mmol), resulting in a slightly cloudy light green/yellow solution. The solution was stirred at ambient temperature for 1 hour, during which the solution cloudiness dissipated. The volatiles were removed under reduced pressure, and the resulting solid was extracted into pentane (6 mL). The solution was concentrated to ~1 mL and placed in the freezer at -35 °C for 16 h, resulting in the precipitation of Ph_3Sb as determined by ^{1}H NMR spectroscopy. The mother liquor was isolated and volatiles were then removed under reduced pressure. The resulting residue was extracted into HMDSO (2 mL), concentrated to ~0.8 mL and placed in the freezer at -35 °C for 16 h, resulting in solid **2.6** (0.0440 g). By ^{1}H NMR, 0.093 eq. of Ph_3Sb remained in the solid isolated, which could not be purified further. The yield of **2.6** was thus reduced to 0.0423 g (52.2%). ^{1}H NMR (600 MHz, C_6D_6, 293 K): δ 3.77 (sept, C*H*Me$_2$, 6H), 2.27 (s, C*H*$_2$SiMe$_3$, 2H), 1.71 (s, NC(C*H*$_3$)N, 9H), 1.32 (d, CH*Me*$_2$, 36H), 0.21 (s, CH$_2$Si*Me*$_3$, 9H). ^{13}C{^{1}H} NMR (151 MHz, C_6D_6, 293 K): δ = 173.4 (N*C*N), 48.7 (Me$_2$*C*H), 28.1 (*C*H$_2$SiMe$_3$), 25.2 (*Me*$_2$CH), 14.6 (NC(*C*H$_3$)N), -1.0 (CH$_2$Si*Me*$_3$). Anal. Calcd for

$C_{28}H_{62}N_6SiS_2Th$ (807.1): C, 41.67; H, 7.74; N, 10.41. Found: C, 41.23; H, 7.20; N, 9.32. Anal. Calcd for $C_{28}H_{62}N_6SiSTh$ w/0.093 eq. $C_{18}H_{15}Sb$: C, 42.43; H, 7.61; N, 10.00. Mp: 89-97 °C. FTIR (Nujol): 1335 (s), 1248 (m), 1197 (s), 1173 (m), 1123 (w), 1052 (w), 1013 (w), 844 (s), 805 (m), 774 (w), 729 (s), 696 (m). Crystals suitable for X-ray diffraction studies were grown from a concentrated HMDSO solution stored at -35 °C for 24 h.

Th(SeCH$_2$SiMe$_3$)(MeC(N^{i}Pr)$_2$)$_3$ (2.7): Solid **2.2** (0.300 g, 0.404 mmol) and Me_3P=Se (0.0656 g, 0.423 mmol) were combined in a 100 mL Schlenk flask, and toluene (10 mL) was added *via* cannula. The solution was then stirred at 60 °C under an inert atmosphere of nitrogen for 24 h. The volatiles were removed under reduced pressure, and the resulting solid was triturated with hexane (10 mL) and extracted into pentane (6 mL). The solution was filtered through Celite, concentrated to ~1.5 mL and placed in the freezer at -35 °C for 16 h, resulting in colorless crystals of **2.7** (0.245 g, 73.8%). ^{1}H NMR (600 MHz, C_6D_6, 293 K): δ 3.64 (sept, C*H*Me$_2$, 6H), 2.25 (s, C*H*$_2$SiMe$_3$, 2H), 1.64 (s, NC(C*H*$_3$)N, 9H), 1.31 (d, CH*Me*$_2$, 36H), 0.44 (s, CH$_2$Si*Me*$_3$, 9H). ^{13}C{^{1}H} NMR (126 MHz, C_6D_6, 293 K): δ = 173.8 (N*C*N), 48.9 (Me$_2$*C*H), 25.0 (*Me*$_2$CH), 13.3 (NC(*C*H$_3$)N), 2.33 (*C*H$_2$SiMe$_3$), -0.2 (CH$_2$Si*Me*$_3$). ^{77}Se{^{1}H} (76.3 MHz, C_6D_6, 293 K): δ 221 (s, $\nu_{1/2}$ = 19 Hz). Anal. Calcd for $C_{28}H_{62}N_6SiSeTh$ (821.9): C, 40.92; H, 7.60; N, 10.22. Found: C, 40.38; H, 7.58; N, 10.27. Mp: 92-96 °C. FTIR (Nujol): 1486 (s), 1361 (s), 1336 (s), 1314 (s), 1242 (m), 1200 (s), 1174 (m), 1123 (m), 1054 (m), 1014 (m), 857 (m), 835 (m), 807 (m), 777 (w), 721 (w), 684 (w), 619 (w), 575 (w), 543 (w). Crystals suitable for single-crystal X-ray diffraction studies were grown from a concentrated pentane solution stored at -35 °C for 16 h.

Th(TeCH$_2$SiMe$_3$)(MeC(N^{i}Pr)$_2$)$_3$ (2.8): Solid **2.2** (0.300 g, 0.404 mmol) was added to a 20 mL scintillation vial containing a magnetic stir bar and was dissolved in 2 mL toluene. To this stirred solution was added a toluene solution (4 mL) of Cy_3P=Te (0.165 g, 0.404 mmol) dropwise over 2 minutes. The resulting light-yellow solution was allowed to stir at ambient temperature for 1 hour. The volatiles were removed under reduced pressure, and the resulting solid was triturated with hexane (6 mL) and extracted into hexane (6 mL). The solution was placed in the freezer at -35 °C for 16 h, resulting in a pale-yellow solid, which by ^{1}H NMR contained trace PCy_3. Removal of the mother liquor, and recrystallization of the isolated solid from hexane (4 mL) resulted in pure **2.8** as a pale-yellow solid (0.235 g, 66.9%). ^{1}H NMR (600 MHz, C_6D_6, 293 K): δ 3.59 (sept, C*H*Me$_2$, 6H), 2.20 (s, C*H*$_2$SiMe$_3$, 2H) 1.61 (s, NC(C*H*$_3$)N, 9H), 1.29 (d, CH*Me*$_2$, 36H), 0.46 (s, CH$_2$Si*Me*$_3$, 9H). ^{13}C{^{1}H} (126 MHz, C_6D_6, 293 K): δ 174.1 (N*C*N), 49.0 (Me$_2$*C*H), 25.0 (*Me*$_2$CH), 13.2 (NC(*C*H$_3$)N), 0.6 (CH$_2$Si*Me*$_3$), -24.2 (*C*H$_2$SiMe$_3$). ^{125}Te{^{1}H} (189 MHz, C_6D_6, 293 K): δ -13 (s, $\nu_{1/2}$ = 25 Hz). Anal. Calcd for $C_{28}H_{62}N_6SiTeTh$ (870.6): C, 38.63; H, 7.18; N, 9.65. Found: C, 38.26; H, 7.13; N, 9.34. Mp: 115-120 °C. FTIR (Nujol): 1362 (s), 1336 (s), 1312 (s), 1240 (m), 1196 (s), 1175 (s), 1136 (w), 1123 (m), 1050 (w), 1013 (m), 857 (s), 831 (s), 805 (m), 767 (w), 715 (w), 617 (w), 575 (w), 543 (w). Crystals suitable for single-crystal X-ray diffraction studies were grown from a concentrated Et_2O solution stored at -35 °C for 16 h.

Crystallographic Procedures. Single-crystal X-ray diffraction experiments were performed at the UC Berkeley CHEXRAY crystallographic facility. Measurements of all complexes were performed on either a Bruker APEX-I or APEX-II CCD area detector using Mo Kα radiation (λ = 0.71073 Å). Crystals were kept at 100(2) K throughout collection. Data collection was performed with Bruker APEX2 software (v. 2014.11). Data refinement and reduction were performed with Bruker SAINT (V8.34A). All structures were solved with

SHELXT.53.[84] Structures were refined with SHELXL-2014.[85] Molecular graphics were computed with Mercury 3.10. All non-hydrogen atoms were refined anisotropically, and hydrogen atoms were included at the geometrically calculated positions and refined using a riding model.

Computational Details. All calculations were carried out in the UC Berkeley Molecular Graphics and Computation Facility with the Gaussian 09 program (G09),[86] employing the B3PW91 functional with standard 6-31G(d,p) basis set for C, H, N, O, Si, S, and Se elements and Stuttgart RLC ECP from EMSL basis set exchange (https://bse.pnl.gov/bse/portal) for the Th element,[87] to fully optimize the geometries of the complexes (no symmetry restrictions imposed (C_1)). For crystallographically characterized complexes (**2.2, 2.4,** and **2.7**), the atomic coordinates from X-ray diffraction studies were used as the initial input for these calculations. All resultant stationary points were subsequently characterized by vibrational analyses, from which their respective Gibbs Free Energies (ΔG) were extracted at 298 K and 1 atm of pressure in the gas phase.

References

(1) Burns, C. J.; Eisen, M. S. In *The Chemistry of the Actinide and Transactinide Elements*; Morss, L. R., Edelstein, N. M., Fuge, J., Eds.; Springer: Berlin, Heidelberg, 2006; Vol. *5*.
(2) Jones, M. B.; Gaunt, A. J. *Chem. Rev.* **2013**, *113*, 1137-1198.
(3) Hayton, T. W. *Chem. Commun*. **2013**, *49*, 2956−2973.
(4) Liddle, S. T. *Angew. Chem. Int. Ed.* **2015**, *54*, 2-40.
(5) Ephritikhine, M. *Organometallics* **2013**, *32*, 2464−2488.
(6) *Fuel Cycle Stewardship in a Nuclear Renaissance*; The Royal Society Science Policy Centre Report 10/11; The Royal Society: London, 2011; ISBN 978-0-85403-891-6.
(7) Hudson, M. J.; Harwood, L. M.; Laventine, D. M.; Lewis, F. W. *Inorg. Chem.* **2013**, *52*, 3414-3428.
(8) Love, J. B. *Dalton Trans.* **2015**, *44*, 2515-2516.
(9) Jensen, M. P.; Bond, A. H. *J. Am. Chem. Soc.* **2002**, *124*, 9870-9877.
(10) Miguirditchian, M.; Guillaneux, D.; Guillaumont, D.; Moisy, P.; Madic, C.; Jensen, M. P.; Nash, K. L. *Inorg. Chem.* **2005**, *44*, 1404-1412.
(11) Ingram, K. I. M.; Tassell, M. J.; Gaunt, A. J.; Kaltsoyannis, N. *Inorg. Chem.* **2008**, *47*, 7824-7833.
(12) Smiles, D. E.; Wu, G.; Hayton, T. W. *New J. Chem.* **2015**, *39*, 7563-7566.
(13) Smiles, D. E.; Wu, G.; Hayton, T. W. *Inorg. Chem.* **2014**, *53*, 10240-10247.
(14) Matson, E. M.; Breshears, A. T.; Kiernicki, J. J.; Newell, B. S.; Fanwick, P. E.; Shores, M. P.; Walensky, J. R.; Bart, S. C. *Inorg. Chem.* **2014**, *53*, 12977-12985.
(15) Zhou, E.; Ren, W.; Hou, G.; Zi, G.; Fang, D.-C.; Walter, M. D. *Organometallics* **2015**, *34*, 3637-3647.
(16) Ren, W.; Song, H.; Zi, G.; Walter, M. D. *Dalton Trans.* **2012**, *41*, 5965-5973.
(17) Ren, W.; Zi, G.; Walter, M. D. *Organometallics* **2012**, *31*, 672-679.
(18) Behrle, A. C.; Barnes, C. L.; Kaltsoyannis, N.; Walensky, J. R. *Inorg. Chem.* **2013**, *52*, 10623-10631.
(19) Smiles, D. E.; Wu, G.; Hrobárik, P.; Hayton, T. W. *J. Am. Chem. Soc.* **2016**, *138*, 814-825.
(20) Rehe, D.; Kornienko, A. Y.; Emge, T. J.; Brennan, J. G. *Inorg. Chem.* **2016**, *55*, 6961-6967.
(21) Romanelli, M.; Kumar, G. A.; Emge, T. J.; Riman, R. E.; Brennan, J. G. *Angew. Chem. Int. Ed.* **2008**, *47*, 6049-6051.
(22) Kornienko, A.; Emge, T. J.; Kumar, G. A.; Riman, R. E.; Brennan, J. G. *J. Am. Chem. Soc.* **2005**, *127*, 3501-3505.
(23) Banerjee, S.; Kumar, G. A.; Riman, R. E.; Emge, T. J.; Brennan, J. G. *J. Am. Chem. Soc.* **2007**, *129*, 5926-5931.
(24) Marks, T. J. *Acc. Chem. Res.* **1992**, *25*, 57-65.
(25) Manriquez, J. M.; Fagan, P. J.; Marks, T. J.; Day, C. S.; Day, V. W. *J. Am. Chem. Soc.* **1978**, *100*, 7112-7114.
(26) Yang, X.; Stern, C. L.; Marks, T. J. *Organometallics* **1991**, *10*, 840-842.
(27) Lauke, H.; Swepston, P. J.; Marks, T. J. *J. Am. Chem. Soc.* **1984**, *106*, 6841-6843.
(28) Manriquez, J. M.; Fagan, P. J.; Marks, T. J. *J. Am. Chem. Soc.* **1978**, *100*, 3939-3941.

(29) Bruno, J. W.; Kalina, D. G.; Mintz, E. A.; Marks, T. J. *J. Am. Chem. Soc.* **1982**, *104*, 1860-1869.
(30) Jantunen, K. C.; Burns, C. J.; Castro-Rodriguez, I.; Da Re, R. E.; Golden, J. T.; Morris, D. E.; Scott, B. L.; Taw, F. L.; Kiplinger, J. L. *Organometallics* **2004**, *23*, 4682-4692.
(31) Evans, W. J.; Walensky, J. R.; Ziller, J. W.; Rheingold, A. L. *Organometallics* **2009**, *28*, 3350-3357.
(32) Siladke, N. A.; Webster, C. L.; Walensky, J. R.; Takase, M. K.; Ziller, J. W.; Grant, D. J.; Gagliardi, L.; Evans, W. J. *Organometallics* **2013**, *32*, 6522-6531.
(33) Haskel, A.; Straub, T.; Dash, A. K.; Eisen, M. S. *J. Am. Chem. Soc.* **1999**, *121*, 3014-3024.
(34) Monreal, M. J.; Diaconescu, P. L. *Organometallics* **2008**, *27*, 1702-1706.
(35) Simpson, S. J.; Turner, H. W.; Andersen, R. A. *Inorg. Chem.* **1981**, *20*, 2991-2995.
(36) Cruz, C. A.; Emslie, D. J. H.; Robertson, C. M.; Harrington, L. E.; Jenkins, H. A.; Britten, J. F. *Organometallics* **2009**, *28*, 1891-1899.
(37) Wedler, M.; Knösel, F.; Edelmann, F. T.; Behrens, U. *Chem. Ber.* **1992**, *125*, 1313-1318.
(38) Kincaid, K.; Gerlach, C. P.; Giesbrecht, G. R.; Hagadorn, J. R.; Whitener, G. D.; Shafir, A.; Arnold, J. *Organometallics* **1999**, *18*, 5360-5366.
(39) Hagadorn, J. R.; Arnold, J. *Organometallics* **1998**, *17*, 1355-1368.
(40) Hagadorn, J. R.; Arnold, J. *J. Am. Chem. Soc.* **1996**, *118*, 893-894.
(41) Hagadorn, J. R.; Arnold, J. *Angew. Chem. Int. Ed.* **1998**, *37*, 1729-1731.
(42) Schmidt, J. A. R.; Arnold, J. *Chem. Commun.* **1999**, 2149-2150.
(43) Camp, C.; Settineri, N.; Lefèvre, J.; Jupp, A. R.; Goicoechea, J. M.; Maron, L.; Arnold, J. *Chem. Sci.* **2015**, *6*, 6379-6384.
(44) Cantat, T.; Scott, B. L.; Kiplinger, J. L. *Chem. Commun*. **2010**, *46*, 919–921.
(45) Hao, S.; Gambarotta, S.; Bensimon, C.; Edema, J. J. H. *Inorg. Chim. Acta.* **1993**, *213*, 65-74.
(46) Fendrick, C. M.; Mintz, E. A.; Schertz, L. D.; Marks, T. J. *Organometallics* **1984**, *3*, 819-821.
(47) Butcher, R. J.; Clark, D. L.; Grumbine, S. K.; Scott, B. L.; Watkin, J. G. *Organometallics* **1996**, *15*, 1488-1496.
(48) Cruz, C. A.; Emslie, D. J. H.; Harrington, L. E.; Britten, J. F.; Robertson, C. M. *Organometallics* **2007**, *26*, 692-701.
(49) Clark, D. L.; Grumbine, S. K.; Scott, B. L.; Watkin, J. G. *Organometallics* **1996**, *15*, 949-957.
(50) Cruz, C. A.; Emslie, D. J. H.; Robertson, C. M.; Harrington, L. E.; Jenkins, H. A.; Britten, J. F. *Organometallics* **2009**, *28*, 1891-1899.
(51) Jantunen, K. C.; Batchelor, R. J.; Leznoff, D. B. *Organometallics* **2004**, *23*, 2186-2193.
(52) Bruno, J. W.; Smith, G. M.; Marks, T. J.; Fair, C. K.; Schultz, A. J.; Williams, J. M. *J. Am. Chem. Soc.* **1986**, *108*, 40-56.
(53) Rabinovich, E.; Aharonovich, S.; Botoshansky, M.; Eisen, M. S. *Dalton Trans.* **2010**, *39*, 6667-6676.
(54) Karmel, I. S. R.; Elkin, T.; Fridman, N.; Eisen, M. S. *Dalton Trans.* **2014**, *43*, 11376-11387.
(55) Karmel, I. S. R.; Fridman, N.; Eisen, M. S. *Organometallics* **2015**, *34*, 636-643.
(56) Kepp, K. P. *Inorg. Chem.* **2016**, *55*, 9461-9470.
(57) Holm, R. H. *Chem. Rev.* **1987**, *87*, 1401-1449.

(58) Pool, J. A.; Scott, B. L.; Kiplinger, J. L. *J. Am. Chem. Soc.* **2005**, *127*, 1338-1339.
(59) Hayes, C. E.; Sarazin, Y.; Katz, M. J.; Carpentier, J.-F.; Leznoff, D. B. *Organometallics* **2013**, *32*, 1183-1192.
(60) Berg, J. M.; Clark, D. L.; Huffman, J. C.; Morris, D. E.; Sattelberger, A. P.; Streib, W. E.; Van Der Sluys, W. G.; Watkin, J. G. *J. Am. Chem. Soc.* **1992**, *114*, 10811-10821.
(61) Clark, D. L.; Huffman, J. C.; Watkin, J. G. *J. Chem. Soc., Chem. Commun.* **1992**, 266-268.
(62) Clark, D. L.; Watkin, J. G. *Inorg. Chem.* **1993**, *32*, 1766-1772.
(63) Veith, M.; Rammo, A. *Z. Anorg. Allg. Chem.* **1997**, *623*, 861-872.
(64) Capps, K. B.; Wixmerten, B.; Bauer, A.; Hoff, C. D. *Inorg. Chem.* **1998**, *37*, 2861-2864.
(65) Evans, W. J.; Miller, K. A.; Kozimor, S. A.; Ziller, J. W.; DiPasquale, A. G.; Rheingold, A. L. *Organometallics* **2007**, *26*, 3568-3576.
(66) Smiles, D. E.; Wu, G.; Kaltsoyannis, N.; Hayton, T. W. *Chem. Sci.* **2015**, *6*, 3891-3899.
(67) Lin, Z.; Brock, C. P.; Marks, T. J. *Inorg. Chim. Acta.* **1988**, *141*, 145-149.
(68) Shaver, A.; Hartgerink, J.; Lal, R. D. *Organometallics* **1983**, *2*, 938-940.
(69) Legzdins, P.; Sánchez, L. *J. Am. Chem. Soc.* **1985**, *107*, 5525-5526.
(70) Evans, S. V.; Legzdins, P.; Rettig, S. J.; Sánchez, L.; Trotter, J. *Organometallics* **1987**, *6*, 7-9.
(71) Kanney, J.; Noll, B. C.; DuBois, M. R. *Organometallics* **2000**, *19*, 4925-4928.
(72) Galardon, E.; Tomas, A.; Selkti, M.; Roussel, P.; Artaud, I. *Inorg. Chem.* **2009**, *48*, 5921-5927.
(73) Siladke, N. A.; Ziller, J. W.; Evans, W. J. *J. Am. Chem. Soc.* **2011**, *133*, 3507-3516.
(74) Ren, W.; Zi, G.; Fang, D.-C.; Walter, M. D. *Chem. Eur. J.* **2011**, *17*, 12669-12682.
(75) Wrobleski, D. A.; Cromer, D. T.; Ortiz, J. V.; Rauchfuss, T. B.; Ryan, R. R.; Sattelberger, A. P. *J. Am. Chem. Soc.* **1986**, *108*, 174-175.
(76) Hector, A. L.; Levason, W.; Reid, G.; Reid, S. D.; Webster, M. *Chem. Mater.* **2008**, *20*, 5100-5106.
(77) Howard, W. A.; Trnka, T. M.; Parkin, G. *Inorg. Chem.* **1995**, *34*, 5900-5909.
(78) Werkema, E. L.; Andersen, R. A.; Maron, L.; Eisenstein, O. *Dalton Trans.* **2010**, *39*, 6648-6660.
(79) Giesbrecht, G. R.; Whitener, G. D.; Arnold, J. *Organometallics* **2000**, *19*, 2809-2812.
(80) McDonough, J. E.; Mendiratta, A.; Curley, J. J.; Fortman, G. C.; Fantasia, S.; Cummins, C. C.; Rybak-Akimova, E. V.; Nolan, S. P.; Hoff, C. D. *Inorg. Chem.* **2008**, *47*, 2133-2141.
(81) Garcia-Rodriguez, R.; Liu, H. *J. Am. Chem. Soc.* **2012**, *134*, 1400-1403.
(82) Provendier, H.; Santini, C. C.; Basset, J.-M.; Carmona, L. *Eur. J. Inorg. Chem.* **2003**, 2139-2144.
(83) Tötsch, W.; Peringer, P.; Sladky, F. *J. Chem. Soc., Chem. Commun.* **1981**, *16*, 841-842.
(84) Sheldrick, G. M. *Acta. Crystallogr. Sect. A* **2015**, *71*, 3-8.
(85) Sheldrick, G. M. *Acta. Crystallogr. Sect. A* **2008**, *64*, 112-122.
(86) Frisch, M. J.; Trucks, G. W.; Schlegel, H. B.; Scuseria, G. E.; Robb, M. A.; Cheeseman, J. R.; Scalmani, G.; Barone, V.; Mennucci, B.; Petersson, G. A.; Nakatsuji, H.; Caricato, M.; Li, X.; Hratchian, H. P.; Izmaylov, A. F.; Bloino, J.; Zheng, G.; Sonnenberg, J. L.; Hada, M.; Ehara, M.; Toyota, K.; Fukuda, R.; Hasegawa, J.; Ishida, M.; Nakajima, T.; Honda, Y.; Kitao, O.; Nakai, H.; Vreven, T.; Montgomery, J. A. J.; Peralta, J. E.; Ogliaro, F.;

Bearpark, M.; Heyd, J. J.; Brothers, E.; Kudin, K. N.; Staroverov, V. N.; Kobayashi, R.; Normand, J.; Raghavachari, K.; Rendell, A.; Burant, J. C.; Iyengar, S. S.; Tomasi, J.; Cossi, M.; Rega, N.; Millam, J. M.; Klene, M.; Knox, J. E.; Cross, J. B.; Bakken, V.; Adamo, C.; Jaramillo, J.; Gomperts, R.; Stratmann, R. E.; Yazyev, O.; Austin, A. J.; Cammi, R.; Pomelli, C.; Ochterski, J. W.; Martin, R. L.; Morokuma, K.; Zakrzewski, V. G.; Voth, G. A.; Salvador, P.; Dannenberg, J. J.; Dapprich, S.; Daniels, A. D.; Farkas, O.; Foresman, J. B.; Ortiz, J. V.; Cioslowski, J.; Fox, D. J. Gaussian, Inc.: Wallingford CT 2009.

(87) Kuechle, W.; Dolg, M.; Stoll, H.; Preuss, H. *Mol. Phys*. **1991**, *74*, 1245-1263.

Chapter 3

Insertion, Protonolysis and Photolysis Reactivity of a Thorium Monoalkyl Amidinate Complex

Chapter 3

Overview

Reactivity of metal-alkyl bonds has been a subject of intense research for decades, and although transition metals have received most of the attention there has been a significant effort by a number of chemists to investigate the reactivity of actinide alkyl complexes, specifically that of uranium and thorium, over the past four decades. While this reactivity has been extensively explored, it is well known that the ancillary ligand framework can have dramatic effects on how these metal-alkyl bonds react with substrates, and to date most of the reactivity of thorium-alkyl bonds has been examined with carbocyclic ligands as supporting ligands, specifically cyclopentadienyl derivatives. The following chapter describes the reactivity of the previously reported thorium monoalkyl complex supported by a tris-amidinate framework, which displayed, at times, divergent and unique reactivity compared to that seen with analogous cyclopentadienyl complexes. Portions of this chapter have previously been published in: Settineri, N. S. and Arnold, J. "Insertion, protonolysis and photolysis reactivity of a thorium monoalkyl amidinate complex." *Chem. Sci.*, **2018**, *9*, 2831-2841.

Introduction

The synthesis and reactivity of metal alkyl complexes have been a focus for organometallic chemists for decades due to their fundamental interest and relevance to catalytic and industrial processes. Studies of f-block alkyl complexes have been performed to a lesser extent, particularly those containing actinide metal centers. Actinide complexes display divergent coordination chemistry compared to the rest of the periodic table, and their large size combined with the accessibility of various oxidation states makes them particularly interesting for structural, electronic and reactivity studies.[1-6] Much of the focus concerning organoactinide investigations has been devoted to uranium, due to its redox capabilities.[4] Fewer studies have involved thorium, despite a fundamental question regarding whether thorium acts more as an actinide or Group IV metal.[7,8] Marks pioneered much of the work regarding thorium organometallic species bearing carbocyclic ancillary ligands (C_5R_5),[9-15] and many groups have continued to explore the reactivity of these systems.[16-20] Others have turned to non-carbocyclic ligands, in an attempt to investigate how complex stability and reactivity is affected by modifying the steric and electronic properties of the ancillary ligand framework.[21-28]

Having used a variety of non-carbocyclic ligand frameworks to stabilize and explore the reactivity of both transition metal and actinide complexes,[29-34] our group endeavored to expand these studies to thorium alkyl species. We have previously reported on the synthesis of a thorium monoalkyl species utilizing a tris-amidinate ancillary framework, specifically $Th(CH_2SiMe_3)(BIMA)_3$ (where BIMA = $MeC(N^iPr)_2$) (**2.2**), and its ability to insert chalcogen atoms to generate rare thorium chalcogenolate complexes.[35] In addition to the chalcogen insertion reactivity, the increased electrophilicity of the metal center with respect to analogous Cp-based systems led to the rare C-H activation of trimethylamine *N*-oxide. Inspired by this result, we sought to investigate how the unique properties of this system would impact the reactivity of **2.2** with a

variety of small molecules. Here we report on the reactivity of **2.2** with organic azides, isocyanide, CO, nitrile, 9-BBN, and various protic substrates, as well as the stability of **2.2** under photolytic conditions.

Results and Discussion

Insertion reactivity of Th(CH$_2$SiMe$_3$)(BIMA)$_3$. Having previously established the ability of **2.2** to undergo chalcogen atom insertion and generate unique thorium chalcogenolates,[35] we next sought to examine potential insertion chemistry of this monoalkyl system with various small molecules. Evans has described the insertion of carbodiimides and organic azides into one alkyl moiety of a $Cp^*_2ThR_2$ system;[16] with this in mind, we targeted the synthesis of a tetrakis(amidinate) complex through the reaction of **2.2** with *N,N'*-diisopropylcarbodiimide (Scheme 3.1). However, despite forcing conditions (100 °C), carbodiimide insertion into the Th-C bond was not observed, most likely a result of steric saturation around the metal center. Regardless, the alternative salt metathesis route using one equiv of $ThCl_4(DME)_2$[36] and 4.05 equiv of Li(BIMA)(THF)[37] and heating to 90 °C for 5 d afforded the desired homoleptic complex Th(BIMA)$_4$ (**3.1**) as colorless crystals in 66% yield (Scheme 3.1). The ^{1}H NMR spectrum of **3.1** reflects averaged C_4-symmetry in solution, with one set of peaks observed for the equivalent amidinate ligands. The molecular

Scheme 3.1. Attempted Insertion and Salt Metathesis Routes to Tetrakis(amidinate) Species

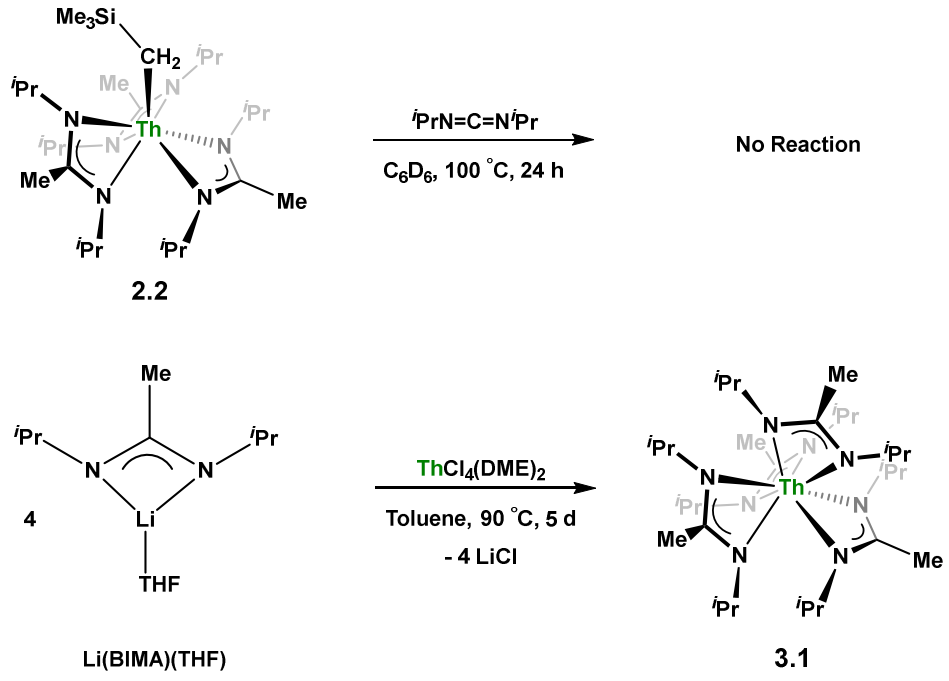

structure of **3.1**, determined by single-crystal X-ray diffraction studies, shows a pseudo-tetrahedral geometry of the amidinate ligands around the thorium center (Figure 3.1). The Th-N_{amid} bond lengths vary between 2.49 and 2.62 Å, a noticeably larger range than that seen in **2.2** (2.49-2.54 Å), indicating the significant steric congestion imposed by the isopropyl groups of the amidinate ligands. The structural parameters of **3.1** combined with the reaction conditions necessary to form **3.1** support the notion that insertion of carbodiimide into the Th-C bond was hindered by steric crowding and indicate that related insertion reactions might be subject to this constraint. Due to the steric protection afforded by the tetrakis(amidinate) framework and inspired by the work of Evans regarding low-valent thorium chemistry,[38] we attempted the reduction of **3.1** with KC_8 in the presence of 18-crown-6; nevertheless, no color change was observed and only starting material was isolated.

Reaction of **2.2** with an equivalent of *p*-tolyl azide resulted in insertion to form the triazenido complex Th[(*p*-tolyl)NNN(CH_2SiMe_3)-$\kappa^2N^{1,2}$](BIMA)$_3$ (**3.2**) in 83% yield (Scheme 3.2). ^{1}H NMR spectroscopy revealed the diagnostic downfield shift of the methylene resonance which was also observed to result from chalcogen insertion.[35] In the present case, we observed a shift from δ -0.08 ppm in **2.2** to δ 3.99 ppm in **3.2**, alongside shifted amidinate resonances and the appearance of resonances attributable to the *p*-tolyl group. Single-crystal X-ray diffraction studies revealed a $\kappa^2N^{1,2}$ coordination mode of the triazenido moiety (Figure 3.2), similar to that observed by Evans in the thorium metallocene system.[16] The metrical parameters relating to the N_3 fragment

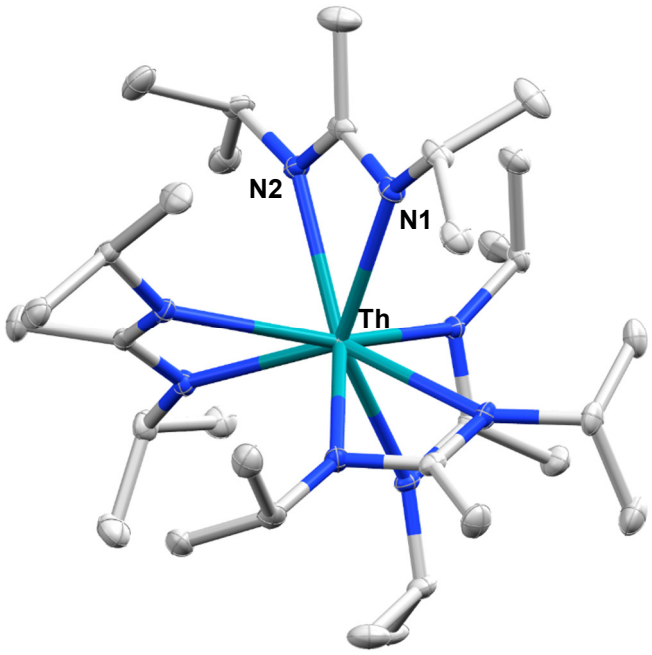

Figure 3.1. Molecular structure of **3.1**. Thermal ellipsoids drawn at the 50% probability level. Hydrogen atoms omitted for clarity.

Scheme 3.2. Synthesis of **3.2** and Thermal Decomposition to **3.3**

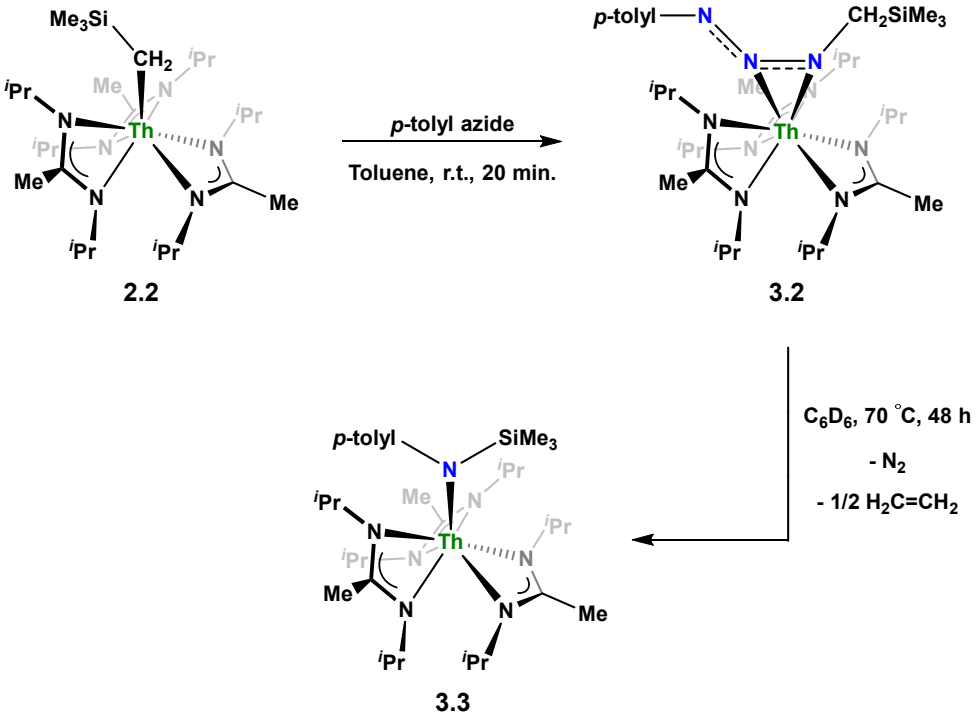

show the effect of electron delocalization, with bond lengths of 1.314(6) and 1.285(6) Å for N7-N8 and N8-N9, respectively, revealing a difference of only ~0.03 Å. In contrast, Evans' system that utilized adamantyl azide exhibited a more localized bonding for the analogous nitrogens, with bond lengths of 1.360(3) and 1.243(3) Å, a difference of ~0.12 Å.[16] The Th-N7 distance of 2.474(4) Å is ~0.1 Å longer than that seen in the thorium metallocene system, while the Th-N8 distance of 2.597(4) Å is the same in both. This indicates that the Th-N7 interaction is best described as anionic, whereas Th-N8 is more dative. The difference between **3.2** and Evans' metallocene system is likely a combination of both steric and electronic effects. Insertion with *tert*-butyl azide was also achieved; however, a mixture of two species was always observed, with the major product slowly converting to the minor product in solution until a ratio of ~4:1 was established. Heating did not alter this ratio, although elevated temperatures (100 °C) induced decomposition of the products. We postulate that the two products are both triazenido complexes that differ only in their coordination mode, with the $\kappa^2N^{1,2}$ and $\kappa^2N^{1,3}$ species present in solution. Exposing **3.2** to elevated temperatures in solution to see if a similar change in coordination mode would occur brought about a different result; **3.2** undergoes clean thermal decomposition to a new complex, with significantly shifted *p*-tolyl aromatic resonances and, most notably, no methylene resonance. Complete conversion was achieved within 48 h heating at 70 °C. This new product was stable to further heating. Close inspection of the ^{1}H NMR spectrum revealed a resonance attributable to ethylene.

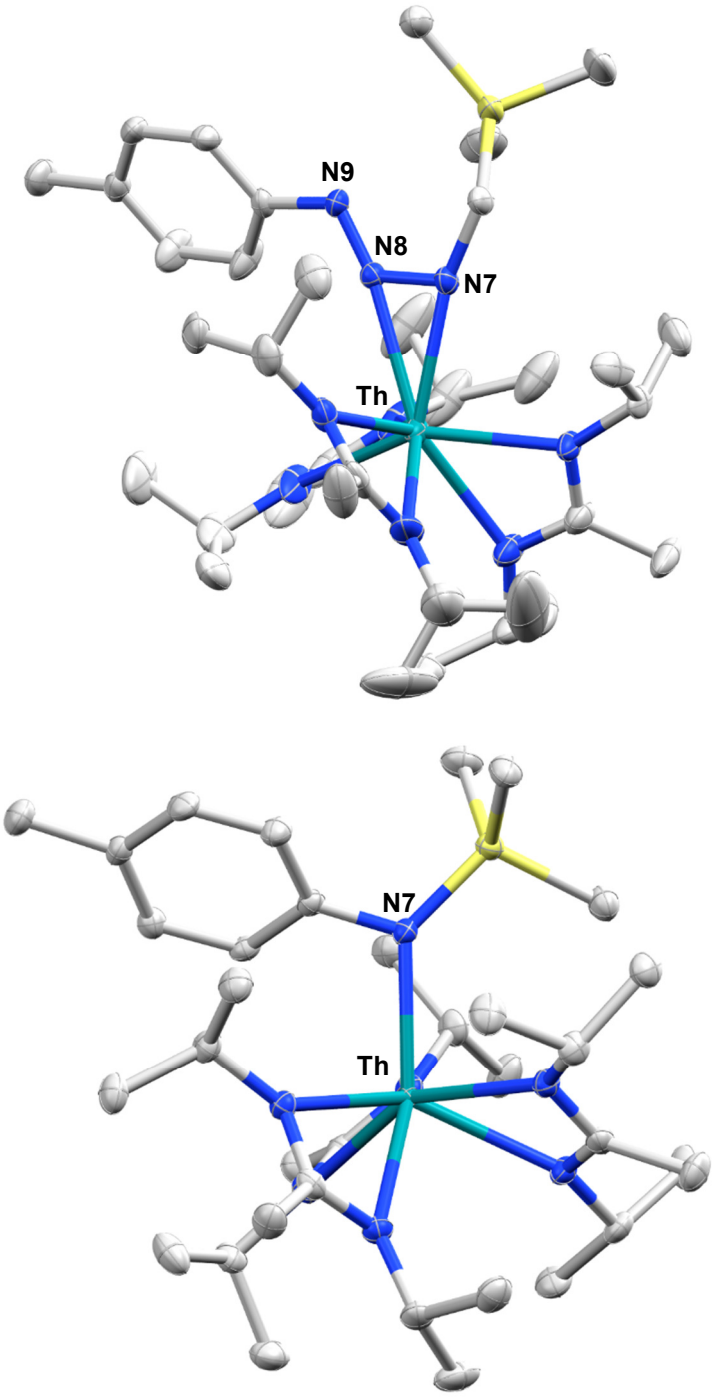

Figure 3.2. Molecular structures of **3.2** (top) and **3.3** (bottom). Thermal ellipsoids drawn at the 50% probability level. Hydrogen atoms omitted for clarity.

With this information we envisioned that **3.2** was losing diazomethane (N_2CH_2), which then decomposed to dinitrogen and ethylene,[39] resulting in the thorium amido species Th[(*p*-

tolyl)N(SiMe$_3$)$_3$](BIMA)$_3$ (**3.3**, Scheme 3.2). Ethylene formation may be the result of singlet methylene[40] generation and coupling upon N_2CH_2 decomposition. In order to try and trap the transient singlet methylene, similar heating experiments were conducted in the presence of 2-butyne and 1,1-diphenylethylene and monitored by ^{1}H NMR spectroscopy. Although it was difficult to unambiguously identify the trapped products (1,2-dimethylcyclopropene and 1,1-diphenylcyclopropane, respectively), the formation of ethylene was not seen with either trapping reagent, and a singlet at δ 1.13 ppm was observed in the 1,1-diphenylethylene experiment, which we tentatively assign to 1,1-diphenylcyclopropane.[41] We were able to confirm the identity of **3.3** as the thorium amido complex by X-ray diffraction studies (Figure 3.2). To the best of our knowledge, this is the first example of clean thermal decomposition of an actinide triazenido complex to the corresponding amido species. Bart and co-workers have observed thermal instability in certain uranium triazenido species, which has led to intractable mixtures of products.[42] However, the thermal decomposition of L^{tBu}Fe(η^2-HNNNAd) (where L^{tBu} = *tert*-butyl substituted-*N*,*N*′-diaryl-β-diketiminate, aryl = 2,6-^{i}Pr$_2$-C$_6$H$_3$) to the corresponding primary amido species L^{tBu}FeNHAd has been observed.[43] This was rationalized based on the instability of free H_2NNNR compounds with respect to loss of dinitrogen. The Th-N7 bond distance of 2.399(2) Å in **3.3** is very close to the Th-N bond distance of 2.389(2) Å observed by Walter and co-workers in [η^5-1,2,4-(Me$_3$C)$_3$C$_5$H$_2$]$_2$Th(Cl)-[N(*p*-tolyl)SiH$_2$Ph], which has a similar silyl amide environment.[44] The nitrogen atom of the amido exhibits a trigonal planar geometry ($\Sigma\angle \approx 360°$), also consistent with Walter's complex. A series of NMR scale experiments revealed the thermal decomposition to be concentration dependent, with higher concentrations of **3.2** leading to the generation of the silyl amine (*p*-tolyl)NH(SiMe$_3$) (as determined by ^{1}H NMR spectroscopy) and a mixture of unknown species. The identity of these products, along with mechanistic studies regarding the formation of **3.3** from **3.2**, has not yet been determined.

Although achieved with both transition metal[45-48] and uranium[49-52] species, isocyanide insertion into thorium alkyl bonds to form the corresponding η^2-iminoacyl complexes has not yet been reported. While sterics precluded the insertion of *N,N'*-diisopropylcarbodiimide, isocyanide insertion was realized with one equivalent of 2,6-dimethylphenylisocyanide and moderate heating, resulting in Th[η^2-(C=N)-2,6-Me$_2$-C$_6$H$_3$(CH$_2$SiMe$_3$)](BIMA)$_3$ (**3.4**) as a colorless, crystalline solid in 81% yield (Scheme 3.3). To the best of our knowledge this is the first thorium η^2-iminoacyl complex. Monitoring the reaction by ^{1}H NMR spectroscopy confirms that this insertion proceeds slowly at room temperature (>95% conversion after 96 h), presumably due to the steric clash between the xylyl moiety and amidinate ligands. As expected, the diagnostic downfield shift of the methylene singlet to δ 2.85 ppm indicated successful isocyanide insertion, along with new methyl and aromatic resonances corresponding to the xylyl group. X-ray diffraction studies reveal the η^2-coordination mode of the imine moiety, with the N7-C29 bond length of 1.299(4) Å falling in the range seen for other transition metal iminoacyl species (Figure 3.3).[45-52] The Th-N7 distance of 2.469(2) Å is noticeably shorter than that typically observed for a dative Th-N bond,[53-56] while the Th-C29 bond length of 2.529(3) Å is in the range observed for other σ-bonded alkyl moieties.[14,19,57] This insertion differs from that observed by Andersen and co-workers in their

Scheme 3.3. Insertion Reactivity of **2.2**

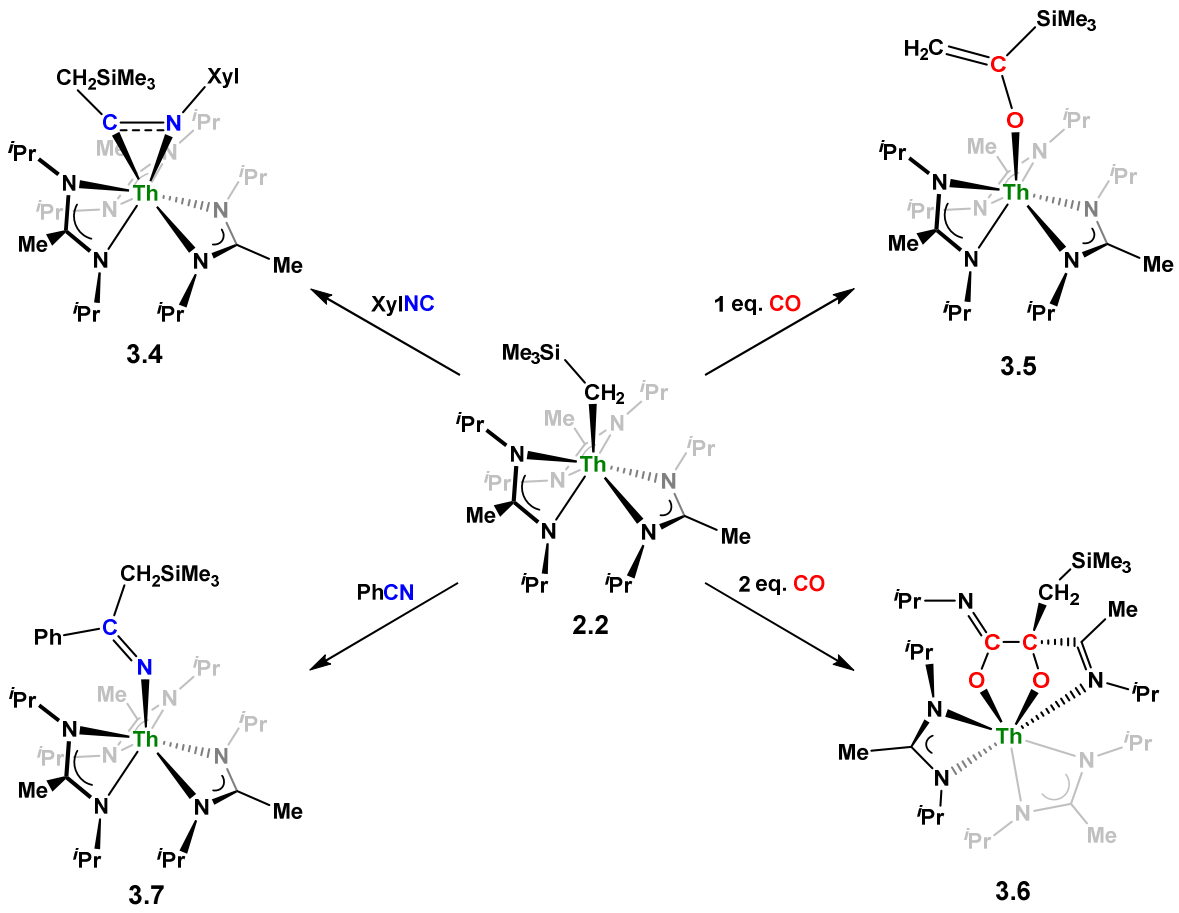

Th(*C*H$_2$SiMe$_2$*N*SiMe$_3$)(NR$_2$)$_2$ (where R = N(SiMe$_3$)$_2$) complex, which undergoes insertion of *tert*-butyl isocyanide into the C-Si bond of the metallacycle to produce Th[(^{t}Bu)*N*C(=CH$_2$)SiMe$_2$*N*SiMe$_3$)](NR$_2$)$_2$.[58] Similar reactivity was observed with CO in Andersen's system, resulting in Th[(*O*C(=CH$_2$)SiMe$_2$*N*SiMe$_3$)](NR$_2$)$_2$. Exposing **2.2** to 1 atm of CO resulted in the formation of two products with similar solubilities in non-polar solvents, precluding their clean isolation and characterization, despite yields of ~80% for the bulk mixture. The major species, as identified by ^{1}H NMR spectroscopy, exhibited inequivalent methylene protons that are consistent with those observed in Th[(*O*C(=CH$_2$)SiMe$_2$*N*SiMe$_3$)](NR$_2$)$_2$. This inequivalency would not be seen in the ^{1}H NMR spectrum of the thorium acyl species generated by simple CO insertion into the Th-C bond; thus, we postulated that it was likely a similar insertion into the C-Si bond of **2.2** occurred (Scheme 3.3). This insertion reactivity was confirmed by X-ray diffraction studies, as a few X-ray quality crystals were isolated from a very concentrated pentane solution stored at -35 °C for 3 days, confirming the identity of the CO insertion as the enolate

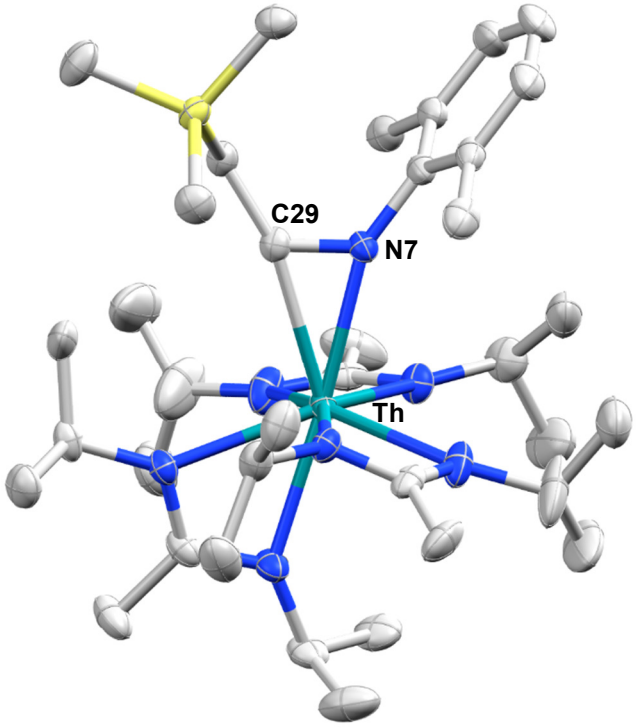

Figure 3.3. Molecular structure of **3.4**. Thermal ellipsoids drawn at the 50% probability level. Hydrogen atoms omitted for clarity.

complex Th[OC(=CH_2)$SiMe_3$](BIMA)$_3$ (**3.5**) (Figure 3.4). Complex **3.5** crystallized with two independent molecules in the asymmetric unit due to disorder in the enolate moiety; thus, the metrical parameters of only the nondisordered molecule will be discussed. The Th-O1 bond length of 2.216(2) Å is slightly longer than the Th-O bond length of 2.166(2) Å seen in Th(OCH_2NMe_2)(BIMA)$_3$,[35] while the C25-C26 bond length of 1.338(5) Å is consistent with a carbon-carbon double bond, and the trigonal planar geometry of C25 ($\Sigma\angle \approx 360°$) indicates sp^2 hybridization. This type of reactivity has precedent in both uranium and thorium systems,[52,58-61] and has been explained by initial CO insertion into the M-C bond to form the metal acyl, which then isomerizes to form a carbene-like intermediate that can then insert into the Si-C bond (Scheme 3.4). Alongside crystals of **3.5** were crystals of a different product, which we have tentatively assigned to the other resonances observed in the ^{1}H NMR spectrum of the bulk material. X-ray diffraction studies reveal this product to be Th[OC(N^{i}Pr)C(CH_2SiMe_3)(C(Me)N(^{i}Pr))O-κ^2O,O′](BIMA)$_2$ (**3.6**), the result of reductive CO coupling and insertion into an amidinate ligand (Figure 3.4). The Th-O1 and Th-O2 bond lengths of 2.220(2) and 2.290(2) Å, respectively, are slightly longer than that seen in **3.5** and Th(OCH_2NMe_2)(BIMA)$_3$,[35] while the bond length of 2.764(3) Å for Th-N5 is indicative of a dative interaction.[53-56] A single bond length of 1.558(5) Å is observed for C22-C23, whereas imine bonds are seen for C23-N6 and C20-N5 (1.266(4) and 1.282(4) Å, respectively). This type of CO coupling mimics the enediolate formation observed

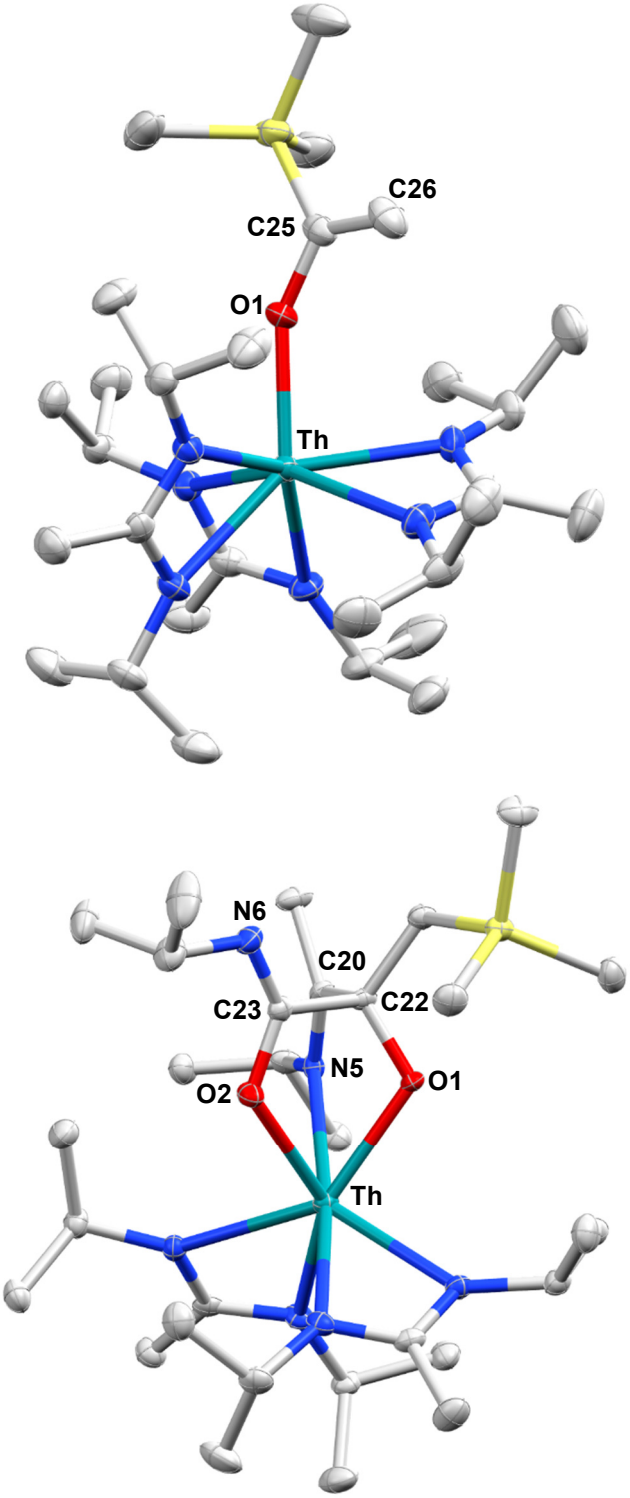

Figure 3.4. Molecular structures of **3.5** (top) and **3.6** (bottom). Ellipsoids drawn at the 50% probability level. Hydrogen atoms omitted for clarity.

with various actinide dialkyl systems.[59,62] Regarding the formation of **3.6**, it seems unlikely that this product is obtained from the interaction of a molecule of CO with **3.5**, due to the intact nature of the trimethylsilylmethyl alkyl fragment. Instead, it is likely that **3.6** results from "trapping" of

Scheme 3.4. Proposed pathways for the formation of **3.5** and **3.6**

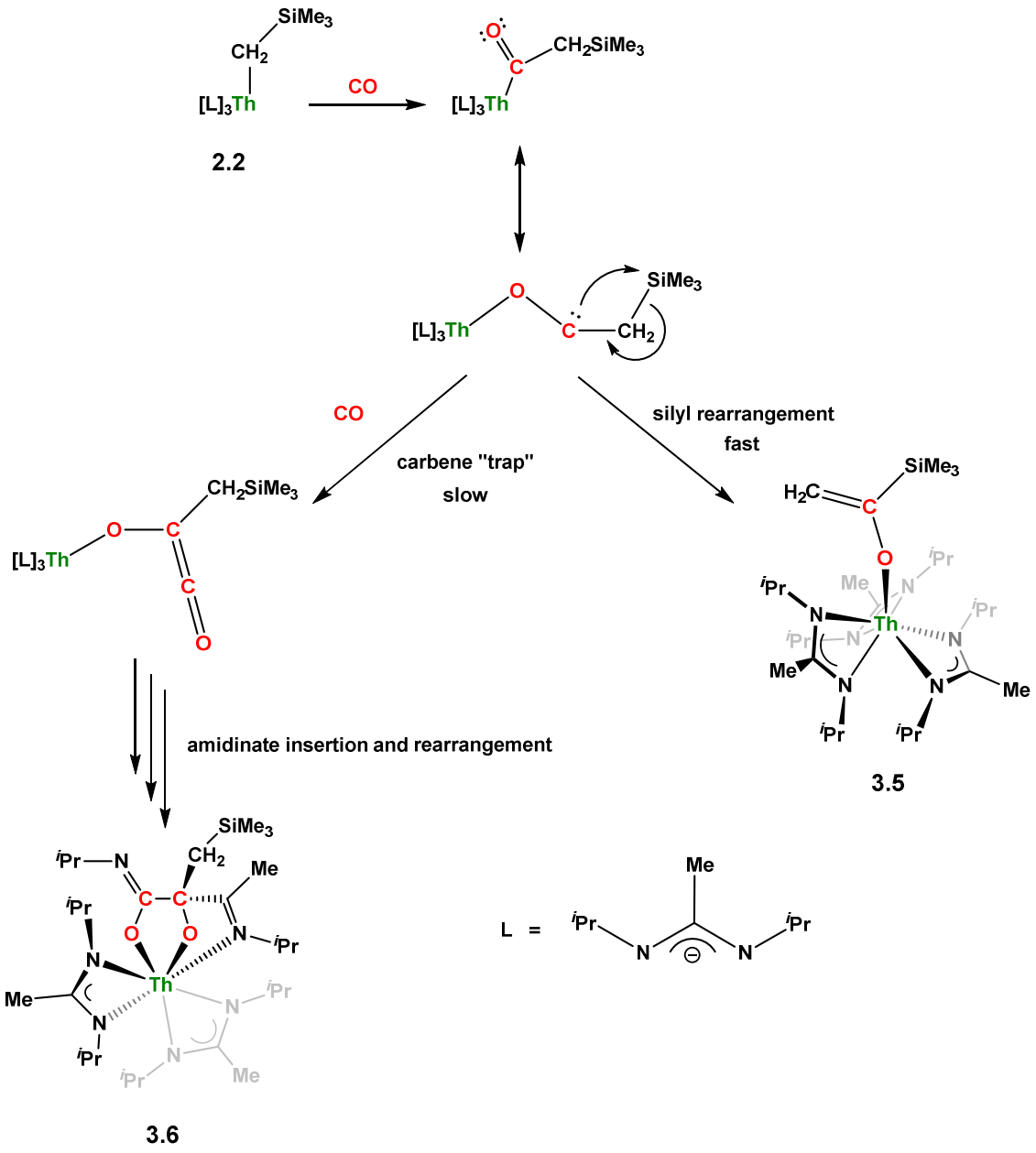

the carbene-like intermediate, which precedes formation of **3.5**, by another molecule of CO to form a transient ketene,[63] and subsequent insertion and rearrangement steps lead to **3.6** as the final product (Scheme 3.4). Kinetically this intermolecular process is slower than the intramolecular attack by the carbene intermediate on the C-Si bond, producing **3.5** as the major product. Exposing a mixture of **3.5** and **3.6** to additional CO did not change the ratio of products observed, confirming that **3.6** is not generated from **3.5**. In an attempt to avoid the formation of **3.6**, the slow addition of 1 eq. of CO to a stirred hexanes solution of **2.2** was conducted, resulting in clean formation of **3.5** in 64% yield. A synthetic strategy to produce **3.6** has not yet been developed. Looking to other small molecules, insertion reactivity with CO_2 and CS_2 did not proceed cleanly, yielding intractable mixtures.

Nitrile insertion was examined by the NMR-scale reaction of **2.2** and benzonitrile. The reaction was sufficiently complete (>95% conversion by ^{1}H NMR spectroscopy) upon heating to 100 °C for 72 h, resulting in the ketimide complex Th[-N=C(Ph)(CH_2SiMe_3)](BIMA)$_3$ (**3.7**) (Scheme 3.3). The methylene singlet is seen downfield at δ 2.73 ppm, along with new resonances corresponding to the aromatic protons of the phenyl ring, as well as aromatic resonances corresponding to the cyclotrimerization product of benzonitrile, 2,4,6-triphenyl-1,3,5-triazine.[64] The Lewis acid-catalysed cyclotrimerization of benzonitrile has been previously reported for lanthanide-imido species,[64] although the active species in this transformation has not been identified.

Protonolysis Reactivity of Th(CH$_2$SiMe$_3$)(BIMA)$_3$. Looking to exploit the basic nature of the alkyl moiety of **2.2**, protonolysis reactivity was explored with a variety of protic substrates, the results of which are summarized in Scheme 3.5. NMR scale experiments were carried out with **2.2** and 2,6-diisopropylaniline, resulting in the primary amido species Th(NH-2,6-^{i}Pr$_2$-C$_6$H$_3$)(BIMA)$_3$ (**3.8**), as well as **2.2** and 2,6-di-*tert*-butylphenol, resulting in the aryloxide complex Th(O-2,6-*t*-Bu$_2$C$_6$H$_3$)(BIMA)$_3$ (**3.9**), as determined by ^{1}H NMR spectroscopy. While phenol addition and subsequent elimination of $SiMe_4$ occurred within 12 h at room temperature, deprotonation of the aniline required extended reaction times at elevated temperatures before conversion to **3.8** was achieved. This can be rationalized on the basis of the higher pK_a of the aniline (~30 vs. 16.8 in DMSO),[65,66] as the sterics imposed by the 2,6-di-*tert*-butylphenol are greater than that of 2,6-diisopropylaniline. Similar NMR experiments were also performed with primary and secondary phosphines, namely mesitylphosphine and diphenylphosphine, resulting in the thorium phosphido complexes Th(PHMes)(BIMA)$_3$ (**3.10**) (Mes = 2,4,6,-trimethylphenyl) and Th(PPh$_2$)(BIMA)$_3$ (**3.11**), respectively, as determined by ^{1}H and ^{31}P NMR spectroscopy. Complex **3.10** exhibits a doublet at δ -45.4 ppm in the ^{31}P NMR spectrum with a $^1J_{P,H}$ coupling constant of 195 Hz; the corresponding doublet in the ^{1}H NMR is observed at δ 3.41 ppm. In the ^{31}P NMR spectrum of **3.11** a singlet is observed at δ 89.5 ppm corresponding to the thorium phosphido, alongside peaks consistent with the dehydrocoupled product Ph$_2$P-PPh$_2$ (δ -14.9 ppm)[67] and an unidentified phosphorus-containing species (δ 106 ppm). These ^{31}P chemical shifts are in the range reported for other primary and secondary thorium phosphido species.[68-70] The dehydrocoupling of phosphines has been reported with zirconium phosphido complexes under similar reaction

conditions.[71] Both complexes **3.10** and **3.11** required elevated temperatures and prolonged reaction times to reach completion. We sought a more scalable strategy to synthesize **3.10** without the need for harsh reaction conditions, as complex **3.10** has the potential to form a thorium phosphinidene via deprotonation of the phosphide ligand. With few examples of thorium phosphinidenes available, this would provide valuable information regarding metal-ligand multiple bonding between thorium and the heavier pnictogens.[72-74] Salt metathesis between the previously reported $ThCl(BIMA)_3$[35] and KPHMes[70] provided a more direct route to **3.10** as bright yellow crystals in 58% yield. Examination of the $^{13}C\{^1H\}$ NMR spectrum of **3.10** reveals rare through-space

Scheme 3.5. Protonolysis Reactivity of **2.2**

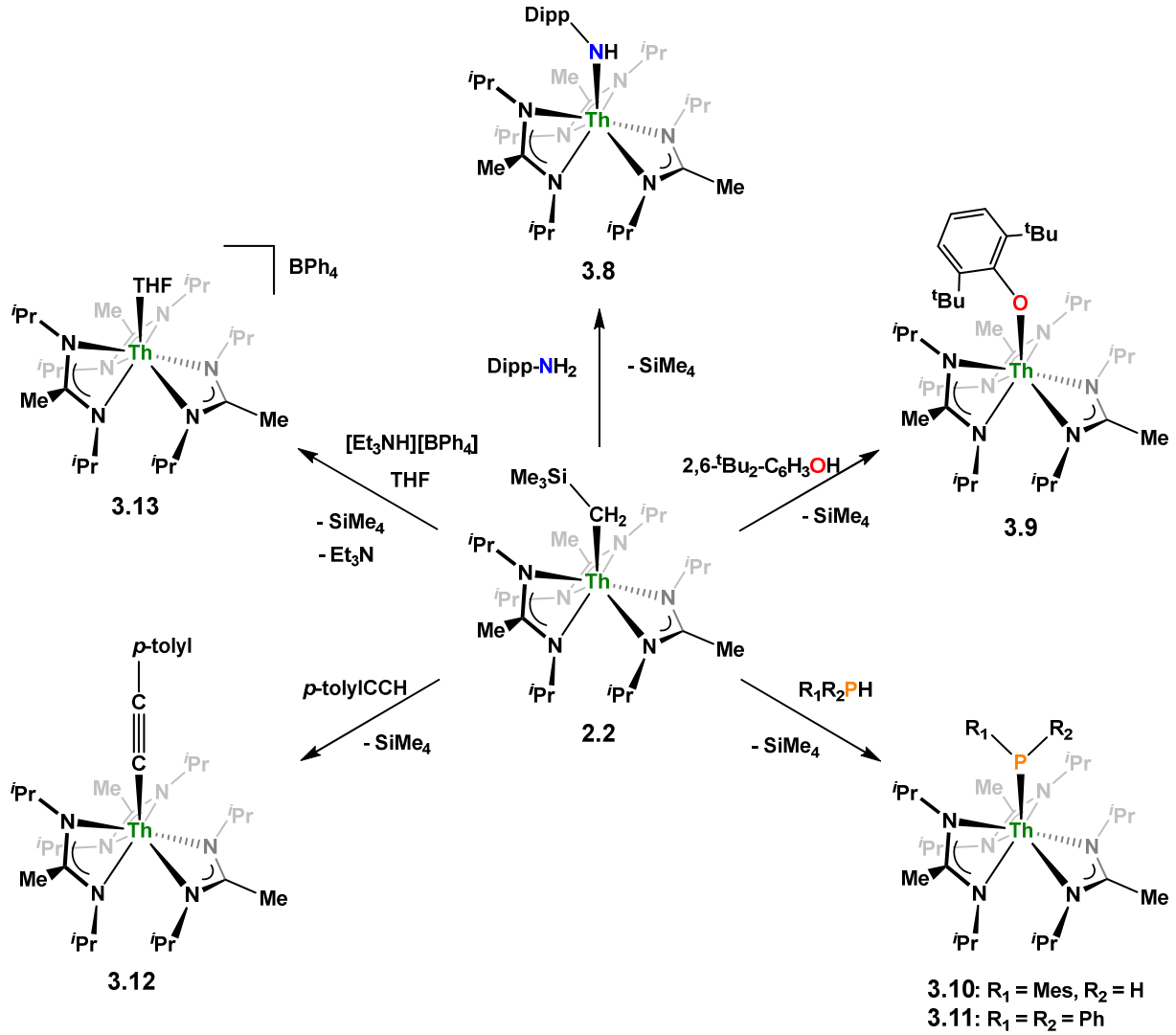

coupling of the phosphorus atom and the isopropyl methyl carbons of the BIMA ligand ($^{TS}J_{P,C}$ = 2.1 Hz), as well as the *ortho*-methyls of the mesitylene ring ($^{TS}J_{P,C}$ = 9.6 Hz).[75-78] This coupling is supported by the X-ray crystal structure of **3.10**, which displays a close proximity of the phosphorus atom to one of the BIMA isopropyl methyls (3.746(4) and 3.779(4) Å) and mesityl methyls (3.062(3) and 3.070(3) Å), along with significant pyramidalization at P ($\Sigma\angle \approx 311°$) in the two independent molecules found in the asymmetric unit (Figure 3.5). The orientation of the phosphorus lone pair toward these carbon atoms facilitates this spin-spin interaction. This is the first crystallographically characterized example of a thorium monophosphido species bearing a primary phosphide ligand; to date, only a handful of primary bis(phosphido)-thorium species have been isolated and characterized.[70,72,79] The Th-P bond lengths seen in the two molecules in the asymmetric unit (3.0497(8) and 3.0404(8) Å) are ~0.15 Å longer than those observed in the previously reported bis(phosphido)-thorium complexes. Attempts to deprotonate **3.10** to form the corresponding thorium phosphinidene have thus far proven unsuccessful.

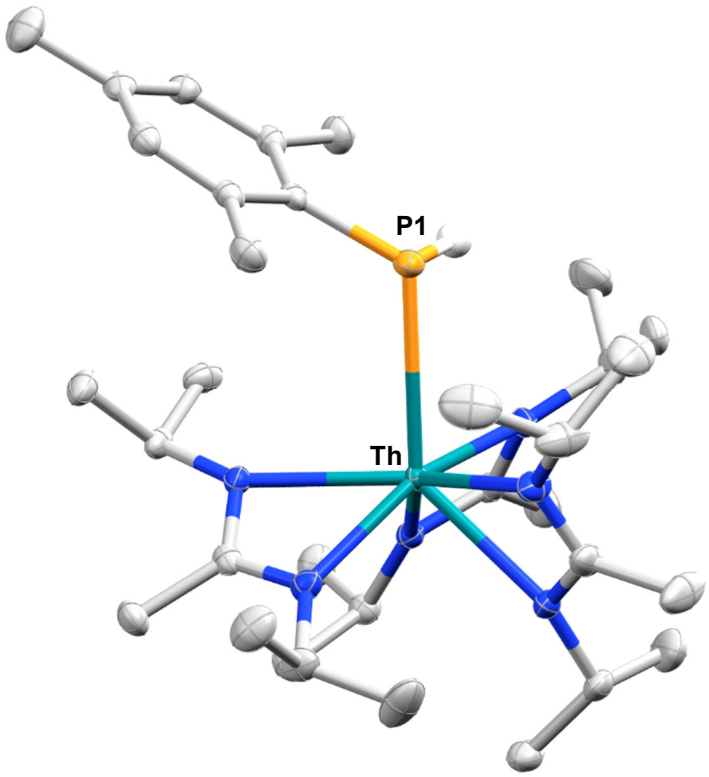

Figure 3.5. Molecular structure of **3.10**. Thermal ellipsoids drawn at the 50% probability level. Non-phosphorus-bound hydrogen atoms omitted for clarity.

The reaction of **2.2** with *p*-tolylacetylene proceeds cleanly, providing the thorium acetylide complex Th(C≡C-*p*-tolyl)(BIMA)$_3$ (**3.12**) as colorless crystals in 95% yield. This new alkynyl species may serve as a useful starting material for future chemistry, as other thorium acetylide complexes have been shown to be active catalysts for the linear oligomerization of terminal alkynes.[80] The ^{1}H NMR spectrum displays a C_3-symmetric amidinate environment along with resonances attributable to the *p*-tolyl group, while the $^{13}C\{^1H\}$ NMR spectrum features a downfield resonance of δ 189.2 ppm corresponding to the thorium-bound carbon atom of the alkyne, consistent with other thorium and group IV acetylides.[81-84] The IR spectrum exhibits a characteristic signal at 2061 cm^{-1} assigned to the C≡C stretch. X-ray diffraction studies reveal a near-linear Th-C≡C bond angle of 175.7(2)° and bond lengths of 2.542(2) and 1.219(3) Å for Th-C25 and C25-C26, respectively (Figure 3.6). The Th-C bond length in **3.12** is ~0.05 Å longer than that of the few other thorium acetylide species to have been characterized crystallographically,

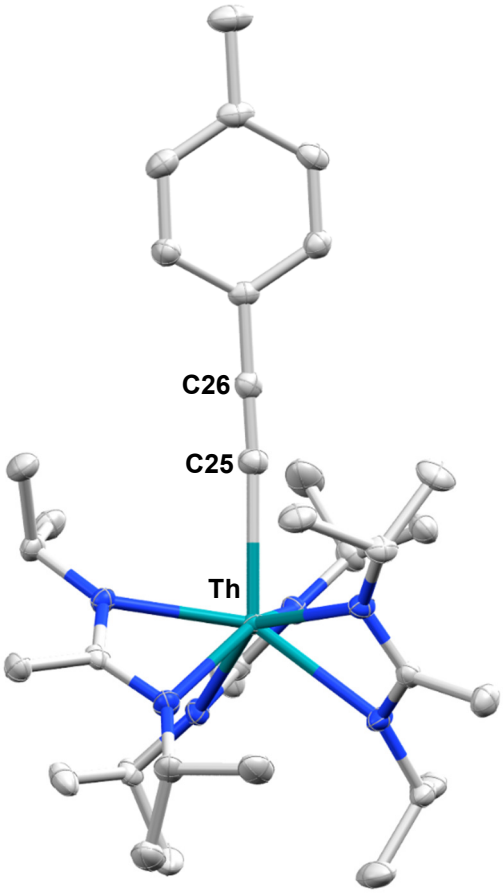

Figure 3.6. Molecular structure of **3.12**. Thermal ellipsoids drawn at the 50% probability level. Hydrogen atoms omitted for clarity.

namely [(L)Th(C≡CSiMe$_3$)$_2$] and [(L)Th(C≡CSi^{i}Pr$_3$)$_2$] (where L = *trans*-calix[2]benzene[2]pyrrolide), and Th(Bc^{Mes})$_2$(C≡C-*p*-tolyl)$_2$ (where Bc^{Mes} = mesityl-substituted bis(NHC)borate, NHC = N-heterocyclic carbene), which were only recently reported.[27,75]

A cationic species was targeted as a potential precursor to a Th(III) amidinate complex, as Evans has shown that reduction of a mixed cyclopentadienyl amidinate thorium cation, namely {(C$_5$Me$_5$)$_2$[^{i}PrNC(Me)N^{i}Pr]Th}{BPh$_3$Me}, can be achieved with KC$_8$.[85] Treatment of **2.2** with [Et$_3$NH][BPh$_4$][86] in THF led to the isolation of [Th(THF)(BIMA)$_3$][BPh$_4$] (**3.13**) as colorless crystals in 81% yield. The NH$_3$ and SiMe$_4$ byproducts were easily removed under vacuum upon workup, and X-ray diffraction studies show a well separated ion pair with one THF molecule coordinated to the thorium center and another co-crystallized in the lattice (Figure 3.7). The Th-N$_{amid}$ bond lengths are noticeably shorter (2.45-2.48 Å) than that of **2.2** or **3.1**, likely due to reduced steric congestion and higher electrophilicity of the metal center. The Th-O1 distance of 2.504(2) Å is in the range observed for other THF-bonded thorium complexes.[87-90] The second equivalent

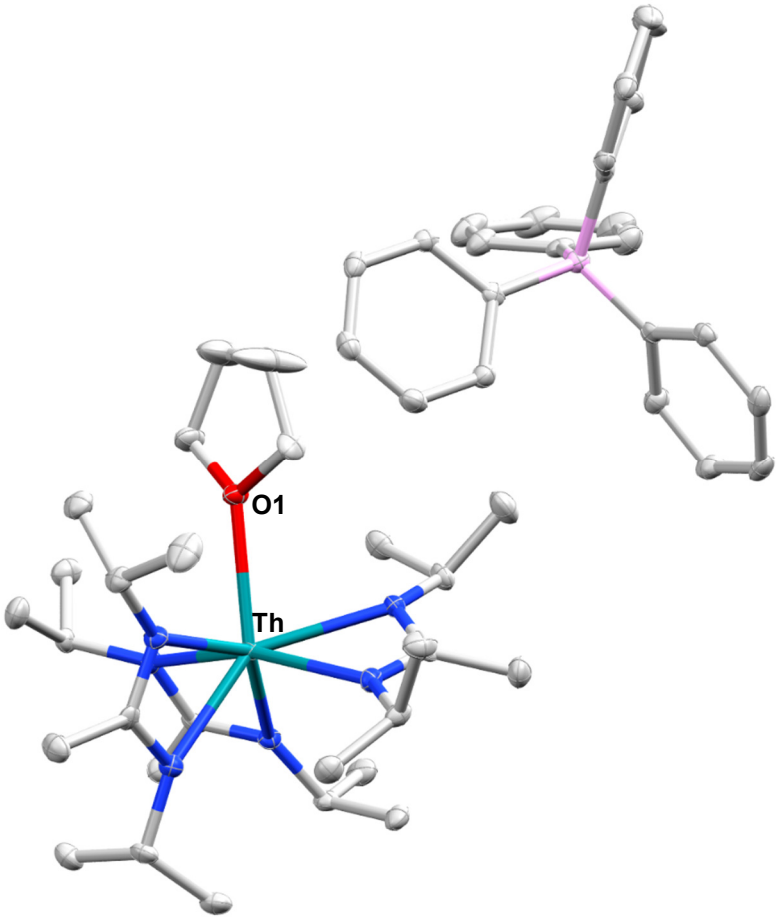

Figure 3.7. Molecular structure of **3.13**. Thermal ellipsoids drawn at the 50% probability level. Hydrogen atoms and THF solvent molecule omitted for clarity.

of THF can be removed under high vacuum. The ^{1}H NMR spectrum of dried **3.13** in $CDCl_3$ displays equivalent amidinate resonances, the aromatic peaks of the BPh_4 anion, and one set of resonances corresponding to coordinated THF. The complex displays appreciable stability in $CDCl_3$ but begins to decompose after ~24 h at room temperature. Attempted reduction of **3.13** with KC_8 in THF led to the isolation of **3.1**. No color change was observed throughout the reaction. Increasing the sterics of the R groups on the amidinate nitrogens may help stabilize a tris-amidinate Th(III) complex. Attempts to utilize H_2 as a protic substrate and form a thorium hydride complex were not successful.

Complex **2.2** undergoes ligand exchange with one equivalent of 9-borabicyclo[3.3.1]nonane (9-BBN), affording $(BIMA)_3Th(\mu\text{-}H)_2[B(C_8H_{14})]$ (**3.14**) alongside one equivalent of $(C_8H_{14})B(CH_2SiMe_3)$, as determined by $^{11}B\{^{1}H\}$ NMR spectroscopy (resonance observed at δ 84.3 ppm in C_6D_6).[91] Complex **3.14** was isolated in 66% crystalline yield after workup (Scheme 3.6). The thorium borohydride complex exhibits equivalent amidinate ligands in solution according to ^{1}H NMR spectroscopy. Additionally, broad μ-*H* resonances and several multiplets corresponding to the C_8H_{14} fragment are observed. The $^{11}B\{^{1}H\}$ NMR spectrum

Scheme 3.6. Ligand Exchange and Photolytic Reactivity of **2.2**

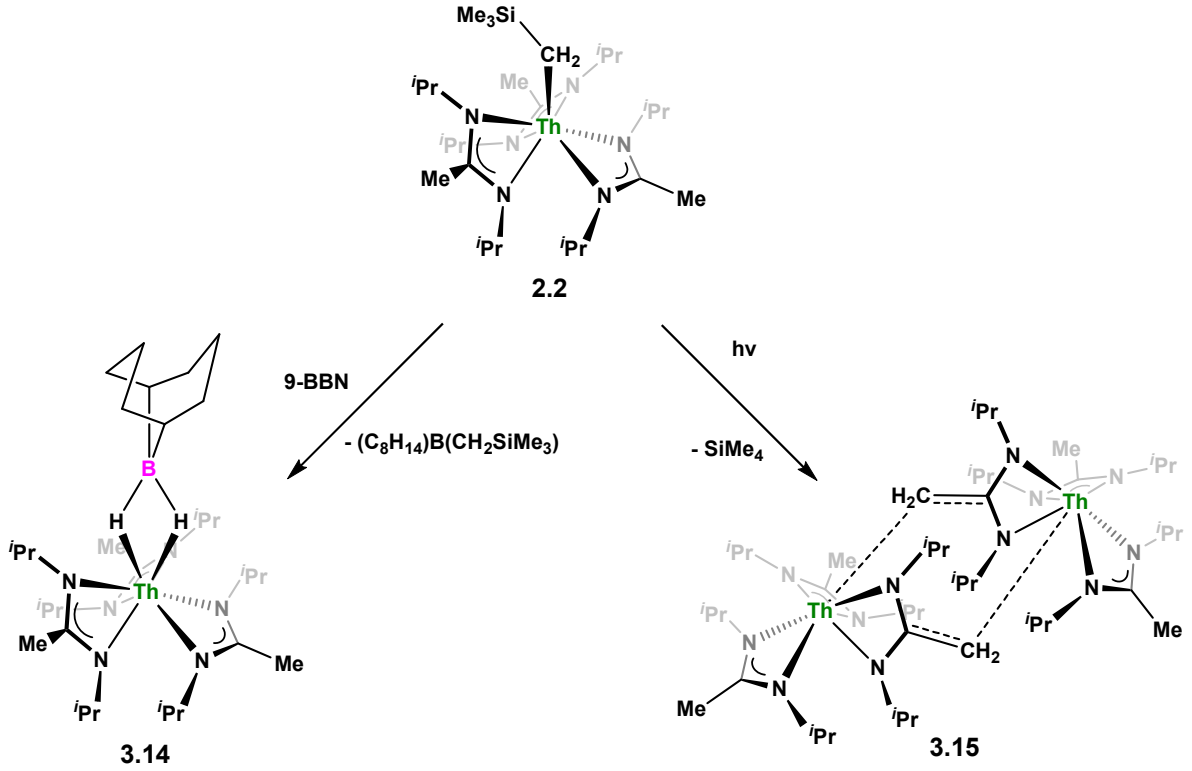

exhibits a single resonance at δ 4.90 ppm, which is in the range typically observed for boron hydrides.[92] FTIR spectroscopy reveals a broad B-H stretch centered at 2021 cm^{-1}. X-ray diffraction studies show an eight-coordinate thorium center bearing bridging hydrides bound to the 9-BBN moiety (Figure 3.8). The hydrides were located in the Fourier difference map and refined isotropically. The Th-B1 distance of 2.952(9) Å is significantly longer than typically observed with other thorium complexes containing bridging borohydrides (2.49(6)-2.670(2) Å),[93-97] but is within the range observed by Girolami and co-workers in the complexes $[Th(H_3BNMe_2BH_3)_4]$ and $[Th(H_3BNMe_2BH_3)_2(BH_4)_2]$, which exhibit Th-B distances between 2.848(9) to 3.193(5) Å.[97] Complex **3.14** is surprisingly stable both under photolytic and elevated temperature conditions, with no decomposition or elimination of H_2 observed.

Photolysis Reactivity of Th(CH$_2$SiMe$_3$)(BIMA)$_3$. Storage of **2.2** at room temperature under dry nitrogen for several weeks led to slight discoloration of the crystalline solid. While the ^{1}H NMR spectrum of this material showed very little change from that of pure **2.2**, we decided to investigate the stability of **2.2** under photolytic conditions. The UV-Vis spectrum of **2.2** features an absorption with λ_{max} = 295 nm, likely a ligand-based π-π* transition. Irradiation of **2.2** with UV-light centered at 253 nm in C_6D_6 and monitoring by ^{1}H NMR spectroscopy showed

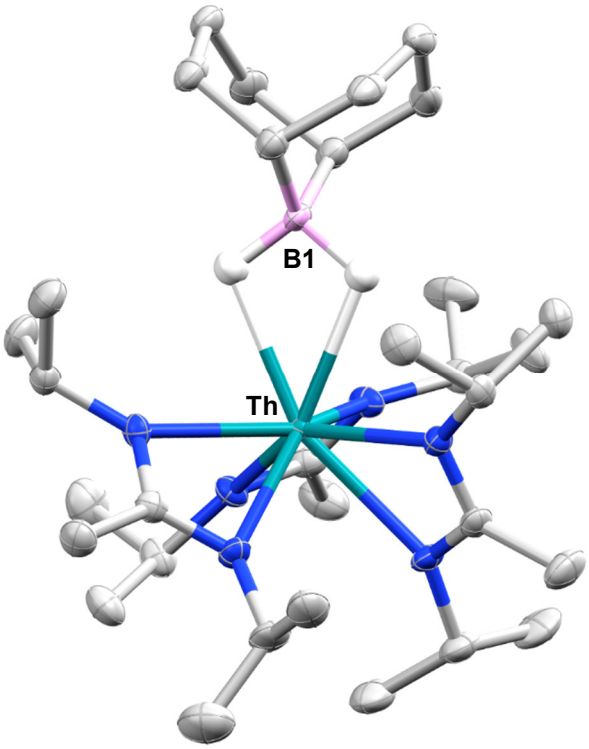

Figure 3.8. Molecular structure of **3.14**. Thermal ellipsoids drawn at the 50% probability level. Non-hydride hydrogen atoms omitted for clarity.

elimination of $SiMe_4$ alongside the production of a single new product, which displayed inequivalent amidinate ligands. Reaction times ranged from 24 h to 10 days, depending on the concentration of **2.2** in the sample (~0.02 – 0.45 M), with higher concentrations taking longer. Optimization of the reaction conditions, by use of a quartz reaction vessel, cyclohexane-d_{12} and a xenon arc lamp, resulted in significantly reduced reaction times (~2 h for ~0.03 M solution). Removal of $SiMe_4$ under vacuum and crystallization from toluene afforded $Th(BIMA)_2(BIMA^*)$ (**3.15**) in 53% yield [BIMA* = (^{i}Pr)NC(CH_2)N(^{i}Pr)]. Heating a solution of **2.2** at 100 °C for 24 h and monitoring by ^{1}H NMR spectroscopy showed no decomposition of **2.2** or production of **3.15**, eliminating the possibility that conversion of **2.2** to **3.15** was thermally-induced. Irradiation of **2.2** results in C-H activation of a methyl group on an amidinate ligand by the alkyl moiety, eliminating $SiMe_4$ and reducing the activated amidinate to a dianionic ligand (Scheme 3.6). Heterolytic bond cleavage of the Th-C bond resulting in a -CH_2SiMe_3 anion, which then attacks the methyl backbone of an amidinate ligand, is a possible explanation for the C-H activation and subsequent ligand reduction observed. This is a rare example of an amidinate dianion,[64] and the first generated under photolytic conditions. The ^{1}H NMR spectrum of **3.15** exhibits a set of equivalent amidinate resonances, alongside the resonances attributable to the amidinate dianion, specifically a 2H septet at δ 4.24 ppm, a 2H singlet at δ 3.44 ppm, and a 12H doublet at δ 1.53 ppm. The 6H singlet corresponding to the methyl groups of the monoanionic amidinates also appears at δ 1.53 ppm. In the $^{13}C\{^1H\}$ NMR spectrum the terminal methylene carbon resonance is observed noticeably downfield at δ 53.3 ppm, shifted by ~40 ppm from the amidinate methyls seen at δ 12.2 ppm, but further upfield than that typically seen with alkenes. The $^1J_{C\text{-}H}$ coupling constant of 157.6 Hz (as measured from the ^{13}C satellites observed in the ^{1}H NMR spectrum) is consistent with sp^2 hybridization and similar to that observed for ethylene.[98] The *ipso*-carbon of the amidinate dianion is shifted upfield to δ 154.2 from δ 172.8 ppm as observed for the monoanionic amidinates. X-ray diffraction studies reveal a dimeric structure where the thorium centers are bridged by the methylene carbon of the dianionic amidinate ligand (Figure 3.9). Complex **3.15** crystallizes in $P\bar{1}$ with the asymmetric unit containing only the monomer unit; the dimer is generated through inversion symmetry. The Th-C21 bond distance of 2.749(3) Å is significantly longer than the Th-C bond observed in **2.2** (2.557(3) Å), but shorter than the long Th-σ-alkyl bond distance of 2.875(9) Å observed by Liddle and co-workers in $Th\{N(CH_2CH_2NSiMe_2{}^t Bu)_2(CH_2CH_2NSiMe{}^t Bu\text{-}\mu\text{-}CH_2)\}]_2$.[90] The C20-C21 bond distance of 1.438(4) is longer by ~0.1 Å than typically observed for C-C double bonds, but this lengthening may be a result of delocalized electron density involved in the Th-C contact, reminiscent of a three-center two-electron bond. This is also manifested in the lack of planarity seen in the -N(CH_2)CN- unit of the amidinate dianion.

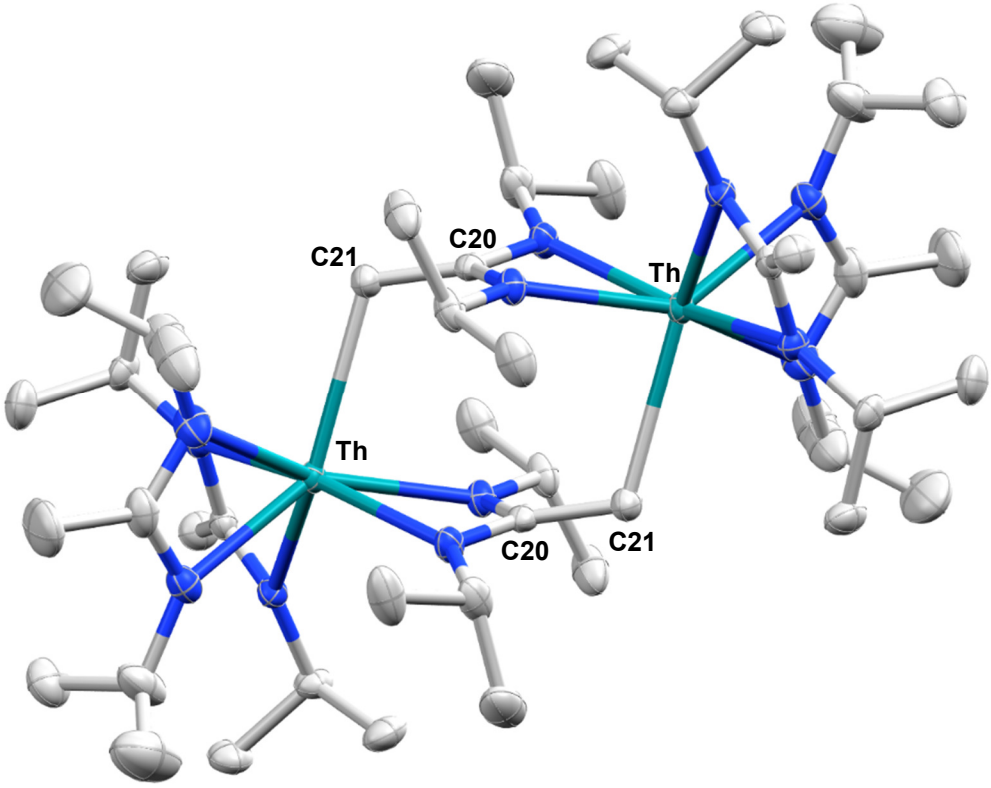

Figure 3.9. Molecular structure of **3.15**. Thermal ellipsoids drawn at the 50% probability level. Hydrogen atoms and toluene solvent molecular omitted for clarity.

Table 3.1. Crystal and Refinement Data for Complexes **3.1-3.6**, **3.10**, **3.12-3.15**

Complex	**3.1**	**3.2**	**3.3**	**3.4**	**3.5**	**3.6**
Chemical formula	$C_{32}H_{68}N_8Th$	$C_{35}H_{69}N_9SiTh$	$C_{34}H_{67}N_7SiTh$	$C_{37}H_{71}N_7SiTh$	$C_{29}H_{62}N_6OSiTh$	$C_{30}H_{62}N_6O_2SiTh$
Formula weight	796.99	876.12	834.07	874.15	770.97	798.98
Temperature (K)	100(2)	100(2)	100(2)	100(2)	100(2)	100(2)
Crystal system	Triclinic	Monoclinic	Monoclinic	Monoclinic	Triclinic	Triclinic
Space group	P-1	P 21/c	P 21/n	P 21/n	P-1	P-1
a (Å)	10.3830(4)	16.9023(9)	12.6373(9)	10.9839(5)	12.986(4)	9.4981(19)
b (Å)	11.3585(5)	11.4723(6)	17.8743(14)	20.9900(8)	16.992(5)	11.950(2)
c (Å)	17.4827(8)	21.7432(12)	17.1544(13)	18.2460(8)	17.337(4)	16.888(3)
α (°)	89.7768(18)	90	90	90	103.843(10)	90.32(3)
β (°)	89.4038(16)	95.127(3)	90.033(3)	93.4600(18)	97.592(10)	99.06(3)
γ (°)	63.7604(15)	90	90	90	93.871(12)	102.29(3)
V (Å^3)	1849.26(14)	4199.3(4)	3874.9(5)	4199.0(3)	3662.2(17)	1848.0(7)
Z	2	4	4	4	2	2
Densitiy (Mg m^{-3})	1.431	1.386	1.430	1.383	1.398	1.436
F(000)	812	1784	1696	1784	1560	808
Radiation Type	MoK_α	MoK_α	MoK_α	MoK_α	MoK_α	MoK_α
μ (mm^{-1})	4.063	3.613	3.910	3.612	4.132	4.099
Meas. Refl.	53843	142853	176871	60423	118651	148820
Indep. Refl.	6800	15081	7927	7751	15074	5516
R(int)	0.0291	0.0441	0.0315	0.0279	0.0399	0.0422
Final R indices [I > 2σ(I)]	R = 0.0107 R_w = 0.0273	R = 0.0317 R_w = 0.0700	R = 0.0153 R_w = 0.0309	R = 0.0220 R_w = 0.0470	R = 0.0273 R_w = 0.0556	R = 0.0198 R_w = 0.0453
GOF	1.090	1.089	1.062	1.072	1.109	1.099
$\Delta\rho_{max}$, $\Delta\rho_{min}$ (e Å^{-3})	0.499, -0.498	1.383, -1.210	1.145, -0.484	1.103, -1.137	3.302, -2.439	2.310, -0.709

Table 3.1 (Cont.). Crystal and Refinement Data for Complexes **3.1-3.6**, **3.10**, **3.12-3.15**

Complex	**3.10**	**3.12**	**3.13**	**3.14**	**3.15**
Chemical formula	$C_{33}H_{63}N_6PTh$	$C_{33}H_{58}N_6Th$	$C_{56}H_{87}N_6O_2BTh$	$C_{32}H_{67}BN_6Th$	$C_{24}H_{50}N_6Th$
Formula weight	806.92	770.91	1119.16	778.76	654.74
Temperature (K)	100(2)	100(2)	100(2)	100(2)	100(2)
Crystal system	Monoclinic	Monoclinic	Monoclinic	Monoclinic	Triclinic
Space group	P 21/n	P 21/c	P 21/c	P 21/n	P-1
a (Å)	22.5782(10)	19.0249(9)	18.6971(7)	12.1573(13)	11.5082(5)
b (Å)	13.2908(6)	10.3942(5)	15.8036(5)	18.4711(18)	12.3194(5)
c (Å)	25.4828(11)	19.1330(9)	18.9111(6)	16.3766(18)	12.8462(5)
α (°)	90	90	90	90	61.8432(7)
β (°)	100.332(2)	110.1048(18)	103.688(2)	90.215(5)	79.1570(8)
γ (°)	90	90	90	90	86.2752(8)
V (Å^3)	7522.9(6)	3553.0(3)	5429.2(3)	3677.5(7)	1576.47(11)
Z	4	4	4	4	1
Densitiy (Mg m^{-3})	1.425	1.441	1.369	1.407	1.468
F(000)	3264	1552	2304	1584	694
Radiation Type	MoK_α	MoK_α	MoK_α	MoK_α	MoK_α
μ (mm^{-1})	3.613	4.226	4.129	4.083	4.753
Meas. Refl.	169945	81894	138819	193336	47536
Indep. Refl.	18721	6536	10015	6764	5773
R(int)	0.0414	0.0265	0.0508	0.0484	0.0263
Final R indices [I > 2σ(I)]	R = 0.0252 R_w = 0.0510	R = 0.0148 R_w = 0.0320	R = 0.0204 R_w = 0.0407	R = 0.0207 R_w = 0.0452	R = 0.0207 R_w = 0.0488
Goodness-of-fit	1.042	1.102	1.068	1.103	1.117
$\Delta\rho_{max}$, $\Delta\rho_{min}$ (e Å^{-3})	1.986, -1.880	1.363, -0.615	1.452, -0.967	1.291, -0.758	2.661, -1.099

Conclusions

The amidinate-supported thorium monoalkyl complex **2.2** exhibits a variety of reactivity with small molecules, including insertion, protonolysis and photolysis. The insertion of *p*-tolyl azide leads to the thorium triazenido complex **3.2** which undergoes clean thermal decomposition at low concentrations to the corresponding amido complex **3.3**, through the loss of the unstable "N_2CH_2" fragment. This is the first example of an actinide complex undergoing this rare transformation. Insertion of xylyl isocyanide results in the first crystallographically characterized thorium iminoacyl complex. This insertion reactivity differs from that observed with CO, which instead results in the corresponding enolate species **3.5** upon CO insertion and rearrangement, as well as the unique double CO insertion and amidinate cleavage product **3.6**. The utility of the alkyl moiety as an internal base was demonstrated with a variety of protic substrates, with the thorium phosphido complex **3.10** generated via both protonolysis and salt metathesis routes, the latter providing a more scalable option for the synthesis of **3.10**. The photolytic elimination of $SiMe_4$ concomitant with the reduction of an amidinate ligand to form complex **3.15** is unprecedented reactivity with amidinate-supported metal complexes, and a rare example of a complex bearing a dianionic amidinate ligand.

Experimental Details

***General Procedures*.** Unless otherwise stated, all reactions were performed under an atmosphere of dry N_2 using standard Schlenk line techniques or in an MBraun N_2 atmosphere glovebox (<1.0 ppm of O_2/H_2O). All solvents were dried and degassed using a commercially available Phoenix SDS from JC Meyer Solvent Systems. All glassware, syringes, and cannulas were stored in a 140 °C oven for a minimum of 16 h prior to use. Deuterated solvents were vacuum-transferred from flasks containing sodium/benzophenone (C_6D_6, C_6D_{12}) or calcium hydride ($CDCl_3$), degassed with three freeze−pump−thaw cycles, and stored over molecular sieves. $ThCl_4(DME)_2$,[36] Li(BIMA)(THF),[37] $ThCl(BIMA)_3$ (**2.1**),[35] $Th(CH_2SiMe_3)(BIMA)_3$ (**2.2**),[35] *p*-tolyl azide,[99] and KPHMes[70] were prepared according to previously reported literature procedures. 2,6-diisopropylaniline was purchased from SigmaAldrich and distilled prior to use. 2,6-di-*tert*-butylphenol was sublimed prior to use. Benzonitrile was dried over CaH_2 and distilled prior to use. CO gas was purchased from Praxair, Inc. and used directly from the cylinder without purification. All other reagents were purchased from commercial sources and used as received. Unless otherwise stated, NMR spectra were collected at ambient temperature on a Bruker AV-300, AVB-400, AV-500, or AV-600 spectrometer. ^1H and $^{13}C\{^1H\}$ NMR chemical shifts (δ) are reported in ppm and were calibrated to residual solvent peaks. $^{11}B\{^1H\}$ and ^{31}P NMR shifts (δ) are referenced to an external standard ($BF_3{\cdot}Et_2O$ and H_3PO_4, respectively). Photo-activation reactions were conducted using a Rayonet reactor (model RPR-100) centered at 253 nm or a Newport 67005 Arc Lamp Housing containing a xenon arc lamp operating at 300 W. Melting points were determined on an Optimelt SRS instrument using capillary tubes sealed under dry N_2. Elemental analysis samples were sealed under vacuum and analyzed at either the London Metropolitan University or the University of California, Berkeley. Infrared spectra were collected on a Thermo Scientific Nicolet iS10 FTIR spectrophotometer using Nujol mulls pressed between KBr plates.

$Th(MeC(N^iPr)_2)_4$ (3.1): Solid $ThCl_4(DME)_2$ (2.49 g, 4.49 mmol) and Li(BIMA)(THF) (4.01 g, 18.2 mmol) were added to a 250 mL Schlenk flask containing a magnetic stir bar and suspended in toluene (60 mL). The suspension was then heated to 90 °C and stirred for 5 d, upon which the solution became slightly orange and contained a colorless precipitate. The volatiles were removed under reduced pressure, and the resulting solid was triturated with hexanes (2 x 30 mL), extracted into hexanes (2 x 50 mL), filtered through Celite, and concentrated to 15 mL. The solution was stored at -40 °C overnight, yielding **3.1** as analytically pure, colorless crystals (2.35 g, 65.6%). ^1H NMR (600 MHz, C_6D_6, 293 K): δ 3.72 (sept, C*H*Me$_2$, 8H, $^3J_{H,H}$ = 6.6 Hz), 1.80 (s, NC(C*H*$_3$)N, 12H), 1.30 (d, CH*Me*$_2$, 48H, $^3J_{H,H}$ = 6.6 Hz). $^{13}C\{^1H\}$ (151 MHz, C_6D_6, 293 K): δ 174.2 (N*C*N), 48.9 (*C*HMe$_2$), 25.3 (CH*Me*$_2$), 14.8 (NC(*C*H$_3$)N). Anal. Calcd for $C_{32}H_{68}N_8Th$ (797.0): C, 48.23; H, 8.60; N, 14.06. Found: C, 48.25; H, 8.71; N, 13.93. Mp: 150 °C (decomp.). FTIR (Nujol): 2595 (w), 1495 (s), 1358 (s), 1340 (s), 1310 (s), 1187 (s), 1175 (s), 1137 (m), 1118 (s), 1044 (m), 1007 (s), 943 (w), 798 (s), 722 (w), 618 (s), 577 (m), 542 (m). Crystals

suitable for single-crystal X-ray diffraction studies were grown from a concentrated hexanes solution stored at -35 °C for 16 h.

Th[(*p*-tolyl)NNN(CH$_2$SiMe$_3$)-κ^{2}N^{1,2}](MeC(N^{i}Pr)$_2$)$_3$ (3.2): Solid **2.2** (0.303 g, 0.408 mmol) was added to a 20 mL scintillation vial containing a magnetic stir bar and dissolved in 4 mL toluene. To this stirred solution was added neat *p*-tolyl azide (0.056 g, 0.421 mmol), resulting in an immediate solution color change from colorless to gold. The solution was allowed to stir at ambient temperature for 20 min. The volatiles were removed under reduced pressure, and the resulting solid was triturated with hexane (2 x 4 mL) and extracted into HMDSO (6 mL). The solution was concentrated to 2 mL, filtered through Celite, and placed in the freezer at -35 °C for 16 h, resulting in isolation of **3.2** as a tan solid (0.295 g, 83.4%). ^{1}H NMR (600 MHz, C_6D_6, 293 K): δ 7.81 (m, C*H*$_{ptolyl}$, 2H), 7.19 (m, C*H*$_{ptolyl}$, 2H), 3.99 (s, C*H*$_2$SiMe$_3$, 2H), 3.64 (sept, C*H*Me$_2$, 6H, $^3J_{H,H}$ = 6.6 Hz), 2.26 (s, C*H*$_{3,ptolyl}$, 3H), 1.68 (s, NC(C*H*$_3$)N, 9H), 1.16 (d, CH*Me*$_2$, 36H, $^3J_{H,H}$ = 6.6 Hz), 0.45 (s, CH$_2$Si*Me*$_3$, 9H). ^{13}C{^{1}H} NMR (151 MHz, C_6D_6, 293 K): δ 174.0 (N*C*N), 150.8 (*C*$_{ptolyl}$), 132.0 (*C*$_{ptolyl}$), 129.2 (*C*$_{ptolyl}$), 120.8 (*C*$_{ptolyl}$), 49.9 (*C*H$_2$SiMe$_3$), 48.6 (*C*HMe$_2$), 25.1 (CH*Me*$_2$), 21.2 (H$_3$*C*$_{ptolyl}$), 13.7 (NC(*C*H$_3$)N), 1.55 (CH$_2$Si*Me*$_3$). Anal. Calcd for $C_{35}H_{69}N_9SiTh$ (876.1): C, 47.98; H, 7.94; N, 14.39. Found: C, 47.98; H, 7.88; N, 14.18; Mp: 180 °C (decomp.) FTIR (Nujol): 1489 (s), 1344 (s), 1312 (m), 1243 (w), 1199 (m), 1173 (w), 1123 (w), 1051 (w), 1013 (w), 980 (w), 852 (m), 821 (w), 805 (w), 722 (w). Crystals suitable for single-crystal X-ray diffraction studies were grown from a concentrated diethyl ether solution stored at -35 °C for 48 h.

Generation of Th[(*p*-tolyl)N(SiMe$_3$)](MeC(N^{i}Pr)$_2$)$_3$ (3.3): Solid **3.2** (0.010 g, 0.0114 mmol) was added to a 4 mL dram vial and dissolved in C_6D_6 (0.6 mL). The solution was transferred to a *J*-Young NMR tube sealed with a Teflon screw cap and heated at 70 °C for 48 h, resulting in clean conversion to **3.3** as judged by ^{1}H NMR spectroscopy. ^{1}H NMR (600 MHz, C_6D_6, 293 K): δ 7.22 (m, C*H*$_{ptolyl}$, 2H), 7.11 (m, C*H*$_{ptolyl}$, 2H), 3.60 (sept, C*H*Me$_2$, 6H, $^3J_{H,H}$ = 6.5 Hz), 2.26 (s, C*H*$_{3,ptolyl}$, 3H), 1.74 (s, NC(C*H*$_3$)N, 9H), 1.20 (d, CH*Me*$_2$, 36H, $^3J_{H,H}$ = 6.5 Hz), 0.55 (s, Si*Me*$_3$, 9H). ^{13}C{^{1}H} NMR (151 MHz, C_6D_6, 293 K): δ 174.4 (N*C*N), 151.0 (*C*$_{ptolyl}$), 130.5 (*C*$_{ptolyl}$), 123.5 (*C*$_{ptolyl}$), 48.4 (*C*HMe$_2$), 25.1 (CH*Me*$_2$), 20.8 (H$_3$*C*$_{ptolyl}$), 15.6 (NC(*C*H$_3$)N), 3.40 (Si*Me*$_3$). Crystals suitable for single-crystal X-ray diffraction studies were grown from a concentrated pentane solution stored at -35 °C for 7 d.

Th[η^2-(C=N)-2,6-Me$_2$-C$_6$H$_3$(CH$_2$SiMe$_3$)](MeC(N^{i}Pr)$_2$)$_3$ (3.4): Solid **2.2** (0.400 g, 0.538 mmol) and 2,6-dimethylphenyl isocyanide (0.0717 g, 0.547 mmol) were combined in a 100 mL Schlenk flask containing a magnetic stir bar and dissolved in toluene (10 mL). The solution was then heated to 65 °C and stirred for 16 h. The volatiles were removed under reduced pressure, and the resulting solid was triturated with hexane (2 x 4 mL) and extracted into HMDSO (6 mL). The solution was then filtered through Celite, concentrated to ~0.6 mL and placed in the freezer at -35 °C for 16 h, resulting in off-white crystals of **3.4** (0.383 g, 81.3%). ^{1}H NMR (600 MHz, C_6D_6, 293 K): δ 7.06 (d, *m*-C*H*$_{Xyl}$, 2H, $^3J_{H,H}$ = 7.5 Hz), 6.96 (t, *p*-C*H*$_{Xyl}$, 1H, $^3J_{H,H}$ = 7.5 Hz), 3.85 (sept, C*H*Me$_2$, 6H, $^3J_{H,H}$ = 6.6 Hz), 2.85 (s, C*H*$_2$SiMe$_3$, 2H), 2.18 (s, C*H*$_{3,Xyl}$, 6H), 1.78 (s, NC(C*H*$_3$)N, 9H), 1.28 (d, CH*Me*$_2$, 36H, $^3J_{H,H}$ = 6.6 Hz), 0.11 (s, CH$_2$Si*Me*$_3$, 9H). ^{13}C{^{1}H} NMR

(151 MHz, C_6D_6, 293 K): δ 289.2 (-*C*=$NH_3C_6Me_2$), 174.3 (N*C*N), 152.6 (C_{Xyl}), 129.2 (C_{Xyl}), 128.2 (C_{Xyl}), 124.2 (C_{Xyl}), 48.4 (*C*HMe_2), 35.0 (*C*H_2SiMe_3), 25.4 (CH*Me*$_2$), 19.2 (-C=$NH_3C_6Me_2$), 15.5 (NC(*C*H_3)N), 1.1 (CH_2Si*Me*$_3$). Anal. Calcd for $C_{37}H_{71}N_7SiTh$ (874.2): C, 50.84; H, 8.19; N, 11.22. Found: C, 50.73; H, 8.00; N, 11.44. Mp: 198(4) °C. FTIR (Nujol): 1497 (s, $\nu_{C=N}$), 1377 (s), 1357 (s), 1336 (s), 1316 (s), 1248 (m), 1196 (s), 1174 (s), 1124 (m), 1093 (m), 1051 (m), 1012 (m), 860 (s), 802 (m), 762 (m), 692 (w), 672 (w), 622 (w), 575 (w), 481 (w), 431 (w). Crystals suitable for single-crystal X-ray diffraction studies were grown from a concentrated pentane solution stored at -35 °C for 16 h.

Th[OC(=CH$_2$)SiMe$_3$](MeC(N^{i}Pr)$_2$)$_3$ (3.5): Solid **2.2** (0.500 g, 0.673 mmol) was added to a 100 mL Schlenk tube containing a magnetic stir bar and dissolved in hexanes (30 mL). CO gas (16.5 mL, 0.673 mmol) was slowly added via syringe directly into the stirred solution over the course of two minutes at ambient temperature, during which the colorless solution became light green. The solution was then sealed off and allowed to stir at ambient temperature for 24 h. During this time the solution became nearly colorless. The volatiles were removed under reduced pressure, and the resulting residue was extracted into pentane (10 mL), filtered through Celite, and concentrated to <0.5 mL. The super saturated solution was placed in the freezer at -35 °C for 16 h, resulting in colorless crystals of **3.5** (0.330 g, 63.6%). ^{1}H NMR (600 MHz, C_6D_6, 293 K): δ 5.07 (d, *H*$_2$C=, 1H, $^2J_{H,H}$ = 1.0 Hz), 4.79 (d, *H*$_2$C=, 1H, $^2J_{H,H}$ = 1.0 Hz), 3.66 (sept, C*H*Me_2, 6H, $^3J_{H,H}$ = 6.3 Hz), 1.71 (s, NC(C*H*$_3$)N, 9H), 1.28 (d, CH*Me*$_2$, 36H, $^3J_{H,H}$ = 6.3 Hz), 0.39 (s, Si*Me*$_3$, 9H). ^{13}C{^{1}H} NMR (151 MHz, C_6D_6, 293 K): δ 173.0 (N*C*N), 104.7 (=*C*H$_2$), 48.5 (*C*HMe_2), 25.2 (CH*Me*$_2$), 13.0 (NC(*C*H_3)N), -0.6 (CH_2Si*Me*$_3$). Anal. Calcd for $C_{29}H_{62}N_6OSiTh$ (771.0): C, 45.18; H, 8.11; N, 10.90. Found: C, 44.96; H, 8.04; N, 10.94. Mp: 130 °C (decomp.). FTIR (Nujol): 1490 (s, $\nu_{C=C}$), 1377 (s), 1360 (s), 1331 (s), 1314 (s), 1254 (w), 1243 (m), 1219 (m), 1200 (s), 1174 (m), 1123 (m), 1051 (w), 1014 (m), 996 (s), 850 (s), 837 (s), 804 (m), 754 (w), 722 (w), 678 (w), 621 (w), 575 (w), 543 (w). X-ray quality crystals were grown from a mixture of **3.5** and **3.6**, as described below.

Generation of Th[OC(=CH$_2$)SiMe$_3$](MeC(N^{i}Pr)$_2$)$_3$ (3.5) and Th[OC(N^{i}Pr)C(CH$_2$SiMe$_3$)(C(Me)N(^{i}Pr))O-κ^2O,O′](MeC(N^{i}Pr)$_2$)$_2$ (3.6): Solid **2.2** (0.500 g, 0.673 mmol) was added to a 75 mL Schlenk tube containing a magnetic stir bar and dissolved in toluene (10 mL). CO was vigorously bubbled through this stirred solution for 5 min., during which the colorless solution became light green. The bubbling was then discontinued, and the tube sealed under an atmosphere of CO. The solution was then stirred at ambient temperature for 1 h, at which point the solution had become colorless. The volatiles were removed under reduced pressure, and the resulting residue was triturated with pentane (2 x 5 mL) and extracted into pentane (10 mL). The solution was filtered through Celite and concentrated to <0.5 mL. The super saturated solution was then placed in the freezer at -35 °C for 48 h, resulting in a microcrystalline solid (0.425 g) which contained both **3.5** and **3.6**. Despite repeated crystallization attempts, separation of **3.5** and **3.6** could not be achieved due to their similar solubility in non-polar solvents. Complex **3.5** could be identified by ^{1}H NMR spectroscopy. X-ray quality crystals were grown from a concentrated pentane solution stored at -35 °C for 72 h.

Individual crystals of **3.5** and **3.6** were selected from a mixture of crystals and distinguished based upon their unit cell.

Generation of Th[-N=C(Ph)(CH_2SiMe_3)](MeC(N^iPr)$_2$)$_3$ (3.7): Solid **2.2** (0.020 g, 0.027 mmol) was added to a 4 mL dram vial and dissolved in C_6D_6 (0.3 mL). In a separate dram vial, benzonitrile (0.0083 g, 0.081 mmol) was weighed out and dissolved in C_6D_6 (0.3 mL). The two solutions were then combined and added to a *J*-Young NMR tube sealed with a Teflon screw cap. The solution was then heated at 100 °C for 3 d, resulting in >95% conversion to **3.7** as judged by ^{1}H NMR spectroscopy. ^{1}H NMR (300 MHz, C_6D_6, 293 K): δ 7.89 (m, C*H*$_{Ar}$, 2H), 7.17-7.27 (m, C*H*$_{Ar}$, 3H), 3.67 (sept, C*H*Me$_2$, 6H, $^3J_{H,H}$ = 6.4 Hz), 2.73 (s, C*H*$_2$SiMe$_3$, 2H), 1.73 (s, NC(C*H*$_3$)N, 9H), 1.23 (d, CH*Me*$_2$, 36H, $^3J_{H,H}$ = 6.4 Hz), 0.20 (s, CH$_2$Si*Me*$_3$, 9H). It was also observed that ~0.33 eq. of 2,4,6-triphenyl triazine was also generated along with the ketimide product, as determined by its characteristic ^{1}H NMR resonances. ^{1}H NMR (300 MHz, C_6D_6): δ 8.85 (m, C*H*$_{Ar}$, 6H), 7.31 (m, C*H*$_{Ar}$, 9H).

Generation of Th(NH-2,6-*i*Pr$_2$-C$_6$H$_3$)(MeC(N^iPr)$_2$)$_3$ (3.8): Solid **2.2** (0.020 g, 0.027 mmol) was added to a 4 mL dram vial and dissolved in C_6D_6 (0.3 mL). In a separate dram vial, 2,6-diisopropylaniline (0.005 g, 0.028 mmol) was weighed out and dissolved in C_6D_6 (0.3 mL). The two solutions were then combined and added to a *J*-Young NMR tube sealed with a Teflon screw cap. The solution was then heated at 100 °C for 5 d, resulting in >90% conversion to **3.8** as judged by ^{1}H NMR spectroscopy. ^{1}H NMR (300 MHz, C_6D_6, 293 K): δ 7.25 (d, C*H*$_{Ar}$, 2H, $^3J_{H,H}$ = 7.5 Hz), 6.91 (t, C*H*$_{Ar}$, 1H, $^3J_{H,H}$ = 7.5 Hz), 4.94 (brs, N*H*, 1H), 3.65 (sept, C*H*Me$_2$, 6H, $^3J_{H,H}$ = 6.5 Hz), 3.54 (sept, C*H*Me$_2$, 2H, $^3J_{H,H}$ = 6.7 Hz), 1.70 (s, NC(C*H*$_3$)N, 9H), 1.42 (d, CH*Me*$_2$, 12H, $^3J_{H,H}$ = 6.7 Hz), 1.17 (d, CH*Me*$_2$, 36H, $^3J_{H,H}$ = 6.5 Hz).

Generation of Th(O-2,6-*t*Bu$_2$-C$_6$H$_3$)(MeC(N^iPr)$_2$)$_3$ (3.9): Solid **2.2** (0.021 g, 0.028 mmol) was added to a 4 mL dram vial and dissolved in C_6D_6 (0.3 mL). In a separate dram vial, 2,6-di-*tert*-butylphenol (0.006 g, 0.029 mmol) was weighed out and dissolved in C_6D_6 (0.3 mL). The two solutions were then combined and added to a *J*-Young NMR tube sealed with a Teflon screw cap. The solution was allowed to stand at ambient temperature for 12 h, at which point full conversion to **3.9** had been achieved as judged by ^{1}H NMR spectroscopy. ^{1}H NMR (600 MHz, C_6D_6, 293 K): δ 7.40 (d, C*H*$_{Ar}$, 2H, $^3J_{H,H}$ = 7.7 Hz), 6.85 (t, C*H*$_{Ar}$, 1H, $^3J_{H,H}$ = 7.7 Hz), 3.71 (sept, C*H*Me$_2$, 6H, $^3J_{H,H}$ = 6.5 Hz), 1.74 (s, NC(C*H*$_3$)N, 9H), 1.73 (s, C(C*H*$_3$)$_3$, 18H), 1.20 (d, CH*Me*$_2$, 36H, $^3J_{H,H}$ = 6.5 Hz).

Th(PHMes)(MeC(N^iPr)$_2$)$_3$ (3.10): Solid ThCl(MeC(N^iPr)$_2$)$_3$ (**2.1**) (0.243 g, 0.352 mmol) was added to a 20 mL scintillation vial containing a magnetic stir bar and dissolved in diethyl ether (2 mL). To this stirred solution was added KPHMes (0.082 g, 0.431 mmol) in THF (2 mL) dropwise, resulting in a light orange/yellow, cloudy solution. The reaction was allowed to stir at room temperature for 48 h, at which point the reaction appeared bright yellow. The volatiles were removed under reduced pressure, and the resulting solid was triturated with hexanes (2 x 2 mL), extracted into pentane (6 mL), filtered through Celite and concentrated to ~1.5 mL. The solution was then placed in the freezer at -35 °C for 16 h, resulting in yellow crystals of **3.10** (0.164 g, 57.8%) ^{1}H NMR (600 MHz, C_6D_6, 293 K): δ 7.01 (s, C*H*$_{Ar}$, 2H), 3.60

(sept, C*H*Me$_2$, 6H, $^3J_{H,H}$ = 6.4 Hz), 3.42 (d, P*H*, $^1J_{P,H}$ = 195 Hz, 1H), 2.74 (s, *o*-C*H*$_3$, 6H), 2.42 (s, *p*-C*H*$_3$, 3H), 1.63 (s, NC(C*H*$_3$)N, 9H), 1.22 (d, CH*Me*$_2$, 36H, $^3J_{H,H}$ = 6.4 Hz). $^{13}C\{^1H\}$ (151 MHz, C_6D_6, 293 K): δ 174.3 (N*C*N), 147.5 (d, $C_{Ar,ipso}$, $^1J_{P,C}$ = 35.2 Hz), 137.5 (d, $C_{Ar,o}$, $^2J_{P,C}$ = 9.1 Hz), 129.9 ($C_{Ar,p}$), 127.7 (d, $C_{Ar,m}$, $^3J_{P,C}$ = 2.7 Hz), 48.8 (*C*HMe$_2$), 25.7 (d, H$_3C_{Ar,o}$, $^{TS}J_{P,C}$ = 9.6 Hz), 24.7 (d, CH*Me*$_2$, $^{TS}J_{P,C}$ = 2.1 Hz), 21.0 (H$_3C_{Ar,p}$), 13.9 (NC(*C*H$_3$)N). ^{31}P NMR (162 MHz, C_6D_6, 293 K): δ -45.4 (d, $^1J_{P,H}$ = 195 Hz). Anal. Calcd for $C_{33}H_{63}N_6PTh$ (806.9): C, 49.12; H, 7.87; N, 10.42. Found: C, 48.79; H, 7.85; N, 10.36. Mp: 102(2) °C. FTIR (Nujol): 2337 (w, ν_{P-H}), 1337 (m), 1314 (m), 1196 (m), 1174 (w), 1122 (w), 1056 (w), 1013 (w), 847 (w), 806 (w), 722 (m), 620 (w). Crystals suitable for single-crystal X-ray diffraction studies were grown from a concentrated pentane solution stored at -35 °C for 16 h.

Generation of Th(PPh$_2$)(MeC(N^{i}Pr)$_2$)$_3$ (3.11): Solid **2.2** (0.021 g, 0.028 mmol) was added to a 4 mL dram vial and dissolved in C_6D_6 (0.3 mL). In a separate dram vial, PHPh$_2$ (0.0052 g, 0.028 mmol) was weighed out and dissolved in C_6D_6 (0.3 mL). The two solutions were then combined and added to a *J*-Young NMR tube sealed with a Teflon screw cap. The solution was then heated at 100 °C for 4 d, resulting in a bright orange solution and >95% conversion to **3.11** as judged by ^1H NMR spectroscopy. ^1H NMR (600 MHz, C_6D_6, 293 K): δ 7.81 (m, C*H*$_{Ar}$, 4H), 7.22 (m, C*H*$_{Ar}$, 4H), 6.96 (m, C*H*$_{Ar}$, 2H), 3.60 (sept, C*H*Me$_2$, 6H, $^3J_{H,H}$ = 6.4 Hz), 1.63 (s, NC(C*H*$_3$)N, 9H), 1.20 (d, CH*Me*$_2$, 36H, $^3J_{H,H}$ = 6.4 Hz). $^{31}P\{^1H\}$ NMR (162 MHz, C_6D_6, 293 K): δ 89.5. It was also observed that the dehydrocoupled product, Ph$_2$P-PPh$_2$, was generated in small quantities as determined by its characteristic ^{31}P NMR resonance in C_6D_6 (δ -14.9) as well as an unidentified phosphorus-containing species (^{31}P: δ 106). Synthesis of **3.10** via protonolysis of **2.2** with mesitylphosphine followed identical reaction conditions.

Th(C≡C-*p*-tolyl)(MeC(N^{i}Pr)$_2$)$_3$ (3.12): Solid **2.2** (0.400 g, 0.538 mmol) was added to a 20 mL scintillation vial containing a magnetic stir bar and dissolved in hexanes (10 mL). To this stirred solution was added neat *p*-tolylacetylene (0.065 g, 0.560 mmol) dropwise, resulting in a faint yellow solution which was allowed to stir at ambient temperature for 1 h. The volatiles were removed under reduced pressure, and the resulting solid was extracted into hexanes (10 mL), concentrated to 6 mL, and placed in the freezer at -35 °C for 16 h, resulting in colorless crystals of **3.12** (0.392 g, 94.5%). ^{1} H NMR (600 MHz, C_6D_6, 293 K): δ 7.69 (d, C*H*$_{ptolyl}$, 2H, $^3J_{H,H}$ = 8.0 Hz), 6.96 (d, C*H*$_{ptolyl}$, 2H, $^3J_{H,H}$ = 8.0 Hz), 3.66 (sept, C*H*Me$_2$, 6H, $^3J_{H,H}$ = 6.3 Hz), 2.04 (s, C*H*$_{3,ptolyl}$, 3H), 1.66 (s, NC(C*H*$_3$)N, 9H), 1.42 (d, CH*Me*$_2$, 36H, $^3J_{H,H}$ = 6.3 Hz). $^{13}C\{^1H\}$ NMR (151 MHz, C_6D_6, 293 K): δ 189.2 (Th*C*≡C), 172.7 (N*C*N), 134.9 (C_{ptolyl}), 131.0 (C_{ptolyl}), 128.8 (C_{ptolyl}), 124.7 (C_{ptolyl}), 107.8 (ThC≡*C*), 48.3 (*C*HMe$_2$), 24.6 (CH*Me*$_2$), 20.9 (C$_6$H$_4$*Me*) 11.8 (NC(*C*H$_3$)N). Anal. Calcd for $C_{33}H_{58}N_6Th$ (770.9): C, 51.42; H, 7.58; N, 10.90. Found: C, 51.72; H, 7.55; N, 10.60. Mp: 131(2) °C. FTIR (Nujol): 2599 (w), 2061 (w, $\nu_{C\equiv C}$), 1358 (s), 1332 (s), 1313 (s), 1198 (s), 1173 (s), 1137 (w), 1125 (m), 1051 (w), 1016 (m), 819 (s), 803 (s), 711 (w), 618 (w), 569 (w), 546 (w), 534 (w), 464 (m). Crystals suitable for single-crystal X-ray diffraction studies were grown from a concentrated hexanes solution stored at -35 °C for 16 h.

Th[(THF)(MeC(N^{i}Pr)$_2$)$_3$][BPh$_4$] (3.13): Solid **2.2** (0.300 g, 0.404 mmol) was added to a 20 mL scintillation vial containing a magnetic stir bar and dissolved in THF (4 mL). To this

stirred solution was added a THF solution (2 mL) of [Et_3NH][BPh_4] (0.170 g, 0.403 mmol), and the resulting colorless solution was allowed to stir at ambient temperature for 2 h. The volatiles were removed under reduced pressure, and the resulting solid was re-dissolved in THF (6 mL), concentrated to 2 mL, and placed in the freezer at -35 °C for 16 h, resulting in colorless crystals of **3.13** (0.368 g, 81.4%). The complex crystallizes with an equivalent of THF in the lattice, which can be removed under vacuum. ^{1}H NMR (600 MHz, $CDCl_3$, 293 K): δ 7.43 (br s, C*H*$_{Ar}$, 8H), 7.06 (m, C*H*$_{Ar}$, 8H), 6.91 (m, C*H*$_{Ar}$, 4H), 3.94 (m, ^{THF}C*H*$_2$, 4H), 3.84 (sept, C*H*Me$_2$, 6H, $^3J_{H,H}$ = 6.4 Hz), 2.02 (s, NC(C*H*$_3$)N, 9H), 1.91 (m, ^{THF}C*H*$_2$, 4H), 1.16 (d, CH*Me*$_2$, 36H, $^3J_{H,H}$ = 6.4 Hz). ^{11}B{^{1}H} NMR (192 MHz, $CDCl_3$, 293 K): -7.16 (s). ^{13}C{^{1}H} (151 MHz, $CDCl_3$, 293 K): δ 176.4 (N*C*N), 164.4 (B-*C*$_{Ph}$, $^1J_{B,C}$ = 49.7 Hz), 136.4 (*C*$_{Ph}$), 125.5 (*C*$_{Ph}$), 121.6 (*C*$_{Ph}$), 69.6 (^{THF}*C*H$_2$), 48.7 (*C*HMe$_2$), 25.6 (^{THF}*C*H$_2$), 25.2 (CH*Me*$_2$), 14.0 (NC(*C*H$_3$)N). Anal. Calcd for $C_{52}H_{78}N_6O_1B_1Th$ (1046.1): C, 59.71; H, 7.52; N, 8.03. Found: C, 59.38; H, 7.53; N, 8.21. Mp: 183(5) °C. FTIR (Nujol): 1378 (s), 1345 (m), 1315 (m), 1194 (m), 1174 (w), 1124 (w), 1015 (w), 806 (w), 742 (w), 730 (m), 706 (m), 614 (w), 605 (w), 424 (w). Crystals suitable for single-crystal X-ray diffraction studies were grown from a concentrated THF solution stored at -35 °C for 16 h.

(MeC(N*i*Pr)$_2$)$_3$Th(μ-H)$_2$[B(C$_8$H$_{14}$)] (3.14): Solid **2.2** (0.251 g, 0.338 mmol) was added to a 20 mL scintillation vial containing a magnetic stir bar and dissolved in 2 mL toluene. To this stirred solution was added a toluene solution (3 mL) of 9-BBN dimer (0.082 g, 0.336 mmol) dropwise over 1 minute. The resulting colorless solution was allowed to stir at ambient temperature for 48 h. The volatiles were removed under reduced pressure, and the resulting solid was triturated with hexane (2 x 4 mL) and extracted into HMDSO (8 mL), leaving behind a small amount of insoluble, colorless solid. The HMDSO extract was then filtered through Celite, concentrated to 5 mL, and placed in the freezer at -35 °C for 16 h, resulting in colorless crystals of **3.14** (0.173 g, 65.8%). ^{1}H NMR (300 MHz, C_6D_6, 293 K): δ 4.67-5.30 (br, μ-*H*, 2H), 3.68 (sept, C*H*Me$_2$, 6H, $^3J_{H,H}$ = 6.5 Hz), 2.25-2.41 (m, BBN, 10H), 2.06 (m, BBN, 2H), 1.78 (brs, BBN, 2H), 1.66 (s, NC(C*H*$_3$)N, 9H), 1.23 (d, CH*Me*$_2$, 36H, $^3J_{H,H}$ = 6.5 Hz). ^{11}B{^{1}H} NMR (192 MHz, C_6D_6, 293 K): δ 4.90 (s). ^{13}C{^{1}H} (126 MHz, C_6D_6, 293 K): δ 174.6 (N*C*N), 48.7 (*C*HMe$_2$), 34.5 (BBN), 25.8 (BBN), 24.7 (CH*Me*$_2$), 14.6 (NC(*C*H$_3$)N). Anal. Calcd for $C_{32}H_{67}BN_6Th$ (778.8): C, 49.35; H, 8.67; N, 10.79. Found: C, 49.30; H, 8.59; N, 10.68; Mp: 207(2) °C. FTIR (Nujol): 2021 cm^{-1} (br, B-H), 1377 (s), 1334 (s), 1313 (s), 1283 (s), 1197 (s), 1171 (s), 1119 (m), 1051 (m), 1011 (m), 919 (w), 805 (m), 775 (w), 723 (m), 618 (w), 575 (w), 543 (w). Crystals suitable for single-crystal X-ray diffraction studies were grown from a concentrated pentane solution stored at -35 °C for 16 h.

Th(MeC(N*i*Pr)$_2$)$_2$((*i*Pr)NC(CH$_2$)N(*i*Pr)) (3.15): Solid **2.2** (0.500 g, 0.673 mmol) was added to a 4 mL dram vial and dissolved in 1.5 mL C_6D_6. The solution was transferred to a *J*-Young NMR tube and sealed with a Teflon screw cap. The *J*-Young tube was then placed in the photolysis reactor and irradiated for 10 days, at which point the solution had changed from colorless to green, and **2.2** was completely consumed as observed by ^{1}H NMR spectroscopy. The *J*-Young tube was then brought into the glovebox and emptied into a 20 mL scintillation vial,

and the tube was rinsed with toluene (2 mL). This rinse was combined with the C_6D_6 solution, and the volatiles were then removed under reduced pressure. The resulting solid was then extracted into toluene (4 mL), concentrated to 1 mL and placed in the freezer at -35 °C for 16 h, resulting in colorless crystals of **3.15** (0.232 g, 52.7%). ^{1}H NMR (600 MHz, C_6D_6, 293 K): δ 4.24 (sept, C*H*Me$_2$*, 2H, $^3J_{H,H}$ = 6.2 Hz), 3.57 (sept, C*H*Me$_2$, 4H, $^3J_{H,H}$ = 6.2 Hz), 3.44 (s, NC(C*H*$_2$)N*, 2H), 1.54 (d, CH*Me*$_2$*, 12H, $^3J_{H,H}$ = 6.2 Hz), 1.53 (s, NC(C*H*$_3$)N, 6H), 1.15 (d, CH*Me*$_2$, 24H, $^3J_{H,H}$ = 6.2 Hz). ^{13}C{^{1}H} NMR (151 MHz, C_6D_6, 293 K): δ 172.8 (N*C*N), 154.2 (N*C*N*), 53.3 (NC(*C*H$_2$)N*), 49.1 (Me$_2$*C*H*), 48.3 (Me$_2$*C*H), 26.0 (*Me*$_2$CH*), 25.7 (*Me*$_2$CH), 12.2 (NC(*C*H$_3$)N). Anal. Calcd for $C_{24}H_{50}N_6Th$ (654.7): C, 44.03; H, 7.70; N, 12.84. Found: C, 43.77; H, 7.67; N, 12.46. Mp: 170 °C (decomp.). FTIR (Nujol): 1496 (s), 1414 (s), 1308 (s), 1197 (s), 1169 (m), 1123 (m), 1049 (m), 1010 (m), 886 (w), 796 (s), 722 (w), 695 (m), 620 (w), 577 (w), 546 (w), 456 (w), 433 (w). Crystals suitable for single-crystal X-ray diffraction studies were grown from a concentrated toluene solution stored at -35 °C for 16 h. Alternatively, solid **2.2** (0.009 g, 0.012 mmol) was added to a 4 mL dram vial and dissolved in 0.4 mL C_6D_{12}. The solution was transferred to a quartz EPR tube custom-fitted with a *J*-Young neck and sealed with a Teflon screw cap. The tube was then placed in front of a xenon arc lamp and irradiated for 2 h, at which point the solution had changed from colorless to green, and **2.2** was completely consumed as observed by ^{1}H NMR spectroscopy.

Crystallographic Procedures. Single-crystal X-ray diffraction experiments were performed at the UC Berkeley CHEXRAY crystallographic facility. Measurements of all complexes were performed on a Bruker APEX-II CCD area detector using Mo Kα radiation (λ = 0.71073 Å). Crystals were kept at 100(2) K throughout collection. Data collection was performed with Bruker APEX2 software (v. 2014.11). Data refinement and reduction were performed with Bruker SAINT (V8.34A). All structures were solved with SHELXT.53.[100] Structures were refined with SHELXL-2014.[101] Molecular graphics were computed with Mercury 3.10. All non-hydrogen atoms were refined anisotropically, and hydrogen atoms were included at the geometrically calculated positions and refined using a riding model.

References

(1) Burns, C. J.; Eisen, M. S. In *The Chemistry of the Actinide and Transactinide Elements*; Morss, L. R., Edelstein, N. M., Fuge, J., Eds.; Springer: Berlin, 2006; Vol. 5.
(2) Hayton, T. W. *Chem. Commun*. **2013**, *49*, 2956-2973.
(3) Jones, M. B.; Gaunt, A. J. *Chem. Rev.* **2013**, *113*, 1137-1198.
(4) Liddle, S. T. *Angew. Chem., Int. Ed.* **2015**, *54*, 2-40.
(5) Ephritikhine, M. *Organometallics* **2013**, *32*, 2464-2488.
(6) Fox, A. R.; Bart, S. C.; Meyer, K.; Cummins, C. C. *Nature* **2008**, *455*, 341-349.
(7) Jantunen, K. C.; Scott, B. L.; Kiplinger, J. L. *J. Alloys Compd.* **2007**, *444*, 363-368.
(8) Yahia, A.; Maron, L. *Organometallics* **2009**, *28*, 672-679.
(9) Marks, T. J.; Wachter, W. A. *J. Am. Chem. Soc.* **1976**, *98*, 703-710.
(10) Kalina, D. G.; Marks, T. J.; Wachter, W. A. *J. Am. Chem. Soc.* **1977**, *99*, 3877-3879.
(11) Bruno, J. W.; Kalina, D. G.; Mintz, E. A.; Marks, T. J. *J. Am. Chem. Soc.* **1982**, *104*, 1860-1869.
(12) Bruno, J. W.; Marks, T. J.; Day, V. W. *J. Am. Chem. Soc.* **1982**, *104*, 7357-7360.
(13) Moloy, K. G.; Marks, T. J. *J. Am. Chem. Soc.* **1984**, *106*, 7051-7064.
(14) Bruno, J. W.; Smith, G. M.; Marks, T. J.; Fair, C. K.; Schultz, A. J.; Williams, J. M. *J. Am. Chem. Soc.* **1986**, *108*, 40-56.
(15) Moloy, K. G.; Fagan, P. J.; Manriquez, J. M.; Marks, T. J. *J. Am. Chem. Soc.* **1986**, *108*, 56-67.
(16) Evans, W. J.; Walensky, J. R.; Ziller, J. W.; Rheingold, A. L. *Organometallics* **2009**, *28*, 3350-3357.
(17) Jantunen, K. C.; Burns, C. J.; Castro-Rodriguez, I.; Da Re, R. E.; Golden, J. T.; Morris, D. E.; Scott, B. L.; Taw, F. L.; Kiplinger, J. L. *Organometallics* **2004**, *23*, 4682-4692.
(18) Pool, J. A.; Scott, B. L.; Kiplinger, J. L. *J. Am. Chem. Soc.* **2005**, *127*, 1338-1339.
(19) Butcher, R. J.; Clark, D. L.; Grumbine, S. K.; Scott, B. L.; Watkin, J. G. *Organometallics* **1996**, *15*, 1488-1496.
(20) Schelter, E. J.; Yang, P.; Scott, B. L.; Da Re, R. E.; Jantunen, K. C.; Martin, R. L.; Hay, P. J.; Morris, D. E.; Kiplinger, J. L. *J. Am. Chem. Soc.* **2007**, *129*, 5139-5152.
(21) Cruz, C. A.; Emslie, D. J. H.; Harrington, L. E.; Britten, J. F.; Robertson, C. M. *Organometallics* **2007**, *26*, 692-701.
(22) Cruz, C. A.; Emslie, D. J. H.; Harrington, L. E.; Britten, J. F. *Organometallics* **2008**, *27*, 15-17.
(23) Cruz, C. A.; Emslie, D. J. H.; Robertson, C. M.; Harrington, L. E.; Jenkins, H. A.; Britten, J. F. *Organometallics* **2009**, *28*, 1891-1899.
(24) Gardner, B. M.; Cleaves, P. A.; Kefalidis, C. E.; Fang, J.; Maron, L.; Lewis, W.; Blake, A. J.; Liddle, S. T. *Chem. Sci.* **2014**, *5*, 2489-2497.
(25) Seaman, L. A.; Walensky, J. R.; Wu, G.; Hayton, T. W. *Inorg. Chem.* **2013**, *52*, 3556-3564.

(26) Behrle, A. C.; Myers, A. J.; Rungthanaphatsophon, P.; Lukens, W. W.; Barnes, C. L.; Walensky, J. R. *Chem. Commun.* **2016**, *52*, 14373-14375.
(27) Suvova, M.; O'Brien, K. T. P.; Farnaby, J. H.; Love, J. B.; Kaltsoyannis, N.; Arnold, P. L. *Organometallics* **2017**, *36*, 4669-4681.
(28) Mora, E.; Maria, L.; Biswas, B.; Camp, C.; Santos, I. C.; Pécaut, J.; Cruz, A.; Carretas, J. M.; Marçalo, J.; Mazzanti, M. *Organometallics* **2013**, *32*, 1409-1422.
(29) Lohrey, T. D.; Bergman, R. G.; Arnold J. *Angew. Chem., Int. Ed*. **2017**, *56*, 14241-14245.
(30) Hohloch, S.; Garner, M. E.; Parker, B. F.; Arnold, J. *Dalton Trans.* **2017**, *46*, 13768-13782.
(31) Ziegler, J. A.; Buckley, H. L.; Arnold, J. *Dalton Trans*. **2017**, *46*, 780-785.
(32) Garner, M. E.; Hohloch, S.; Maron, L.; Arnold J. *Organometallics* **2016**, *35*, 2915-2922.
(33) Camp, C.; Settineri, N.; Lefevre, J.; Jupp, A. R.; Goicoechea, J. M.; Maron, L.; Arnold, J. *Chem. Sci.* **2015**, *6*, 6379-6384.
(34) Boreen, M. A.; Parker, B. F.; Lohrey, T. D.; Arnold, J. *J. Am. Chem. Soc.* **2016**, *138*, 15865-15868.
(35) Settineri, N. S.; Garner, M. E.; Arnold, J. *J. Am. Chem. Soc.* **2017**, *139*, 6261-6269.
(36) Cantat, T.; Scott, B. L.; Kiplinger, J. L. *Chem. Commun.* **2010**, *46*, 919-921.
(37) Hao, S.; Gambarotta, S.; Bensimon, C.; Edema, J. J. H. *Inorg. Chim. Acta* **1993**, *213*, 65-74.
(38) Langeslay, R. R.; Fieser, M. E.; Ziller, J. W.; Furcher, F.; Evans, W. J. *Chem. Sci.* **2015**, *6*, 517-521.
(39) Kurogi, T.; Mane, M. V.; Zheng, S.; Carroll, P. J.; Baik, M.-H.; Mindiola, D. J. *Angew. Chem., Int. Ed.* **2018**, *57*, 1978-1981.
(40) Hoffmann, R.; Gleiter, R.; Mallory, F. B. *J. Am. Chem. Soc.* **1970**, *92*, 1460-1466.
(41) Waterman, R.; Hillhouse, G. L. *J. Am. Chem. Soc.* **2003**, *125*, 13350-13351.
(42) Kraft, S. J.; Fanwick, P. E.; Bart, S. C. *Organometallics* **2013**, *32*, 3279-3285.
(43) Yu, Y.; Sadique, A. R.; Smith, J. M.; Dugan, T. R.; Cowley, R. E.; Brennessel, W. W.; Flaschenriem, C. J.; Bill, E.; Cundari, T. R.; Holland, P. L. *J. Am. Chem. Soc.* **2008**, *130*, 6624-6638.
(44) Zhou, E.; Ren, W.; Hou, G.; Zi, G.; Fang, D.-C.; Walter, M. D. *Organometallics* **2015**, *34*, 3637-3647.
(45) Thorn, M. G.; Lee, J.; Fanwick, P. E.; Rothwell, I. P. *J. Chem. Soc., Dalton Trans.* **2002**, *17*, 3398-3405.
(46) Nechayev, M.; Gianetti, T. L.; Bergman, R. G.; Arnold, J. *Dalton Trans.* **2015**, *44*, 19494-19500.
(47) Amor, F.; Butt, A.; du Plooy, K. E.; Spaniol, T. P.; Okuda, J. *Organometallics* **1998**, *17*, 5836-5849.
(48) Fandos, R.; Otero, A.; Rodriguez, A. M.; Suizo, S. *Organometallics* **2012**, *31*, 1849-1856.
(49) Evans, W. J.; Takase, M. K.; Ziller, J. W.; Rheingold, A. L. *Organometallics* **2009**, *28*, 5802-5808.
(50) Siladke, N. A.; Ziller, J. W.; Evans, W. J. *J. Am. Chem. Soc.* **2011**, *133*, 3507-3516.

(51) Evans, W. J.; Walensky, J. R.; Ziller, J. W. *Organometallics* **2010**, *29*, 945-950.
(52) Evans, W. J.; Siladke, N. A.; Ziller, J. W. *Chem. Eur. J.* **2010**, *16*, 796-800.
(53) Ren, W.; Zi, G.; Fang, D.-C.; Walter, M. D. *J. Am. Chem. Soc.* **2011**, *133*, 13183-13196.
(54) Barnhart, D. M.; Clark, D. L.; Gordon, J. C.; Huffman, J. C.; Watkin, J. G. *Inorg. Chem.* **1994**, *33*, 3939-3944.
(55) Kiplinger, J. L.; Scott, B. L.; Schelter, E. J.; Tournear, J. A. P. D. *J. Alloys Compd.* **2007**, *444*, 477-482.
(56) Clark, D. L.; Watkin, J. G. *Inorg. Chem.* **1993**, *32*, 1766-1772.
(57) Fendrick, C. M.; Mintz, E. A.; Schertz, L. D.; Marks, T. J. *Organometallics* **1984**, *3*, 819−821.
(58) Simpson, S. J.; Andersen, R. A. *J. Am. Chem. Soc.* **1981**, *103*, 4063-4066.
(59) Manriquez, J. M.; Fagan, P. J.; Marks, T. J.; Day, C. S.; Day, V. W. *J. Am. Chem. Soc.* **1978**, *100*, 7112-7114.
(60) Bénaud, O.; Berthet, J.-C.; Thuéry, P.; Ephritikhine, M. *Inorg. Chem.* **2010**, *49*, 8117-8130.
(61) Arnold, P. L.; Turner, Z. R.; Germeroth, A. I.; Casely, I. J.; Nichol, G. S.; Bellabarba, R.; Tooze, R. P. *Dalton Trans*. **2013**, *42*, 1333-1337.
(62) Tatsumi, K.; Nakamura, A.; Hofmann, P.; Hoffmann, R.; Moloy, K. G.; Marks, T. J. *J. Am. Chem. Soc.* **1986**, *108*, 4467-4476.
(63) Radu, N. S.; Engeler, M. P.; Gerlach, C. P.; Tilley, T. D.; Rheingold, A. L. *J. Am. Chem. Soc.* **1995**, *117*, 3621-3622.
(64) Cui, D.; Nishiura, M.; Hou, Z. *Angew. Chem. Int. Ed.* **2005**, *44*, 959-962.
(65) Bordwell, F. G.; Algrim, D. J. *J. Am. Chem. Soc.* **1988**, *110*, 2964-2968.
(66) Bordwell, F. G. *Acc. Chem. Res.* **1988**, *21*, 456-463.
(67) Beachley, O. T., Jr.; MacRae, D. J.; Kovalevsky, A. Y. *Organometallics* **2003**, *22*, 1690-1695.
(68) Wrobleski, D. A.; Ryan, R. R.; Wasserman, H. J.; Salazar, K. V.; Paine, R. T.; Moody, D. C. *Organometallics* **1986**, *5*, 90-94.
(69) Hall, S. W.; Huffman, J. C.; Miller, M. M.; Avens, L. R.; Burns, C. J.; Arney, D. S. J.; England, A. F.; Sattelberger, A. P. *Organometallics* **1993**, *12*, 752-758.
(70) Garner, M. E.; Arnold, J. *Organometallics* **2017**, *36*, 4511-4514.
(71) Waterman, R. *Organometallics* **2007**, *26*, 2492-2494.
(72) Behrle, A. C.; Castro, L.; Maron, L.; Walensky, J. R. *J. Am. Chem. Soc.* **2015**, *137*, 14846-14849.
(73) Wildman, E. P.; Balázs, G.; Wooles, A. J.; Scheer, M.; Liddle, S. T. *Nat. Commun.* **2016**, *7*, 12884-12895.
(74) Duttera, M. R.; Day, V. W.; Marks, T. J. *J. Am. Chem. Soc.* **1984**, *106*, 2907-2912.
(75) Garner, M. E.; Parker, B. F.; Hohloch, S.; Bergman, R. G.; Arnold, J. *J. Am. Chem. Soc.* **2017**, *139*, 12935-12938.
(76) Hierso, J.-C.; Ivanov, V. V.; Amardeil, R.; Richard, P.; Meunier, P. *Chem. Lett.* **2004**, *33*, 1296-1297.

(77) Marchenko, A.; Hurieva, A.; Koidan, H.; Rampazzi, V.; Cattey, H.; Pirio, N.; Kostyuk, A. N.; Hierso, J.-C. *Organometallics* **2012**, *31*, 5986-5989.
(78) Hierso, J.-C. *Chem. Rev.* **2014**, *114*, 4838-4867.
(79) Behrle, A. C.; Walensky, J. R. *Dalton Trans.* **2016**, *45*, 10042-10049.
(80) Haskel, A.; Straub, T.; Dash, A. K. Eisen, M. S. *J. Am. Chem. Soc.* **1999**, *121*, 3014-3024.
(81) Dash, A. K.; Wang, J. Q.; Eisen, M. S. *Organometallics* **1999**, *18*, 4724-4741.
(82) Pappas, I.; Chirik, P. J. *Angew. Chem. Int. Ed.* **2014**, *53*, 6241-6244.
(83) Podiyanachari, S. K.; Fröhlich, R.; Daniliuc, C. G.; Petersen, J. L.; Mück-Lichtenfeld, C.; Kehr, G.; Erker, G. *Angew. Chem. Int. Ed.* **2012**, *51*, 8830-8833.
(84) Vaid, T. P.; Veige, A. S.; Lobkovsky, E. B.; Glassey, W. V.; Wolczanski, P. T.; Liable-Sands, L. M.; Rheingold, A. L.; Cundari, T. R. *J. Am. Chem. Soc.* **1998**, *120*, 10067-10079.
(85) Walensky, J. R.; Martin, R. L.; Ziller, J. W.; Evans, W. J. *Inorg. Chem.* **2010**, *49*, 10007-10012.
(86) Berthet, J.-C.; Villiers, C.; Le Maréchal, J.-F.; Delavaux-Nicot B.; Lance, M.; Nierlich, M.; Vigner, J.; Ephritikhine, M. *J. Organomet. Chem.* **1992**, *440*, 53-65.
(87) Travia, N. E.; Monreal, M. J.; Scott, B. L.; Kiplinger, J. L. *Dalton Trans.* **2012**, *41*, 14514-14523.
(88) Behrle, A. C.; Levin, J. R.; Kim, J.-E.; Drewett, J. M.; Barnes, C. L.; Schelter, E. J.; Walensky, J. R. *Dalton Trans.* **2015**, *44*, 2693-2702.
(89) Zalkin, A.; Templeton, D. H.; Le Vanda, C.; Streitwieser, A., Jr. *Inorg. Chem.* **1980**, *19*, 2560-2563.
(90) Gardner, B. M.; Lewis, W.; Blake, A. J.; Liddle, S. T. *Organometallics* **2015**, *34*, 2386-2394.
(91) Soderquist, J. A.; Najafi, M. R. *J. Org. Chem.* **1986**, *51*, 1330-1336.
(92) Eaton, G. R. *J. Chem. Educ.* **1969**, *46*, 547-556.
(93) Shinomoto, R.; Gamp, E.; Edelstein, N. M.; Templeton, D. H.; Zalkin, A. *Inorg. Chem.* **1983**, *22*, 2351-2355.
(94) Turner, H. W.; Andersen, R. A.; Zalkin, A.; Templeton, D. H. *Inorg Chem.* **1979**, *18*, 1221-1224.
(95) McKinven, J.; Nichol, G. S.; Arnold, P. L. *Dalton Trans.* **2014**, *43*, 17416-17421.
(96) Trnka, T. M.; Bonanno, J. B.; Bridgewater, B. M.; Parkin, G. *Organometallics* **2001**, *20*, 3255-3264.
(97) Daly, S. R.; Piccoli, P. M. B.; Schultz, A. J.; Todorova, T. K.; Gagliardi, L.; Girolami, G. S. *Angew. Chem. Int. Ed.* **2010**, *49*, 3379-3381.
(98) Kaski, J.; Lantto, P.; Vaara, J.; Jokisaari, J. *J. Am. Chem. Soc.* **1998**, *120*, 3993-4005.
(99) Zhao, J.; Li, Z.; Yan, S.; Xu, S.; Wang, M.; Fu, B.; Zhang, Z. *Org. Lett.* **2016**, *18*, 1736-1739.
(100) Sheldrick, G. M. *Acta. Crystallogr. Sect. A* **2015**, *71*, 3-8.
(101) Sheldrick, G. M. *Acta. Crystallogr. Sect. A* **2008**, *64*, 112-122.

Chapter 4

Two-Electron Oxidation of a Homoleptic U(III) Guanidinate Complex by Diphenyldiazomethane

Chapter 4

Overview

While actinide amidinate chemistry is still decidedly less explored than that of Cp-based systems, the chemistry of actinide guanidinate complexes is almost nonexistent. To this extent, only two uranium complexes have been characterized containing guanidinate ligands, and the ability of these frameworks to support unique, reactive moieties has not been investigated. Guanidinates, with their stronger electron-donating ability compared to that of amidinates, seemed like an ideal candidate for the synthesis of rare actinide-heteroatom linkages, particularly with a redox-active metal like uranium. The following chapter describes the synthesis, characterization and reactivity of the first U(III) homoleptic guanidinate complex; this species was able to undergo two-electron oxidation reactions with diphenyldiazomethane, *p*-tolyl azide, and pyridine *N*-oxide to form terminal U(V) imidos and oxos. The imido complex formed with diphenyldiazomethane is the first isolable example of a U(V) imido formed with this specific moiety and is a testament to the stabilizing nature of the *N, N, N', N''*-tetraisopropylguanidinate (TIG) ligand, the specific guanidinate employed in these studies.

Introduction

With the redox chemistry of uranium primarily governed by one-electron processes, effecting two-electron transformations similar to those seen with transition-metals is an ongoing challenge.[1-4] Two-electron oxidation at uranium is generally facilitated by reactions with organic azides or oxygen-atom transfer reagents, resulting in terminal imido and oxo complexes, respectively.[5-10] Diphenyldiazomethane has been shown to act as both a one-[11] and two-electron[12-14] oxidant towards uranium, forming amido- and imido-like bonds, although these oxidative transformations have been limited to U(III) to U(IV) or U(IV) to U(VI). No stable U(V) diphenyldiazomethane complex has been isolated, with putative U(V) species undergoing disproportionation or comproportionation.[13]

Our group has recently explored the viability of amidinates as an alternative ancillary ligand (to the more ubiquitous cyclopentadienyl fragment[15]) to support actinide metal centers and promote new reactivity and metal-atom linkages.[16-18] In addition to amidinates, we also endeavored to explore guanidinates as a suitable ligand platform, considering the dearth of actinide guanidinate complexes currently known,[19,20] as well as the possibility of comparative reactivity studies with analogous amidinate systems to probe the effect of the greater electron-donating ability of the guanidinates.[21] We envisioned the electronic properties of the guanidinate ligand, combined with an appropriate steric profile, would prove capable of supporting a variety of uranium-ligand multiple bonds. Herein, we present the synthesis and characterization of both U(IV) and U(III) guanidinate complexes, the latter of which is the first homoleptic U(III) guanidinate species reported. The U(III) complex undergoes two-electron oxidation upon reaction with diphenyldiazomethane, generating the tris-guanidinate U(V) diphenyldiazomethane product, which contains a short, terminal U-N bond indicative of uranium-nitrogen multiple bonding.

Additionally, two-electron oxidation of the U(III) species with an organic azide and an oxygen-atom transfer reagent leads to the corresponding U(V) imido and U(V) oxo complexes, respectively.

Results and Discussion

Synthesis of Uranium Guanidinate Systems. Choice of guanidinate ligand was important, as we had observed in previous studies with amidinates where proper steric and electronic support led to isolable actinide complexes. After screening a number of guanidinate ligands, we settled on the *N,N,N',N''*-tetraisopropylguanidinate (TIG) ligand for its ease of synthesis as well as its ability to generate isolable actinide complexes in high yield. Salt metathesis of UCl_4[22] with 3 equiv. of Li(TIG)(THF)[23] afforded $UCl(TIG)_3$ (**4.1**) as green crystals in 93% yield upon crystallization from toluene. The molecular structure of **4.1** was determined by X-ray diffraction studies, revealing a seven-coordinate uranium center with a U-Cl1 bond distance of 2.662(1) Å, and U-N_{guan} bond distances ranging from 2.361(4) to 2.518(3) Å, with an average U-N_{guan} distance of 2.44(4) Å (Figure 4.1). This is the first mononuclear actinide complex bearing only guanidinates as supporting ligands. Reduction of **4.1** with KC_8 in THF led to an immediate color change from

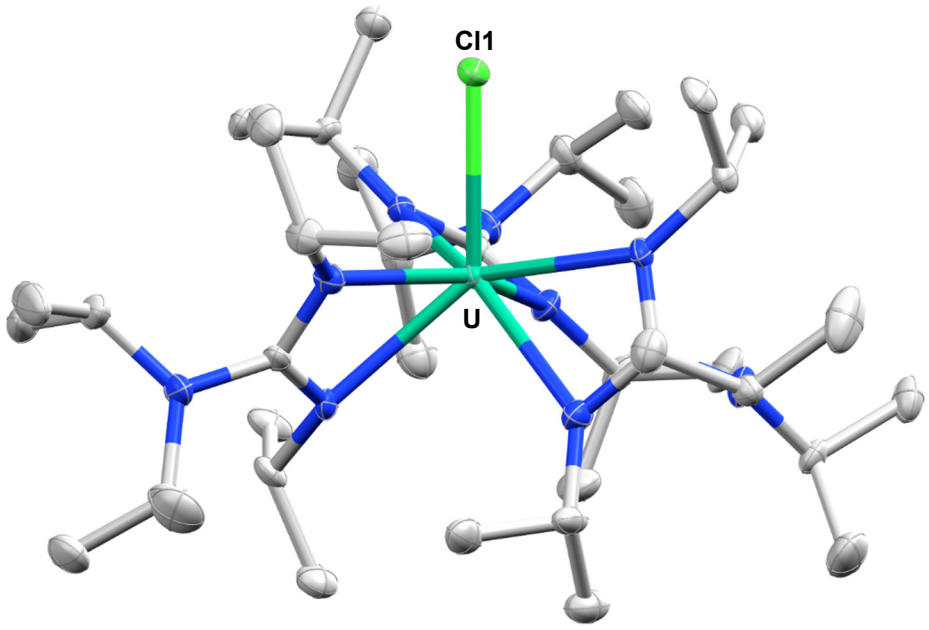

Figure 4.1. Molecular structure of **4.1**. Thermal ellipsoids drawn at the 50% probability level. Hydrogen atoms and hexane solvent molecules omitted for clarity.

green to dark blue, and the U(III) homoleptic guanidinate complex $U(TIG)_3$ (**4.2**) was isolated in 81% yield upon workup and crystallization from HMDSO. Alternatively, reaction of $UI_3(1,4\text{-dioxane})_{1.5}$[24] with 3.5 equiv. of Li(TIG)(THF) afforded **4.2** in 73% yield (Scheme 4.1). Complexes **4.1** and **4.2** represent rare examples of uranium guanidinate species, with **4.2** being the first homoleptic U(III) guanidinate complex isolated and characterized. The molecular structure of **4.2** was determined by X-ray diffraction studies and features three guanidinate ligands enclosing the six-coordinate uranium center in a propeller-like fashion (Figure 4.2). The average $U\text{-}N_{guan}$ bond distance has increased to 2.49(3) Å, in accordance with the larger size of U(III) vs. U(IV), and the uranium center sits in-between the planes created by the nitrogen atoms of the guanidinate ligands, encapsulating the metal center in a trigonal antiprism. For both **4.1** and **4.2** the C-N bond lengths of the NCN chelating fragment of the guanidinate ligands fall within the range of 1.33-1.35 Å, indicating delocalization of electron density. ^{1}H NMR spectroscopy for **4.1** and **4.2** reveals paramagnetically shifted resonances; however, while **4.1** displays broad, overlapping resonances, **4.2** exhibits six sharp resonances ranging from 30 to -10 ppm integrating to a ratio of 1:1:3:3:3:3, reflecting averaged C_3-symmetry of **4.2** in solution (Figure 4.3).

Scheme 4.1. Syntheses of **4.1** and **4.2**

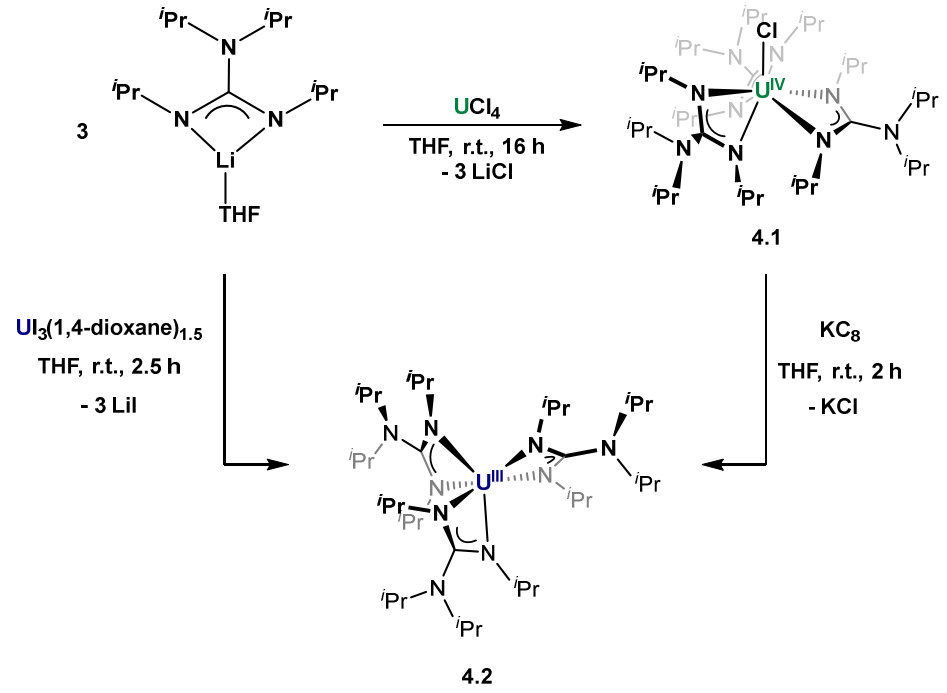

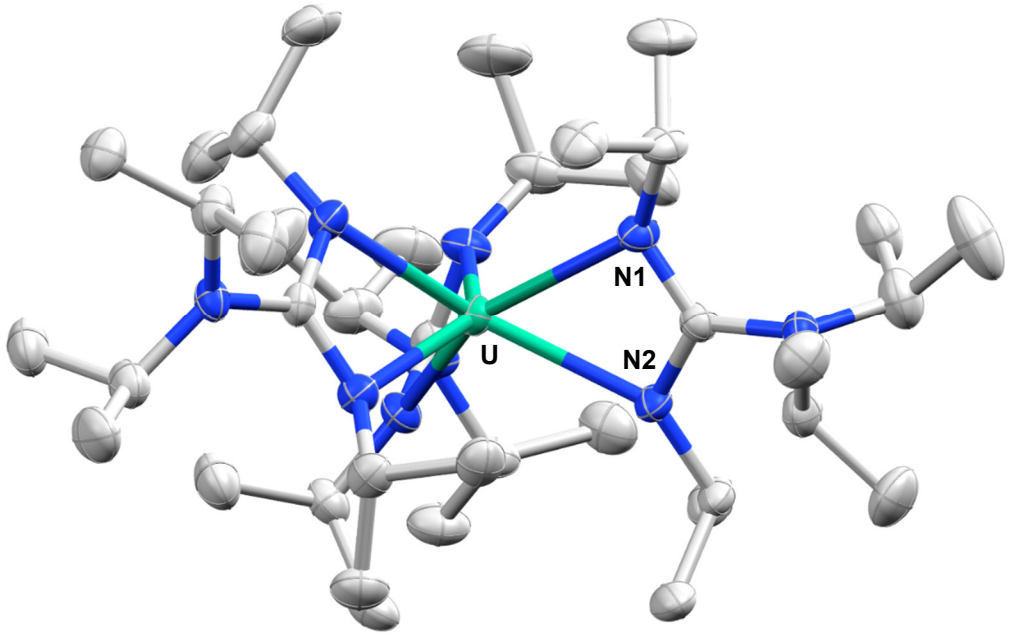

Figure 4.2. Molecular structure of **4.2**. Thermal ellipsoids drawn at the 50% probability level. Hydrogen atoms omitted for clarity.

Two-Electron Oxidation of U(TIG)$_3$. With **4.2** in hand, we investigated the ability of the tris-guanidinate framework to support uranium-ligand multiple bonds. We initially looked at the use of diphenyldiazomethane as a carbene source, with precedent in transition-metal chemistry for the elimination of dinitrogen to form the corresponding transition-metal diphenylcarbene complexes,[25-27] although no such success has been achieved with the actinides. Upon mixing a magenta solution of diphenyldiazomethane[28] in hexane with a dark blue solution of **4.2** in hexane, an immediate color change to dark red-brown occurred, with no effervescence of gas observed. Subsequent workup and crystallization from pentane afforded U(N_2CPh_2)(TIG)$_3$ (**4.3**) as dark red-brown crystals in 72% yield (Scheme 4.2). The ^{1}H NMR spectrum of **4.3** shows four paramagnetically shifted resonances ranging from 21 to -3 ppm; the two sharp resonances appearing at δ 9.74 and 8.16 ppm can be assigned to the aromatic protons of the diphenyldiazomethane moiety, while the two very broad resonances observed at δ 20.99 and -2.82 ppm correspond to the methine and methyl protons of the TIG ligand, respectively. The molecular structure of **4.3** was determined by X-ray diffraction studies, which revealed a short U-N10 bond distance of 2.060(3) Å, and a near-linear U-N10-N11 bond angle of 165.8(3)°. This information, coupled with the reduction of the N10-N11 bond length to 1.299(4) Å (compared to ~1.13 Å for free diphenyldiazomethanes[29]), is consistent with a two-electron reduction of the diphenyldiazomethane moiety by the uranium center, resulting in a U(V) imido complex (Figure

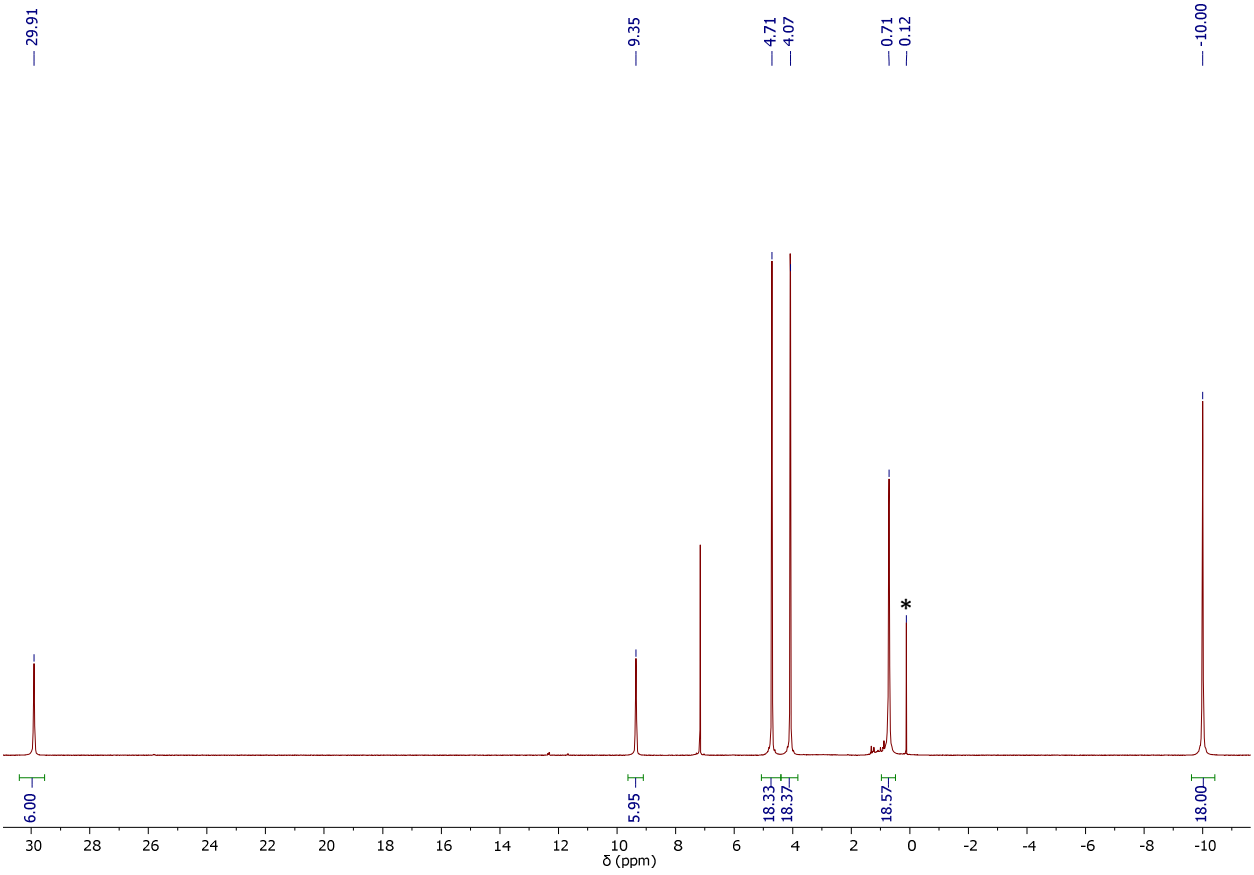

Figure 4.3. ^{1}H NMR spectrum of **4.2** at 298 K in C_6D_6. *HMDSO

4.4). To the best of our knowledge, this is the first example of a U(V) imido complex employing diphenyldiazomethane as a multiply-bonded ligand. Although the U-N_{imido} bond length is longer than typically observed with U(V) monoimido systems (average 1.97 Å[30]), it agrees well with the imido bonds observed with diphenyldiazomethane in other U(IV) and U(VI) systems.[12,13] The U-N_{guan} bond lengths average 2.47(3) Å, and the C-N bond distances in the NCN chelating fragment of the guanidinate ligands fall in the range of 1.32-1.34 Å, indicating no reduction of any of the guanidinate ligands. The room temperature magnetic moment (established by Evans method) of **4.3** is $\mu_{eff} = 2.68\ \mu_B$, whereas the magnetic moments of **4.1** and **4.2** are $\mu_{eff} = 2.93\ \mu_B$ and $\mu_{eff} = 3.34\ \mu_B$, respectively, all consistent with oxidation state assignments of **4.1** – U(IV), **4.2** – U(III), and **4.3** – U(V).[1] Attempts to eliminate N_2 from **4.3**, via photolysis or heating at elevated temperature, and generate a uranium carbene species only resulted in decomposition.

In order to properly assign the short U-N bond distance in **4.3** as an imido, we sought to synthesize a structural comparison through the two-electron oxidation of **4.2** by an organic azide. We were also curious if the $U(TIG)_3$ framework could support the formation of a terminal U(V) oxo in order to probe this system's ability to form stable U(V) complexes through two-electron

Scheme 4.2. Syntheses of Complexes **4.3-4.5**

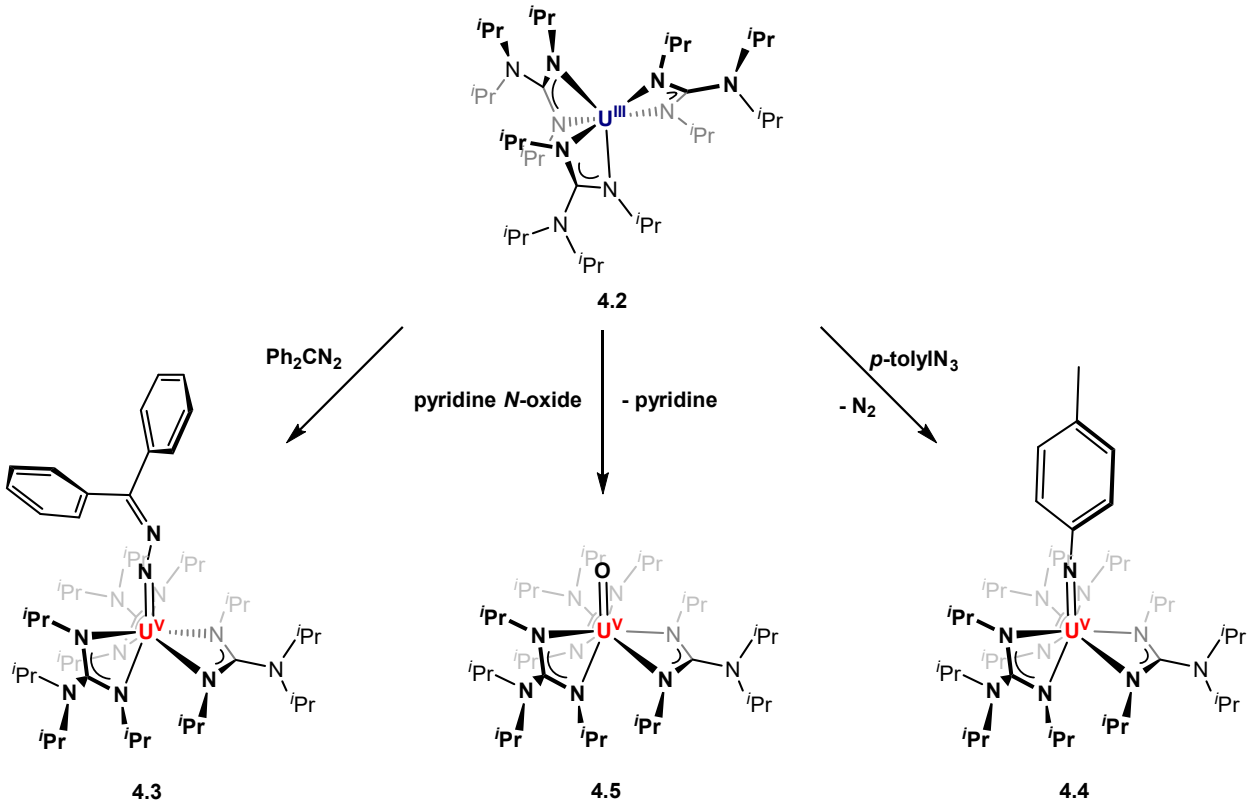

oxidation processes (Scheme 4.2). Lastly, a U(IV) analog containing an amido or azido moiety would serve to clearly demonstrate that the imido bond in **4.3** was not comparable to a U(IV)-N single bond. Treatment of a dark blue hexane solution of **4.2** with a hexane solution of *p*-tolyl azide[31] resulted in an immediate color change to dark red-brown accompanied by bubbling of the solution. Workup and crystallization from pentane afforded U(N-*p*tolyl)(TIG)$_3$ (**4.4**) as red-brown crystals in 76% yield. The identity of **4.4** as the U(V) imido complex was confirmed by X-ray diffraction studies, which revealed a U-N10 bond length of 1.984(4) Å, as well as a U-N10-C40 bond angle of 172.6(4)° (Figure 4.5). The U-N$_{imido}$ bond lengths in **4.3** and **4.4** differ by 0.08 Å, which may be the result of the larger steric profile of the diphenyldiazomethane ligand compared to the *p*-tolyl moiety. Both bond lengths and angles seen in **4.3** and **4.4** are consistent with that seen in other uranium-imido species.[3,30] The room temperature magnetic moment of **4.4** is μ_{eff} = 2.67 μ_B, which is nearly identical to that seen in **4.3**. Redox events for **4.3** and **4.4** were probed using cyclic voltammetry; voltammograms were recorded for **4.3** and **4.4** in dichloromethane using a 0.1 M [Bu$_4$N][PF$_6$] electrolyte. The CV of complex **4.4** exhibits two reversible events (Figure 4.6). Both oxidative U(VI)/U(V) and reductive U(V)/U(IV) processes show negative $E_{1/2}$ values

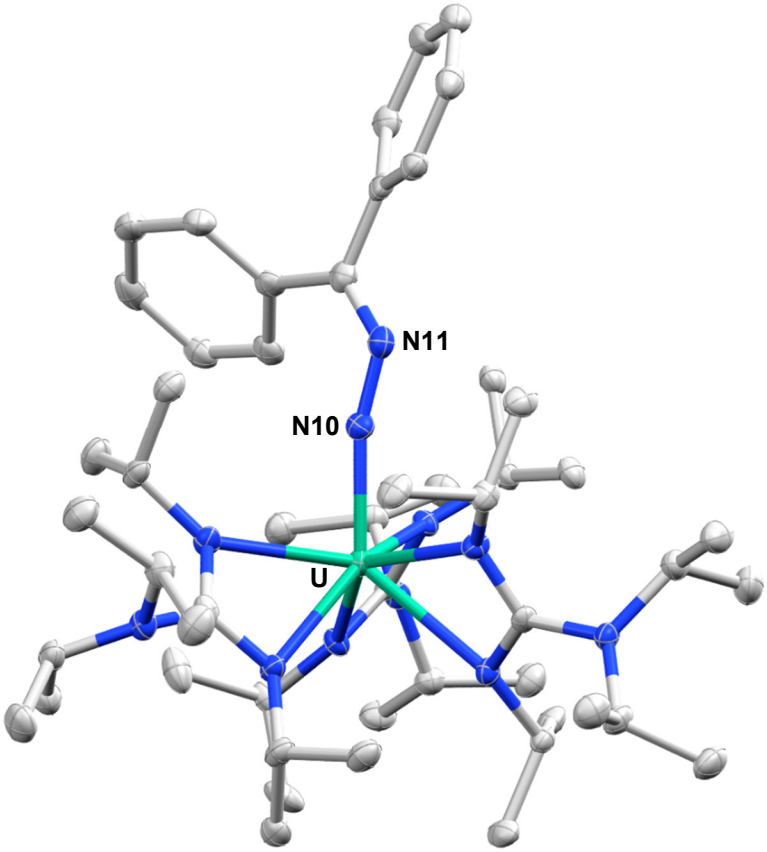

Figure 4.4. Molecular structure of **4.3**. Thermal ellipsoids drawn at the 50% probability level. Hydrogen atoms and pentane solvent molecule omitted for clarity.

(V vs. Fc/Fc^{+}) of -0.83 and -2.7, respectively. Compared to $E_{1/2}$ values previously reported for metallocene[32] and amide[33] supported U(V) imido complexes, the potentials of the redox processes of **4.4** are shifted negatively by almost 800 mV, consistent with the strongly electron-donating nature of the TIG ligand. The CV of **4.3** shows no reversible redox processes. Attempts at chemical oxidation of both **4.3** and **4.4** to access the corresponding U(VI) species were not successful; free N_2CPh_2 was observed by its characteristic stretching frequency in the IR spectra of crude reaction mixtures of **4.3** exposed to various oxidants.

With an analogous imido complex established in **4.4**, we turned our attention to eliciting other U(V) complexes via two-electron oxidation, specifically the $U(O)(TIG)_3$ complex. We envisioned this could be done with an oxygen transfer reagent, such as pyridine *N*-oxide or trimethylamine *N*-oxide. Reaction of **4.2** with pyridine *N*-oxide resulted in an immediate color

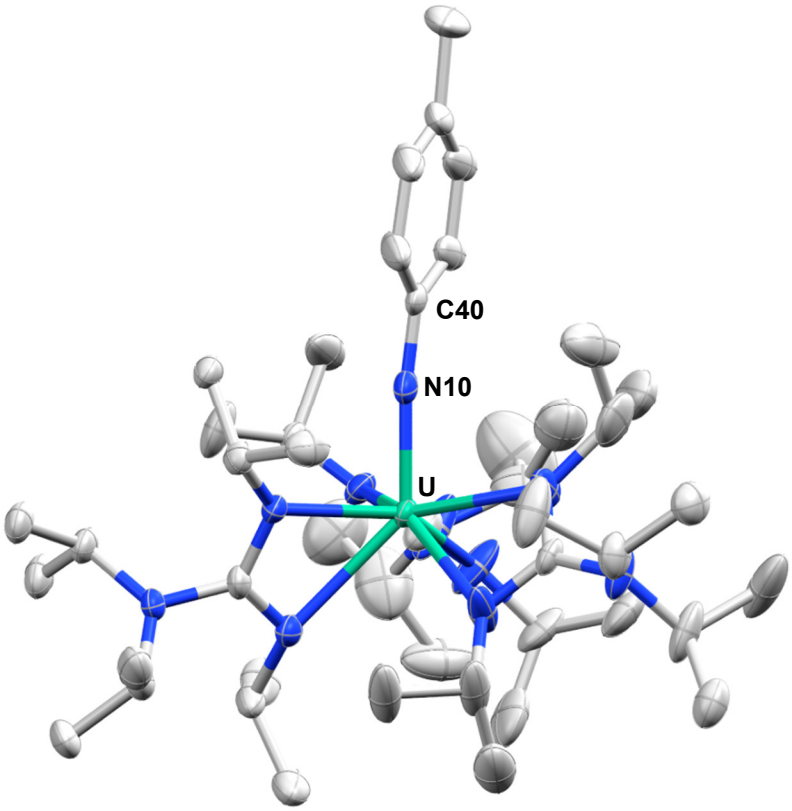

Figure 4.5. Molecular structure of **4.4**. Thermal ellipsoids drawn at the 50% probability level. Hydrogen atom and hexane solvent molecule omitted for clarity.

change from dark blue to dark red, and the U(V) terminal oxo complex U(O)(TIG)$_3$ (**4.5**) was isolated in 89% yield upon workup and isolation from pentane. The terminal nature of the oxo moiety, as well as the lack of coordinated pyridine, was confirmed by X-ray diffraction studies, which revealed a U-O1 bond length of 1.831(2) Å, typical of that seen in other U(V) terminal oxo species (Figure 4.7).[30,34-37] The U-N_{guan} and NCN bond lengths are similar to those observed in complexes **4.3** and **4.4**. The room temperature magnetic moment is μ_{eff} = 2.31 μ_B, less than that seen with **4.3** and **4.4**, but greater that observed by Liddle and co-workers in their terminal U(V) nitride complex [UN(Tren^{TIPS})][Na(12C4)$_2$].[38] Despite the lack of steric protection directly at the oxo moiety, the bulky nature of the tris-guanidinate framework is sufficient to prevent dimerization or decomposition. It was observed by ^{1}H NMR spectroscopy that **4.5** could also be generated from the reaction of **4.2** with trimethylamine *N*-oxide, although this reaction was significantly slowed by the poor solubility of trimethylamine *N*-oxide in C_6D_6.

Having accessed a direct structural comparison to **4.3** through the synthesis of **4.4** and investigated the ability of **4.2** to support other two-electron oxidation processes through the

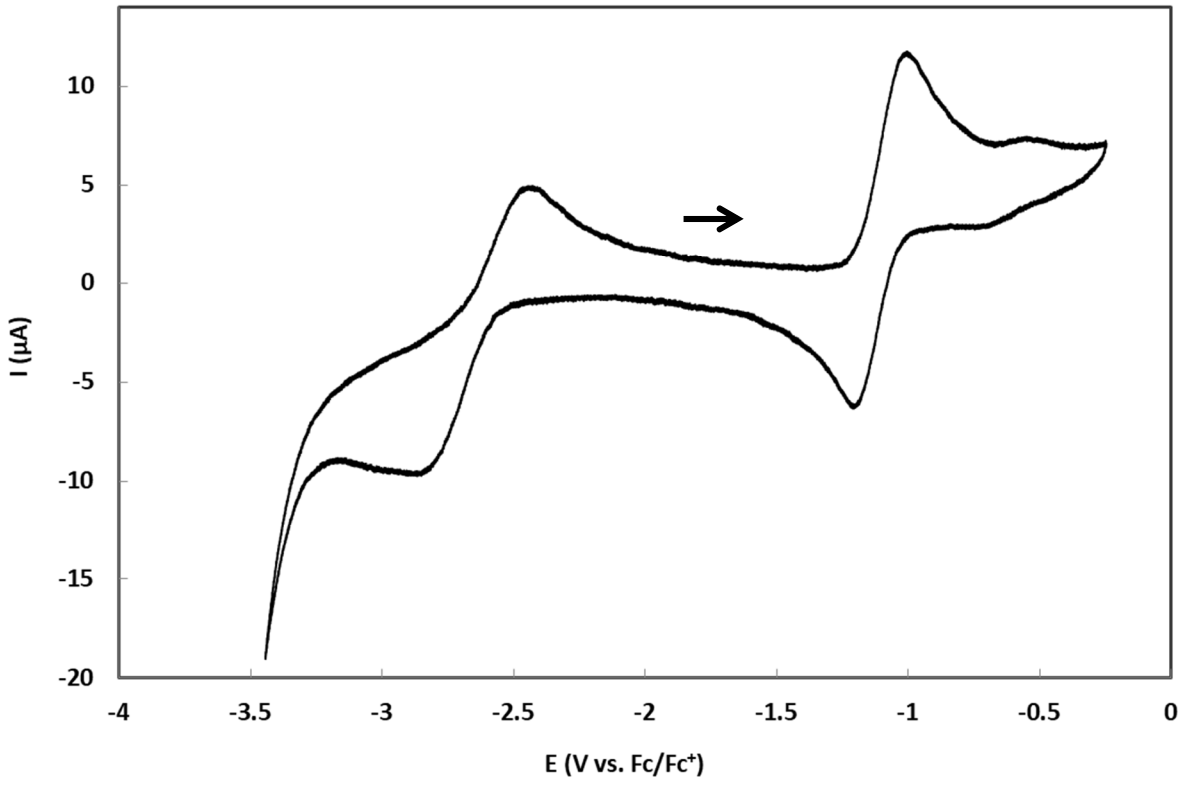

Figure 4.6. Cyclic voltammogram of **4.4**. The scan rate is 100 mV/s. The solvent is dichloromethane. The electrolyte solution is 0.1 M $[Bu_4N][PF_6]$.

generation of **4.5**, we looked to synthesize the corresponding U(IV) amido species in order to determine the U-N_{amido} single bond length for our tris-guanidinate system. However, the synthesis of a U(IV) amido analogue has proved challenging, with single-crystal formation remaining elusive. We turned to installing an azido moiety, as this would still provide a U-N single bond with uranium in the 4+ oxidation state. Salt metathesis of **4.1** with NaN_3 in THF over a period of two days cleanly affords green crystals of $U(N_3)(TIG)_3$ (**4.6**) in 65% yield upon workup and crystallization from diethyl ether (Scheme 4.3). The incorporation of the azido moiety in **4.6** was confirmed by the X-ray crystal structure, which displayed typical azide bond lengths and angles (1.189(3) Å, 1.154(3) Å, and 167.8(2)° for N10-N11, N11-N12, and U-N10-N11, respectively), as well as a U-N10 bond distance of 2.326(2) Å, consistent with other U(IV) azido species (Figure 4.8).[39,40] The strong azide stretching frequency is observed at 2088 cm^{-1} in the FTIR spectrum. Taken together, the data from these structural comparisons further support that **4.3** is best described as a U(V) imido; the U-N_{imido} bond length is much closer to that observed in **4.4** (difference of ~0.08 Å) than the U(IV)-N_{azido} bond length seen in **4.6** (difference of ~0.27 Å).

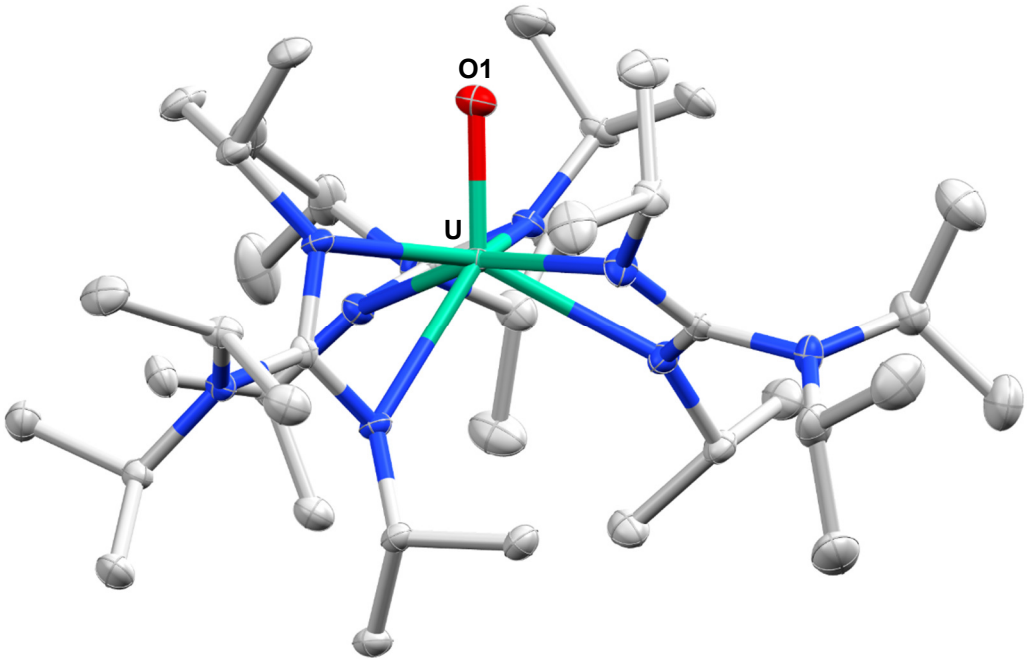

Figure 4.7. Molecular structure of **4.5**. Thermal ellipsoids drawn at the 50% probability level. Hydrogen atoms omitted for clarity.

Scheme 4.3. Synthesis of **4.6**

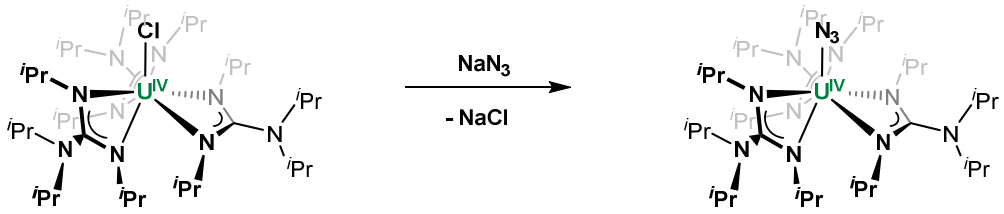

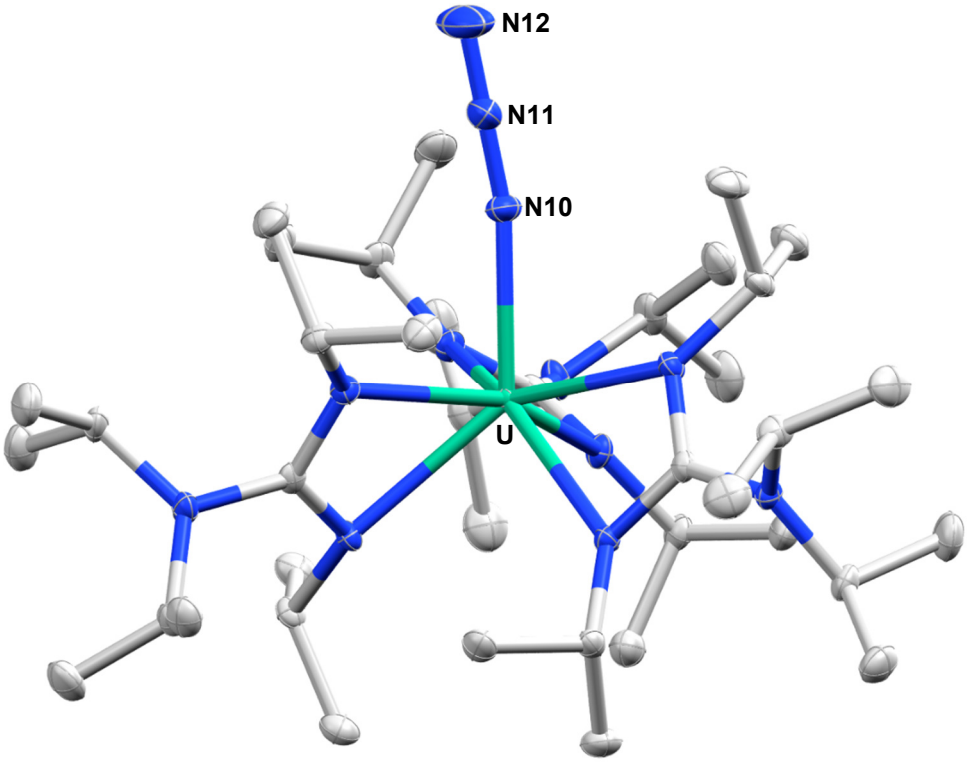

Figure 4.8. Molecular structure of **4.6**. Thermal ellipsoids drawn at the 50% probability level. Hydrogen atoms omitted for clarity.

Table 4.1. Selected Bond Lengths (Å) and Angles (°) for Complexes **4.1-4.6**

Complex	**4.1**	**4.2**	**4.3**	**4.4**	**4.5**	**4.6**
Bond Lengths (Å)						
U-X	2.662(1)	-	2.060(3)	1.984(4)	1.831(2)	2.326(2)
U-N_{guan} (avg.)	2.44(4)	2.49(3)	2.47(3)	2.46(6)	2.46(2)	2.44(2)
Bond Angles (°)						
U-N10-Y	-	-	165.8(3)	172.6(4)	-	167.8(2)

*X is the atom bound directly to U not coming from the amidinate ligands. Y is the atom bound directly to N10 in the structures (N11 for **4.3, 4.6** and C40 for **4.4**).*

Table 4.2. Crystal and Refinement Data for Complexes **4.1-4.6**

Complex	**4.1**	**4.2**	**4.3**	**4.4**	**4.5**	**4.6**
Chemical formula	$C_{39}H_{84}N_9ClU \cdot 1.5(C_6H_{14})$	$C_{39}H_{84}N_9U$	$C_{52}H_{94}N_{11}U \cdot C_5H_{12}$	$C_{46}H_{91}N_{10}U \cdot 0.5(C_6H_{14})$	$C_{39}H_{84}N_9OU$	$C_{39}H_{84}N_{12}U$
Formula weight	1081.88	917.18	1183.55	1065.40	933.19	959.21
Temperature (K)	100(2)	100(2)	100(2)	100(2)	100(2)	100(2)
Crystal system	Monoclinic	Monoclinic	Triclinic	Monoclinic	Monoclinic	Triclinic
Space group	P 21/c	P 21/c	P-1	C 2/c	P 21/c	P-1
a (Å)	11.6454(4)	13.2890(11)	12.3599(6)	39.246(4)	19.9133(19)	13.0981(2)
b (Å)	37.8373(10)	19.9565(16)	12.6609(6)	14.3692(16)	12.7998(16)	13.2024(2)
c (Å)	13.3431(4)	18.7099(14)	21.0290(11)	19.965(2)	19.1902(16)	17.7597(2)
α (°)	90	90	88.8639(11)	90	90	96.1010(10)
β (°)	109.795(3)	110.091(3)	77.3174(11)	109.062(9)	109.856(4)	103.8660(10)
γ (°)	90	90	79.3741(11)	90	90	119.6380(10)
V (Å^3)	5532.0(3)	4659.9(6)	3154.7(3)	10641(2)	4600.5(8)	2497.88(7)
Z	4	4	2	8	4	2
Densitiy (Mg m^{-3})	1.299	1.307	1.246	1.330	1.347	1.275
F(000)	2260	1892	1234	4432	1924	988
Radiation Type	MoK$_\alpha$	MoK$_\alpha$	MoK$_\alpha$	MoK$_\alpha$	MoK$_\alpha$	MoK$_\alpha$
μ (mm^{-1})	3.020	3.517	2.614	3.091	3.566	3.286
Meas. Refl.	61124	246388	50668	88992	109654	58226
Indep. Refl.	11297	8549	11131	9820	9404	12188
R(int)	0.0816	0.0714	0.0338	0.0457	0.0492	0.0589
Final R indices [I > 2σ(I)]	R = 0.0395 R_w = 0.0830	R = 0.0295 R_w = 0.0589	R = 0.0315 R_w = 0.0726	R = 0.0424 R_w = 0.0987	R = 0.0184 R_w = 0.0404	R = 0.0232 R_w = 0.0515
GOF	1.042	1.089	1.115	1.070	1.031	1.041
$\Delta\rho_{max}$, $\Delta\rho_{min}$ (e Å^{-3})	1.855, -1.469	3.202, -1.116	3.501, -0.778	1.850, -1.266	0.682, -0.347	0.798, -0.540

Conclusions

In summary, we have synthesized a number of rare uranium guanidinate complexes, including the first homoleptic U(III) guanidinate and the first diphenyldiazomethane imido complex of uranium in the 5+ oxidation state. Comparative structural studies between other imido and azido analogues clearly demonstrate the multiple-bond character of the U-N linkage in **4.3**, with additional spectroscopic data supporting the U(V) assignment. The stabilization of this U(V) species, as well as the U(V) terminal oxo complex, is tied to the encumbering steric profile provided by the tris-guanidinate framework. The electron richness of the TIG ligand is manifested in the cyclic voltammetry observed for **4.4** and is another important factor in the stability of these complexes. Future studies will involve the comparative reactivity of the imido functionalities in **4.3** and **4.4**.

Experimental Details

General procedures. Unless otherwise stated, all reactions were performed under an atmosphere of dry N_2 using standard Schlenk line techniques or in an MBraun N_2 atmosphere glovebox (<1.0 ppm of O_2/H_2O). Toluene, *n*-hexane, *n*-pentane, THF, and diethyl ether were dried and degassed using a commercially available Phoenix SDS from JC Meyer Solvent Systems. Hexamethyldisiloxane (HMDSO) was distilled from sodium/benzophenone, degassed by sparging with nitrogen, and stored over molecular sieves. All glassware, syringes, and cannulas were stored in a 140 °C oven for a minimum of 16 h prior to use. Deuterated solvents (C_6D_6, tol-d_8) were vacuum-transferred from a flask containing sodium/benzophenone, degassed with three freeze−pump−thaw cycles, and stored over molecular sieves. UCl_4,[22] Li(TIG)(THF),[23] UI_3(1,4-dioxane)$_{1.5}$,[24] N_2CPh_2,[28] and *p*-tolyl azide[31] were prepared according to previously reported literature procedures. Pyridine *N*-oxide was sublimed prior to use. All other reagents were purchased from commercial sources and used as received. Unless otherwise stated, NMR spectra were collected at ambient temperature on an AV-600 spectrometer. ^{1}H NMR chemical shifts (δ) are reported in ppm and were calibrated to residual solvent peaks. Melting points were determined on an Optimelt SRS instrument using capillary tubes sealed under dry N_2. Elemental analysis samples were sealed under vacuum and analyzed at either the London Metropolitan University or the University of California, Berkeley. Infrared spectra were collected on a Thermo Scientific Nicolet iS10 FTIR spectrophotometer using Nujol mulls pressed between KBr plates. Solution magnetic moments were obtained by Evans Method.

UCl(^{i}Pr$_2$NC(N^{i}Pr)$_2$)$_3$ (4.1): UCl_4 (0.939 g, 2.47 mmol) was added to a 250 mL Schlenk flask containing a magnetic stir-bar and dissolved in 30 mL of THF. A THF solution (50 mL) of Li(TIG)(THF) (2.26 g, 7.40 mmol) was added to the dark green solution. Over the course of 4 h, the reaction mixture became a suspension of a light green precipitate in a brown-green solution. Volatiles were removed under reduced pressure and the resulting solid was extracted into toluene (50 mL). A gray-green solid was filtered away, and the brown-green solution was concentrated to 20 mL. Storage of this solution at -40 °C yielded **4.1** as analytically pure, green crystals (2.18 g, 92.8%) ^{1}H NMR (600 MHz, tol-d_8, 293 K): δ 21.69, 18.47, 4.37, 2.95, 0.99. Anal. Calcd for $C_{39}H_{84}N_9ClU$ (952.6): C, 49.17; H, 8.89; N, 13.23. Found: C, 49.42; H, 8.78; N, 12.99. Mp: 168 °C (decomp). FTIR(Nujol): 1408 (w), 1378 (w), 1308 (s), 1212 (s), 1178 (w), 1156 (w), 1133 (m), 1061 (s), 1014 (m), 976 (m), 940 (w), 862 (m), 815 (w), 722 (w), 681 (w), 666 (m), 576 (w), 507 (w), 458 (w), 416 (w). μ_{eff} = 2.93 μ_B. Crystals suitable for single-crystal X-ray diffraction studies were grown from a concentrated *n*-hexane solution stored at -35 °C for 16 h.

U(^{i}Pr$_2$NC(N^{i}Pr)$_2$)$_3$ (4.2): UI_3(1,4-dioxane)$_{1.5}$ (0.500 g, 0.666 mmol) was added to a 20 mL scintillation vial containing a magnetic stir-bar and suspended in 4 mL of THF, resulting in a dark blue-purple suspension. A solution of Li(TIG)(THF) (0.626 g, 2.05 mmol) in THF (12 mL) was added to the reaction mixture; the dark blue solution was stirred at ambient temperature for 3 h. Volatiles were removed under reduced pressure, and the sticky blue-gray solid was triturated with *n*-hexane (2 x 2 mL). The blue-gray solid was then extracted with 8 mL of *n*-hexane and filtered

away from the gray precipitate. Volatiles were removed under reduced pressure, resulting in dark blue and yellow solids. HMDSO (8 mL) was used to extract the blue solid. The solution was filtered, concentrated to 3 mL, and stored at -35 °C to yield **4.2** as analytically pure, dark blue, block crystals (0.445 g, 72.9%). ^{1}H NMR (600 MHz, C_6D_6, 293 K): δ 30.04 (s, C*H*Me$_2$, 6H), 9.36 (m, C*H*Me$_2$, 6H), 4.72 (d, CHC*H*$_3$CH$_3$, 18 H), 4.09 (d, CHC*H*3CH3, 18 H), 0.71 (s, CHC*H*3CH3, 18H), -10.01 (s, CHC*H*$_3$CH$_3$, 18H). Anal. Calcd for $C_{39}H_{84}N_9U$ (917.2): C, 51.07; H, 9.23; N, 13.74. Found: C, 50.74; H, 9.25; N, 13.54. Mp: 165 – 170 °C. FTIR (Nujol): 1631 (w), 1404 (w), 1377 (s), 1362 (m), 1314 (s), 1212 (s), 1133 (m), 1058 (s), 1017 (m), 971 (w), 863 (w), 722 (m), 666 (w), 574 (w), 450 (w). μ_{eff} = 3.34 μ_B. UV-Vis: 614 nm (ε = 323 L/mol·cm). Crystals suitable for single-crystal X-ray diffraction studies were grown from a concentrated HMDSO solution stored at -35 °C for 16 h.

Alternative synthesis of 4.2: Solid **4.1** (0.698 g, 0.733 mmol) was added to a 100 mL Schlenk flask containing a magnetic stir-bar and was dissolved in 40 mL of THF. KC_8 (0.107 g, 0.792 mmol) was added to this green solution. The color of the reaction mixture immediately turned dark teal, then dark blue. This solution was stirred at ambient temperature for 2 h. Volatiles were removed under reduced pressure, and the solid was extracted with HMDSO (20 mL). The solution was filtered through Celite, concentrated to ~3 mL, and stored at -35 °C for 16 h, resulting in dark blue crystals of **4.2** (0.544 g, 81.0%).

U(N$_2$CPh$_2$)(*i*Pr$_2$NC(N*i*Pr)$_2$)$_3$ (4.3): Solid **4.2** (0.300 g, 0.327 mmol) was added to a 20 mL scintillation vial containing a magnetic stir-bar and dissolved in *n*-hexane (5 mL). A magenta solution of diphenyldiazomethane (0.063 g, 0.324 mmol) in *n*-hexane (2 mL) was added slowly to the dark blue U(TIG)$_3$ solution. Immediately upon the addition, the dark blue solution becomes dark red-brown. The reaction mixture was stirred at ambient temperature for 16 h. Volatiles were removed under reduced pressure, resulting in a sticky red-brown solid. Recrystallization of this solid from 2 mL of *n*-pentane yielded **4.3** as analytically pure, dark red-brown crystals (0.263 g, 72.4%). ^{1}H NMR (600 MHz, C_6D_6, 293 K): δ 20.99, 9.74, 8.16, -2.82. Anal. Calcd for $C_{52}H_{94}N_{11}U$ (1110.4): C, 56.20; H, 8.53; N, 13.86. Found: C, 56.01; H, 8.61; N, 13.53. Mp: 129 – 132 °C. FTIR (Nujol): 1596 (w), 1493 (w), 1405 (m), 1378 (m), 1362 (m), 1317 (m), 1209 (s), 1175 (m), 1158 (w), 1132 (m), 1060 (s), 1015 (w), 974 (m), 935 (w), 863 (w), 768 (m), 758 (m), 723 (w), 698 (m), 681 (w), 666 (m), 507 (m), 456 (w). μ_{eff} = 2.68 μ_B. UV-Vis: 467 nm (ε = 1,268 L/mol·cm). Crystals suitable for single-crystal X-ray diffraction studies were grown from a concentrated *n*-pentane solution stored at -35 °C for 16 h.

U(N-*p*tolyl)(*i*Pr$_2$NC(N*i*Pr)$_2$)$_3$ (4.4): Solid **4.2** (0.216 g, 0.236 mmol) was added to a 20 mL scintillation vial containing a magnetic stir bar and dissolved in *n*-hexane (6 mL). In a smaller vial, *p*-tolyl azide was weighed out (0.034 g, 0.255 mmol) and dissolved in 0.5 mL of *n*-hexane. When the azide solution was added slowly to the U(TIG)$_3$ solution, bubbling occurred and the solution color immediately changed from dark blue to dark red-brown. The reaction was then stirred at ambient temperature for 3 h. Volatiles were removed under reduced pressure, resulting in a foamy brown solid. This solid was dissolved in *n*-pentane, concentrated, and stored at -35 °C for 48 h, resulting in red-brown block crystals of **4.4** (0.182 g, 75.6%). ^{1}H NMR (600 MHz, C_6D_6, 293 K):

δ 20.30, 19.89, 10.07, 6.12, 3.62, -1.97. Anal. Calcd for $C_{46}H_{91}N_{10}U$ (1022.3): C, 54.04; H, 8.97; N, 13.70. Found: C, 53.67; H, 8.97; N, 13.48. Mp: 132 – 139 °C. FTIR (Nujol): 1631 (w), 1377 (w), 1362 (m), 1315 (m), 1259 (m), 1211 (s), 1171 (m), 1131 (m), 1057 (s), 973 (w), 901 (w), 859 (w), 813 (m), 722 (m), 681 (w), 665 (w), 506 (w). μ_{eff} = 2.67 μ_B. UV-Vis: 473 nm (ε = 2,842 L/mol·cm). Crystals suitable for single-crystal X-ray diffraction studies were grown from a concentrated *n*-pentane solution stored at -35 °C for 16 h.

U(O)(*i*Pr$_2$NC(N*i*Pr)$_2$)$_3$ (4.5): Solid **4.2** (0.199 g, 0.217 mmol) was added to a 20 mL scintillation vial containing a magnetic stir bar and dissolved in toluene (2 mL). To this stirred solution was added a solution of pyridine *N*-oxide (0.022 g, 0.231 mmol) in toluene (4 mL), resulting in an immediate color change from dark blue to dark red. The reaction was stirred at ambient temperature for 15 min. Volatiles were removed under reduced pressure, and the resulting red solid was triturated with *n*-hexane (4 mL), extracted into *n*-pentane (6 mL), filtered through Celite, concentrated to ~1 mL and stored at -35 °C for 16 h, resulting in red block crystals of **4.5** (0.180 g, 88.9%). ^{1}H NMR (600 MHz, C_6D_6, 293 K): δ 7.88, -1.52, -1.71. Mp: 158-162 °C. FTIR (Nujol): 1378 (s), 1363 (s), 1315 (s), 1211 (s), 1174 (m), 1156 (m), 1132 (m), 1060 (m), 1011 (w), 974 (w), 862 (w), 782 (m), 723 (w), 683 (w), 666 (w), 499 (w). μ_{eff} = 2.31 μ_B. UV-Vis: 486 nm (ε = 874 L/mol·cm) Anal. Calcd for $C_{39}H_{84}N_9OU$ (933.2): C, 50.20; H, 9.07; N, 13.51. Found: C, 49.90; H, 8.72; N, 13.43. Crystals suitable for single-crystal X-ray diffraction studies were grown from a concentrated *n*-pentane solution stored at -35 °C for 72 h.

U(N$_3$)(*i*Pr$_2$NC(N*i*Pr)$_2$)$_3$ (4.6): In a 20 mL scintillation vial containing a magnetic stir bar, NaN_3 (0.010 g, 0.154 mmol) was suspended in 3 mL of THF. A light green, THF solution (10 mL) of **4.1** (0.151 g, 0.159 mmol) was added to the stirring suspension, and the reaction mixture was stirred at ambient temperatures for two days. The reaction mixture became cloudy. Volatiles were removed under reduced pressure and the pale green solid was extracted into diethyl ether. A white precipitate was filtered away, and the pale green solution was concentrated and stored at -35 °C, yielding green crystals of **4.6** (0.099 g, 65.3%). ^{1}H NMR (600 MHz, C_6D_6, 293 K): δ 17.40, 16.45, 10.78, 5.86, 1.81, 0.14, -1.02, -2.43, -6.19. Anal. Calcd for $C_{39}H_{84}N_{12}U$ (959.2): C, 48.83; H, 8.83; N, 17.52. Found: C, 49.14; H, 8.62; N, 17.23. Mp: 225 °C (decomp). FTIR (Nujol): 2088 (s), 1377 (m), 1309 (w), 1210 (s), 1181 (m), 1158 (m), 1132 (m), 1061 (m), 1013 (w), 975 (w), 863 (w), 722 (w), 682 (w), 665 (w), 505 (w). Crystals suitable for single-crystal X-ray diffraction studies were grown from a concentrated *n*-pentane solution stored at -35 °C for 24 h.

Crystallographic Procedures. Single-crystal X-ray diffraction experiments were performed at the UC Berkeley CHEXRAY crystallographic facility. Measurements for compounds **4.1**, **4.6** were performed on a Rigaku XtaLAB P200 rotating anode equipped with a Pilatus 200K hybrid pixel array detector. Data were collected using Mo Kα radiation (λ = 0.71073 Å). Crystals were kept at 100(2) K throughout collection. Data collection was performed with CrysAlis^{Pro}.[41] Data processing was done using CrysAlis^{Pro} and included a multi-scan absorption correction applied using the SCALE3 ABSPACK scaling algorithm within CrysAlis^{Pro}. Measurements for compounds **4.2-4.5** were performed on a Bruker APEX-II area detector using Mo Kα radiation (λ = 0.71073 Å). Crystals were kept at 100(2) K throughout collection. Data collection was performed

with Bruker APEX2 software (v. 2014.11). Data refinement and reduction were performed with Bruker SAINT (V8.34A). All structures were solved with SHELXT.53.[42] Structures were refined with SHELXL-2014.[43] Molecular graphics were computed with Mercury 3.10. All non-hydrogen atoms were refined anisotropically, and hydrogen atoms were either included at the geometrically calculated positions and refined using a riding model or located as Q peaks in the Fourier difference map. Compounds **4.3**, **4.4**, and **4.6** contained highly disordered outer sphere solvent molecules that could not be accurately modeled; the data for these structures were treated with the SQUEEZE routine included in PLATON.[44]

References

(1) Liddle, S. T. *Angew. Chem., Int. Ed.*, **2015**, *54*, 2-40.
(2) Gardner, B. M.; Kafalidis, C. E.; Lu, E.; Patel, D.; McInnes, E. J. L.; Tuna, F.; Wooles, A. J.; Maron, L.; Liddles, S. T. *Nat. Commun.* **2017**, *8*, 1898 (2017).
(3) Seyam, A. M. *Inorg. Chim. Acta*, **1982**, *58*, 71-74.
(4) Kraft, S. J.; Fanwick, P. E.; Bart, S. C. *J. Am. Chem. Soc.* **2012**, *134*, 6160-6168.
(5) Hayton, T. W. *Dalton Trans.* **2010**, *39*, 1145-1158.
(6) Hayton, T. W. *Chem. Commun.* **2013**, *49*, 2956-2973.
(7) Andersen, R. A. *Inorg. Chem.* **1979**, *18*, 1507-1509.
(8) Arney, D. S. J.; Burns, C. J.; Smith, D. C. *J. Am. Chem. Soc.* 1992, *114*, 10068-10069.
(9) Roussel, P.; Boaretto, R.; Kingsley, A. J.; Alcock, N. W.; Scott, P. *J. Chem. Soc.*, *Dalton Trans.* **2002**, 1423-1428.
(10) Castro-Rodriguez, I.; Olsen, K.; Gantzel, P.; Meyer, K. *J. Am. Chem. Soc.* **2003**, *125*, 4565-4571.
(11) Lam, O. P.; Feng, P. L.; Heinemann, F. W.; O'Connor, J. M.; Meyer, K. *J. Am. Chem. Soc.* **2008**, *130*, 2806-2816.
(12) Kiplinger, J. L.; Morris, D. E.; Scott, B. L.; Burns, C. J. *Chem. Commun.* **2002**, 30-31.
(13) Cantat, T.; Graves, C. R.; Scott, B. L.; Kiplinger, J. L. *Angew. Chem., Int. Ed.* **2009**, *48*, 3681-3684.
(14) Matson, E. M.; Fanwick, P. E.; Bart, S. C. *Eur. J. Inorg. Chem.* **2012**, 5471-5478.
(15) Ephritikhine, M. *Organometallics* **2013**, *32*, 2464-2488.
(16) Camp, C.; Settineri, N.; Lefevre, J.; Jupp, A. R.; Goichoechea, J. M.; Maron, L.; Arnold, J. *Chem. Sci.* **2015**, *6*, 6379-6384.
(17) Settineri, N. S.; Garner, M. E.; Arnold, J. *J. Am. Chem. Soc.* **2017**, *139*, 6261-6269.
(18) Settineri, N. S.; Arnold, J. *Chem. Sci.* **2018**, *9*, 2831-2841.
(19) Villiers, C.; Thuéry, P.; Ephritikhine, M. *Chem. Commun.* **2007**, 2832-2834.
(20) Montalvo, E.; Ziller, J. W.; DiPasqule, A. G.; Rheingold, A. L.; Evans, W. J. *Organometallics* **2010**, *29*, 2104-2110.
(21) Maity, A. K.; Metta-Magaña, A. J.; Fortier, S. *Inorg. Chem.* **2015**, *54*, 10030-10041.
(22) Kiplinger, J. L.; Morris, D. E.; Scott, B. L.; Burns, C. J. *Organometallics* **2002**, *21*, 5978-5982.
(23) Pang, X.-A.; Yao, Y.-M.; Wang, J.-F.; Sheng, H.-T.; Zhang, Y.; Shen, Q. *Chin. J. Chem.* **2005**, *23*, 1193-1197.
(24) Monreal, M. J.; Thomson, R. K.; Cantat, T.; Travia, N. E.; Scott, B. L.; Kiplinger, J. L. *Organometallics* **2011**, *30*, 2031-2038.
(25) Schwab, P.; Mahr, N.; Wolf, J.; Werner, H. *Angew. Chem., Int. Ed.* **1993**, *32*, 1480-1482.
(26) Herrmann, W. A.; Hubbard, J. L.; Bernal, I.; Korp, J. D.; Haymore, B. L.; Hillhouse, G. L. *Inorg. Chem.* **1984**, *23*, 2978-2983.

(27) Ortmann, D. A.; Weberndörfer, B.; Schöneboom, J.; Werner, H. *Organometallics* **1999**, *18*, 952-954.
(28) Javed, M. I.; Brewer, M. *Org. Synth.* **2008**, *85*, 189.
(29) Iikubo, T.; Itoh, T.; Hirai, K.; Takahashi, Y.; Kawano, M.; Ohashi, Y.; Tomioka, H. *Eur. J. Org. Chem.* **2004**, 3004-3010.
(30) Boreen, M. A.; Arnold, J. "Multiple Bonding in Actinide Chemistry. " In *Encyclopedia of Inorganic and Bioinorganic Chemistry*. **2018**, doi.org/10.1002/9781119951438.eibc2535.
(31) Zhao, J.; Li, Z.; Yan, S.; Xu, S.; Wang, M.; Fu, B.; Zhang, Z. *Org. Lett.* **2016**, *18*, 1736-1739.
(32) Thomson, R. K.; Cantat, T.; Scott, B. L.; Morris, D. E.; Batista, E. R.; Kiplinger, J. L. *Nat. Chem.* **2010**, *2*, 723-729.
(33) Graves, C. R.; Yang, P.; Kozimor, S. A.; Vaughn, A. E.; Clark, D. L.; Conradson, S. D.; Schelter, E. J.; Scott, B. L.; Thompson, J. D.; Hay, J.; Morris, D. E.; Kiplinger, J. L. *J. Am. Chem. Soc.* **2008**, *130*, 5272-5285.
(34) Bart, S. C.; Anthon, C.; Heinemann, F. W.; Bill, E.; Edelstein, N. M.; Meyer, K. *J. Am. Chem. Soc.* **2008**, *130*, 12536-12546.
(35) Fortier, S.; Kaltsoyannis, N.; Wu, G.; Hayton, T. W. *J. Am. Chem. Soc.* **2011**, *133*, 14224-14227.
(36) Fortier, S.; Brown, J. L.; Kaltsoyannis, N.; Wu, G.; Hayton, T. W. *Inorg. Chem.* **2012**, *51*, 1625-1633.
(37) Arney, D. S. J.; Burns, C. J. *J. Am. Chem. Soc.* **1993**, *115*, 9840-9841.
(38) King, D. M.; Tuna, F.; McInnes, E. J. L.; McMaster, J.; Lewis, W.; Blake, A. J.; Liddle, S. T. *Science*, **2012**, *337*, 717-720.
(39) Castro-Rodriguez, I.; Nakai, H.; Zakharov, L. N.; Rheingold, A. L.; Meyer, K. *Science* **2004**, *305*, 1757-1759.
(40) Mullane, K. C.; Carroll, P. J.; Schelter, E. J. *Chem. Eur. J.* **2017**, *23*, 5748-5757.
(41) Rigaku Oxford Diffraction, (2015), CrysAlisPro Software system, version 1.171.39.7a, Rigaku Corporation, Oxford, UK.
(42) Sheldrick, G. M. *Acta. Crystallogr.* **2015**, *A71*, 3-8.
(43) Sheldrick, G. M. *Acta. Crystallogr.* **2008**, *A64*, 112-122.
(44) Spek, A. L. *Acta. Crystallogr., Sect. C: Cryst. Struct. Commun.*, **2015**, *71*, 9-18.

Chapter 5

Dioxygen Reactivity with Thorium Dialkyls Supported by Amidinate and Guanidinate Frameworks

Chapter 5

Overview

While the reactivity of transition-metal alkyl complexes has been extensively explored over the past few decades, the reactivity of these species with molecular oxygen has been limited to mostly late transition-metals, with only a handful of early transition-metals capable of productive reactivity. Actinides, in general, are very susceptible to decomposition via exposure to molecular oxygen; many of the actinide metals are prone to oxidation, and formation of the corresponding actinide oxides is very thermodynamically favorable. However, thorium has been shown to often act in an analogous fashion to group IV metals, and several examples of early transition-metal reactivity with molecular oxygen were seen with group IV complexes. The following chapter describes the synthesis, characterization and reactivity of thorium dialkyl complexes supported by amidinate and guanidinate ligand frameworks, which undergo insertion of molecular oxygen to form the corresponding dialkoxide species.

Introduction

The chemical oxidation of relatively inert C-H bonds of hydrocarbons to produce value-added products is a major goal of academic and industrial research due to its far-reaching implications in commercial processes.[1,2] Molecular oxygen presents itself as an ideal oxidant, due its natural abundance, non-existant environmental impact, and inexpensive cost, and thus many industries have learned to utilize molecular oxygen as their oxidant of choice.[1] However, the use of expensive and environmentally hazardous oxidants still maintains a prominent role in many industies,[3] as oxidation with molecular oxygen can be difficult to control, often leading to undesirable side reactions such as overoxidation.[4] Transition-metal complexes, particularly those of late transition-metals, have proven themselves to be powerful tools for the generation of value-added produts,[3,5] although combining this efficacy with the use of molecular oxygen has proven difficult,[6] due to a poor understanding of how oxygen reacts with these metal species. Significant work in this field has been achieved by the Goldberg group, who have investigated a number of mechanistic steps in the reaction of oxygen with various late transition-metal complexes.[7-12] However, a major drawback to these systems is the high cost of the precious metals involved.

While the use of early transition-metals to faciliate such reactions would have the added benefit of low financial cost due to the relative earth abundance of these metals, even less is known about how oxygen reacts with d^0 transition-metal complexes.[13-20] Wolczanski and co-workers were able to observe insertion of molecular oxygen into titanium and zirconium dialkyl species containing the tritox supporting ligand (tritox = $(^t\text{Bu})_3\text{CO}$) to form the corresponding alkoxide complexes.[13] Mechanistic investigations on this system seemed to indicate a radical propagation mechanism was responsible for the observed reactivity, and the poorly electron-donating nature of the tritox ligand (and thus increased electrophilicity of the metal center) was partly responsible for the inner sphere attack by either oxygen or the propagating radical species (Scheme 5.1).[14]

Scheme 5.1. Proposed Mechanism for the Reactivity of O_2 with $(Tritox)_2M(Me_2)$

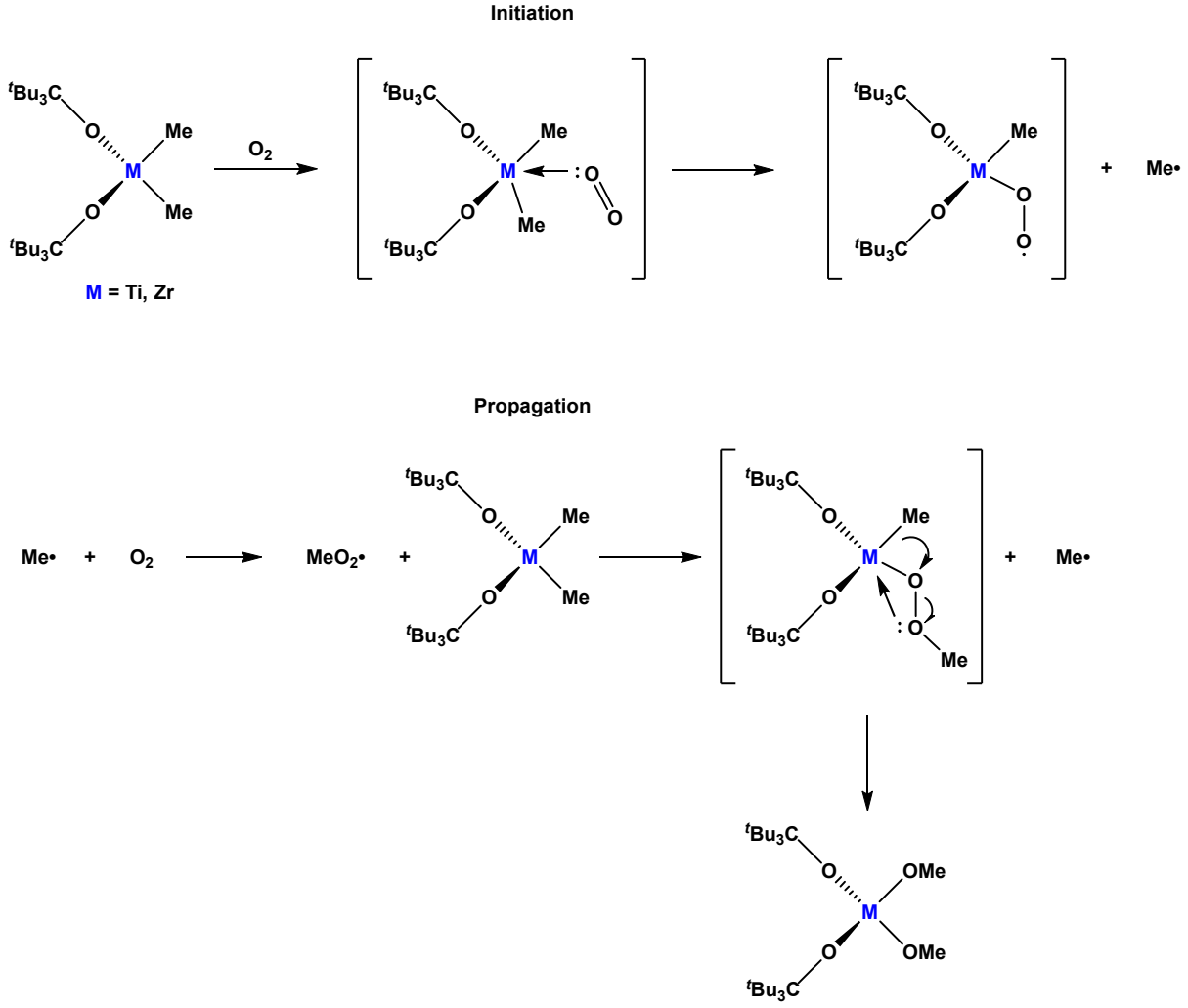

Intrigued by the results observed with group IV metals, we were curious to see if appropriately tailored thorium complexes would undergo similar molecular oxygen reactivity, as the debate regarding whether thorium behaves more like a transition-metal or actinide is still ongoing.[21] While there have been studies regarding the reactivity of thorium and oxygen in argon and neon matrices at 10 and 4 K, respectively,[22] there have no been molecular thorium species which have exhibited similar reactivity to that observed in early transition-metal systems. Our group has previously reported on the reactivity of a thorium monoalkyl complex supported by a tris-amidinate framework with chalcogen-atom transfer reagents[23] and a variety of small molecules;[24] we envisioned a similar, bis-amidinate, dialkyl thorium system may be suitable for reactivity with molecular oxygen. Similarly, the more electron-donating guanidinate ligand,[25] of

which there are no current thorium complexes known, would serve as a useful comparison regarding the effect of metal electrophilicity on reaction kinetics. Herein, we present the synthesis and characterization of thorium dialkyl complexes featuring both amidinate and guanidinate supporting frameworks, as well as their reactivity towards molecular oxygen.

Results and Discussion

Synthesis of Amidinate-Supported Thorium Dialkyls. Although previous studies had employed the bis(isopropyl)methylamidinate (BIMA) ligand, attempted syntheses of a $ThX_2(BIMA)_2$ complex (where X = halide) were unsuccessful. Eisen and co-workers were successfully able to synthesize a thorium bis-amidinate complex utilizing a bulkier *N*,*N*'-bis(trimethylsilyl)-2-pyridylamidinate ligand,[26] so we decided to investigate *N*,*N*'-bis(trimethylsilyl)benzamidinate (BTBA), due to its ease of synthesis and its prior use with actinide metals.[27,28] Salt metathesis of $ThCl_4(DME)_2$[29] with 2 equiv. of Li(BTBA)(TMEDA)[30] (TMEDA = tetramethylethylenediamine) afforded $Th(BTBA)_2Cl(\mu\text{-}Cl)_2Li(TMEDA)$ (**5.1**) as large, colorless blocks in 78% yield (Scheme 5.2). The ^{1}H NMR spectrum of **5.1** exhibits

Scheme 5.2. Synthesis of Complexes **5.1** and **5.2** from Li(BTBA)(TMEDA)

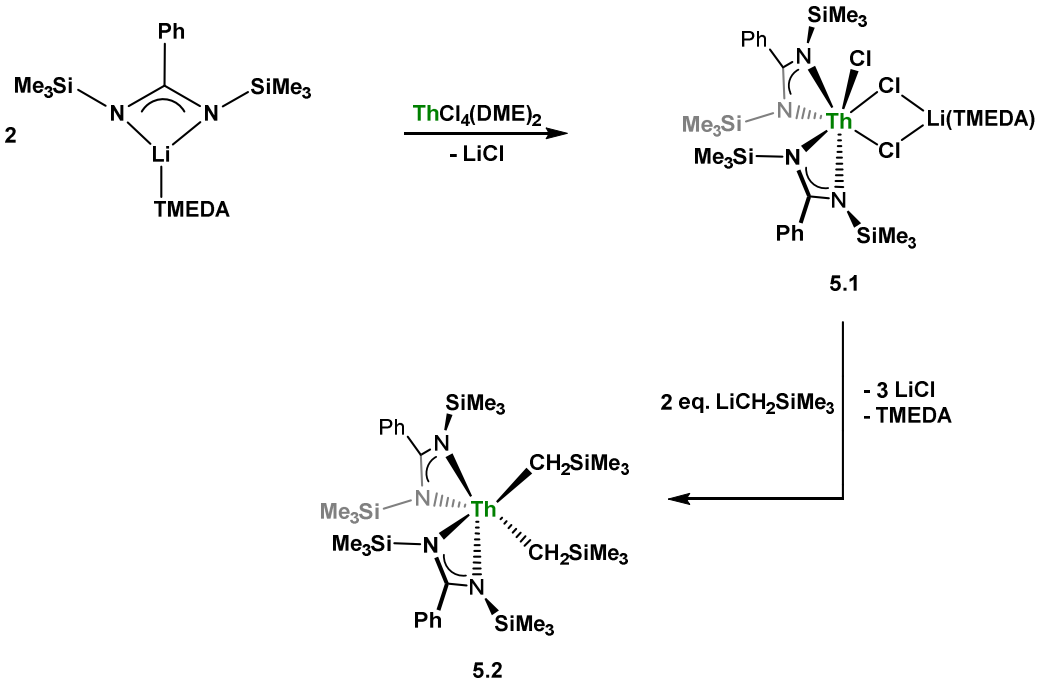

equivalent amidinate ligands in solution, with only one observable resonance for the -$SiMe_3$ protons at δ 0.34 ppm and phenyl resonances appearing at δ 7.35 and 7.03 ppm, as well as two singlets at δ 2.07 and 1.72 ppm corresponding to the TMEDA-methyl and methylene protons, respectively. The molecular structure of **5.1** was determined by single-crystal X-ray diffraction studies (Figure 5.1). The Th-N_{amid} bond distances are typical of that observed with previous thorium amidinate complexes,[23,24,26,29] while the terminal Th-Cl1 bond length of 2.7030(8) Å is noticeably shorter than the bond lengths observed for the bridging chlorides (2.8148(8) and 2.7999(6) Å for Th-Cl2 and Th-Cl3, respectively), as expected. The thorium, lithium and two bridging chlorides exhibit a dihedral angle of ~9° and thus form a nearly flat metallacycle. This is similar to that observed with the 2-pyridyl system reported by Eisen (dihedral angle of ~5°).[26] Electron delocalization is observed throughout the amidinate ligands, as all the C-N bond lengths fall between 1.33-1.34 Å.

With **5.1** in hand, we looked to synthesize the corresponding dialkyl complex; addition of 2 equiv. of $LiCH_2SiMe_3$ to a stirred solution of **5.1** in toluene resulted in immediate precipitation of LiCl, followed by a gradual color change from colorless to orange. This orange color could be avoided by decreasing the reaction time to only a few minutes, and upon workup and crystallization from hexane the dialkyl complex $Th(BTBA)_2(CH_2SiMe_3)_2$ (**5.2**) was isolated as colorless crystals

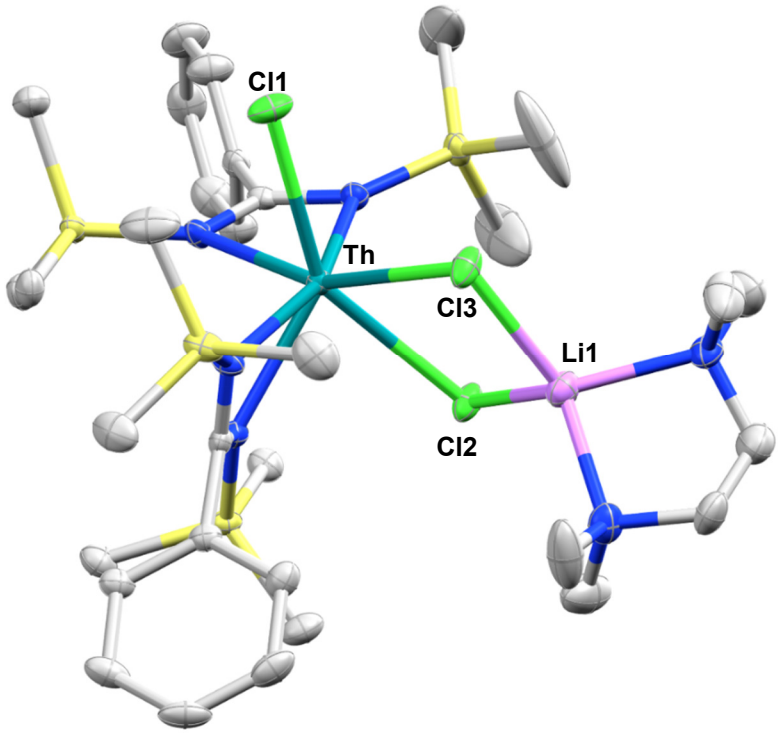

Figure 5.1. Molecular structure of **5.1**. Thermal ellipsoids drawn at the 50% probability level. Hydrogen atoms omitted for clarity.

in 76% yield (Scheme 5.2). ^{1}H NMR spectroscopy of **5.2** shows incorporation of the alkyl moieties with singlets attributable to the methylene and -SiMe$_3$ protons at δ 0.42 and 0.51 ppm, respectively. The molecule exhibits averaged C_2-symmetry in solution, as there is only a single set of peaks corresponding to the alkyl and amidinate ligands. Interestingly, the alkyl methylene resonance is significantly more downfield than that observed in Th(CH$_2$SiMe$_3$)(BIMA)$_3$ (**2.2**, δ -0.08 ppm).[23] This may be indicative of an even more electrophilic thorium center in **5.2** than in **2.2**. The methylene singlet serves as a very diagnostic NMR handle for determining the success of insertion reactions. Unlike in **2.2**, there are no indications of any C-H-Th α-agostic interactions in **5.2**. Single-crystals of **5.2** were grown from a concentrated hexane solution, and the molecular structure was determined by X-ray diffraction studies (Figure 5.2). Two molecules crystallize in the asymmetric unit, thus the metrics discussed are an average of the two molecules. Although the thorium center is six-coordinate, the ligand geometry around the metal center is pseudo-tetrahedral, similar to that seen in Th(BIMA)$_4$ (**3.1**). The average Th-C bond length of 2.492(5) Å is shorter than that seen in **2.2** (2.557(3) Å), but is typical of that seen with other thorium (IV)

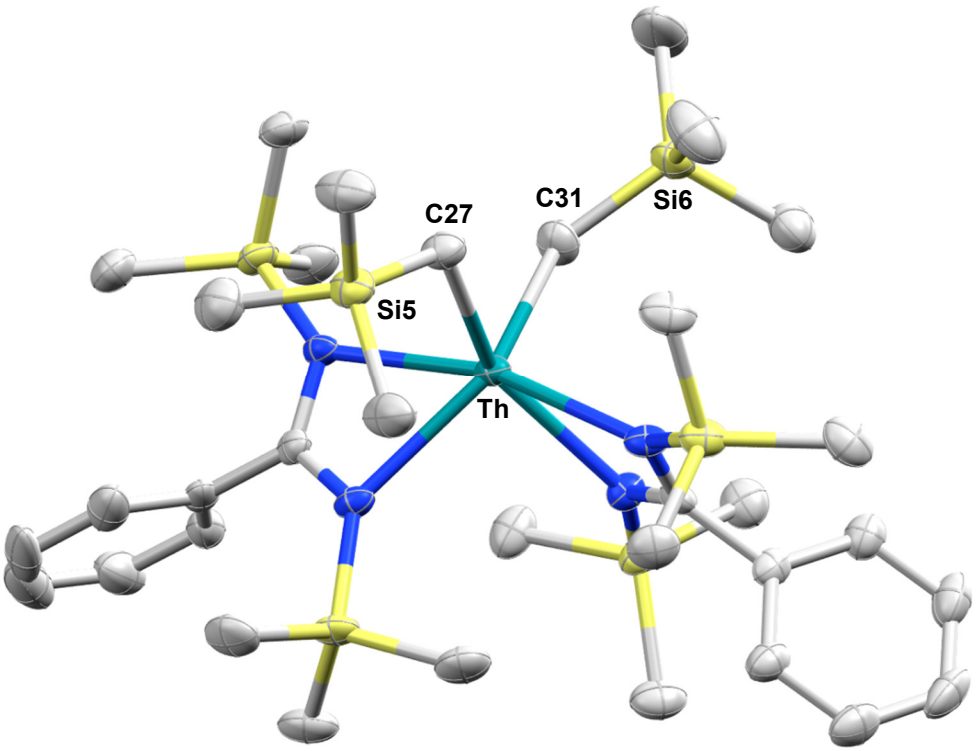

Figure 5.2. Molecular structure of **5.2**. Thermal ellipsoids drawn at the 50% probability level. Hydrogen atoms omitted for clarity.

complexes bearing the -CH_2SiMe_3 ligand.[31-36] The Th-C-Si bond angle of 125.1(2)° is ~10° lower than in **2.2**; this may be due to the less congested nature of the bis-amidinate system. Th-N_{amid} bond distances range from 2.440(3) to 2.566(3) Å while the C-N bonds within the amidinates fall between 1.32-1.35 Å, typical of that seen with other thorium amidinate complexes.[23,24,37-39]

With **5.2** successfully synthesized, we looked to see if this complex would mimic the reactivity with molecular oxygen previously seen by Wolczanski's group IV tritox systems.[13,14] Exposure of a C_6D_6 solution of **5.2** to dry oxygen resulted in conversion to a new product in less than five minutes. In cases where solutions of **5.2** contained a pale-orange hue (due to extended reaction times during the synthesis of **5.2**), addition of dry oxygen lead to an instantaneous change from pale-orange to colorless, with ^{1}H NMR spectroscopy revealing full conversion to the new product. Looking at the ^{1}H NMR spectrum, the most striking change is the methylene resonance of the alkyl substituents, which shifts downfield from δ 0.42 to δ 4.18 ppm (Figure 5.3). This was an indication that O_2 insertion was successfully achieved, as the downfield shift is due to the deshielding nature of the oxygen atom on the methylene protons. This new product was tentatively

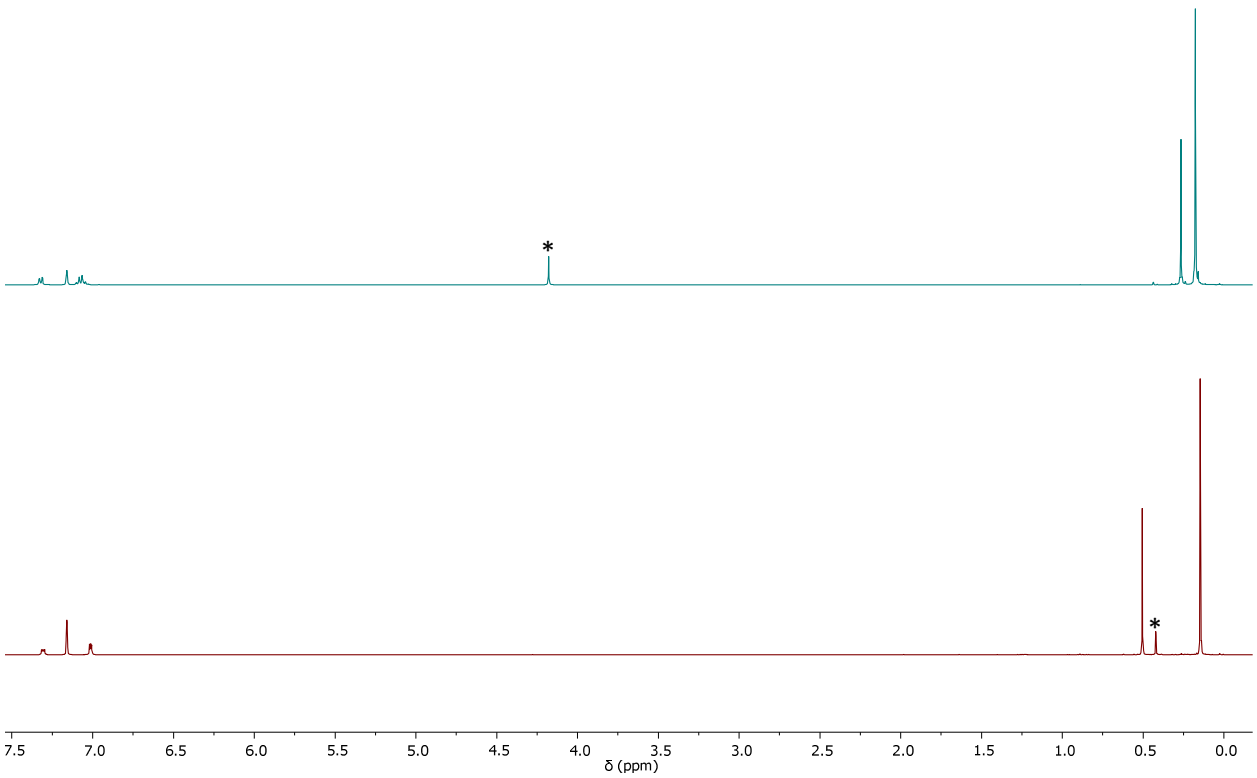

Figure 5.3. Stacked ^{1}H NMR spectrum of **5.2** (bottom) and **5.3** (top) in C_6D_6 at 293 K. *Indicates the methylene resonance in each complex.

assigned as $Th(BTBA)_2(OCH_2SiMe_3)_2$ (**5.3**, Scheme 5.3). Scaling up the reaction revealed the highly soluble nature of **5.3**, which had to be isolated from <1 mL of hexamethyldisiloxane (HMDSO) on a 550 mg scale. Fortuitously, X-ray quality crystals were obtained from a highly concentrated HMDSO solution of **5.3** stored at -35 °C for 24 h, confirming the identity of **5.3** as the O_2 insertion product (Figure 5.4). The Th-O1 and Th-O2 bond distances of 2.133(4) and 2.127(4) Å, respectively, are similar to the Th-O bond length of 2.1663(15) Å seen in $Th(OCH_2NMe_2)(BIMA)_3$ (**2.4**) and fall in the range observed for known thorium alkoxide and aryloxide species.[40-43] The near linear Th-O1-C27 and Th-O2-C31 bond angles of 175.4(3)° and 169.4(3)°, respectively, are also consistent with those previously mentioned thorium alkoxy complexes. The Th-N_{amid} bond distances range from 2.508(4) to 2.577(4) Å, while the C-N bond distances in the amidinate fall in between 1.32-1.34 Å. Mechanistically, we were curious if this

Scheme 5.3. Synthesis of **5.3** via O_2 insertion

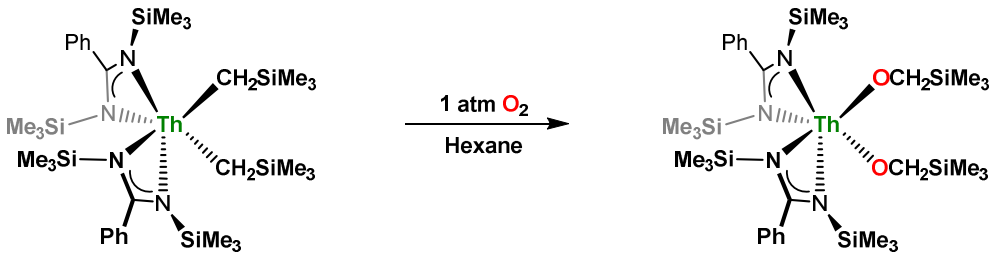

5.2 **5.3**

was operating by a radical mechanism analogous to what Wolczanski had observed with the group IV tritox complexes. However, carrying out the converison of **5.2** to **5.3** in the presence of 1,4-cyclohexadiene produced no appreciable amount of tetramethylsilane (the product formed from the scavenging of C_6H_{10} allylic hydrogens by propagating $\bullet CH_2SiMe_3$ radical species), and the rate of **5.3** formation was not noticeably affected. This does not disprove the radical-based mehanism, though, as the kinetics of formation of **5.3** may be significantly faster than radical abstraction by 1,4-cyclohexadiene. Continued mechanistic investigations are discussed later in this chapter.

Having successfully synthesized **5.3**, we were curious if other chalcogenolate species could be synthesized with this system. While gaseous versions of sulfur, selenium and tellurium are not synthetically accessible for Schlenk chemistry, many chalcogen-atom transfer reagents are readily available for this purpose. Of the reagents tested, only $Ph_3P{=}Se$ and $Me_3P{=}Se$ were able to successfully insert into **5.2** to generate a dichalcogenolate species, specifically $Th(BTBA)_2(SeCH_2SiMe_3)_2$ (**5.4**, Scheme 5.4). Monitoring the reaction by ^1H NMR spectroscopy,

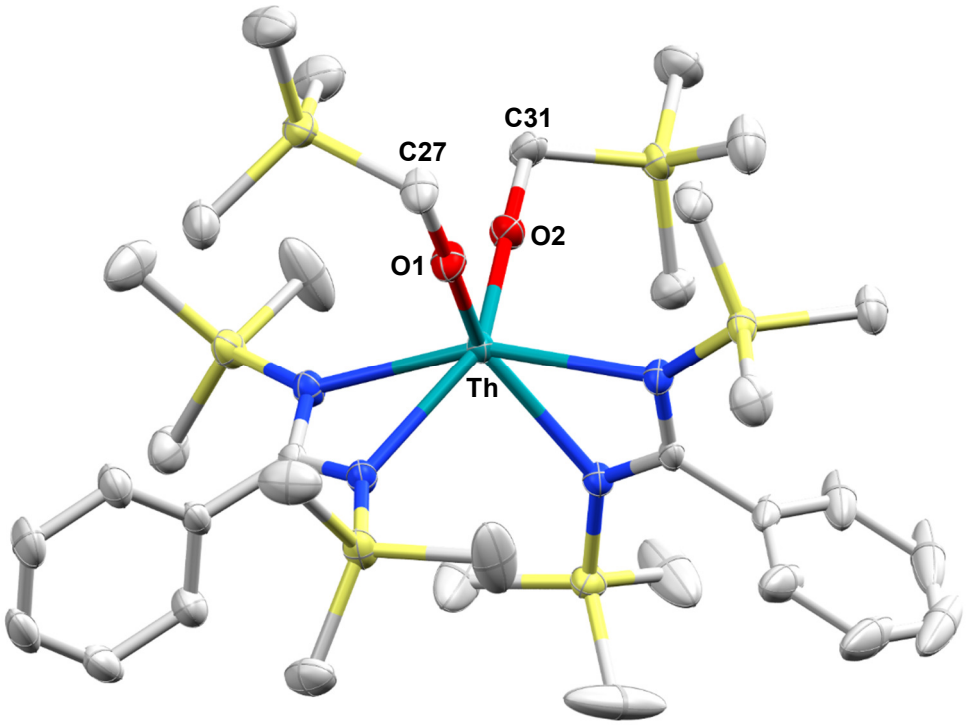

Figure 5.4. Molecular structure of **5.3**. Thermal ellipsoids drawn at the 50% probability level. Hydrogen atoms omitted for clarity.

Scheme 5.4. Synthesis of **5.4** via Selenium Atom Transfer

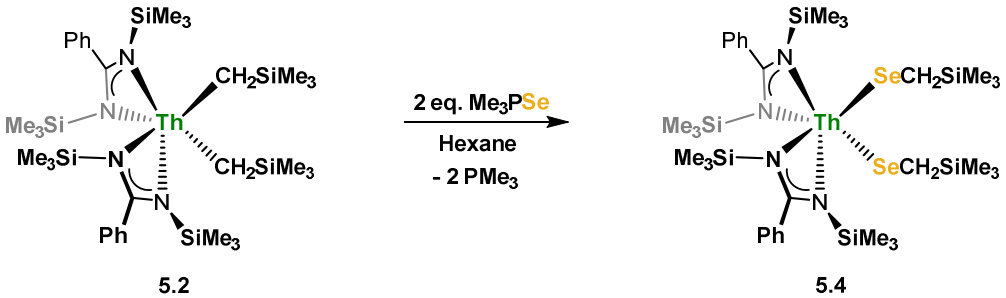

the methylene singlet shifts downfield to δ 2.18 ppm, similar to that seen with $Th(SeCH_2SiMe_3)(BIMA)_3$ (**2.7**, δ 2.25 ppm), indicating successful insertion of selenium into the Th-C bonds. The use of $Me_3P{=}Se$ was preferable over $Ph_3P{=}Se$, as the volatile PMe_3 by-product could be removed under reduced pressure. The identity of **5.4** as the diselenolate complex was confirmed by X-ray diffraction studies (Figure 5.5). The Th-Se1 and Th-Se2 bond lengths of 2.8870(5) and 2.8465(6) Å, respectively, are shorter than the distance of 2.9317(5) Å seen in **2.7**, but are in the range observed for previously reported Th-Se complexes.[44-49] Again, the most striking feature of this molecular structure is the sharply acute Th-Se1-C27 and Th-Se-C31 bond angles of 80.3(1)° and 83.1(1)°, respectively, which are similar to that seen in **2.7** (80.98(13)°). We had previously attributed this angle largely to crystal packing effects due to the shallow potential energy well calculated for **2.7**, which shows a minimal (~2 kcal mol^{-1}) energy difference over a 20° range for the Th-Se-C bond angle in the gas phase.[23] We believe crystal packing effects are still the dominant forces governing this acute angle, as the $^1J_{C,H}$ coupling constant of 125 Hz for the methylene resonance in **5.4** (as measured from the ^{13}C satellites observed in the ^1H NMR spectrum) is in the range expected for a sp^3-hybridized carbon atom, unlike that seen with **2.2** and other actinide alkyl systems that have been proposed to contain C-H-Th α-agostic

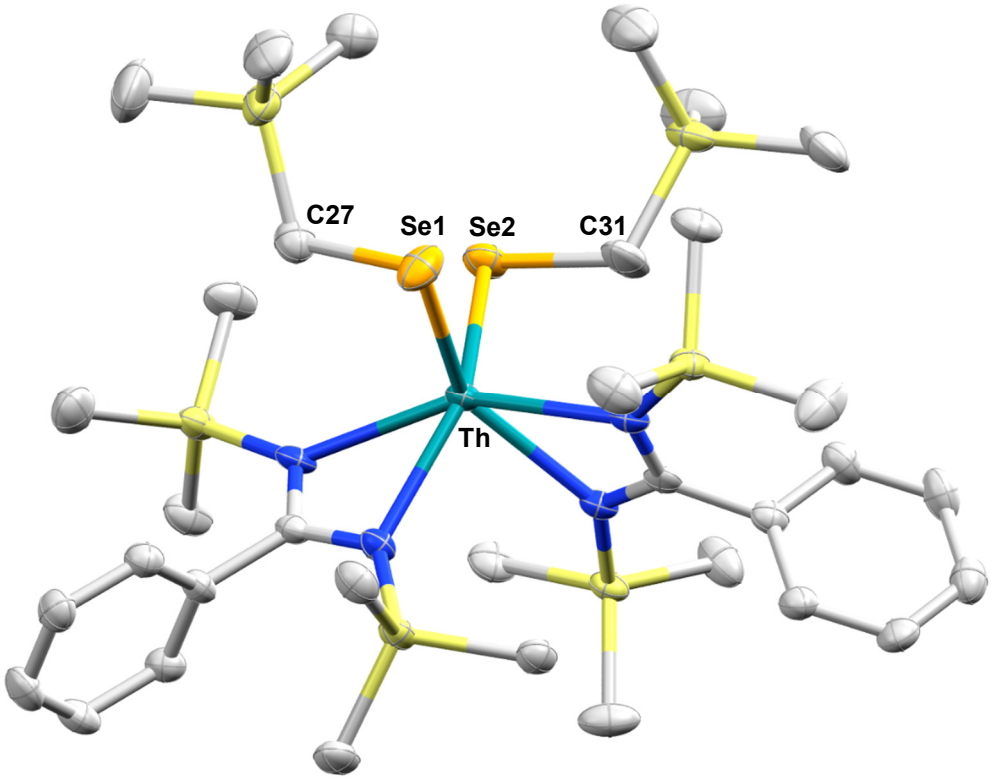

Figure 5.5. Molecular structure of **5.4**. Thermal ellipsoids drawn at the 50% probability level. Hydrogen atoms omitted for clarity.

interactions.[31-35,50] The Th-C27 and Th-C31 distances of 3.215(6) and 3.270(5) Å, respectively, are close to that observed for **2.7** (3.281(5) Å). The use of various sulfur or tellurium transfer reagents led to products that no longer contained the -CH_2SiMe_3 alkyl moieties, as determined by ^{1}H NMR spectroscopy.

Synthesis of Guanidinate-Supported Thorium Dialkyls. With the amidinate dialkyl complex successfully able to insert O_2 to form the dialkoxide, we turned our attention to synthesizing an analogous thorium guanidinate complex in order to probe the effect the more electron-donating guanidinates would have on O_2 insertion. While it is difficult to keep the steric profile of the ligands the exact same, the success of the *N, N, N', N''*-tetraisopropylguanidinate (TIG) in synthesizing uranium complexes prompted us to utilize this ligand for the synthesis of our analogous thorium species. Salt metathesis of $ThCl_4(DME)_2$ with 2 equiv. of Li(TIG)(THF)[51] afforded $Th(TIG)_2Cl_2(THF)$ (**5.5**) in moderate yield (Scheme 5.5). Slow addition of Li(TIG)(THF) is critical for this synthesis, as the tris-guanidinate complex $Th(TIG)_3Cl$ is readily formed in the presence of excess Li(TIG)(THF). The bound THF molecule in **5.5** can be removed under dynamic vacuum. The ^{1}H NMR spectrum of **5.5** exhibits the two different isopropyl environments on the TIG ligand, with two septets and two doublets observed in total, indicative of averaged C_2-symmetry of the molecule in solution. The molecular structure of **5.5** features two Th-Cl distances of 2.673(1) and 2.746(1) Å, a Cl1-Th-Cl2 bond angle of 115.19(3)°, and a Th-O1 bond length of 2.564(3) Å; these values are typical of that seen in similar thorium dichloride complexes with a bound THF molecule (Figure 5.6).[52,53] Exposing **5.5** to 2 equiv. of $LiCH_2SiMe_3$ afforded the desired bis-guanidinate thorium dialkyl complex $Th(TIG)_2(CH_2SiMe_3)_2$ (**5.6**, Scheme 5.5) in good yield. The ^{1}H NMR spectrum of **5.6** is as expected, with one new set of peaks attributable to the alkyl moieties; however, the methylene singlet is now seen further upfield at δ 0.21 ppm (compared to δ 0.42 in **5.2**), likely indicative of a more electron-rich metal center. The molecular structure of **5.6** was determined by X-ray diffraction studies (Figure 5.7); **5.6** crystallizes in the monoclinic

Scheme 5.5. Synthesis of Complexes **5.1** and **5.2** from Li(TIG)(THF)

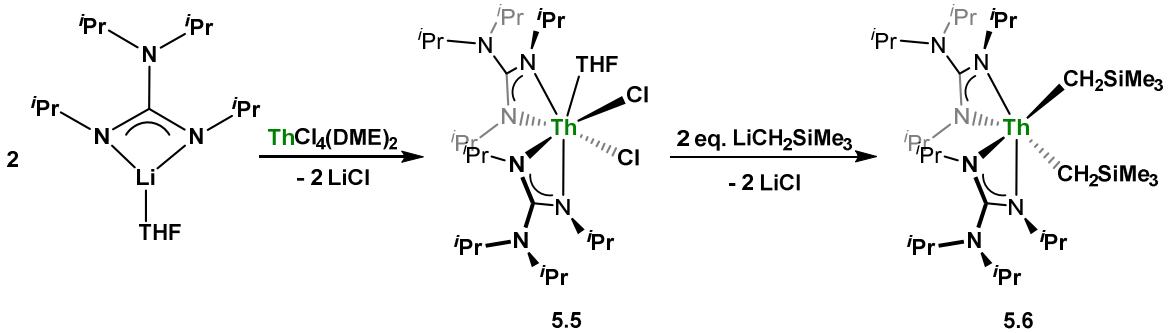

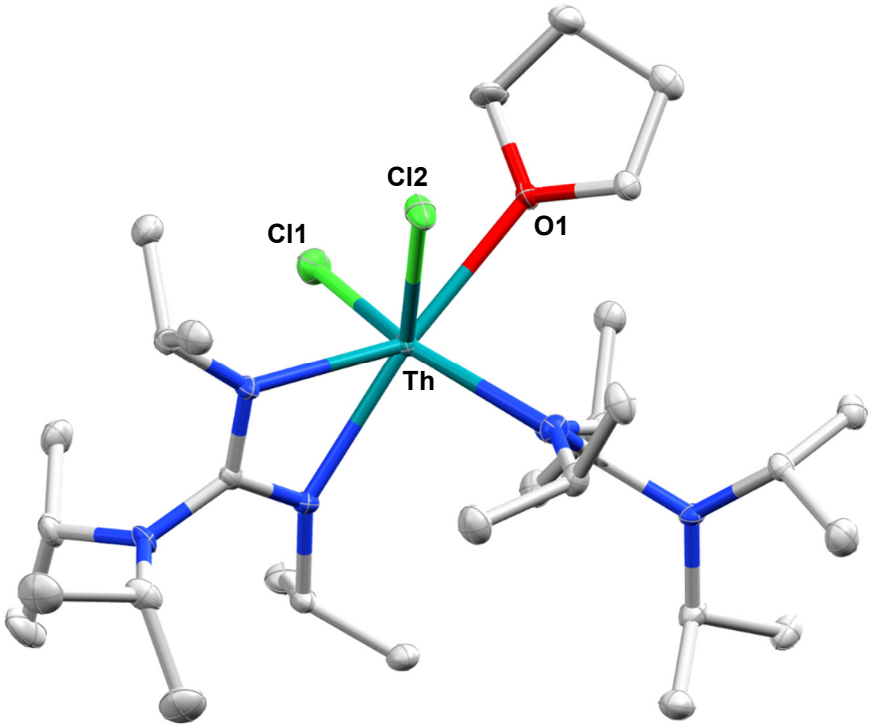

Figure 5.6. Molecular structure of **5.5**. Thermal ellipsoids drawn at the 50% probability level. Hydrogen atoms omitted for clarity.

space group C2/c, with half of the molecule in the asymmetric unit and the other half generated by symmetry. The Th-C14 bond length of 2.528(2) Å is similar to that seen in **2.2** and **5.2**, and the Th-C14-Si1 bond angle of 126.22(10)° is only 1° larger than that observed in **5.2**. All other crystallographic metrics are unremarkable.

Exposing a C_6D_6 solution of **5.6** to 1 atm of O_2 resulted in the formation of a new product with a downfield singlet appearing in the ^{1}H NMR spectrum at δ 4.22 ppm, along with shifted resonances corresponding to the TIG ligand and -$SiMe_3$ protons on the alkyl moieties. Based on these results, we concluded that O_2 insertion had been achieved and $Th(TIG)_2(OCH_2SiMe_3)_2$ (**5.7**) had been formed (Scheme 5.6). This transformation occurred more slowly than that seen with **5.2**, with completion times routinely taking >3 h when monitored by ^{1}H NMR spectroscopy. We postulated that the kinetics of O_2 insertion had indeed been slowed due to the increased electron-richness of the thorium metal center as a result of the greater electron-donating ability of the TIG

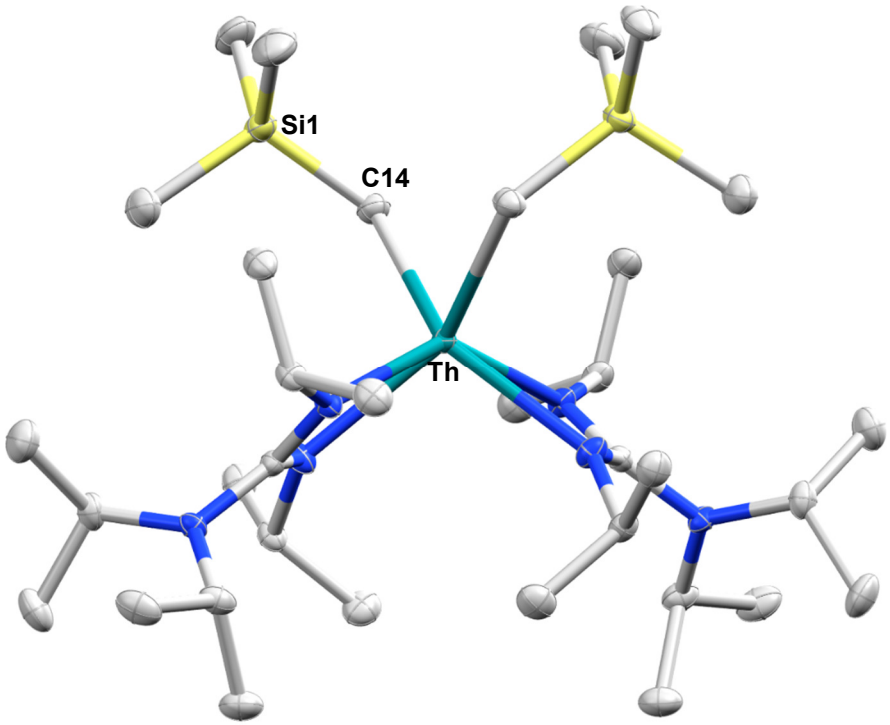

Figure 5.7. Molecular structure of **5.6**. Thermal ellipsoids drawn at the 50% probability level. Hydrogen atoms omitted for clarity.

Scheme 5.6. Synthesis of **5.7** via O_2 insertion

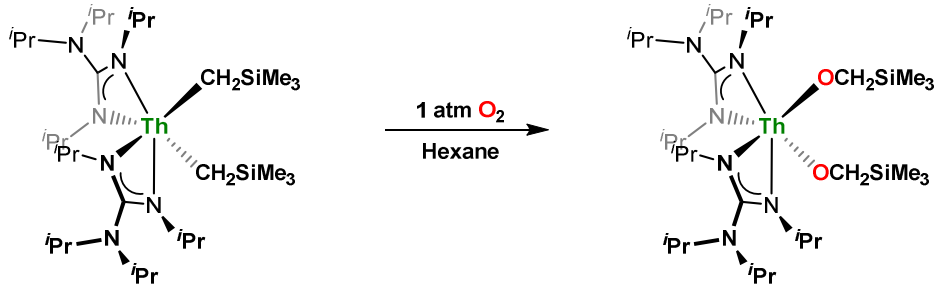

5.6 **5.7**

ligand, although the role of the different steric profile of TIG vs. BTBA cannot be discounted. Due to the poorer solubility of the TIG framework, **5.7** could be isolated as a colorless, block crystals in 89% yield from hexane. The molecular structure of **5.7** was determined by X-ray diffraction studies (Figure 5.8); like that observed with **5.6**, complex **5.7** crystallizes in the monoclinic space group C2/c, with half of the molecule in the asymmetric unit. Perhaps the most noticeable feature of this structure is the orientation of the alkyl groups, with the moieties almost eclipsed in their positioning; the dihedral angle between the $SiMe_3$ groups is 21.9(1)° in **5.7** (compared to 164.8(3)° in **5.3**). Although this kind of packing was not observed in **5.3**, it is presumably the lowest energy conformation for this molecule, as opposed to any indication of additional interactions. However, this configuration has not been observed in any metal complex bearing two -OCH_2SiMe_3 moieties; in fact, all such examples feature bridging oxos rather than terminal alkoxides.[54-57] The Th-O1 bond length of 2.1525(18) Å and Th-O1-C14 bond angle of 170.52(16)° are all consistent with what was observed in **5.3**. Selected bond lengths and angles of complexes **5.1-5.7** are listed in Table 5.1.

With the kinetics of O_2 insertion slowed for **5.6** compared to that of **5.2**, we looked to see if we could perform the same trapping experiment we had attempted using 1,4-cyclohexadiene in

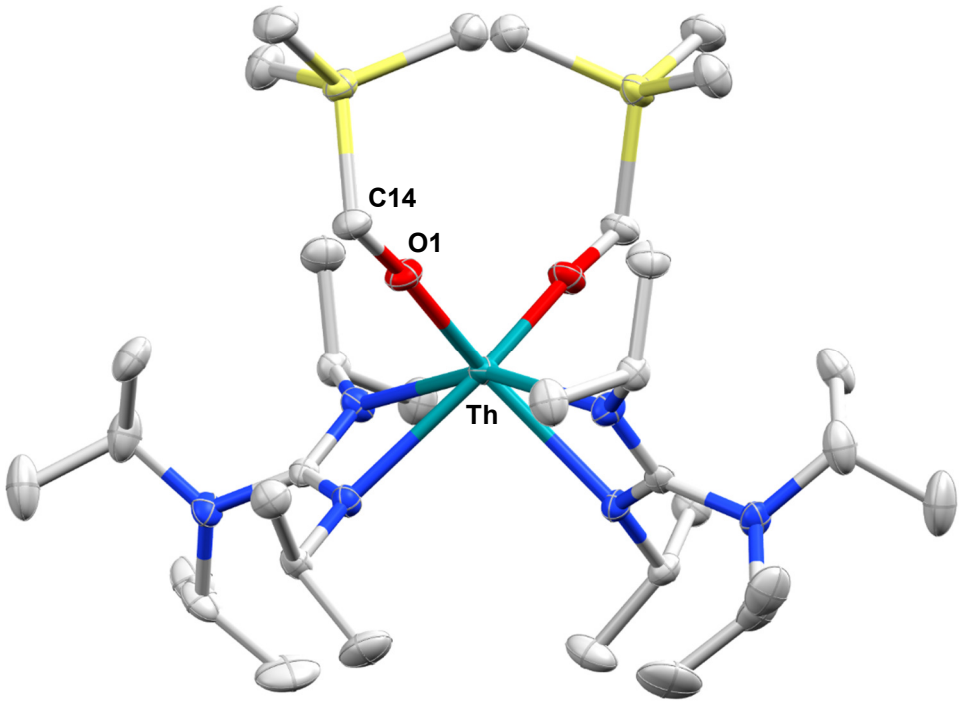

Figure 5.8. Molecular structure of **5.7**. Thermal ellipsoids drawn at the 50% probability level. Hydrogen atoms omitted for clarity.

order to find evidence for a radical-based mechanism. Three NMR-scale experiments were run in Teflon-capped *J*-Young NMR tubes simultaneously in order to test this: first, as a control, a sample of **5.6** was subjected to 1,4-cyclohexadiene in C_6D_6 and monitored over a period of 5 days, which brought about no observable change to the ^{1}H NMR spectrum. Second, a sample of **5.6** in C_6D_6 was subjected to dry O_2, and the rate of formation of **5.7** was monitored over a period of 5 days, as judged by the ratio of **5.7**:**5.6**. Lastly, a sample of **5.6** in C_6D_6 containing 1,4-cyclohexadiene was subjected to dry O_2, and the rate of formation of **5.7** was monitored over a period of 5 days, as judged by the ratio of **5.7**:**5.6**. All samples contained an internal standard of hexamethylbenzene. What was observed from these experiments was significant generation of tetramethylsilane when the O_2 experiment was carried out in the presence of 1,4-cyclohexadiene, as well as a decrease in the rate of formation of **5.7**. Additional experiments showed that increasing the amount of 1,4-cyclohexadiene in the sample decreased the amount of **5.7** formed and increased the amount of tetramethylsilane generated. Considering this evidence and prior literature precedent,[14] we do believe that a radical-based mechanism is operative in the formation of **5.3** and **5.7**, and that the greater electron-donating nature of the guanidinate ligand plays a role in affecting the kinetics of the reaction. This is consistent with Wolczanski's assertion that the electrophilicity of the metal center is important in synthesizing systems capable of this reactivity.

Table 5.1. Selected Bond Lengths (Å) and Angles (°) for Complexes **5.1-5.7**

Complex	**5.1**	**5.2**	**5.3**	**5.4**	**5.5**	**5.6**
Bond Lengths (Å)						
Th-Cl	2.773(7)[a]	-	-	-	2.710(1)[a]	-
Th-C	-	2.492(5)[a]	-	-	-	2.528(2)
Th-E	-	-	2.130(4)[a]	2.867(6)[a]	-	-
Bond Angles (°)						
Th-X-Y	-	125.1(2)[a]	172.4(3)[a]	81.7(1)[a]	-	126.22(10)

Complex	**5.7**
Bond Lengths (Å)	
Th-Cl	-
Th-C	-
Th-E	2.1525(18)
Bond Angles (°)	
Th-X-Y	170.52(16)

*E is the chalcogen atom bound directly to thorium. X and Y are the atoms of the alkyl moiety (C and Si for **5.2** and **5.6**; O and C for **5.3** and **5.7**; Se and C for **5.4**).*

[a]Average bond lengths and angles.

Table 5.2. Crystal and Refinement Data for Complexes **5.1-5.7**

Complex	**5.1**	**5.2**	**5.3**	**5.4**	**5.5**	**5.6**
Chemical formula	$C_{32}H_{62}N_6Si_4Cl_3LiTh$	$C_{34}H_{68}N_4Si_6Th$	$C_{34}H_{68}N_4Si_6O_2Th$	$C_{34}H_{68}N_4Si_6Se_2Th$	$C_{30}H_{64}Cl_2ON_6Th$	$C_{34}H_{78}N_6Si_2Th$
Formula weight	988.56	933.49	965.50	1091.42	827.81	859.24
Temperature (K)	100(2)	100(2)	100(2)	100(2)	100(2)	100(2)
Crystal system	Monoclinic	Monoclinic	Monoclinic	Triclinic	Triclinic	Monoclinic
Space group	P 21/c	P 21/c	P 21/c	P-1	P-1	C 2/c
a (Å)	18.8563(10)	26.240(5)	23.380(3)	10.7397(6)	9.9544(16)	24.340(2)
b (Å)	12.1439(6)	18.585(5)	9.8979(11)	11.3177(6)	12.545(2)	11.7801(11)
c (Å)	23.6059(13)	20.796(5)	20.423(2)	20.9355(12)	15.474(3)	18.3484(17)
α (°)	90	90	90	104.9130(10)	85.589(8)	90
β (°)	108.474(2)	113.178(5)	90.519(2)	96.0730(10)	84.718(8)	123.5780(10)
γ (°)	90	90	90	96.3560(10)	72.616(7)	90
V (Å^3)	5126.9(5)	9323(4)	4726.0(9)	2419.8(2)	1833.7(6)	4383.0(7)
Z	4	8	4	2	2	4
Densitiy (Mg m^{-3})	1.281	1.330	1.357	1.498	1.499	1.302
F(000)	1984	3792	1960	1084	836	1768
Radiation Type	MoK$_\alpha$	MoK$_\alpha$	MoK$_\alpha$	MoK$_\alpha$	MoK$_\alpha$	MoK$_\alpha$
μ (mm^{-1})	3.183	3.378	3.338	4.760	4.242	3.484
Meas. Refl.	76942	61389	97328	71997	78388	67790
Indep. Refl.	9424	16763	8708	8877	6699	4018
R(int)	0.0255	0.0345	0.0419	0.0274	0.0733	0.0248
Final R indices [I > 2σ(I)]	R = 0.0175 R_w = 0.0430	R = 0.0285 R_w = 0.0527	R = 0.0341 R_w = 0.0789	R = 0.0307 R_w = 0.0743	R = 0.0262 R_w = 0.0548	R = 0.0137 R_w = 0.0326
GOF	1.053	1.039	1.122	1.096	1.124	1.332
$\Delta\rho_{max}$, $\Delta\rho_{min}$ (e Å^{-3})	1.17, -0.43	1.550, -0.959	3.030, -1.065	2.449, -0.698	2.222, -0.537	1.568, -0.814

Table 5.2 (Cont.). Crystal and Refinement Data for Complexes **5.1-5.7**

Complex	**5.7**
Chemical formula	$C_{34}H_{78}N_6O_2Si_2Th$
Formula weight	891.24
Temperature (K)	100(2)
Crystal system	Monoclinic
Space group	C 2/c
a (Å)	23.921(5)
b (Å)	11.822(2)
c (Å)	19.372(4)
α (°)	90
β (°)	126.690(6)
γ (°)	90
V (Å^3)	4392.8(15)
Z	4
Densitiy (Mg m^{-3})	1.348
F(000)	1832
Radiation Type	MoK_α
μ (mm^{-1})	3.482
Meas. Refl.	68882
Indep. Refl.	4035
R(int)	0.0317
Final R indices [I > 2σ(I)]	R = 0.0194 R_w = 0.0463
GOF	1.118
$\Delta\rho_{max}$, $\Delta\rho_{min}$ (e Å^{-3})	3.321, -0.966

Conclusions

The amidinate- and guanidinate-supported thorium dialkyl complexes **5.2** and **5.6** are capable of undergoing oxygen atom insertion through the cleavage of O_2. This unique reactivity is seldom seen with early metal systems and has not been observed with the oxophilic actinides. Probing the mechanism of this reactivity produced evidence for a radical-based mechanism, as tetramethylsilane was produced when **5.6** was exposed to O_2 along with a decrease in total production of **5.7.** This is consistent with the mechanism likely operative with other group IV metal systems. While atom transfer with the heavier chalcogens proved more difficult, selenium insertion into the Th-C bonds in **5.2** was achieved with $Me_3P{=}Se$, resulting in the diselenolate complex **5.4**, which features two acute Th-Se-C bond angles. The electrophilicity of the metal center plays an important role in the ability of O_2 to react with these actinide systems, as was evidenced by the kinetic differences in the amidinate and guanidinate frameworks.

Experimental Details

General procedures. Unless otherwise stated, all reactions were performed under an atmosphere of dry N_2 using standard Schlenk line techniques or in an MBraun N_2 atmosphere glovebox (<1.0 ppm of O_2/H_2O). All solvents were dried and degassed using a commercially available Phoenix SDS from JC Meyer Solvent Systems. All glassware, syringes, and cannulas were stored in a 140 °C oven for a minimum of 16 h prior to use. Deuterated solvents were vacuum-transferred from flasks containing sodium/benzophenone (C_6D_6), degassed with three freeze−pump−thaw cycles, and stored over molecular sieves. $ThCl_4(DME)_2$,[30] Li(BTBA)(TMEDA),[27] Li(TIG)(THF),[51] and $Me_3P{=}Se$[58] were prepared according to previously reported literature procedures. O_2 gas was purchased from Praxair, Inc. and used directly from the cylinder without purification. (Trimethylsilyl)methyllithium was purchased from SigmaAldrich as a 1.0 M solution in pentane; solid $LiCH_2SiMe_3$ was obtained by crystallization from this pentane solution at -40 °C. All other reagents were purchased from commercial sources and used as received. Unless otherwise stated, NMR spectra were collected at ambient temperature on a Bruker AV-300, AVB-400, AV-500, DRX-500 or AV-600 spectrometer. ^1H and $^{13}C\{^1H\}$ NMR chemical shifts (δ) are reported in ppm and were calibrated to residual solvent peaks. Melting points were determined on an Optimelt SRS instrument using capillary tubes sealed under dry N_2. Elemental analysis samples were sealed under vacuum and analyzed at either the London Metropolitan University or the University of California, Berkeley. Infrared spectra were collected on a Thermo Scientific Nicolet iS10 FTIR spectrophotometer using Nujol mulls pressed between KBr plates.

$Th(PhC(NSiMe_3)_2)_2Cl(\mu\text{-}Cl)_2Li(TMEDA)$ (5.1): $ThCl_4(DME)_2$ (2.50 g, 4.52 mmol) was added to a 250 mL Schlenk flask containing a magnetic stir-bar and dissolved in 40 mL of THF. A THF solution (40 mL) of Li(BTBA)(TMEDA) (3.48 g, 9.00 mmol) was slowly added to this stirred solution, resulting in a faint pink solution which was allowed to stir at ambient temperature for 2 h. Volatiles were removed under reduced pressure and the resulting solid was triturated with hexane (2 x 30 mL), and extracted into toluene (75 mL). The solution was filtered away from the colorless LiCl precipitate, concentrated to 20 mL, and stored at -40 °C for 16 h, yielding **5.1** as large, colorless blocks (3.484 g, 78.1%). ^1H NMR (600 MHz, C_6D_6, 293 K): δ 7.35 (m, 4H, CH_{Ar}), 7.03 (m, 6H, CH_{Ar}), 2.07 (s, 12H, NMe_2), 1.72 (s, 4H, CH_2), 0.34 (s, 36H, SiMe_3). $^{13}C\{^1H\}$ NMR (151 MHz, C_6D_6, 293 K): δ 180.9 (N*C*N), 142.8 (C_{Ar}), 126.8 (C_{Ar}), 56.5 ($C_{TMEDA}H_2$), 45.8 (NMe_2), 2.8 (SiMe_3). Anal. Calcd for $C_{32}H_{62}Cl_3N_6Si_4LiTh$ (988.6): C, 38.88; H, 6.32; N, 8.50. Found: C, 38.79; H, 6.38; N, 8.42. Mp: 194-202 °C. FTIR (Nujol): 2797 (m), 1291 (m), 1247 (s), 1180 (w), 1160 (w), 1129 (w), 1066 (w), 1034 (m), 1017 (m), 1006 (m), 981 (s), 947 (w), 924 (w), 839 (s), 787 (m), 762 (m), 720 (s), 706 (s), 689 (m), 481 (s), 439 (m). Crystals suitable for single-crystal X-ray diffraction studies were grown from a concentrated toluene solution stored at -35 °C for 16 h.

$Th(PhC(NSiMe_3)_2)_2(CH_2SiMe_3)_2$ (5.2): Solid **5.1** (3.17 g, 3.21 mmol) was added to a 250 mL Schlenk flask containing a magnetic stir-bar and dissolved in 40 mL of toluene. A toluene solution (60 mL) of $LiCH_2SiMe_3$ (0.608 g, 6.46 mmol) was slowly added to this stirred solution,

resulting in immediate precipitation of a colorless solid. This solution was allowed to stir at ambient temperature for 5 minutes. Volatiles were removed under reduced pressure, and the resulting solid was extracted into hexane (40 mL) and filtered away from the LiCl precipitate. The resulting solution was concentrated to 5 mL and stored at -40 °C for 16 h, yielding **5.2** as colorless crystals (2.283 g, 76.4%). ^{1}H NMR (500 MHz, C_6D_6, 293 K): δ 7.31 (m, 4H, C*H*$_{Ar}$), 7.01 (m, 6H, C*H*$_{Ar}$), 0.51 (s, 18H, CH_2Si*Me*$_3$), 0.42 (s, 4H, C*H*$_2$SiMe$_3$), 0.15 (s, 36H, Si*Me*$_3$). ^{13}C{^{1}H} NMR (126 MHz, C_6D_6, 293 K): δ 182.5 (N*C*N), 143.5 (*C*$_{Ar}$), 128.9 (*C*$_{Ar}$) 126.2 (*C*$_{Ar}$), 95.2 (*C*H$_2$SiMe$_3$), 4.6 (CH_2Si*Me*$_3$), 2.5 (Si*Me*$_3$). Anal. Calcd for $C_{34}H_{68}N_4Si_6Th$ (933.5): C, 43.75; H, 7.34; N, 6.00. Found: C, 43.61; H, 7.32; N, 6.16. Mp: 76-77 °C. FTIR (Nujol): 1384 (s), 1248 (s), 1164 (w), 1075 (w), 1003 (m), 994 (m), 975 (s), 919 (m), 838 (s), 785 (s), 759 (s), 744 (m), 714 (s), 604 (w), 479 (m), 439 (w). Crystals suitable for single-crystal X-ray diffraction studies were grown from a concentrated hexane solution stored at -35 °C for 16 h.

Th(PhC(NSiMe$_3$)$_2$)$_2$(OCH$_2$SiMe$_3$)$_2$ (5.3): Solid **5.2** (0.550 g, 0.589 mmol) was added to a 100 mL Schlenk flask containing a magnetic stir bar and dissolved in hexane (20 mL). The solution was freeze-pump-thawed once, and the evacuated flask was then filled with O_2 gas (1 atm) via the vacuum manifold of the Schlenk line. The colorless solution was allowed to stir at ambient temperature for 20 minutes. Volatiles were removed under reduced pressure, and the resulting residue was extracted into HMDSO (12 mL). The extract was concentrated to <1 mL and placed in a freezer at -35 °C for 16 h, yielding **5.3** as colorless crystals (0.295 g, 51.8%). ^{1}H NMR (400 MHz, C_6D_6, 293 K): δ 7.32 (m, 4H, C*H*$_{Ar}$), 7.06 (m, 6H, C*H*$_{Ar}$), 4.18 (s, 4H, C*H*$_2$), 0.27 (s, 18H, CH_2Si*Me*$_3$), 0.18 (s, 36H, Si*Me*$_3$). ^{13}C{^{1}H} NMR (126 MHz, C_6D_6, 293 K): δ 180.5 (N*C*N), 144.6 (*C*$_{Ar}$), 126.2 (*C*$_{Ar}$), 69.1 (*C*H$_2$SiMe$_3$), 2.4 (Si*Me*$_3$), -3.0 (CH_2Si*Me*$_3$). Anal. Calcd for $C_{34}H_{68}N_4Si_6O_2Th$ (965.5): C, 42.30; H, 7.10; N, 5.82. Found: C, 41.99; H, 6.74; N, 6.15. Mp: 145-150 °C. FTIR (Nujol): 1246 (s), 1087 (m), 1060 (s), 1002 (m), 978 (s), 919 (w), 842 (s), 785 (w), 759 (m), 723 (w), 700 (m), 474 (m). Crystals suitable for single-crystal X-ray diffraction studies were grown from a concentrated HMDSO solution stored at -35 °C for 16 h.

Th(PhC(NSiMe$_3$)$_2$)$_2$(SeCH$_2$SiMe$_3$)$_2$ (5.4): Solid **5.2** (0.498 g, 0.533 mmol) was added to a 20 mL scintillation vial containing a magnetic stir-bar and dissolved in toluene (5 mL). To this stirred solution was added a toluene solution (5 mL) of Me_3P=Se (0.166 g, 1.07 mmol), and the clear solution was allowed to stir at ambient temperature for 30 minutes. Volatiles were removed under reduced pressure, and the resulting solid was extracted into hexane (12 mL). The hexane extract was concentrated to 4 mL and stored at -35 °C for 16 h, yielding **5.4** as colorless crystals (0.478 g, 82.1%). ^{1}H NMR (600 MHz, C_6D_6, 293 K): δ 7.22 (m, 4H, C*H*$_{Ar}$), 7.00 (m, 6H, C*H*$_{Ar}$), 2.18 (s, 4H, C*H*$_2$SiMe$_3$), 0.47 (s, 18H, CH_2Si*Me*$_3$), 0.19 (s, 36H, Si*Me*$_3$). ^{13}C{^{1}H} NMR (151 MHz, C_6D_6, 293 K): δ 182.3 (N*C*N), 142.5 (*C*$_{Ar}$), 129.0 (*C*$_{Ar}$), 128.5 (*C*$_{Ar}$), 126.1 (*C*$_{Ar}$), 2.5 (Si*Me*$_3$), 0.57 (*C*H$_2$SiMe$_3$), -0.04 (CH_2Si*Me*$_3$). Anal. Calcd for $C_{34}H_{68}N_4Si_6Se_2Th$ (1091.4): C, 37.42; H, 6.28; N, 5.13. Found: C, 37.42; H, 6.12; N, 5.16. Mp: 164-167 °C. FTIR (Nujol): 1249 (s), 1002 (w), 992 (w), 975 (m), 839 (s), 784 (w), 761 (m), 701 (m), 481 (m), 440 (w). Crystals suitable for single-crystal X-ray diffraction studies were grown from a concentrated toluene solution stored at -35 °C for 16 h.

Th(^{i}Pr$_2$NC(N^{i}Pr)$_2$)$_2$Cl$_2$(THF) (5.5): Solid $ThCl_4(DME)_2$ (0.500 g, 0.902 mmol) was added to a 20 mL scintillation vial containing a magnetic stir-bar and dissolved in THF (10 mL). A THF solution (5 mL) of Li(TIG)(THF) (0.552 g, 1.81 mmol) was then added dropwise to this colorless solution. Over the course of this addition, the reaction mixture turned pale yellow and cloudy; the reaction was stirred at ambient temperature for 16 h. Volatiles were removed under reduced pressure, resulting in a colorless solid, which was then triturated with hexane (3 mL) and extracted into toluene (2 x 5 mL). The solution was filtered through Celite. After volatiles were removed under reduced pressure, the resulting colorless powder was washed with 1 mL diethyl ether (to remove trace amounts of $Th(TIG)_3Cl$), and dissolved in 2 mL of THF. Storing this concentrated solution at -40 °C overnight yielded **5.5** as analytically pure, colorless block crystals (0.390 g, 55.7%). The molecule of coordinated THF could be removed under reduced pressure. ^{1}H NMR (600 MHz, C_6D_6, 293 K): δ 4.04 (sept, C*H*Me$_2$, 4H), 3.64 (m, THF: OC*H*$_2$CH$_2$, 2H), 3.28 (sept, C*H*Me$_2$, 4H), 1.50 (d, CH*Me*$_2$, 24H), 1.42 (m, THF: OCH$_2$C*H*$_2$, 2H), 1.06 (d, CH*Me*$_2$, 24H). ^{13}C{^{1}H} NMR (151 MHz, C_6D_6, 293 K): δ 172.0 (N*C*N), 68.1 (THF: O*C*H$_2$CH$_2$), 49.5 (*C*HMe$_2$), 47.5 (*C*HMe$_2$), 25.8 (THF: OCH$_2$*C*H$_2$), 25.7 (CH*Me*$_2$), 23.2 (CH*Me*$_2$). Anal. Calcd for $C_{26}H_{56}Cl_2N_6Th$ (754.4): C, 41.32; H, 7.47; N, 11.12. Found: C, 41.50; H, 7.36; N, 10.90. Mp: 199 °C (decomp). FTIR (Nujol): 1413 (s), 1324 (m), 1261 (w), 1207 (m), 1180 (w), 1138 (m), 1066 (m), 1019 (m), 800 (s), 722 (m), 665 (w), 513 (w), 460 (w). Crystals suitable for single-crystal X-ray diffraction studies were grown from a concentrated solution of THF stored at -35 °C for 16 h.

Th(^{i}Pr$_2$NC(N^{i}Pr)$_2$)$_2$(CH$_2$SiMe$_3$)$_2$ (5.6): Solid **5.5** (0.322 g, 0.389 mmol) was added to a 20 mL scintillation vial containing a magnetic stir-bar and dissolved in 10 mL of toluene. The addition of a toluene solution (5 mL) of $LiCH_2SiMe_3$ (0.074 g, 0.786 mmol) to this solution resulted in the precipitation of a colorless solid. The suspension was further stirred at ambient temperature for 2 h. The reaction mixture was filtered through Celite and the colorless solution was concentrated to 10 mL. Storage of this solution at -35 °C overnight yielded **5.6** as analytically pure, colorless microcrystals (0.322 g, 96.2%). ^{1}H NMR (300 MHz, C_6D_6, 293 K): δ 4.11 (sept, C*H*Me$_2$, 4H), 3.37 (sept, C*H*Me$_2$, 4H), 1.40 (d, CH*Me*$_2$, 24H), 1.14 (d, CH*Me*$_2$, 24H), 0.47 (s, CH$_2$Si*Me*$_3$, 18H), 0.21 (s, C*H*$_2$SiMe$_3$, 4H). ^{13}C{^{1}H} NMR (151 MHz, C_6D_6, 293 K): δ 172.9 (N*C*N), 91.9 (Th*C*H$_2$SiMe$_3$), 50.1 (*C*HMe$_2$), 47.2 (*C*HMe$_2$), 26.2 (CH*Me*$_2$), 23.6 (CH*Me*$_2$), 4.8 (ThCH$_2$Si*Me*$_3$). Anal. Calcd for $C_{34}H_{78}N_6Si_2Th$ (858.6): C, 47.53; H, 9.15; N, 9.78. Found: C, 47.65; H, 9.20; N, 10.04. Mp: 128 °C (decomp). FTIR (Nujol): 1317 (m), 1249 (w), 1236 (m), 1208 (m), 1182 (w), 1133 (m), 1122 (m), 1064 (s), 977 (m), 891 (m), 847 (s), 815 (m), 734 (m), 681 (w), 665 (m), 493 (w), 451 (w), 406 (w). Crystals suitable for single-crystal X-ray diffraction studies were grown from a concentrated solution of hexane, stored at -35 °C for 48 h.

Th(^{i}Pr$_2$NC(N^{i}Pr)$_2$)$_2$(OCH$_2$SiMe$_3$)$_2$ (5.7): Solid **5.6** (0.157 g, 0.183 mmol) was added to a 10 mL Schlenk flask containing a magnetic stir-bar and suspended in 5 mL of hexane. The hexane solution was frozen and the N_2 atmosphere was removed under reduced pressure. After the solution warmed up to room temperature, O_2 (1 atm) was introduced to the flask. The reaction mixture was stirred at ambient temperature for 16 hours, over which the solution became clear. After removal of the O_2 atmosphere, all volatiles were removed under reduced pressure, resulting in a colorless

solid. This solid was dissolved in 1 mL of hexane and the solution was concentrated to ~0.5 mL; storing this solution at -35 °C afforded **5.7** as analytically pure, colorless block crystals (0.138 g, 88.7%). ^{1}H NMR (400 MHz, C_6D_6, 293 K): δ 4.22 (s, ThOC*H*$_2$SiMe$_3$, 4H), 4.10 (sept, C*H*Me$_2$, 4H), 3.41 (sept, C*H*Me$_2$, 4H), 1.41 (d, CH*Me*$_2$, 24H), 1.19 (d, CH*Me*$_2$, 24H), 0.23 (s, CH$_2$Si*Me*$_3$, 18H). ^{13}C{^{1}H} NMR (151 MHz, C_6D_6, 293 K): δ 169.3 (N*C*N), 68.7 (ThO*C*H$_2$SiMe$_3$), 49.2 (*C*HMe$_2$), 46.8 (*C*HMe$_2$), 26.4 (CH*Me*$_2$), 23.6 (CH*Me*$_2$), -2.9 (ThOCH$_2$Si*Me*$_3$). Anal. Calcd for $C_{34}H_{78}N_6Si_2O_2Th$ (891.3): C, 45.82; H, 8.82; N, 9.43. Found: C, 46.09; H, 8.56; N, 9.27. Mp: 158–161 °C. FTIR (Nujol): 1310 (m), 1244 (m), 1214 (m), 1191 (w), 1136 (w), 1084 (m), 1064 (s), 1019 (m), 856 (s), 722 (m), 670 (m). Crystals suitable for single-crystal X-ray diffraction studies were grown from a concentrated solution of hexane stored at -35 °C for 16 h.

Formation of 5.7 in the Presence of 1,4-Cyclohexadiene: Three NMR-scale experiments were run simultaneously using 0.020 g portions of **5.6** (0.023 mmol) in C_6D_6. An internal standard of hexamethylbenzene (3.78 mg, 0.023 mmol) was used for each experiment. (1) 22 μL of 1,4-cyclohexadiene (0.023 mmol) was added to the first sample. Over the course of 5 days, all peaks corresponding to **5.6** remained unchanged; a small, insignificant amount of tetramethylsilane, however, was generated. (2) After three freeze-pump-thaw cycles, an atmosphere of dry O_2 was introduced to the second sample. The rate of formation of **5.7** was monitored for 5 days, as judged by the ratio of OCH_2SiMe_3:CH_2SiMe_3. A small, insignificant amount of tetramethylsilane was generated over the course of these 5 days. (3) 22 μL of 1,4-cyclohexadiene (0.023 mmol) was added to the third sample, along with an atmosphere of dry O_2, following the same freeze-pump-thaw procedure described previously. Over a period of 5 days, it was noted that the rate of the formation of **5.7** was significantly slower than that of the reaction in the absence of 1,4-cyclohexadiene. A significant amount of tetramethylsilane was also generated, presumably from the scavenging of C_6H_{10} allylic hydrogens by propagating •CH_2SiMe_3. In similar trials, increasing the amount of inhibitor decreased the amount of **5.**7 and increased the amount of tetramethylsilane generated, relative to the control.

Crystallographic Procedures. Single-crystal X-ray diffraction experiments were performed at the UC Berkeley CHEXRAY crystallographic facility. Measurements of all complexes were performed on a Bruker APEX-II CCD area detector using Mo Kα radiation (λ = 0.71073 Å). Crystals were kept at 100(2) K throughout collection. Data collection was performed with Bruker APEX2 software (v. 2014.11). Data refinement and reduction were performed with Bruker SAINT (V8.34A). All structures were solved with SHELXT.53.[59] Structures were refined with SHELXL-2014.[60] Molecular graphics were computed with Mercury 3.10. All non-hydrogen atoms were refined anisotropically, and hydrogen atoms were included at the geometrically calculated positions and refined using a riding model.

References

(1) Cavani, F.; Teles, J. H. *ChemSusChem* **2009**, *2*, 508-534.
(2) Boisvert, L.; Goldberg, K. I. *Acc. Chem. Res.* **2012**, *45*, 899-910.
(3) Sheldon, R. A.; Arends, I.; Hanefeld, U. *Green Chemistry and Catalysis*; Wiley-VCH: Weinheim, Germany, 2007; Chapter 4.
(4) *Active Oxygen in Chemistry*; Foote, C. S., Valentine, J. S., Greenberg, A., Liebman, J. F., Eds.; Blackie Academic & Professional: London, 1995.
(5) Arpe, H.-J. *Industrial Organic Chemistry*, 5th ed.; Wiley-VCH: Weinheim, Germany, 2010.
(6) Punniyamurthy, T.; Velusamy, S.; Iqbal, J. *Chem. Rev.* **2005**, *105*, 2329-2363.
(7) Wick, D. D.; Goldberg, K. I. *J. Am. Chem. Soc.* **1997**, *119*, 10235-10236.
(8) Williams, B. S.; Goldberg, K. I. *J. Am. Chem. Soc.* **2001**, *123*, 2576-2587.
(9) Jensen, M. P.; Wick, D. D.; Reinartz, S.; White, P. S.; Templeton, J. L.; Goldberg, K. I. *J. Am. Chem. Soc.* **2003**, *125*, 8614-8624.
(10) Smythe, N. A.; Grice, K. A.; Williams, B. S.; Goldberg, K. I. *Organometallics* **2009**, *28*, 277-288.
(11) Fulmer, G. R.; Muller, R. P.; Kemp, R. A.; Goldberg, K. I. *J. Am. Chem. Soc.* **2009**, *131*, 1346-1347.
(12) Fulmer, G. R.; Herndon, A. N.; Kaminsky, W.; Kemp, R. A.; Goldberg, K. I. *J. Am. Chem. Soc.* **2011**, *133*, 17713-17726.
(13) Lubben, T. V.; Wolczanski, P. T. *J. Am. Chem. Soc.* **1985**, *107*, 701-703.
(14) Lubben, T. V.; Wolczanski, P. T. *J. Am. Chem. Soc.* **1987**, *109*, 424-435.
(15) Stanciu, C.; Jones, M. E.; Fanwick, P. E.; Abu-Omar, M. M. *J. Am. Chem. Soc.* **2007**, *129*, 12400-12401.
(16) Tilley, T. D. *Organometallics* **1985**, *4*, 1452-1457.
(17) Hunter, S. C.; Chen, S.-J.; Steren, C. A.; Richmond, M. G.; Xue, Z.-L. *Organometallics* **2015**, *34*, 5687-5696.
(18) Chen, S.-J.; Xue, Z.-L. *Organometallics* **2010**, *29*, 5579-5584.
(19) Wang, R.; Zhang, X.-H.; Chen, S.-J.; Yu, X.; Wang, C.-S.; Beach, D. B.; Wu, Y.-D.; Xue, Z.-L. *J. Am. Chem. Soc.* **2005**, *127*, 5204-5211.
(20) Van Asselt, A.; Trimmer, M. S.; Henling, L. M.; Bercaw, J. E. *J. Am. Chem. Soc.* **1988**, *110*, 8254-8255.
(21) Yahia, A.; Maron, L. *Organometallics* **2009**, *28*, 672-679.
(22) Andrews, L.; Gong, Y.; Liang, B.; Jackson, V. E.; Flamerich, R.; Li, S.; Dixon, D. A. *J. Phys. Chem. A* **2011**, *115*, 14407-14416.
(23) Settineri, N. S.; Garner, M. E.; Arnold, J. *J. Am. Chem. Soc.* **2017**, *139*, 6261-6269.
(24) Settineri, N. S.; Arnold, J. *Chem. Sci.* **2018**, *9*, 2831-2841.
(25) Maity, A. K.; Metta-Magaña, A. J.; Fortier, S. *Inorg. Chem.* **2015**, *54*, 10030-10041.
(26) Rabinovich, E.; Aharonovich, S.; Botoshansky, M.; Eisen, M. S. *Dalton Trans.* **2010**, *39*, 6667-6676.
(27) Wedler, M.; Roesky, H. W.; Edelmann, F. T. *J. Organomet. Chem.* **1988**, *345*, C1-C3.

(28) Wedler, M.; Knösel, F.; Noltemeyer, M.; Edelmann, F. T. *J. Organomet. Chem.* **1990**, *388*, 21-45.
(29) Cantat, T.; Scott, B. L.; Kiplinger, J. L. *Chem. Commun*. **2010**, *46*, 919−921.
(30) Volkis, V.; Nelkenbaum, E.; Lisovskii, A.; Hasson, G.; Semiat, R.; Kapon, M.; Botoshansky, M.; Eishen, Y.; Eisen, M. S. *J. Am. Chem. Soc.* **2003**, *125*, 2179-2194.
(31) Fendrick, C. M.; Mintz, E. A.; Schertz, L. D.; Marks, T. J. *Organometallics* **1984**, *3*, 819-821.
(32) Butcher, R. J.; Clark, D. L.; Grumbine, S. K.; Scott, B. L.; Watkin, J. G. *Organometallics* **1996**, *15*, 1488-1496.
(33) Cruz, C. A.; Emslie, D. J. H.; Harrington, L. E.; Britten, J. F.; Robertson, C. M. *Organometallics* **2007**, *26*, 692-701.
(34) Clark, D. L.; Grumbine, S. K.; Scott, B. L.; Watkin, J. G. *Organometallics* **1996**, *15*, 949-957.
(35) Cruz, C. A.; Emslie, D. J. H.; Robertson, C. M.; Harrington, L. E.; Jenkins, H. A.; Britten, J. F. *Organometallics* **2009**, *28*, 1891-1899.
(36) Bruno, J. W.; Smith, G. M.; Marks, T. J.; Fair, C. K.; Schultz, A. J.; Williams, J. M. *J. Am. Chem. Soc.* **1986**, *108*, 40-56.
(37) Evans, W. J.; Walensky, J. R.; Ziller, J. W.; Rheingold, A. L. *Organometallics* **2009**, *28*, 3350-3357.
(38) Karmel, I. S. R.; Elkin, T.; Fridman, N.; Eisen, M. S. *Dalton Trans.* **2014**, *43*, 11376-11387.
(39) Karmel, I. S. R.; Fridman, N.; Eisen, M. S. *Organometallics* **2015**, *34*, 636-643.
(40) Hayes, C. E.; Sarazin, Y.; Katz, M. J.; Carpentier, J.-F.; Leznoff, D. B. *Organometallics* **2013**, *32*, 1183-1192.
(41) Berg, J. M.; Clark, D. L.; Huffman, J. C.; Morris, D. E.; Sattelberger, A. P.; Streib, W. E.; Van Der Sluys, W. G.; Watkin, J. G. *J. Am. Chem. Soc.* **1992**, *114*, 10811-10821.
(42) Clark, D. L.; Huffman, J. C.; Watkin, J. G. *J. Chem. Soc., Chem. Commun.* **1992**, 266-268.
(43) Clark, D. L.; Watkin, J. G. *Inorg. Chem.* **1993**, *32*, 1766-1772.
(44) Zhou, E.; Ren, W.; Hou, G.; Zi, G.; Fang, D.-C.; Walter, M. D. *Organometallics* **2015**, *34*, 3637-3647.
(45) Ren, W.; Song, H.; Zi, G.; Walter, M. D. *Dalton Trans.* **2012**, *41*, 5965-5973.
(46) Ren, W.; Zi, G.; Walter, M. D. *Organometallics* **2012**, *31*, 672-679.
(47) Behrle, A. C.; Barnes, C. L.; Kaltsoyannis, N.; Walensky, J. R. *Inorg. Chem.* **2013**, *52*, 10623-10631.
(48) Smiles, D. E.; Wu, G.; Hrobárik, P.; Hayton, T. W. *J. Am. Chem. Soc.* **2016**, *138*, 814-825.
(49) Rehe, D.; Kornienko, A. Y.; Emge, T. J.; Brennan, J. G. *Inorg. Chem.* **2016**, *55*, 6961-6967.
(50) Jantunen, K. C.; Batchelor, R. J.; Leznoff, D. B. *Organometallics* **2004**, *23*, 2186-2193.
(51) Pang, X.-A.; Yao, Y.-M.; Wang, J.-F.; Sheng, H.-T.; Zhang, Y.; Shen, Q. *Chin. J. Chem.* **2005**, *23*, 1193-1197.

(52) Wilson, D. J.; Sebastian, A.; Cloke, F. G. N.; Avent, A. G.; Hitchcock, P. B. *Inorg. Chim. Acta* **2003**, *345*, 89-94.
(53) Arunachalampillai, A.; Crewdson, P.; Korobkov, I.; Gambarotta, S. *Organometallics* **2006**, *25*, 3856-3866.
(54) Liu, X.; Cui, D. *Dalton Trans.* **2008**, 3747-3752.
(55) Goel, S. C.; Hollingsworth, J. A.; Beatty, A. M.; Robinson, K. D.; Buhro, W. E. *Polyhedron* **1998**, *17*, 781-790.
(56) Kennedy, A. R.; Klett, J.; McGrath, G.; Mulvey, R. E.; Robertson, G. M.; Robertson, S. D.; O'Hara, C. T. *Inorg. Chim. Acta* **2014**, *411*, 1-4.
(57) Linti, G.; Frey, R. *Z. Anorg. Allg. Chem.* **1997**, *623*, 531-538.
(58) Garcia-Rodriguez, R.; Liu, H. *J. Am. Chem. Soc.* **2012**, *134*, 1400-1403.
(59) Sheldrick, G. M. *Acta. Crystallogr. Sect. A* **2015**, *71*, 3-8.
(60) Sheldrick, G. M. *Acta. Crystallogr. Sect. A* **2008**, *64*, 112-122.